



The
University
Of
Sheffield.

**Investigation into the level of Cellular Prion Protein
(PrP^c) in Glioblastoma Multiforme (GBM) Cells
Treated with Alkylating Agents and Other Small
Molecules**

Ibrahim Al-Aadily

**A Thesis Submitted in Partial Fulfilment of the
Requirements for the Degree of
Doctor of Philosophy**

Department of Chemistry

University of Sheffield

UK

August 2019

List of Contents

List of Contents	I
List of Figures	VII
Lis of Tables.....	XI
Abstract	XII
Acknowledgements	XIV
Abbreviations	XV
Chapter 1: Introduction and Literature Review	1
1.1 Introduction.....	1
1.2 Review of literature.....	4
1.2.1 Programmed cell death and cancer.....	5
1.2.2 The cell cycle and cancer	8
1.2.3 Glioblastoma Multiforme (GBM)	10
1.2.4 GBM and programmed cell death	11
1.2.5 Human Prion protein	13
1.2.5.1 The structure of human cellular prion protein (PrP ^c).....	14
1.2.5.2 The functions of prion protein	16
1.2.5.2.1 PrP ^c and copper regulation.....	17
1.2.5.2.2 PrP ^c and oxidative stress	17
1.2.5.2.3 PrP ^c and Bcl-2 family proteins	18
1.2.5.2.4 PrP ^c and some signalling pathways.....	21
1.2.5.2.5 PrP ^c and cell proliferation	22
1.2.5.3 Prion protein and cancers.....	23
1.2.5.3.1 PrP ^c and breast cancer.....	23
1.2.5.3.2 PrP ^c and colorectal cancer.....	25
1.2.5.3.3 PrP and pancreatic ductal adenocarcinoma (PDAC)	26
1.2.5.3.4 PrP and gastric cancer.....	26
1.2.5.3.5 PrP and other types of cancers	28
1.2.5.3.6 PrP ^c and Glioblastoma	29
1.2.6 Chemotherapeutics for GBM	31
1.2.7 GBM disease models	35
1.2.8 Thesis aim and objectives	37
Chapter 2: Materials and Methods	42
2.1 Materials.....	42

2.1.1 Reagents and Chemicals.....	42
2.1.2 Equipment and Apparatus	44
2.1.3 Experimental Kits.....	45
2.2 Methods.....	45
2.2.1 Cell line and cell culture.....	45
2.2.1.1 Cell line.....	45
2.2.1.2 Thawing cells.....	45
2.2.1.3 Cell culture medium.....	46
2.2.1.4 Cell subculturing.....	46
2.2.1.5 Freezing of cells.....	46
2.2.2 Cells Viability assay (MTT).....	47
2.2.3 Cell cycle assay	47
2.2.4 Real time quantitative PCR assay	48
2.2.4.1 RNA extraction.....	48
2.2.4.2 Synthesis of cDNA	49
2.2.4.3 Primer design and real time quantitative PCR.....	49
2.2.5 Quantification of protein expression by Western blotting	51
2.2.5.1 Protein quantification.....	51
2.2.5.2 Western blot assay	52
2.2.6 Flow cytometry analysis: protein expression	54
2.2.6.1 Live cells (surface protein) flow cytometry.....	54
2.2.6.2 Fixing and permeabilising cells (cytosolic protein).....	55
2.2.7 ICC by Confocal Microscopy.....	55
2.2.8 ICC screening assay	56
2.2.9 Transfection- siRNA delivery in U87 cells.....	58
2.2.10 LDH assay	59
2.2.11 Alamar Blue assay.....	60
2.2.12 Apoptosis assay	61
2.2.13 Statistical Analyses.....	62
Chapter 3: Evaluation of PrP ^c and PRNP gene expression in different phases of the cell cycle and in U87 cells treated with TMZ or BCNU.....	63
3.1 Introduction.....	63
3.2 The aim.....	64
3.3 Methods.....	65
3.3.1 Preparation of treatments.....	65

3.3.2. Cell viability assay (MTT)	65
3.3.2.1 Growth curve of U87 cells	65
3.3.2.2 MTT assay for treated cells	66
3.3.3. Cell cycle assay by flow cytometry	67
3.3.4. RT-qPCR	68
3.3.5. Protein expression analysis by western blotting	70
3.3.6. PrP ^c expression by flow cytometry	70
3.4 Results	71
3.4.1 U87 growth curve	71
3.4.2 Cell viability of U87 cells	71
3.4.2.1 Cell viability of U87 in DMSO	72
3.4.2.2 Viability of U87 cells treated with TMZ and BCNU	72
3.4.2.3 Viability of U87 cells treated with Nocodazole and Aphidicolin	73
3.4.3 Cell cycle arrest	74
3.4.3.1 Cell cycle arrest by Aphidicolin and Nocodazole	74
3.4.3.2 Cell cycle analysis following treatment with TMZ and BCNU	75
3.4.4 p21 and p53 expression increased in U87 cells treated by TMZ and BCNU	79
3.4.5 PRNP expression by qRT-PCR	80
3.4.6 PrP ^c expression level by Western blotting (Experiment 1, 2 and 3)	82
3.4.7 Characterisation of PrP ^c expression by flow cytometry	85
3.4.7.2 PrP ^c level in U87 cells treated with TMZ and BCNU (Experiment 2)	86
3.4.7.3 PrP ^c level in treated cells with alkylating agents (Experiment 3)	87
3.5 Summary of key experimental results	89
3.6 Discussion	90
Chapter 4: Silencing of PRNP inhibits the proliferation of U87 cells	96
4.1 Introduction	96
4.1 The aim	97
4.2. Methods	98
4.2.1. Cell proliferation and viability MTT assay	98
4.2.2. RT-qPCR	99
4.2.3. PrP ^c expression by flow cytometry	99
4.2.4. PrP ^c , p53 and p21 expressions by western blot	100
4.2.5. Proliferation assay using Alamar Blue	101
4.2.6. Cytotoxicity LDH assay	102
4.2.7. Immunocytochemistry (ICC) by confocal microscopy	103

4.2.8. Apoptosis assay by Annexin V with PI.....	104
4.2.9. Cell cycle assay by flow cytometry.....	104
4.3 Results.....	105
4.3.1 Assessment of U87 cell viability in PRNP siRNA and Darmafect reagents	105
4.3.2 The effectiveness of PRNP gene knockdown in transfected cells	106
4.3.3 PrP ^c expression in knockdown cells.....	107
4.3.3.1 PrP ^c expression in transfected cells by Flow cytometry.....	108
4.3.3.2 PrP ^c expression in transfected cells by Western blot and ICC	109
4.3.4 PRNP knockdown reduces the proliferation of U87 cells.....	112
4.3.5 Knockdown of PrP ^c in U87 cells does not induce cytotoxicity according to LDH assay	113
4.3.6 PrP ^c knockdown inhibits proliferating marker ki67	114
4.3.7 Knockdown of PRNP gene does not induce apoptosis in U87 cells either when treated with TMZ or untreated.....	116
4.3.8 PrP ^c silencing does not influence chemotherapeutic resistance in U87 cells by MTT assay	117
4.3.9 PRNP knockdown cells affect the cell cycle of TMZ treated U87 cells.....	118
4.3.10 p53 and p21 in PRNP knockdown cells treated with TMZ and BCNU....	120
4.4. Summary of key experimental results.....	122
4.5. Discussion	123
Chapter 5: Evaluation of the effect of proteasomal inhibitor, MG132, on PrP ^c in U87 cells and on the apoptosis when combined with TMZ.....	129
5.1 Introduction.....	129
5.2 The aim.....	133
5.3 Methods.....	133
5.3.1 Preparation of treatments.....	133
5.3.2 Cell viability assay	134
5.3.3 Western blot assay	134
5.3.4 Flow cytometry assay for protein level	135
5.3.5 Microscopical assay	135
5.3.6 Annexin V with PI assay	136
5.3.7 Cell cycle assay by flow cytometry.....	136
5.4 Results.....	137
5.4.1 Cell viability for U87 treated with MG132	137
5.4.2. MG132 increases the PrP ^c level according to the western blot assay	138

5.4.3 Assess PrP ^c level in treated cells with MG132 by flow cytometry	140
5.4.4 PrP ^c level in MG132 treated U87 cells using confocal microscopy	141
5.4.5 MG132/TMZ combination does not promote the apoptosis of U87 according to Annexin V with PI staining assay	143
5.4.6 The effect of MG132/TMZ combination upon the proliferation of U87 cells	145
5.4.7 MG132 induces cell cycle arrest	146
5.4.8 MG132 increases the level of p53 and p21	148
5.5 Summary of key experimental results.....	151
5.6 Discussion	151
Chapter 6: Investigation of the effect of small molecules (Fanconi anaemia pathway inhibitors, FAPi) on the level of PrP ^c in U87 cells	156
6.1 Introduction.....	156
6.2 The aim.....	160
6.3 Methods.....	162
6.3.1 Preparation of treatments.....	162
6.3.2. Cell viability assay	162
6.3.3 Western blot assay	163
6.3.3 High throughput and high content small molecule screening method	163
6.3.3.1 Optimisation of ImageXpress Micro as a high content screening assay.....	164
6.2.3.2 Validating the screening method	165
6.3.3.3 The screening of FAPi compounds to evaluate PrP ^c level	165
6.3.4 The analysis of the images	165
6.4 Results.....	166
6.4.1 Cell viability for U87 cells treated with FAPi compounds in combination with TMZ or BCNU	166
6.4.2 FANCD2 expression in treated U87 cells with TMZ or BCNU	168
6.4.3 FAPi compounds suppress FA pathway.....	168
6.4.4 Development of high throughput and high content small molecule screening method.....	171
6.4.4.1 Optimisation and validation of ImageXpress Micro as a high throughput and high content screening assay.....	171
6.4.4.2. PrP ^c expression in treated U87 cells with FAPi compounds/TMZ or BCNU combination using ImageXpress Micro.....	173
6.4.4.3 The expression of PrP ^c in treated U87 cells with FAPi compounds.....	175
6.5 Summary of key experimental results.....	177
6.6 Discussion	177

Chapter 7: Screening of small molecule chemical libraries as anticancer agents using U87 glioblastoma cells.....	181
7.1 Introduction.....	181
7.2 The aim.....	184
7.3 Methods.....	184
7.3.1 Compounds preparation	184
7.3.2 Cell viability by MTT assay	185
7.3.3 Apoptosis assay	185
7.3.4 Cell cycle assay	186
7.3.5 Western blot assay.....	186
7.4 Results.....	186
7.4.1 Cell viability of U87 treated with the small molecules.....	186
7.4.2 Apoptosis assay for the treated U87 cells with small molecules	187
7.4.3 Dose-dependent studies of U87 cells treated with compound 175 over 5 days	190
7.4.4 Cell cycle studies by compound 175.....	190
7.4.5 The level of p21 and p53 by compound 175.....	193
7.4.6 The effect of compound 175 on PrP ^c level in U87 cells	194
7.5 Summary of key experimental results.....	196
7.6 Discussion.....	196
Chapter 8: General discussion, Conclusions and Future perspectives.....	200
References.....	213

List of Figures

Figure (1-1): The apoptotic pathways.....	7
Figure (1-2): Cell cycle in eukaryotic cell.....	9
Figure (1-3): Human PrP structure (Immature PrP ^c).....	16
Figure (1-4): The proposed mechanism for PrP with Bax to suppression of apoptosis	20
Figure (1-5): The mechanism of TMZ action	32
Figure (1-6): The mechanism of BCNU action	33
Figure (2-1): The standard curve for serial dilutions of BSA in RIPA buffer..	51
Figure (2-2): The cassette of western blotting shows the order of the membrane, gel, filter paper and fibre pad according to black and white sides.....	53
Figure (2-3): ImageXpress Micro device.....	57
Figure (2-4): The distribution of samples in 96-well plate used to performed cell viability assay by Alamar blue assay.....	61
Figure (3-1): A summary of the experimental designs showing the different time points and treatments.....	69
Figure (3-2): Growth curve for U87 cells over four days.....	71
Figure (3-3): Cell viability of U87 cells in different concentrations of DMSO	72
Figure (3-4): The viability of U87 cells treated with a series of concentrations of TMZ and BCNU	73
Figure (3-5): Cell viability for U87 cells in synchronised agents.....	74
Figure (3-6): Cell cycle synchronisation of U87 cells by Nocodazole and Aphidicolin.....	75
Figure (3-7): TMZ and BCNU induced cell synchronisation in the G2/M phase.....	77
Figure (3-8): The effect of alkylating agents on the U87 cell cycle.....	78
Figure (3-9) p21 and p53 expression levels in TMZ or BCNU treated cells by western blot.....	79
Figure (3-10): PRNP expression in treated U87 cells.....	82
Figure (3-11): Western blotting for PrP ^c in U87 cells (Experiment 1).....	83
Figure (3-12): Western blotting analysis of PrP ^c in U87 cells (Experiment 2)	84
Figure (3-13): Western blotting analysis for PrP ^c in U87 cells treated 24+48h	

with TMZ and BCNU (Experiment 3).....	85
Figure (3-14): The expression of PrP ^c in treated U87 cells by flow cytometry (Experiment 1).....	86
Figure (3-15): PrP ^c expression in treated U87 cells by flow cytometry (Experiment 2).....	87
Figure (3-16): PrP ^c expression in treated U87 cells by flow cytometry ((Experiment 2).....	88
Figure (4-1): The design of Alamar blue experiment.....	101
Figure (4-2): The experimental design for LDH assay.....	103
Figure (4-3): Quantification of cell viability in transfected U87 cells using MTT assay.....	106
Figure (4-4): Relative PRNP gene expression in transfected and non- transfected U87 cells.....	107
Figure (4-5): Expressions of PrP ^c in transfected U87 cell according to flow cytometry.....	109
Figure (4-6): Expressions of PrP ^c in transfected U87 cells.....	111
Figure (4-7): Cell proliferation of transfected U87 cells.....	113
Figure (4-8): Cytotoxicity of transfection reagents in U87 cells by LDH assay.....	114
Figure (4-9): ICC for ki67 in PRNP knockdown cells.....	115
Figure (4-10): The apoptosis of PrP ^c knockdown cells using Annexin V with PI.....	116
Figure (4-11): Knockdown of PrP ^c in U87 cells does not affect the response to TMZ or BCNU.....	118
Figure (4-12): Determination of cell cycle phases in knockdown cells using PI.....	119
Figure (4-13): Western blot for p53 and p21 in treated and untreated transfected U87 cells.....	121
Figure (5-1): The proteasome structure and its function.....	129
Figure (5-2): The structure of MG132.....	130
Figure (5-3): Diagram showing MG132-induced apoptosis.....	131
Figure (5-4): The experimental design for using confocal microscopy to evaluate PrP ^c in treated cells with MG132.....	135

Figure (5-5): The experimental design for U87 cells treated with MG132 and/or TMZ for apoptosis assay.....	136
Figure (5-6): Viability of U87 cells in different concentrations of MG132.....	138
Figure (5-7): PrP ^c level in U87 treated with MG132 by western blotting.....	139
Figure (5-8): The expression of PrP ^c in MG132 treated U87 cells after 12 h according to flow cytometry assay.....	141
Figure (5-9): PrP ^c expression in MG132 treated and untreated cells by confocal microscopy.....	142
Figure (5-10): Apoptosis assay by flow cytometry for MG132 treated cells ...	144
Figure (5-11): Cell viability for U87 cells treated with MG132 and/or TMZ over 48 h by MTT assay.....	146
Figure (5-12): Cell cycle analysis for MG132 treated U87 cells.....	148
Figure (5-13): The expression of p53 and p21 and in MG132 treated U87 cells with and without TMZ.....	150
Figure (6-1): The mechanism of DNA repair via the FA pathway.	158
Figure (6-2): The structures of FAPi compounds.....	161
Figure (6-3): The experimental design of MTT assay used to evaluate cell viability of U87 cells treated with FAPi compounds/TMZ or BCNU.....	163
Figure (6-4): The experimental design to optimise the PrPc antibodies.	164
Figure (6-5): The design of screening compounds by ImageXpress Micro	165
Figure (6-6): Cell viability assay for U87 cells treated with FAPi compounds in combination with TMZ or BCNU.....	167
Figure (6-7): Western blot for FANCD2 in U87 cells treated with TMZ and BCNU for 24h	168
Figure (6-8): The level of FANCD2 in FAPi treated U87 cells	170
Figure (6-9): The level of PrP ^c by ICC using ImageXpress Micro.....	173
Figure (6-10): FAPi compounds do not affect PrP ^c expression in combination with TMZ or BCNU	175
Figure (6-11): FAPi compounds do not affect PrPc level in U87 cells after 48 h of treatment with 5 μ M FAPi compounds.....	176
Figure (7-1): List of the small molecules subdivided into seven families.....	183
Figure (7-2): The experimental design of MTT assay for the small molecules	185

Figure (7-3): Cell viability of U87 cells treated with eight compounds.....	187
Figure (7-4): The effect of eight small molecules on the apoptosis of U87 cells using Annexin V with PI.....	189
Figure (7-5): Viability of U87 cells in the different concentrations of compound 175	190
Figure (7-6): The cell cycle analysis of U87 cells treated with compound 175	192
Figure (7-7): Compound 175 upregulates p21 and p53 in U87 cells.....	194
Figure (7-8): PrP ^c level in treated U87 cells with compound 175	195

Lis of Tables

Table (1-1): Commonly used cell lines in GBM studies, the information provided by ATCC and European Collection of Authenticated Cell Culture (ECACC).....	36
Table (2-1): List of chemicals and reagents.....	42
Table (2-2): List of the equipment and apparatus.....	44
Table (2-3): List of commercial kits.....	45
Table (2-4): The sequences of primers.....	50
Table (2-5): The examples of siRNA and DarmaFECT volume (μ l) in different cell densities.....	59
Table (3-1): Cell density and incubation time of treated cells in MTT assay.....	67
Table (3-2): Seeding density of U87 cells in cell cycle experiments.....	68
Table (3-3): The incubation times and cell densities of RT-PCR experiment.....	68
Table (4-1): Cell density and the volume of transfection reagents in the proliferation and viability assay.....	98
Table (4-2): Cell density and the volume of transfection reagents used at each time point to determine PRNP level.....	99
Table (4-3): A summary of the cell densities and transfection reagents for all incubation periods in the Alamar blue assay.....	102
Table (6-1): The FA genes and their function.....	157

Abstract

Glioblastoma multiforme (GBM) is a malignant tumour of astrocytes in the brain which accounts for approximately one third of all tumours in the nervous system. Despite the availability of chemotherapy, the median survival rate for all patients is between 15 to 24 months. Temozolomide (TMZ) and carmustine (BCNU) are the most common chemotherapeutic agents used in combination with radiotherapy or surgery to treat GBM. The overexpression of PrP^c in GBM has been reported and its involvement in the resistance to alkylating agents (TMZ and BCNU) was speculated. The exact role of PrP^c in GBM, i.e. how it is affected by chemotherapeutic agents and small molecules, needs to be further investigated.

In this work, the effect of TMZ and BCNU on PrP^c was evaluated using U87 glioblastoma cell line. The results showed that 24 h treatment with TMZ or BCNU followed by 48 h resting gave the highest level of G2/M cells (about 84%) when compared with untreated cells. The upregulations of p53 and p21 are believed to be the key cause for this increment. PRNP gene is also upregulated in TMZ or BCNU treated U87 cells for 24 h treatment followed by 48 h resting and this may contribute to the resistance these cells towards the treatments due to the cytoprotective effect of this protein despite less PrP^c is detected at protein level. Some of these findings are in agreement while others are opposite to those previously reported.

The resistance to chemotherapy is considered as one of the main limitations for the effective treatment of cancer, especially for GBM. PRNP gene in U87 cell line was silenced to determine cell proliferation and chemoresistance. A decrease of 80% in PrP^c level was obtained after 48 h of treatment with transfection reagents. Additionally, the level of the PrP^c knockdown was retained 5 days post-knockdown.

Silencing of the PRNP gene in glioblastoma cell line U87 reduces cell proliferation in a time-dependent manner. In addition, positive cells with proliferation marker ki67 were significantly decreased in knockdown cells after 5 days. This implies that PrP^c contributes to the malignance of the cancer cells. It was also found that there was no significant reduction in cell proliferation in response to TMZ or BCNU in knockdown cells and p21 is upregulated in TMZ or BCNU knockdown cells. Therefore, silencing PRNP gene may impact the function of p21 which contributes to the resistance to alkylating agents TMZ and BCNU.

In an attempt to sensitise U87 cells to TMZ, the combination treatment of MG132 with TMZ did not improve the apoptosis rate and no accumulative effect was observed. High concentration of MG132 increased the level of PrP^c in U87 cells after a short incubation time.

The level of PrP^c was also evaluated in U87 cells treated with the compounds (FAPi) which inhibit the Fancony Anaemia (FA) pathway by reduction of FANCD2 using high content imaging by ImageXpress Micro. These compounds did not affect the level of PrP^c in these cells with or without combination with TMZ or BCNU showing that these FAPi are target specific.

Several novel families of heteroaromatic compounds (30 compounds) previous shown to be cytotoxic to embryonic carcinoma cells (NT2) were screened on U87 cells and eight of them were found to be inhibit the proliferation of the cells. The compound **175** that belongs to the acridine family induced apoptosis for U87 cells. It also arrests U87 cells in G2/M and upregulate p53 and p21 proteins which are regulatory for cell cycle. That may open the door to examine more acridine compounds as anti-glioblastoma agents.

Acknowledgements

I am very grateful to the great and almighty God, Allah. I would like to express my gratitude to my supervisor, Prof. Beining Chen for her constant help, supervision and inspiration during the period of my research. I cannot express enough thanks to Dr Cleide Dos Santos for her help and advice towards this project. I would also like to thank my friends Imane, Zainab, Ahmed, Muhanned and Ali for their support. A special mention should go to my colleague Mehul for his advice and suggestions that were very helpful for my experiments. I would especially like to thank the Department of Biochemistry- Faculty of Medicine, University of Kufa, Iraqi Cultural Attache and the Iraqi Ministry of Higher Education and Scientific Research, who gave me the opportunity to study in the Sheffield University, United Kingdom at their full expense. Special thank goes to Dr Majid Kadhum Hussain for his support. I also wish to thank my extended family members, especially my mother, sisters, brothers, mother-in-law, sisters-in-law, brothers-in-law, who have prayed for me throughout this journey. My deepest appreciation goes to my wonderful wife, Zena Wally for her never-ending support and motivation, particularly during the tough times. A very special thank you to my lovely children Maryam, Mustafa and Mohammed for their understanding and patience during the long hours I spent in the lab and writing this thesis. Finally, I would like to thank my late father Rahem J. Al-Aadily who taught me to love learning. Now I want to dedicate my thesis to his memory.

Abbreviations

19S	Proteasome subunit 19 individual proteins
20S	Proteasome subunit beta type-5
5-FU	Fluorouracil
ADR	Adriamycin
Akt	Protein kinase B
ANOVA	Analysis of variance
Apaf-1	Apoptotic protease activating factor 1
Atg	Autophagy-related protein
Bak	Bcl-2 homologous antagonist/killer
Bax	Bcl-2-associated X protein
BCL-2	B-cell lymphoma 2
BCL-XL	B-cell lymphoma-extra large
BCNU	Carmustine
BH2	BCL-2 homology domain
Bid	BH3 interacting-domain death agonist
BSA	Bovine serum albumin
cAMP/PKA	Cyclic adenosine monophosphate/protein kinase A
CDDP	Cisplatin
cDNA	Complimentary DNA
DAPI	4',6-diamidino-2-phenylindole
DISC	Death-inducing signalling complex
DMSO	Di methyl sulfoxide
DR4	TRAIL receptor 1
DR5	TRAIL receptor 1
DRAM	DNA damage regulated autophagy modulator
EEF2K	Eukaryotic elongation factor-2 kinase
EGFR	epidermal growth factor receptor
ER	Endoplasmic reticulum
ERAD	Endoplasmic-reticulum-associated protein degradation
ERK	Extra-cellular signal related kinase
FADD	Fas-Associated protein with Death Domain
FBS	Fetal bovine serum

FIP200	FAK family-interacting protein
FLNa	Filamin A
FoxO	Forkhead family proteins
FSC	Forward scatter
GAPDH	Glyceraldehyde-3-phosphate dehydrogenase
GBM	Glioblastoma multiforme
GPI	Glycosylphosphatidyl inositol
GPI-PSS	Glycosylphosphatidyl- inositol anchor peptide signal sequence
GR	Glutathione reductase
Grb2	Growth factor receptor-bound protein 2
HBSS	Hanks' Balanced Salt Solution
HDACi	Histone deacetylase inhibitor
IAP	The inhibitor of apoptosis proteins
IC ₅₀	The half maximal inhibitory concentration
IκB	I kappa B proteins
IKK	IκB kinase
LC3	Microtubule-associated protein 1A/1B-light chain 3
LC3-II	LC3-phosphatidylethanolamine conjugate
MAPK	Mitogen-activated protein kinases
Mcl-1	Induced myeloid leukemia cell differentiation protein
MDR	Multidrug-resistant
MG132	Carbobenzoxyl-L-leucyl-L-leucyl-L-leucinal
MGMT	O6-methylguanine-DNA methyltransferase
MGr1-Ag/37LRP	MGr1-antigen human
miRNA	microRNA
mTOR	Mammalian target of rapamycin
MTT	3-[4,5-dimethylthiazol-2-yl]-2,5 diphenyl tetrazolium bromide
NEAA	Non-essential amino acid
NF-κB	Nuclear factor kappa-light-chain-enhancer of activated B cells
nNOS	Neuronal nitric oxide synthase
p21	Cyclin-dependent kinase inhibitor 1

p53	Tumour suppressor p53
P59Fyn	Protein tyrosine kinase fyn
p62	Nucleoporin p62
p-Akt	Phosphorylated Akt
PBS	Phosphate buffer saline
PDGFR	Platelet-derived growth factor receptor
P-gp	P-glycoprotein
PI	Propidium Iodide
PI3 kinase	Phosphoinositide 3-kinase
PI3K/Akt	phosphoinositide-3 kinase
PRND	Doppel protein gene
PRNP	Prion protein gene
PrP	Prion protein
PrP ^c	Cellular prion protein
PrP ^{Sc}	Scrapie prion protein
Pro-PrP	PrP retaining its GPI-PSS or incompletely processed prion protein
PTEN	Phosphatase and tensin homolog
Raf	Rapidly Accelerated Fibrosarcoma
Ras	Family of related proteins
ROS	Reactive oxygen species
rpm	Revolutions per minute
SAHA	Histone deacetylase inhibitor suberoylanilide hydroxamic acid
SD	Standard deviation
siRNA	Small interfering RNA
SMAC	Second mitochondrial protein
SOD	Superoxide dismutase
SOD1	Superoxide dismutase 1
SSC	Side scatter
STI1	Stress inducible protein 1
TBS	Tris buffer saline
TBS-T	Tris buffer saline with triton
TMZ	Temozolomide

TNF	Tumour necrosis factors
TP53	Tumour protein p53
TRAIL	TNF-related apoptosis-inducing ligand
Ub	Monoubiquitin
UPR	Unfolded protein response
VCR	Vincristine
WT	Wild Type

Chapter 1: Introduction and Literature Review

1.1 Introduction

Glioblastoma multiforme (GBM) or Grade IV astrocytoma is a primary malignant brain tumour that can afflict most glial cells. It is an aggressive, and fatal disease, accounting for about one third of all tumours in the nervous system¹. The median survival rate of this type of cancer is very short (up to two years). GBM affects a large number of heterogeneous brain cells and is more aggressive, angiogenic, genetically unstable and chemotherapeutic-resistant tumour than other types of astrocytomas. Radiotherapy followed by temozolomide (TMZ) is a current standard treatment regimen for GBMs after a surgical operation². However, resistance evolves rapidly during the treatment and the cause for the resistance is poorly understood which results in ineffective treatment and poor prognosis. Therefore, further research is required in the area.

Although the exact biological role of cellular prion protein (PrP^c) remains enigmatic, many studies have revealed that PrP^c is involved in various cellular functions, including oxidative stress, apoptosis, cell migration, cell-cell signalling, regulation of the immune system, proliferation and copper metabolism etc. This mix of functions would suggest that PrP^c may plausibly be implicated in various types of cancers³, including GBM⁴. Comincini and co-workers have shown that tissue samples from GBM tumours exhibit a high level of PrP^c expression compared to other grades of brain tumour⁵. TMZ induces cell cycle arrest in the G2/M phase, but it has been noticed *in vitro* that TMZ-resistant GBM cells exhibit an upregulation of PRNP expression at this phase of the cell cycle⁶.

One of the important issues concerning cancer treatment is chemoresistance since this dramatically hampers its clinical applications, particularly for alkylating agents such as TMZ⁷. PrP^c is thought to be involved in chemotherapeutic resistance for many types of cancers⁸, and this poses the question: what is the effect of PrP^c on the resistance of GBM cells treated with alkylating agents?

Recently, proteasome inhibitors have been used to treat cancers such as multiple myeloma and are under examination for other types⁹ because the ubiquitin proteasomal pathway has a crucial role for proteolysis of most intracellular proteins and regulation of many cellular processes such as the differentiation, apoptosis and the cell cycle. In addition, the proteasome is responsible for the regulation of tumour suppressors, cell cycle regulators and transcription factors which are closely related to cancer development¹⁰. The proteasome inhibitor MG132, for example, is a peptide aldehyde that suppresses the growth of many kinds of tumours by arresting the cells in G2/M and inducing apoptosis¹¹. MG132 reduces the aggressiveness of glioma cells by inhibiting their proliferation and promoting apoptosis^{12,13}. Besides the effect of MG132 on apoptosis of glioblastoma cells, it has been found that the PrP^c expression level is increased in neuron cells N2a and N2a-PrP when treated with MG132¹⁴ as will be described in Section 5.1 of Chapter 5 of this thesis. Despite the effect of MG132 on glioma cells, its effect on these cells when used in combination with TMZ has not been investigated. PrP^c level in U87 cells treated with MG132 also needs to be assessed.

The Fanconi anaemia (FA) pathway is a DNA repair pathway and often responds to DNA damage, replication arrest and other disruptions which are produced by alkylating agents such as TMZ and carmustine (BCNU)¹⁵. Interestingly, as

chemotherapeutic agents, TMZ and BCNU have been shown to stimulate the FA pathway by upregulating of FANCD2. Inhibition of the FA pathway by silencing the key part of this pathway (FANCD2) has therefore been found to improve cell sensitivity to TMZ and BCNU¹⁶. Recently, Abhijit *et al.* revealed that FANCD2 expression is upregulated in GBM compared to normal brain tissue and other grades of astrocytoma. The combination of some small molecules with TMZ or BCNU, therefore, served to sensitise glioblastoma cells to these treatments by inhibiting the FA pathway¹⁷. In previous work from our group (unpublished data), many novel small molecules were examined and shown to inhibit the FA pathway. We assume that such molecules may also affect the level of PrP^c in U87 cells because it has also previously been suggested that amide scaffolds can lower the level of PrP^c in T98G glioblastoma cells¹⁸ (this will be detailed in chapter 6).

In this thesis, we hypothesised that the treatment of U87 cells with alkylating agents TMZ and BCNU might influence the prion protein expression level as a result of the accumulation of cells in G2/M and this effect might induce the resistance to these agents. Therefore, we first looked at the expression of PrP^c and its gene in different phases of the cell cycle in U87 cells treated with TMZ or BCNU. Silencing of PRNP gene was performed to study the effect of PrP^c on the sensitivity of U87 cells to TMZ and BCNU treatments. We then examine the impact of the MG132 proteasomal inhibitor on the level of PrP^c in U87 cells and the apoptotic effect of the MG132-TMZ combination on these cells. The possible efficacy of the novel drug combinations that inhibited the FA pathway was also assessed to determine the PrP^c level in U87. The potential anticancer effect of other novel small molecules was also screened here to evaluate their cytotoxicity on U87 cells.

1.2 Review of literature

Through the literature survey, the possible links between the cellular prion protein (PrP^c) in cancers, including GBM, and the challenges associated with the resistance of glioblastoma cells to the chemotherapies (TMZ and BCNU) commonly used to treat this aggressive and often fatal disease can be established. The overexpression of PrP^c in GBM has been identified in many studies as well as its involvement in underpinning resistance to alkylating agents due to interaction with apoptotic pathways. The possibility of the resistance could be attributed to the accumulation of cells in G2/M phase, and PrP^c and its gene may have different expression in the G1 phase compared to the G2/M phase. Specifically, the upregulation of PrP^c may protect GBM cells due to the cytoprotective effect of this protein.

Within the cell cycle, the G2/M phase represents the response to DNA damage induced by various stimuli and is a vitally important staging point to ensure that cells do not trigger mitosis until damaged DNA is sufficiently repaired. p53 plays a crucial role in DNA repair and can regulate the cell cycle with its transcriptional target p21 and arrest the cells in G2/M.

The molecular mechanisms of PrP^c's involvement in the response of GBM cells to chemotherapy have yet to be investigated. Work in this area is promising and may provide significant improvements in how GBM cells respond to chemotherapeutic treatments. We hypothesised that treatment of U87 cells, as a model of glioblastoma, with alkylating agents TMZ and BCNU will result in the upregulation of prion protein due to the accumulation of cells in G2/M. This upregulation may induce resistance toward these treatments. Furthermore, the silencing of the PRNP gene may sensitise U87 cells against TMZ or BCNU. We also speculated that the combination of small

molecules with TMZ or BCNU could inhibit the expression of PrP^c in U87 cells. The following chapters of this thesis will outline a series of investigations, as described in section (1.2.8).

1.2.1 Programmed cell death and cancer

Programmed cell death is a process referring to the normal biological fate of the cell which is carried out by either apoptosis, autophagy or programmed necrosis to keep a balance between the living and dead cells. The apoptosis can be triggered by several biochemical and morphological changes such as nuclei shrinking, DNA fragmentation and condensation, and loss of cell-cell adhesion or extracellular matrix adhesion¹⁹. Autophagy occurs in response to cellular stress resulting from the lack of nutrients or growth factors²⁰. It plays an important role in the preservation of tissue homeostasis and administrates many physiological processes such as cell differentiation, starvation, cell death and survival²¹. In addition to apoptosis and autophagy, programmed necrosis has recently identified as programmed cell death characterised by swelling, organelle dysfunction and cell lysis²². Disruption of any these regulatory mechanisms will in general result in cancer, including GBM.

It is known that cancer can cause various alterations in cell signalling pathways which occur as a result of gene mutation²³. Apoptosis serves to maintain a healthy body system by removing old cells. There are two main pathways inducing apoptosis: the death receptor pathway/ extrinsic pathways and the mitochondrial pathway/ intrinsic pathway²⁴.

The extrinsic pathway is activated by death receptors such as tumour necrosis factor (TNF) receptors: DR4 (TRAIL-R1), DR5 (TRAIL-R2), TNF-R1, Fas, DR3 and DR6²⁵. These receptors bind their related extracellular ligands. Fas binds to its receptor when

exposed to death stimuli, such as DNA damage and drugs, to form the Fas/Fas-L complex. This complex then recruits Fas-Associated protein with Death Domain (FADD) and pro-caspases 8,10 to form the death-inducing signalling complex (DISC) as an initiator to activate caspase 8, which in turn triggers the activation of caspases 3, 6 and 7²⁶. In addition, p53 can transactivate multiple other death receptors, such as DR5 and Fas, through its downstream effect, which is activated in response to DNA damage²⁷. Moreover, BH3 interacting-domain death agonist (Bid) is activated by the active caspase-8. Bid triggers Bax and Bak (pro-apoptotic factors)²⁸ and leads to the continuation of the intrinsic apoptotic pathway (Figure 1-1).

The intrinsic pathway, meanwhile, is regulated by mitochondrial pro-enzymes. Upregulation of oncogenes or DNA damage DNA can stimulate this pathway²⁹. In addition, other factors can also stimulate the intrinsic pathway such as growth factor deficiency, excess Ca^{2+} and DNA damage molecules³⁰. Furthermore, Bcl-2 family proteins play an effective role in the mitochondrial pathway through permeabilisation of the mitochondrial membrane. The activation of mitochondria is regulated by either Bcl-2 pro-apoptotic proteins or Bcl-2 anti-apoptotic proteins³¹. According to several studies, these proteins are upregulated in different kinds of cancer³². Bax and Bak as a pro-apoptotic multi domain BH3 are necessary for mitochondrial apoptosis which activates mitochondria to release cytochrome c³³. Cytochrome c is released from the mitochondria and then binds to apoptotic protease-activating factor 1 (Apaf 1) and procaspase 9 to form the apoptosome. The apoptosome triggers the signalling of caspases which are implicated in apoptosis, such as caspase 3³⁴. Additionally, the pro-apoptotic proteins Bim, Bid and Bad activate Bax/Bak signalling, which is activated by p53³⁵, and this may be inhibited via anti-apoptotic proteins Bcl-2, Bcl-XL, and Mcl-1³⁶. As a tumour suppressor factor p53 has a crucial role in

mitochondrial apoptosis through its activation of Bax³⁷. Bcl-2 suppresses mitochondrial apoptosis by inhibiting transcription of Bax and Bak³⁸ (Figure 1-1).

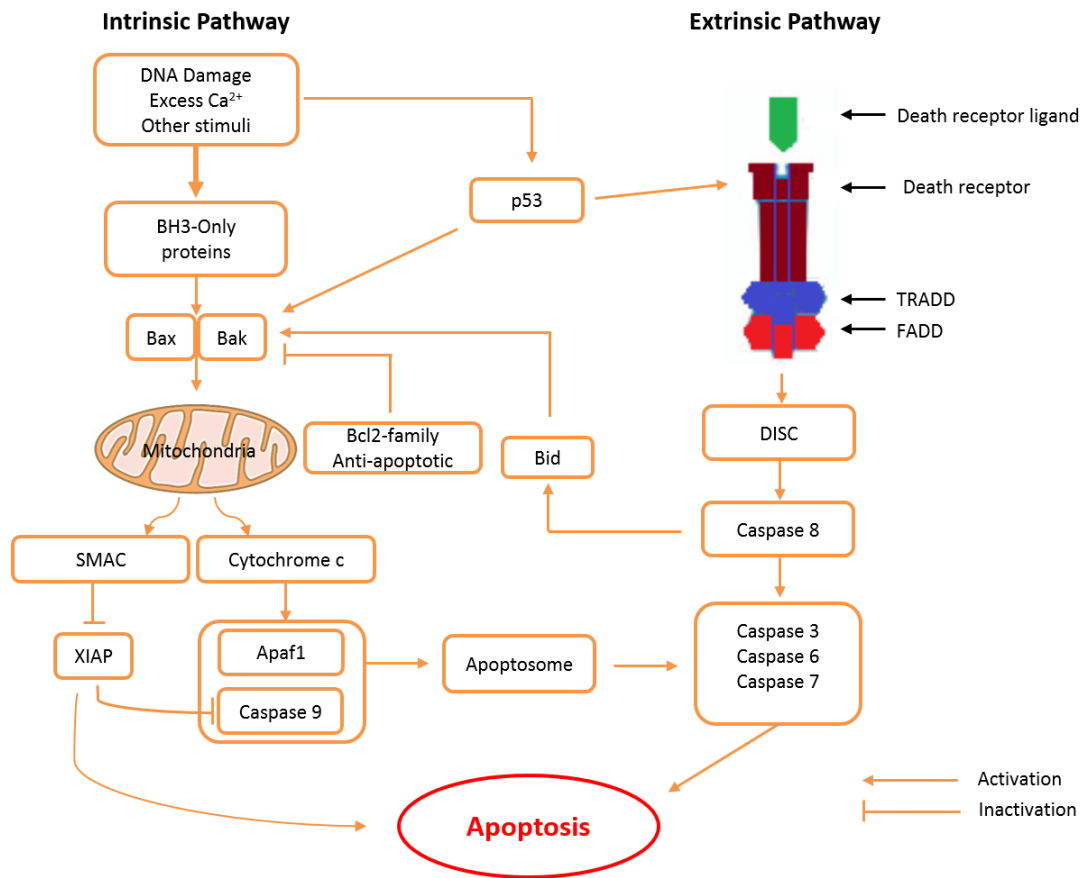


Figure (1-1): The apoptotic pathways. Adapted from Baig *et al.* under the Creative Commons Attributed Licence²⁶.

Autophagy is an evolutionarily catabolic process which occurs under different circumstances such as extra or intracellular stress. In this physiological process, the cells recycle excess cytoplasmic components via lysosomal degradation, which is regulated by some autophagy-related genes³⁹. In cancer, autophagy faces a challenge of whether to protect live cells or to promote cell death. It has been reported that the activity of autophagy protects malignant cells in the early stages of cancer. In contrast, autophagy can decrease the effect of cancer by promoting pro-autophagic genes and suppressing anti-autophagic genes. The autophagic pathway is promoted and

regulated by different cytosolic pathways including LC3, p53, mTORC1/C2, Beclin-1, Bcl-2 and PI3K (Class III and I)⁴⁰.

It has been reported that some forms of necrosis, such as necroptosis, are regulated in various cells under normal physiological conditions²². During this specific cell death process, the components of the cell are released into the extracellular region due to a result of cell membrane damage. This can stimulate immune cells and trigger an inflammatory response. The malignant tumour may provoke topical inflammation via this type of cell death. The activation of programmed necrosis may also participate in the reduction of cancer, however⁴¹. It should be noted that the discovery of the key markers of necrotic cell death, such as receptor-interacting protein kinases (RIPKs), opens the door to the development of more sophisticated theories of programmed necrosis.

1.2.2 The cell cycle and cancer

In eukaryotic cells, the cell cycle consists of a series of events across four phases: gap one or growth 1 (G1), synthesis (S), gap two or growth 2 (G2) and mitosis (M)⁴². In G1, the transcription and translation processes increase to produce cellular proteins which are important for DNA synthesis. In addition, the number of organelles such as ribosomes and mitochondria, also increase in preparation for pre-mitosis steps. This phase occupies the longest period in the cell cycle. In the S phase, DNA is disentangled and duplicated. The replication of DNA is considered a major event in the S phase. Subsequently, during the G2 phase, the cell grows in preparation for cell mitosis. The G2/M checkpoint is stimulated, and the cell will be arrested should DNA damage occur in this phase⁴³. G2 / M is essential for eukaryotic cells to ensure that they do not undergo mitosis before any DNA damage is repaired⁴⁴. Before cell

division, the chromosomes are separated, and cytokinesis divides organelles and the cell membrane into two equal parts. The mitotic (M) phase in animal cells is defined by the action of both mitosis and cytokinesis⁴⁵. Generally, the division in eukaryotic cells is grouped into two main stages: interphase (G1, S and G2 phase) and mitosis (M phase). The M phase consists of four events, including prophase, metaphase, anaphase, and telophase⁴⁶ (Figure 1-2).

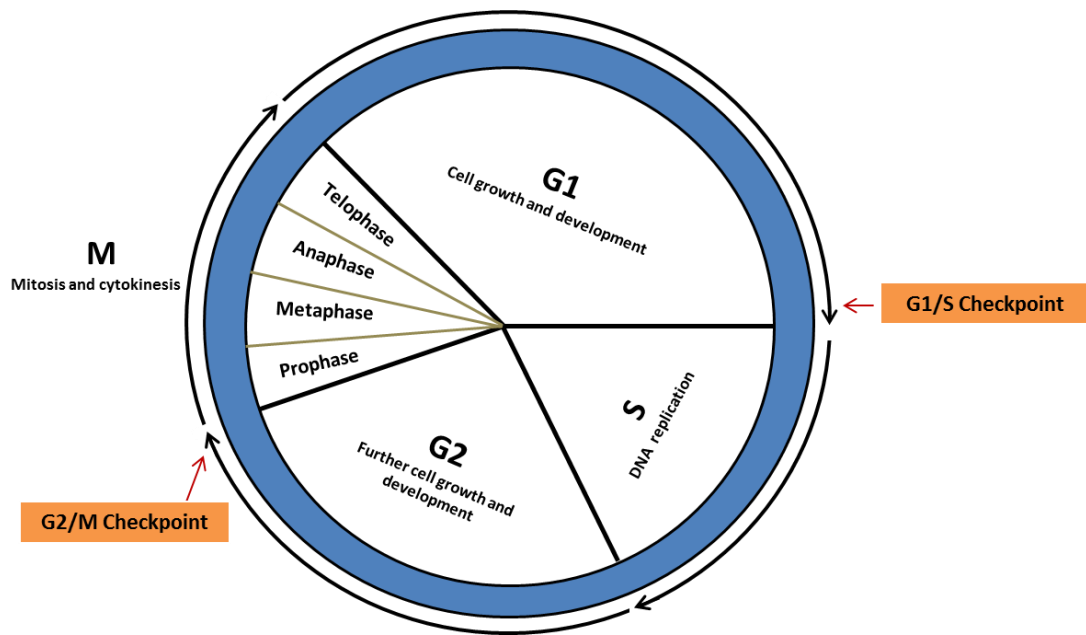


Figure (1-2): Cell cycle in a eukaryotic cell.

It has been reported that in cancer cells the cell cycle is always decontrolled, potentially promoting abnormal cell proliferation and division⁴⁷. The checkpoints in the cell cycle are therefore considered to be good targets for the development of many treatments for cancers due to their potential to inhibit cell progression. One treatment strategy is to control these checkpoints and disrupt the process of cell division. Subsequently, this action activates apoptosis⁴⁸. For instance, 5-fluorouracil inhibits DNA replication and taxol has an effect on microtubules, and these drugs are currently first-line treatments for breast and colorectal cancer, respectively⁴⁹. These treatments are limited, however, in that they are toxic when delivered in high doses⁵⁰.

1.2.3 Glioblastoma Multiforme (GBM)

According to the World Health Organization (WHO), astrocytomas can be classified into four grades in the following (ascending) order of severity.

Grade I is a low grade and very slow-growing tumour which commonly occurs in childhood. It can often be cured with surgical resection alone.

Grade II is a low grade and slow-growing tumour that often recurs and develops into a higher grade malignant tumour (grade III and IV). Patients with a Grade II tumour have a median survival rate of up to 15 years.

Grade III is a high-grade malignant tumour including anaplastic astrocytoma, anaplastic ependymoma, anaplastic oligodendroglioma and anaplastic oligoastrocytoma. It has high mitotic activity and may be transformed to grade IV. Patients with a Grade III tumour have a survival rate of up to 10 years.

Grade IV or glioblastoma multiforme (GBM) is more aggressive than grade III, and it spreads to other portions of the brain rapidly. The median survival rate of GBM is between 15 to 24 months, depending on the prognosis and treatment regimen⁵¹.

GBM or grade IV astrocytoma form about half of all gliomas and is a common type of offensive malignant tumour¹. Bastien and collaborators further categorised GBMs into primary/*de novo* or secondary depending on the clinical history of patients. Primary/*de novo* GBMs are the most common type, accounting for about 90%-95% of all GBMs, and they are more aggressive, with the tumour progressing than with secondary GBMs. Patients with primary glioblastoma are diagnosed without clinical or histological evidence of precursor lesions. Secondary GBMs represent about 5%-10% of the total GBMs and are commonly developed from low-grade astrocytomas

(Grade II or III)^{1,52}. Although GBMs are often aggressive, they do not normally spread to other parts of the CNS and behave similarly to other types of CNS tumours⁵³.

Computed tomography (CT or CAT) scan and magnetic resonance imaging (MRI) are sophisticated imaging systems which can accurately localise GBMs⁵². From pathological, histological and physiological perspectives, all GBMs display clear clinical manifestations, including abnormal proliferation, a decrease in apoptosis, plentiful genomic fluctuation, angiogenesis, vascular thrombosis and a tendency to necrosis⁵⁴.

As with most other types of cancers, the exact aetiology of GBM is unclear, but it is known that risk factors for GBM include exposure to ionising radiation and some rare genetic disorders⁵¹. Nonetheless, GBM shares some common underlying molecular events with all other cancers, as detailed below.

1.2.4 GBM and programmed cell death

In the glioblastoma cells, it was found that there are many regulators for apoptotic and homeostatic processes leading to them being over-expressed, mutated or methylated. For example, the Bcl-2 protein family, p53, growth factor receptors such as phosphoinositide-3 kinase (PI3K)/Akt, mammalian target of rapamycin (mTOR), and the TNFR family are all implicated in GBM cell death and survival⁵⁵.

The expression of the Bcl-2 protein family, whether pro- or anti-apoptotic proteins, is inconsistent in patients with different grades of astrocytoma. Krajewski *et al.* showed that the level of the pro-apoptotic proteins was lower in glioblastoma than other grades of gliomas⁵⁶, while the expression of Bcl-2 positively correlated with the

survival period of patients, regardless of astrocytoma grade⁵⁷. Moreover, *in vitro* studies revealed that cell death is induced in glioblastoma cells by gossypol (an extract from the cotton plant), both alone and in combination with temozolomide (TMZ). Gossypol binds to Bcl-2 and induces cell death in glioblastoma cells⁵⁸. Overall, in U87, MZ-54 and U343 glioblastoma cells, autophagy may be induced by gossypol and gossypol-TMZ increases the sensitivity of these cells to TMZ⁵⁹.

Another set of studies have focused on micro RNA (miRNA), a small RNA that binds to complementary sequences of mRNA, inhibiting the translation of mRNA. Of particular interest is miRNA21. It has been shown that when this is overexpressed in GBM cells, it appears to induce resistance to TMZ by reducing the ratio of Bax/Bcl-2⁶⁰. Furthermore, it has been found that silencing of miRNA-21 promotes caspase-induced cell death⁶¹. Likewise, GBM cells transfected with miRNA-153 also seemed to induce cell death through inhibition of Bcl-2.

The p53 that is encoded by the TP53 gene also has an important role in apoptosis and cell cycle regulation⁶². Indeed, according to the Cancer Genome Atlas Research Network, the signalling of p53 is altered in 87% of all GBM patients.⁶³ Ohgaki *et al.* showed that TP53 mutations frequently occur in GBM and that *de novo* GBM has fewer of these mutations than secondary GBM, 28% to 65%, respectively⁶⁴.

It has also been reported that growth factors such as epidermal growth factor receptor (EGFR), phosphatidylinositol 3-kinases (PI3K/AKT) and mammalian target of rapamycin (mTOR) are involved in facilitating apoptosis in glioblastoma cells. For example, inhibition of PI3K/Akt and mTOR improve survival rates in patients with glioblastoma⁶⁵. Similarly, the inhibition of EGFR/mTOR promoted cell death and

inhibited downstream PI3K pathway signalling in U87 and SF295 glioblastoma cell lines⁶⁶.

During apoptosis of cells, TNF-related apoptosis-inducing ligand (TRAIL) binds to the death receptors DR4 (TRAIL-R1) and DR5 (TRAIL-R2). Although TRAIL binds three other types of TRAIL receptors, these do not induce an apoptotic signal in human cells⁶⁷. Grund *et al.* found that DR5 was highly expressed in grade II gliomas compared with grade III and that the expression of DR5 correlated with the survival time of glioma patients⁶⁸. Consequently, DR5 is suggested to be the key constituent of TRAIL receptors that mediates cell death signalling in human glioma cells⁶⁹. In glioblastoma cells, TRAIL inhibitors cause an intrinsic resistance to apoptosis that may result from the low expression of caspase 8, high levels of TRAIL-R3 and TRAIL-R4, or increasing the expression of TRAIL inhibitors⁷⁰. Many cancer cell types, including glioblastoma, have been found to be resistant to the apoptotic stimuli of TRAIL. To combat this, the combination of TRAIL with small molecules has been found to potentiate its cytotoxicity through the sensitisation of TRAIL-resistant cancer cells⁷¹.

1.2.5 Human Prion protein

Over the last few decades, the prion protein has attracted much attention due to its role in neurodegenerative diseases, including transmissible spongiform encephalopathies (TSE) and Alzheimer's disease⁷². The term "prion" was introduced by Stanley B. Prusiner in 1982 to describe a small proteinaceous infectious particle which causes TSE⁷³. The prion protein has two isoforms, a normal cellular isoform (PrP^c) and an abnormal infectious isoform (PrP^{Sc}) (the superscript Sc refers to scrapie). These two isoforms share the same primary sequences but differ in their secondary

and tertiary structures⁷². The human PrP^c is encoded by the PRNP gene which is located on the short arm of chromosome 20^{74,75}. As well as PrP^c, there are two other members of the prion protein family, Doppal and Shadoo, encoded by PRND, and Shadoo/SPRN genes respectively in mammals⁷⁶. In this study, the focus will be on PrP^c because of its role in many types of cancer.

1.2.5.1 The structure of human cellular prion protein (PrP^c)

PrP^c is a cellular healthy isoform that exists in many organisms. The immature human PrP^c, as a precursor protein, consists of 253 amino acids with a molecular weight of approximately 35-36 kDa. PrP^c consists of a signalling sequence (1-22), an unstructured N-terminal domain (23-113), a hydrophobic region (113-135), a structured C-terminal domain (113-232) and GPI-anchor sequence (232-253), as shown in **Figure (1-3)**^{75,77}. PrP^c is synthesised in the rough endoplasmic reticulum (ER) and glycosylated in the Golgi apparatus where several post-translational modifications take place. It is then transferred to the plasma membrane and attaches to lipid rafts, membrane microdomains enriched in cholesterol and sphingolipids, via a GPI (glycosylphosphatidylinositol) anchor^{78,79}, although a small amount of the unglycosylated proteins remain in the cytoplasm of the cell⁸⁰. This intracellular localisation may be due to the re-translocation of PrP into the proteasome system for degradation⁸¹. PrP^c is converted from immature to mature form (208 amino acids, from 23 to 231) during protein translocation and maturation to the extracellular side of the cell membrane, where the immature PrP^c loses the signal peptides in the N- and C-terminals⁸². The median half-life of PrP^c is approximately five hours. It is then internalised to the cytoplasm through a caveola-dependent mechanism and broken down in the endolysosome compartment^{83,75}.

The signal peptide at the N-terminal guides the PrP into the ER, where it is co-translationally transported and synthesised⁸⁴. The N-terminal region consists of four octapeptide repeats that have a high affinity to copper ions,⁸⁵ implying that PrP^c could be involved in copper metabolism⁷⁵. Another study has suggested that there is a functional interaction between PrP^c and zinc ions via electrostatic interaction⁸⁶. Indeed, the formation of a Zn²⁺-PrP complex is seen in many PrP mutations of inherited prion diseases⁸⁷. The N-terminal polybasic region and octapeptide repeats in PrP^c is also believed to be involved in Zn⁺² flux in neurodegenerative diseases⁸⁸.

The hydrophobic region (~ 113-135) connecting the N and C domains is the most conserved sequence motif of PrP^c in all species known⁸⁹. A hydrophobic sequence may serve as a transmembrane domain in some isoforms of the prion protein⁷⁵ and is involved in misfolding, oligomerisation and intracellular retention of mutant PrP⁹⁰.

The C-terminal domain of PrP^c consists of three α -helices ($\alpha 1$, $\alpha 2$ and $\alpha 3$), and two short antiparallel β -strands ($\beta 1$ and $\beta 2$)⁸⁹. It connects to a single sequence for membrane attachment via a GPI-anchor^{82,77}. The $\alpha 2$ and $\alpha 3$ form the bulk of the globular domain and are covalently bridged via a disulphide bond between Cys179 and Cys214. Two N-linked glycans are also attached at 181 and 197.

The stability of the human PrP^c structure has been attributed to the salt bridges and H-bonding interactions found between $\alpha 3$ - $\alpha 1$ and $\beta 2$ - $\alpha 2$ - $\alpha 3$. These interactions drive the appropriate folding of the C-terminal domain⁸².

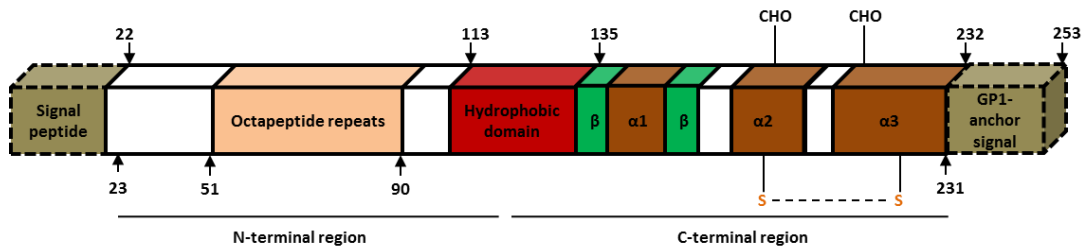


Figure (1-3): Human PrP structure (Immature PrP^c), [consists of 253 amino acids, including a signal peptide (1–22), four octapeptide repeats, a hydrophobic domain (113–135), a disulphide bond between Cys179 and Cys 214, two glycosidic bonds at positions 181 and 197 and a GPI-anchor (232 – 254)]. Adapted from Acevedo-Morantes and Wille under the Creative Commons Attributed Licence⁷⁵.

In TSE, PrP^c is converted into PrP^{Sc} (infectious isoform) via post transformational modifications⁷⁷. Although PrP^c and PrP^{Sc} have an identical primary structure, the secondary structure of PrP^{Sc} consists of β -sheet instead of α -helices. The structural details of PrP^{Sc} are very limited because this protein and its truncated variant (PrP 27-30, amino acids~ 90-231) are insoluble, resistant to protease and have a strong tendency to aggregate⁷⁵. Cryo-electron microscopy and X-ray diffraction at 19.2 Å, however, have shown that the structure of PrP^{Sc} may exist as a four-rung β -solenoid, although this result is subject to validation using higher-resolution imaging⁹¹.

1.2.5.2 The functions of prion protein

Varying levels of expression of PrP^c have been found in many human cells from different parts of the body, such as the brain, nervous system, heart, liver, kidneys and lymphoid tissue^{3,92}. Although the precise function PrP^c is not fully understood, studies have suggested its involvement in various cellular functions, including copper regulation, protection against oxidative stress, anti-apoptosis, cell signalling, proliferation and others. Some of these will be briefly described in the following sections.

1.2.5.2.1 PrP^c and copper regulation

It has been suggested that PrP^c could play a role in the metabolism of copper; that it could serve as a recycling receptor for copper ion which in turn overrates the endocytosis of PrP^c⁹³. Brown and collaborators revealed that copper binds with the octapeptide repeat region of the N-terminal in five to six positions⁹⁴, but that only two of these have higher affinity binding to copper ions⁹⁵. Such high-affinity bindings are necessary to facilitate PrP^c endocytosis via clathrin-mediated pits⁹⁶. In addition, studies of mouse neuroblastoma N2a and the human microglia C13-NJ cells have revealed that PrP^c-copper stimulates the endocytosis of PrP^c via a caveolin-dependent pathway⁹⁷. Cerebellar cells from PrP^c knockout mice contain approximately one-fifth of the copper ions of cerebellar cells in wild-type mice. This result suggested that PrP^c may play an important role in copper binding to proteins in the brain⁹⁴. Moreover, the copper concentration was reduced by nearly 50% in synaptosomal fractions isolated from PrP knockout mice compared to wild type mice⁹⁸.

1.2.5.2.2 PrP^c and oxidative stress

Many studies have reported that oxidative stress causes upregulation of PrP^c expression in many studies⁷⁶. Watt *et al.* demonstrated that PrP plays a vital role in protecting cells against DNA damage induced by reactive oxygen species (ROS)⁹⁹. PrP^c maintains oxidative stress-related homeostasis through the PrP-copper complex which upregulates superoxide dismutase (SOD)¹⁰⁰. In this regard, introducing PrP^c to PrP^{-/-} cells improves cell viability by upregulating SOD, eliminating the superoxide anion, and preventing apoptosis mediated by caspase 3/9¹⁰¹. The oxidative stress markers were significantly increased in brain lysates of PrP^c knockout mice compared to wild type mice^{102,103}. In addition, in an *in vivo* study, the octarepeat region of PrP^c plays an effective role in reducing copper neurotoxicity in hippocampal neurons¹⁰⁴.

Interference of PrP^c with manganese protects neuronal cells against Mn-induced GSH depletion, ROS generation, caspase-3 activation and DNA fragmentation¹⁰⁵. Besides, β -cleavage in the octapeptide repeat region of PrP^c is induced by oxidative stress in the presence of copper, and this cleavage produces an N2 fragment which is capable of reducing the intracellular ROS induced by serum deprivation in neuronal cells and neural stem cells (NSCs)^{106,107}. It has also been suggested that PrP^c activates the base excision repair pathway in response to oxidative stress – mediating DNA damage by interacting with AP endonuclease, an enzyme involving in the DNA base excision repair pathway¹⁰⁸.

Despite these findings concerning the role of PrP^c in oxidative stress, not all results are consistent. For instance, in *in vivo* studies by Hutter *et al.* and Steinacker *et al.* suggest that PrP^c does not contribute to SOD activity in the spinal cord, spleen or brain^{109,110}. Another study showed that N2a neuroblastoma cells were protected against oxidative stress induced by 3-morpholino synonimine hydrochloride in the presence of PrP^c, but that the protein's overexpression made N2a cells were more sensitive to hydrogen peroxide treatment¹¹¹.

1.2.5.2.3 PrP^c and Bcl-2 family proteins

It has been shown that PrP^c plays an essential role in the survival and death of cells. Bcl-2 proteins play a central role in the regulation of cell apoptosis, and the Bcl-2 homology domain 2 (BH2) is essential for the anti-apoptotic function of Bcl-2¹¹². Octapeptide repeats of PrP^c are highly conserved and share some degree of similarity to the BH2 domain of Bcl-2 proteins. PrP^c is found to promote the survival of human primary neurons cells by protecting against Bax-mediated cell death¹¹³. The binding between PrP^c and Bcl-2 was confirmed by a yeast two-hybrid system, Bcl-2 can

survive neurons from apoptosis¹¹⁴. PrP^c increased the survival of mouse neuron cells by upregulation of Bcl-2 and downregulation of Bax¹¹⁵.

Roucou *et al.*, meanwhile, used human neuron cells transfected with Bax plasmid and/or PrP plasmid to investigate the effect of PrP and Bax on apoptosis. The cells encoded with both Bax and PrP plasmid were protected from apoptosis whereas neuron cells injected with Bax plasmid only went into apoptosis¹¹⁶. Conversely, the inhibition of endogenous PrP by PrP antisense in neurons induces cell death mediated by Bax¹¹³. Studies on human primary neurons and breast cancer MCF-7 cells showed that PrP only protected cells from Bax-mediated apoptosis¹¹⁷. Since the role of PrP as an anti-apoptotic factor could be attributed to its interaction with pro-apoptotic proteins which mediated cell death, Westergard and collaborators suggested many mechanisms which may be involved in apoptosis by Bax and PrP (Figure 1-4)¹¹⁸.

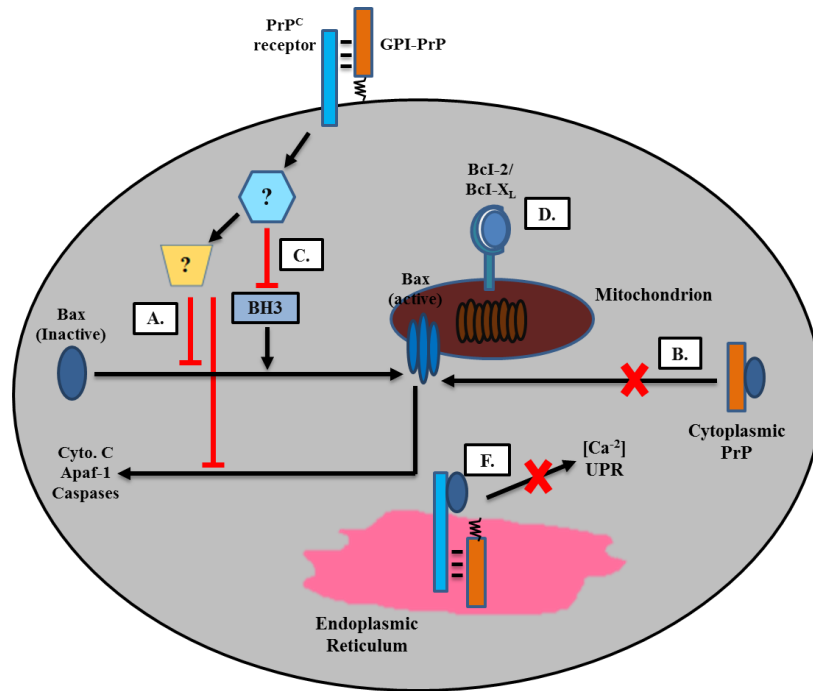


Figure (1-4): The proposed mechanism for PrP with Bax to suppression of apoptosis. The apoptosis pathways that occur under the action of Bax may be suppressed by PrP in many different ways. **A:** because of the location of PrP on the surface of the cell, it may interact with a putative transmembrane receptor and initiate a signal transduction cascade which represses Bax mitochondrial translocation, conformational change or oligomerisation. **B:** PrP in the cytoplasm may interact directly with Bax and produce similar effects. **C:** pro-apoptotic, BH3 only family may be prevented by PrP. **D:** PrP may accelerate the interaction of anti-apoptosis factors such as Bcl-xL and Bcl-2 with Bax. **E:** downstream events in the Bax activation pathway, such as cytochrome c release, activation of Apaf-1 and caspases may be inhibited via PrP. **F:** The function of Bax in the endoplasmic reticulum may be altered by PrP affecting the unfolded protein response (UPR) and intracellular calcium. Adapted from Westergard *et al.* with kind permission of Elsevier Group¹¹⁸.

Indeed, Bax-mediated apoptosis involves a sequence of events: Bax conformational change, mitochondrial translocation and cytochrome c release which finally cause cell death. Roucou and collaborators have reported that through the activation of Bax, PrP^c initially suppresses the conformational change event in breast cancer and neuronal cell lines and protects the cells against Bax-mediated apoptosis¹¹⁹. Furthermore, Westergard *et al.* mentioned that the conformational change of Bax in serum-free medium happened rapidly in PrP^{-/-} hippocampal neurons compared to cells expressing

PrP^{c118}. Another study showed that cytoplasmic PrP has minimal anti-Bax activity and is a predominant form of PrP with anti-Bax function in human neurons and MCF-7 cells¹²⁰. In addition, transfecting cytosolic PrP into neurons protected these cells from apoptosis mediated by Bax¹¹⁶. The above findings support the mechanisms **A and B** in **Figure (1-4)**.

Nevertheless, several studies have shown conflicting results regarding the effect of cytosolic PrP as an anti-Bax agent. Rambold *et al.* stated that cytosolic PrP is cytotoxic rather than cytoprotective in a number of cells¹²¹. Other studies on Chinese hamster ovary and green monkey kidney cells showed that insoluble PrP is produced in the cytosol, which is not affected by proteinase K in the same way as PrP^{Sc122,14}. Furthermore, the accumulation of even small amounts of cytosolic PrP induced neuronal toxicity and caused massive damage in cerebral granule and glial cells in transgenic mice¹²³. Overall, the interaction of PrP with Bax remains unclear.

1.2.5.2.4 PrP^c and some signalling pathways

Several studies have suggested that PrP is involved in transmembrane and intracellular signalling through interaction with signalling molecules such as Src family kinase, Fyn kinase¹²⁴, stress-inducible protein (STI1)^{125,126}, cyclic adenosine monophosphate /protein kinase A (cAMP/PKA)¹²⁷, PI3K/Akt¹²⁸ and others. Some scholars have argued that the flexible structure of the N-terminal region in PrP^c may allow it to bond directly to other proteins¹²⁹. These signalling pathways have been expected to be affected by PrP^c expression or cellular processes which are regulated by PrP^{c76}. In the neuronal differentiation model IC11, the interaction of PrP with the integral membrane protein caveolin activates P59Fyn signalling which regulates cell growth¹³⁰. The interaction of STI1 with PrP has also been shown to induce the activation of the signalling pathway via mitogen-activated protein kinase (MAPK),

which is important in the development of neuron cells¹³¹. Chiarini *et al.* showed that PrP^c-binding peptide stimulates cAMP/PKA and extracellular signal-related kinase (Erk) pathways, and partially protects cells from anisomycin-mediated apoptosis in retinas extracted from neonatal rodents¹²⁷. PrP^c expression affects the activity of both PI3K-Akt and ERK1/2 signalling pathways, which have been reported to be involved in the regulation of protein synthesis¹²⁶ and autophagy^{132,133}. The activation of the PI3K-Akt pathway by PrP^c could also explain how PrP^c affects cell proliferation¹³⁴. Chen *et al.* revealed that PrP^c increased neurite outgrowth and neuronal survival in mouse neuron cells resulting from the activation of the signal transduction pathways, PI3K/Akt, cAMP and MAPK¹¹⁵. It has also been found that PrP^c expression triggers Src family kinases Fyn /Yes and mediates cell adhesion¹³⁵.

On the other hand, the interaction of PrP^c with other proteins may be indirectly regulated by PrP^c since other signalling pathways also participate in this interaction⁷⁶. For instance, although the PI3K-Akt pathway is assumed to enhance cell proliferation¹²⁸, the expression of PrP^c may have contradictory effects on proliferation in different experimental models.

1.2.5.2.5 PrP^c and cell proliferation

Studies have revealed conflicting information about the role of PrP^c in the regulation of proliferating cells. Mice overexpressing PrP^c exhibit higher levels of cellular proliferation in the adult neurogenic region than wild type and knockout mice, but fewer proliferating cells were observed in the hippocampus of knockout mice compared to wild type and mice overexpressing PrP^c¹³⁶. Zhang *et al.* found that PrP^c supported the self-renewal of hematopoietic stem cells (HSCs)¹³⁷. Prion protein has been found to enhance the proliferation of neural stem cells (NSCs), whereas both the N1 and N2 fragments of PrP^c appear to inhibit cellular growth¹³⁸. Overexpression of

PrP^c has also been shown to increase cell proliferation in mouse neuroblastoma cells N2a¹³⁴, the LS 174T colon adenocarcinoma cell line¹³⁹ and cancer stem cells derived from GBM¹⁴⁰. In contrast, the absence of PrP^c increased the proliferation of undifferentiated oligodendrocyte cells¹⁴¹. Moreover, Kim *et al.* showed that PrP-deficient embryonic hippocampus cells exhibited a high proliferation¹⁴². PrP^c also decreased the proliferation rate of intestinal epithelial cells and has a dual function in the regulation of polarisation and proliferation of these cells¹⁴³. As can be seen, the effects of PrP^c on cell proliferation depends on the type of cells.

1.2.5.3 Prion protein and cancers

Several lines of research have demonstrated that PrP^c may be implicated in cancers. While PrP^c appears to contribute to different functions of the cell, such as proliferation, differentiation, adhesion, migration, ion homeostasis, anti-apoptosis and transduction of the signal its exact function in cancer is unclear³. Various studies have observed PrP^c upregulation in different types of cancers (breast¹⁴⁴, colorectal¹⁴⁵, gastric¹⁴⁶, glioblastoma¹⁴⁷, pancreatic ductal adenocarcinoma¹⁴⁸, and osteosarcoma¹⁴⁹). It has been found that knocking out of PrP^c in cancer cells effectively inhibits the growth of cancer cells while, conversely, the overexpression of PrP^c enhances cell survival and/or proliferation¹⁴⁶. The following sections will focus on the suggested roles of PrP^c in different types of cancer.

1.2.5.3.1 PrP^c and breast cancer

Over the last decade, the role of PrP^c in breast cancer has been evaluated and elucidated³. Dery *et al.* revealed that endoplasmic reticulum stress positively regulates the level of PrP mRNA in MCF-7 cells. A positive correlation has also been seen between BiP mRNA and PrP mRNA levels in breast cancer cell lines and tissue¹⁵⁰. Another study found that PrP^c has different expression levels in breast carcinoma cell

lines. The TNF-resistant1001 cell line expressed the PRNP gene seventeen times higher than the TNF-sensitive MCF7 cell line, and this appeared to revert TNF-sensitivity to resistance in these cells¹⁵¹.

Meslin *et al.* examined the relationship between PrP^c and TRAIL using breast cancer cell lines TRAIL-sensitive MCF-7, MCF-7/ADR (resistance to Adriamycin, ADR), and 2101 (resistance to TRAIL). They found that the PrP^c expression increased in both the resistant cell lines. TRAIL induced apoptosis when PrP^c was knocked down in these cells through caspases, Bid cleavage, Mcl-1 degradation, but not through TRAIL receptors. They also found that while knockdown PrP^c reduced the Bcl-2 level, the Bcl-XL and Mcl-1 levels were not affected¹⁵².

Additionally, PrP^c in MCF7/ADR cells interacts with P-glycoprotein (P-gp) to form PrP^c/P-gp complex and this initiates the motility in these cells. Silencing PrP^c or blocking P-gp inhibits paclitaxel (P-gp substrate), inducing the migration *in vitro*. Furthermore, inhibition of the PrP^c/P-gp complex induces cell apoptosis¹⁵³. Using by tissue microarray, analysis of samples from 756 breast cancer patients revealed a negative relationship between PrP^c expression and sensitivity to adjuvant chemotherapy. This study showed that higher PrP^c expression is associated with ER-negative breast cancer subsets, and these ER-negative/PrP^c-positive patients were less susceptible to adjuvant chemotherapy than ER-negative/PrP^c-negative patients¹⁵⁴. In another study, researchers reported the overexpression of PrP^c and CD44 (cell surface adhesion receptor) in MCF-7/ADR cells. When PrP^c or CD44 were inhibited Several cell functions were suppressed, such as migration, invasion and proliferation. In addition, in human breast cancer tissue, the interaction of PrP^c and CD44 was found in the post-neoadjuvant-chemotherapy patients¹⁵⁵.

On the other hand, Yu *et al.* revealed that the knockdown of PrP^c expression in MDA-MB-435 breast cancer cells increased the cell death induced by serum deprivation medium and induced the resistance to doxorubicin and DNA-interacting chemotherapy drugs. Moreover, they found that silencing PrP^c had no significant effect on cell proliferation and colony formation⁸.

1.2.5.3.2 PrP^c and colorectal cancer

PrP^c has been shown to play a role in the function of the cytoskeleton in epithelial cells. It interacts with cytoskeleton-associated proteins and some intracellular proteins such as spectrin, desmoglein 2, in Caco-2/TC7 (Colon adenocarcinoma cells). This interaction improves the cell-cell adhesion and proliferation and is necessary for cell polarisation and differentiation¹⁴³. Furthermore, the knockdown of PrP^c inhibits the proliferation and survival rate in DLD-1 and SW480 colorectal cancer cells by disrupting the Fyn-HIF-2 α pathway and downregulating glucose transporter 1 (Glut1). In addition, the injection of PRNP shRNA in mice reduced the growth of colorectal tumour¹⁵⁶. Wit *et al.* showed that both Glut1 and PrP^c are increased through the progression of adenoma to carcinoma. Thus, they suggested that Glut1 and PrP^c could be used as biomarkers to monitor the progression of malignant tumour in colon cancer¹⁵⁷.

In tissue samples from colorectal cancer patients, the PRNP gene was upregulated in relapsed patients compared to non-relapsed patients. Moreover, PRNP expression was an independent prognostic factor for three-year survival in colorectal carcinoma patients¹⁵⁸. Importantly, PrP^c antibodies decreased the growth of HCT116 colon cancer cells and improved the activity of cancer treatments such as 5-FU, cisplatin, doxorubicin and irinotecan as well as reducing tumour growth *in vivo*^{157,3}. Wang *et al.* revealed that PrP^c expression increased the motility of the colorectal carcinoma cell

line SW480 whereas knockdown of PrP^c in primary human colon adenocarcinoma LIM2405 cells inhibited cell migration. Within the same study, inhibition of PrP^c reduced the metastasis *in vivo*¹⁵⁹.

1.2.5.3.3 PrP and pancreatic ductal adenocarcinoma (PDAC)

Han *et al.* were the first to evaluate the gene expression level of PrP in different pancreatic ductal adenocarcinoma (PDAC) cell lines growing in tissue. Using cDNA microarray analysis, they found that PrP mRNA was upregulated in these cells¹⁶⁰. Another study showed that PrP expression is a marker in different groups of patients with PDAC¹⁴⁸. PrP was expressed, at varying levels, in seven PDAC cell lines¹⁶¹. Indeed, the PrP in cell lines of this cancer exists as pro-PrP (PrP retaining its GPI-PSS)^{161,162}. Li *et al.* demonstrated that pro-PrP GPI-PSS binds to FLNa, an actin-binding protein that participates in the anchoring of membrane proteins and cell signalling. The knockdown of PrP expression disrupted protein-signalling and cytoskeletal organisation. It also decreased the proliferation and migration of PDAC cells as well as the development of tumours *in vivo*¹⁶¹. A recent study by Yang *et al.* also showed that knockout of the PRNP gene in BxPC-3 and PDAC cells inhibited cell migration. They found that multiple gene irregularities in these cells contribute to the formation of pro-PrP, and the binding of FLNa to pro-PrP increased cell migration ability¹⁶².

1.2.5.3.4 PrP and gastric cancer

PrP^c is highly expressed in the gastric mucosa of patients with *Helicobacter pylori* infection¹⁶³. This upregulation may result from hypergastrinemia, a high level of interleukin 1 beta-synthase and increasing prostaglandin E2¹⁶⁴. *Helicobacter pylori* can cause gastric cancer¹⁶⁵ and PrP^c expression was detected in both non-cancerous

and malignant gastric tissues¹⁶⁶. Zhao *et al.* identified that the PRNP gene was one of the upregulated genes in SGC 7901/ADR cells and ADR resistant gastric adenocarcinoma cell line SGC7901, using a PCR-based subtractive hybridisation technique¹⁶⁷.

PrP^c was more highly expressed in SGC7901/ADR (resistant to ADR) cells than SGC7901 cells (sensitive to ADR). The PrP^c overexpression in SGC7901 cells increased the resistance to P-glycoprotein (P-gp)-related drugs, whereas inhibition of P-gp could partially reduce PrP^c-mediated multidrug resistance (MDR) and induce apoptosis. PrP^c also inhibits ADR-mediated apoptosis by increasing Bcl-2 and suppressing Bax expression in gastric cancer cells¹⁶⁸. Additionally, the overexpression of PrP^c in the gastric cancer cells SGC7901 and AGS increased migration and proliferation via activation of PI3K/Akt and promoting G1/S transition by upregulation of Cyclin D1¹⁶⁹. Liang and collaborators suggested that the PI3K/Akt pathway is implicated in PrP^c-induced MDR (ADR and VCR, vincristine) in gastric adenocarcinoma cells and that inhibition of this pathway reduced the resistance exhibited in MDR-gastric cancer cells and decreased the level of P-gp¹⁷⁰. Within the same research group, one octapeptide repeat deletion (1-OPRD) of PrP^c was found in several types of gastric cancer cells. When cells were transfected with PrP^c or PrP^c (1-OPRD) there was the same effect on MDR, cell invasiveness, adhesion or apoptosis but cell proliferation was mainly influenced by PrP^c (1-OPRD) compared to PrP^c due to the activation Cyclin 3 and Cyclin 1¹⁷¹.

It has been shown that PrP^c is overexpressed in the tissue samples of patients with metastatic gastric cancers. PrP^c also promoted cancer metastasis in mice transfected by gastric cancer cell lines. These findings could be attributed to the role of the OPR-containing N terminal domain of PrP^c which induces the invasiveness and metastasis

processes in gastric cancer cells¹⁷². Overall, these studies suggest that PrP^c and MGr1-Ag/37LRP (upregulated protein in gastric cancer drug-resistant cells) may be considered as biomarkers for poor prognostics and chemoresistance in gastric cancer^{173,174}.

1.2.5.3.5 PrP and other types of cancers

The PrP^c expression level in normal skin cells is very low. When the skin is inflamed, however, PrP^c is strongly expressed in keratinocyte and infiltrating mononuclear cells¹⁷⁵. Although the PrP^c is not detected in normal melanocytes, it is overexpressed in melanoma cells. In addition, an *in vitro* study showed that the PrP in M2 and A7 melanoma cells is pro-PrP, which binds with FLNa in A7 cell lines. This binding significantly induces the migration of A7 cells. Inhibition of PrP significantly reduces the migration and invasion of A7 cells, however¹⁷⁶.

In prostate cancer, overexpression of PrP^c is found in prostate spheroids that are associated with ROS and the size of tumour spheroids¹⁷⁷. High levels of expression of PrP^c have been identified in biopsies of prostate tumours, hepatic cancer and oral squamous cell carcinoma³. Another study has shown that PRNP is involved in osteosarcomas. In addition, the expression of this gene was upregulated in human osteosarcoma¹⁴⁹. Conti *et al.* reported that PrP^c was detected in soft tissue sarcomas and it could be one of the novel biomarkers of this cancer. It was one of 16 proteins significantly increased in metastatic sera compared to non-metastatic sera¹⁷⁸. A substantial body of evidence, therefore, supports the involvement of PrP^c in various cancers.

1.2.5.3.6 PrP^c and Glioblastoma

Various studies have shown that PrP^c is involved in astrocytoma and interacts with certain signalling pathways that contribute to multiple cellular functions. Comincini and co-workers evaluated the expression of the PRNP gene in astrocytomas, finding that PRNP is highly expressed in all tumour samples and astrocytoma cells⁵. In T89G glioblastoma cells, Kikuchi *et al.* found that the expression of PrP^c may be associated with the G1 phase of the cell cycle. The amount of PrP^c expression depends on the period of cell culture (in a time-dependent manner) with the protein level on Day 16 being higher than that on Day 4 by about two fold¹⁷⁹.

Lopes *et al.* identified STI1 or protein as a cell surface ligand of PrP^c that activates several signal transduction pathways, some of which modulate the proliferation and cell death of neurons¹⁸⁰. STI1 promotes the proliferation of the glioblastoma cell line A172 through the activation of Erk and PI3K pathways and does not affect normal astrocytes. The binding of PrP^c with STI1 may induce the proliferation of these cells¹⁸¹. Further study has demonstrated that both HOP (Hsp70-Hsp90 complex) and PrP^c are strongly expressed and that this positively correlates with high proliferation and low survival of glioblastoma patients compared to other astrocytoma grades or normal tissue samples. HOP interacts with PrP^c to increase the proliferation of GBM cells (U87 and U251) by activating the PI3K and Erk pathways. Inhibition of this binding, on the other hand, reduces the proliferation of GBM cells. Silencing PrP^c decreases tumour growth and promotes the survival of mice with GBM⁴. In this context, PrP^c and HOP are co-localised and highly expressed in glioblastoma stem-like cells (GSC). Proliferation and self-renewal of GSC cells appear to be affected by disruption to the binding of PrP^c with HOP: for example, exogenous HOP treatment (recombinant) induces the proliferation and self-renewal of GSC, depending on the

PrP^c level, whereas inhibition of HOP reduces the proliferation of these cells. Importantly, knockdown of PrP^c impairs cell migration and reduces cell adhesion, which confirms the important function of PrP^c on the cell surface¹⁸². In addition, the proliferation and migration of GBM95 glioblastoma cells have been shown to increase when cultured in microglia conditioned medium, due to the secretion STII by microglia cells. Remarkably, the anti-PrP^c antibody does not affect the proliferation of GBM95 cells with or without microglia conditioned medium¹⁸³.

Barbieri *et al.* studied the effect of PrP^c on the cell death of glioblastoma *in vitro* and *in vivo*. The results showed that silencing PrP^c using the antisense of the PRNP gene in T98G human glioblastoma cells induced autophagy by promoting LC3-II, Beclin 1 expressions and Bcl-2 downregulation. Silencing PrP^c also reduced the size of the tumour in male mice¹⁸⁴. In another study, knockdown of PrP^c in J889 human glioblastoma cells reduced cell growth and induced apoptosis by elevating caspase 3 activity¹⁸⁵.

Zhuang and co-workers showed that PrP^c is upregulated in the G2/M cell phase in glioblastoma cells U87 and U251 treated with TMZ and that this could induce the resistance to TMZ. On the contrary, cells in phase G1/S displayed a lower level of PrP^c and the sensitivity to TMZ was promoted. Additionally, a flow cytometry assay showed a high rate of apoptosis in TMZ treated G1/S cells compared to G2/M cells⁶. The specific pro-apoptotic effector domain in cancers (SAC) has been identified in many cancer cells¹⁸⁶. In cells treated with TMZ, PrP^c interacts with Par4 (response of prostate apoptosis 4) via SAC. This interaction induces an anti-apoptotic effect by preventing protein kinase A-mediated Par4 phosphorylation and then reducing cell death⁶.

1.2.6 Chemotherapeutics for GBM

Clinical treatments for GBM face many difficulties due to the resistance of tumour cells, the hypersensitivity of brain tissues, the limited ability of brain cells to self-repair and the permeability of drugs across the brain blood barrier¹⁸⁷. Currently, the standard therapy for GBM patients is surgery followed by radiation and chemotherapy¹⁸⁸. Alkylating agents, such as TMZ and BCNU, are the main treatments for malignant brain tumours, but while these have the ability to damage the DNA and promote cell death, the cytotoxic effects of these treatments are associated with the pathways of DNA repair¹⁸⁹.

The chemistry of TMZ as a prodrug is similar to imidazotetrazine compounds. TMZ is reduced in an alkaline or neutral medium to produce triazene methyltriazenoimidazole carboxamide (MTIC), which is then converted to 5-aminoimidazole-4-carboxamide (AIC) and a methyldiazonium ion. The methyldiazonium ion is attacked by the nucleophile on DNA to form methylated DNA, preventing DNA replication and thereby triggering apoptosis (Figure 1-5). The majority of methylations can occur either on guanine-N7 or guanine-N3 site, accounting for 70% and 9% respectively. These N-methylations have no therapeutic value because the lesions are successfully treated with basic excision repair enzymes. The methylation that occurs in guanine-O6 (5%), however, confers the activity of TMZ towards cancer cells¹⁹⁰.

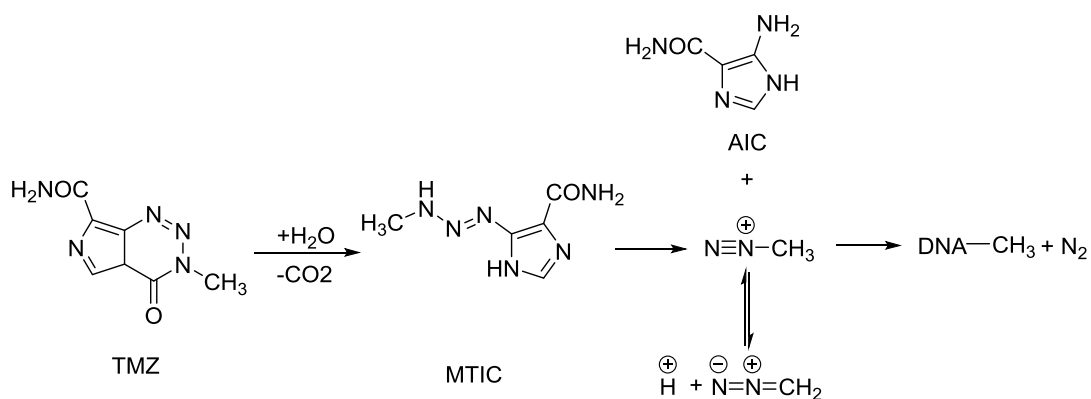


Figure (1-5): The mechanism of TMZ action

The mechanism of action for the chloroethylating agent BCNU involves multiple steps. The first step is to chloroethylate the guanine in DNA (step 1 Figure 1-6), followed by a rearrangement step (step 2 Figure 1-6). Later, the C-O bond is cleaved and the methyl group either attacks the amino group of cytosine (step 3 Figure 1-6) to form DNA interstrand cross-link or is transferred to cysteine through the MGMT enzyme irreversibly to form a DNA-MGMT complex^{191,192}.

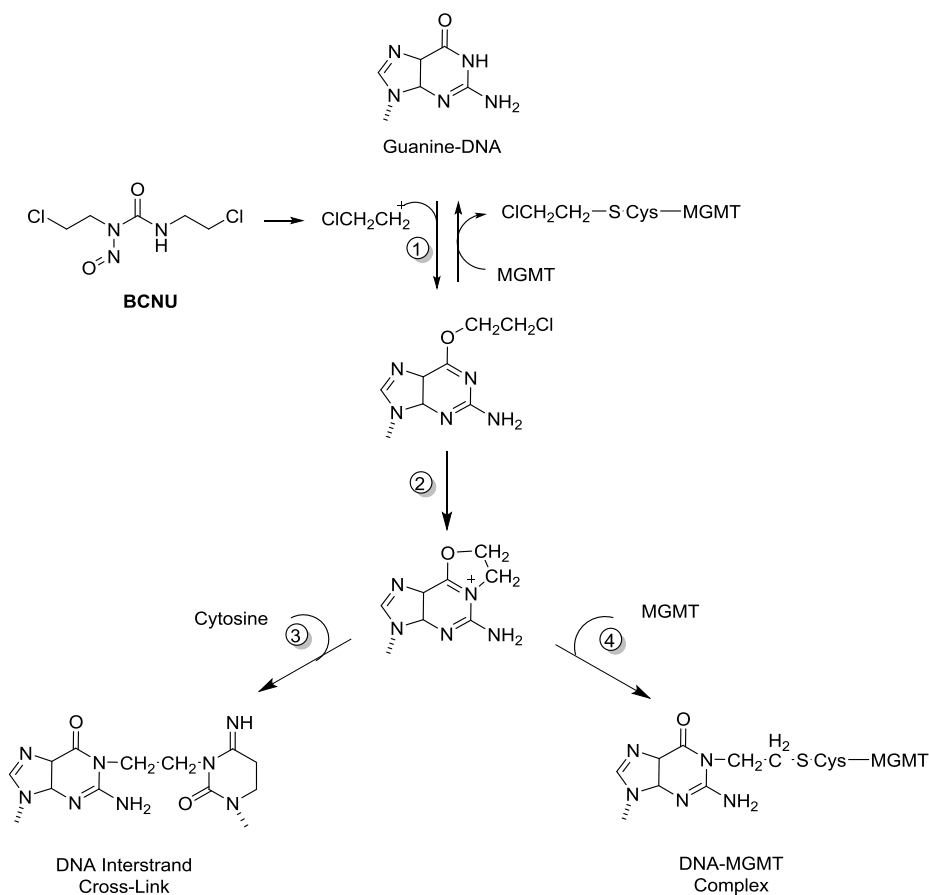


Figure (1-6): The mechanism of BCNU action¹⁹¹

According to clinical studies, TMZ in combination with radiotherapy is the cornerstone of treatment for glioblastoma patients when compared with radiotherapy alone, with survival rates of 14.6 months and 12.1 months respectively^{193,194}. That said, resistance to TMZ is a major issue. O6-methylguanine DNA methyltransferase enzyme (MGMT) reduces the efficacy of TMZ by eliminating the damage wrought by the drug on the methyl groups within cell DNA¹⁹⁵. Inhibition of the MGMT gene increases the response to the alkylating agent and extends the survival time, however^{196,197}. Moreover, it has been shown that the activity of MGMT is diminished in peripheral mononuclear cells by TMZ, depending on the duration of treatment. In a clinical study, inhibition of the MGMT gene improves the survival time by approximately a further 6.2 months through increasing the activity of TMZ¹⁹⁸. The

efficiency of TMZ might also depend on MGMT expression in stem-like cancer cells in GBM since it has been shown that GBM cancer stem cells that express MGMT show no response to TMZ while those without MGMT expression are completely eliminated by TMZ¹⁹⁹.

In spite of the activity of the TMZ-radiotherapy combination in glioblastoma patients, the resistance of tumour cells, poor prognosis and limitations of treatment after recurrent malignancy have promoted researchers to look for different approaches to develop an alternative treatment. Different strategies have been followed to this end, including inhibition of the receptor tyrosine kinases, development of alternative drugs (e.g. etoposide, irinotecan and cisplatin), modifications of treatment delivery (such as BCNU wafers), increasing drug sensitivity by repression of MGMT, using gene therapy or improving immune techniques²⁰⁰.

Expression of the eukaryotic elongation factor-2 kinase (EEF2K) reduces the efficacy of TMZ treatment in glioma cell lines and silencing of this protein increases the sensitivity of cells toward TMZ. The apoptosis which is mediated by alkylating agents is promoted further by inhibiting EEF2K. These findings have also been confirmed *in vivo*²⁰¹. Moreover, it has been shown that p53 plays a significant role in chemotherapy resistance. Inhibition of p53 in U87 glioblastoma cell lines via the small molecule pifithrin- α also induces sensitivity to TMZ and BCNU treatments²⁰². Based on studies in xenograft cells, it has been reported that reduced levels of MGMT lead to an improved response to BCNU and decreased cell growth rates. O⁶-benzylguanine inhibits MGMT⁺ cells for about six hours and increases the sensitivity of these cells to BCNU therapy. The sensitivity of cells to alkylating chemotherapy depends on O⁶-methylguanine deletion, however, and this is mediated by MGMT¹⁸⁹. Xu *et al.*

discovered that the inhibition of CD44 receptor reduces tumour growth and improves the sensitivity of chemotherapeutics such as BCNU and TMZ in GBM patients²⁰³.

A BCNU wafer is a localised therapy that has the advantage of being able to bypass the blood-brain barrier to address the malignant tissue directly. The toxic effect that results from this treatment is decreased compared to other chemotherapeutic regimens²⁰⁴, and this localised BCNU wafer followed by TMZ treatment exhibits a better survival rate in some GBM patients²⁰⁵.

1.2.7 GBM disease models

In order to study cancer biology, disease aetiology and facilitate drug discovery, various models have been developed²⁰⁶. For GBM in particular, disease models can be classified into two main groups in preclinical *in vivo* and *in vitro* models. Current preclinical *in vivo* models are divided into two classes: syngeneic mouse GBM and xenografts. The establishment of syngeneic models are either by development the native glioblastoma cell lines via exposure to a certain risk factors such as radiation or chemical insult, or spontaneously through the genetic engineering to reproduce the tumour. Xenografts model are subdivided into two categories, including GBM cell-line xenografts and patient-derived tissue xenografts²⁰⁷. GBM cell-line xenografts have high growth rate, but drawback includes that it possibly does not retain the histological feature of glioblastoma cells. The patient-derived xenografts are more efficient models because they retain the biological and genetic features of primary tumour²⁰⁸.

In vitro culture models have been widely established for GBM research since the isolation and immortalization of cell lines were achieved. GBM is a fast-growing and the most aggressive primary malignant brain tumour. Of all the primary malignant

cancers, percentage of GBM patients is relatively small (1.35 % in the US)²⁰⁹. Hence, access primary cell to study this disease is limited, not to mention obtaining samples from the brain is fraught with difficulties and is usually not an option. Forty eight human glioblastoma cell lines have been developed and available from biobank²¹⁰. **Table (1-1)** shows the commonly GBM cells used in research. U87 cell line is the most commonly used as a model cell line to study GBM and provided valuable knowledge in brain cancer research. Over the last three decades, U87 has the highest PubMed citation (more than 1900) compare to other commonly used glioblastoma cell models, U251 (more than 1100 citations) and T98G (more than 900 citations)²¹⁰.

Table (1-1): Commonly used cell lines in GBM studies, the information provided by ATCC and European Collection of Authenticated Cell Culture (ECACC).

Name of the cell line	The origin	Morphology
U87	Human brain-Male	Epithelial
U251	Human brain-Male	Astrocytoid
T98G	Human brain-Male	Fibroblast
A172	Human brain-Male	Unknown
U138	Human brain-Male	Polygonal
U118	Human brain-Male	Mixed
LN-18	Human brain-Male	Epithelial
LN-229	Human brain-Female	Epithelial
U373	Human brain	Astrocytoid

Uppsala 87 Malignant Glioma (U87-GM) or U87 is non-neuronal glial brain tumour cell line²⁰⁹. The male cell line has an epithelial morphology and was obtained from a patient of unknown age in 1966 in Uppsala University²¹¹. The currently available version of U78 is from the American Type Culture Collection (ATCC- HTB-14). It was reported as a grade IV glioma cell line derived from a 44-year old male caucasian

patient diagnosed with glioblastoma. The exact nature was reported by Allen *et al*, 2016 from Uppsala University to be different from previous U87 glioblastoma cell lines used in their study²¹¹. In addition to that, ATCC in 2016 updated U87 as unknown age and likely glioblastoma. The genome of this cell line has been sequenced and found that 60 genes are mutated in the U87 cell line and are located in regions that are commonly deleted in GBMs²⁰⁹. U87 cell line has previously been used in many *in vitro* studies to investigate the involvement of prion protein in many processes such as apoptosis and proliferation of GBM^{4,184,212}. Furthermore, previous work in the group used U87 cells in the screening of novel small molecules inhibitors for the FA pathway in search for sensitising agents for chemotherapies of GBM, TMZ and BCNU. Besides, most researchers rely on publicly available cell lines²¹¹. U87MG appears to be a more representative GBM cell line than others because its genomic features are a large number of chromosomal abnormalities, that can be typical of cancer cell lines and primary cancers²¹³. Therefore, in the current study U87 cells were selected to investigate the role of PrP^c in GBM upon the treatment with TMZ and BCNU and identify the FAPi discovered in the previous work would have any impact on PrP^c pathway.

1.2.8 Thesis aim and objectives

PrP^c expression is implicated in many cancers, including GBM. Although the role of PrP^c expression has been investigated in glioblastoma cells, the effect of GMB chemotherapeutic agents (i.e both TMZ and BCNU) on PrP^c expression has not been studied in depth. In addition, PrP^c expression level may influence on the proliferation of U87 cells and their resistance to alkylating agents. The main aim of this thesis was, therefore, to investigate the level of PrP^c expression in glioblastoma cell line U87 treated with alkylating agents TMZ and BCNU and the effects of some small

molecules on its level. In addition, the effect of a collection of potential anticancer novel small molecules (30 compounds) on U87 were evaluated. To achieve these aims, the following tasks were addressed:

- Since the level of PrP^c expression has been suggested to be affected in different cell cycle phases, PRNP and PrP^c expressions in U87 cells treated with TMZ or BCNU were evaluated across the cell cycle. The following experiments were performed (Chapter 3).
 - Cell cycle analysis was used for U87 cells treated with cell cycle modulators, Aphidicolin and Nocadazole, that are known to arrest the cells in G1 and G2/M after 24h respectively. Additionally, U87 cells were treated with alkylating agents TMZ and BCNU, and the cell cycle was analysed at different time points using flow cytometry.
 - The regulators of the cell cycle, p53 and p21, were assessed to confirm the arrest at G2/M in response to alkylating agents.
 - The PRNP gene and PrP^c protein expression levels in U87 treated with Aphidicolin, Nocodazole, TMZ or BCNU were evaluated using qPCR (for gene level), flow cytometry and western blot (for protein level).
 - The cell morphology of treated U87 cells was investigated using actin filament staining.
- PrP^c may play a role in the resistance to alkylating agents demonstrated by U87 cells. We speculated that silencing the PRNP gene may affect the proliferation of U87 cells, whether treated or untreated with alkylating agents. To investigate this speculation the following objectives were carried out (Chapter 4).
 - Knockdown of the PRNP gene in U87 cells using PRNP siRNA.

- Evaluation of the knockdown level using qPCR, flow cytometry, western blot and immunocytochemistry (ICC).
- Assessment of the effect of PRNP knockdown on cell proliferation using MTT and Alamar blue assay. Besides, the proliferation marker ki67 was quantified using ICC.
- Evaluation of the proliferation of knockdown cells treated with TMZ or BCNU using MTT assay.
- Estimation of the cell cycle phases and regulatory cell cycle proteins, p53 and p21, in knockdown U87 cells treated with alkylating agents.
- Proteasome inhibitor MG132 decreases the degradation of PrP^c in some neuron cells. It also promotes apoptosis in various cancer cells, including glioblastoma cells, as reviewed in the relevant chapter ([chapter 5, section 5.1](#)). It is assumed that proteasome inhibitor, MG132 could reduce the degradation of PrP^c, hence increase the protein level in U87 cells. Furthermore, we expected that the combination of MG132 with TMZ may promote the apoptosis of U87 cells. Thus, the following steps were performed to test these speculations. (Chapter 5)
 - Evaluation of cell viability in U87 cells treated with MG132 and calculation of the IC₅₀ using MTT assay.
 - Assessment of the PrP^c expression level in the U87 cells treated with MG132 using flow cytometry western blot and ICC.
 - Evaluation of cell proliferation and apoptosis in cells treated with MG132 and MG132/TMZ combination MTT and annexin V with PI assays, respectively.
 - Estimation of cell cycle phase and the level of p53 and p21 in U87 cells treated with MG132 or MG132/TMZ combination using flow cytometry and western blot assays, respectively.

- Many novel compounds (benzimidazole derivatives) were screened to assess the level of PrP^c expression in U87 cells. These compounds have been synthesised in previous work by this research group (Drs. Matthew Sellwood and Peng Hua) and have been shown to have the ability to inhibit the FA pathway by reducing FANCD2, the key part of FA pathway. These compounds may have a potential to decrease the level of PrP^c expression in U87 cells due to their ability to bind PrP^c. We, therefore, hypothesised that these molecules may affect the PrP^c pathway. To test our hypothesis the following experiments were performed (Chapter 6).
 - Investigation of the effect of these molecules on cell viability in combination with TMZ or BCNU using MTT assay.
 - ICC by ImageXpress Micro as a high content screening assay was used to evaluate the level of PrP^c expression in treated cells with and without TMZ or BCNU combination.
- In a further study, the efficacy of a collection of potential anticancer small molecules (30 compounds) on U87 was evaluated. These compounds were synthesised in previous work by this group. Due to the cytotoxic effect of these compounds on the NT2 stem cells, we expected that these compounds may promote cell death of U87 cells. To address this expectation, the following experiments were carried out (Chapter7).
 - Evaluation of cell viability in U87 cells treated with these compounds using MTT assay.
 - Assessment of the apoptosis in U87 cells treated with these molecules using Annexin V with PI.

- Evaluation of cell cycle phases and the level of p53 and p21 in cells treated with the compound/s that induced apoptosis using flow cytometry and western blot assays, respectively.
- Evaluation of the effect of the compound/s that induced apoptosis on the level of PrP^C expression to determine whether this increases or reduces the level of this protein.

Chapter 2: Materials and Methods

2.1 Materials

2.1.1 Reagents and Chemicals

The reagents and chemicals used in this thesis are detailed in the following table.

Table (2-1): List of chemicals and reagents

Experiment	Chemical /reagent	Source
Cell culture	Fetal Bovine Serum	ThermoFisher
	Non-Essential Amino Acid	Sigma Aldrich
	HBSS (1X)	ThermoFisher
	Trypsin- 0.25 EDTA	ThermoFisher
Cell viability (MTT)	Isopropanol	Sigma Aldrich
	HCl	VWR
	MTT (thiazolyl blue tetrazolium bromide)	Sigma Aldrich
Protein determination	Bradford reagent	Sigma Aldrich
Western blot	Tris-glycine-SDS buffer (10X)	SLS
	Tris-glycine buffer (10X)	SLS
	Colour plus protein marker	Bio-Rad
	Tween 20	Sigma Aldrich
	Milk powder	Sigma Aldrich
	BSA	Sigma Aldrich
	Methanol	Sigma Aldrich
	3F4 anti-prion antibody	BioLegend
	p21 primary antibody	Santa Cruz
	p53 primary antibody	Santa Cruz
	Goat anti-mouse IgG antibody	Insight Biotechnology
	Anti-beta-actin antibody	New England Biolabs
	Goat anti-rabbit IgG antibody	Insight Biotechnology
	ECL solutions	Geneflow

Cell cycle	PI/RNase Staining	ThermoFisher
	Ethanol	VWR
FACS (protein expression)	Tris-base	Fisher
	Sodium Chloride	Fisher
	Hydrochloric acid	VWR
	Sodium azide	Sigma Aldrich
	4% Paraformaldehyde	Alfa Aesar
	8H4 anti-prion antibody	Sigma Aldrich
	Goat anti-mouse IgG -FITC	Santa Cruz
	Donkey anti-mouse IgG Alexa 488	ThermoFisher
	Mouse mAb IgG Isotype control	Cell Signaling
Treatments	DMSO	Sigma Aldrich
	Aphidicolin	Alfa-Aesar
	Nocodazole	Sigma Aldrich
	TMZ	Sigma Aldrich
	BCNU	Sigma Aldrich
	MG132	Sigma Aldrich
Confocal microscopy	Ki67 primary antibody	BD Pharm
Alamar blue assay	Resazurin Sodium Salt	Sigma Aldrich
siRNA Transfection	On-Target plus Human PRNP	Dharmacon
	On-Target plus Non targeting	Dharmacon
	DharmaFECT Transfection Reagent	Dharmacon
	5X siRNA Buffer	Dharmacon
	RNase-free Water	Dharmacon

2.1.2 Equipment and Apparatus

In the following table, the equipment and apparatus used in the thesis are listed.

Table (2-2): List of the equipment and apparatus

Equipment/ Apparatus	Source
Plate reader	BIO-TEK
Minicentrifuge	Eppendorf
Centrifuge 5810	Eppendorf
Incubator	NUAIRE
Fume hood	Labcaire
Water bath	VWR
Dry bath	Grant
Nano drop	Thermo scientific
Roller mixer	Stuart scientific
Flow cytometry (LSRII)	BD Biosciences
ImageXpress Micro	Molecular Devices
Hemocytometer	Sigma Aldrich
Microscop	Olympus
Mx3005P qPCR System	Agilent Technologies
Balance	METTLER TOLEDO
LEICA SP5 microscope	Leica
Micropipette	Eppendorf
PVDF membrane (western blot)	ThermoFisher
Filter paper (western blot)	Bio-Rad
Precast gels	Bio-Rad
Transparencies	USA
Glass slide, size 25 mm × 75 mm	Sigma Aldrich
Coverslips	Sigma Aldrich

2.1.3 Experimental Kits

The commercial kits which were used in this study, are listed in the following table.

Table (2-3): List of commercial kits

Kit	Source
PureLink® RNA Mini Kit	Invitrogen
AMV First Strand cDNA synthesis	BioLabs
PowerUp Sybr Green Master Mix	Applied Biosystems
PureLink® DNase Set	Invitrogen
FITC Annexin V Apoptosis Detection Kit with PI	BioLegend
Pierce LDH Cytotoxicity Assay Kit	Thermo scientific

2.2 Methods

2.2.1 Cell line and cell culture

2.2.1.1 Cell line

The cell culture-based experiments detailed throughout the thesis was performed using a glioblastoma cell line, U87. This cell line was kindly donated by Dr. Spencer Collis, University of Sheffield, Medical School.

2.2.1.2 Thawing cells

Upon retrieval from vapour-phase liquid nitrogen storage, the cryovial was placed immediately in a 37 °C water bath to rapidly thaw cells. After a sterile wipe with 70% ethanol, the contents of the vial were then transferred into a 15 ml centrifuge tube with warm culture medium. The tube was spun down at 1000 rpm for 5 minutes. After the supernatant was discarded, the cells were mixed well by pipetting with 10 ml of fresh medium and transferred into a T75 flask. The flask was incubated at 37 °C in the incubator. The medium was changed after 24 hours.

2.2.1.3 Cell culture medium

Dulbecco's modified eagles medium (DMEM) containing 4.5 g/L glucose, L-glutamine (DMEM, D5796; 500ml; Lonza) and further supplemented with 10% of Fetal Bovine Serum (FBS) and 1% Non-Essential Amino Acid (NEAA) was used to culture the U87 cell line. The medium was stored at 4 °C and warmed to 37 °C in a water bath for at least 30 minutes prior to any experimentation.

2.2.1.4 Cell subculturing

The cells were split every 3-4 days using a T75 flask when the cells reached 70-80% confluence. The cells were washed with PBS (phosphate buffer saline) or HBSS (Hank's Balanced Salt Solution, 1X, thermoFisher) and then detached using 1 ml trypsin (Trypsin- 0.25 EDTA), following 1-2 minutes incubation at 37 °C and 5% CO₂. Nine ml of fresh warm medium was then added into the cells. After the cells were resuspended with a fresh medium by pipetting, 1-2 ml of cell suspension was transferred to a new T75 flask labelled with the number of cell passage and date. An appropriate amount of fresh medium (9 -10 ml) was then added to the flask and finally incubated in the humid incubator.

2.2.1.5 Freezing of cells

Once the cells were 70-80% confluent, they were detached from the flask by trypsinisation and re-suspended in a warm medium. The cells were counted and then spun down at 1000 rpm for 5 minutes. The supernatant was removed and the cells were resuspended with an appropriate volume of cryomedium (10% DMSO and 90% fresh medium). $1-2 \times 10^6$ cells/ml were transferred into the cryovial that was labelled correctly with cell types, the number of passage, initial person's name and date. The cryovial was placed in Mr Frosty freezing container to achieve a -1 °C every minute.

The container was then transferred into -80 °C freezer overnight and for the long-term storage, the vials were placed in the vapor phase of liquid nitrogen.

2.2.2 Cells Viability assay (MTT)

MTT (3-[4,5-dimethylthiazol-2-yl]-2,5 diphenyl tetrazolium bromide) assay was used to assess cell viability. 10 µl of MTT reagent (5mg/ml) was added to each well on a 96-well plate and incubated for 2 hours at 37 °C. Then the medium was aspirated and 60 µl of acidic isopropanol was added to each well. Finally, the absorbance of the sample was measured using a UV plate reader. The optical density was measured at 570 nm with background subtraction at 690 nm. The viability of cells was figured according to the control by a percentage value.

2.2.3 Cell cycle assay

Cells were seeded in T25 flask or 6-well plate and left in the incubator to attach overnight. Cells were then treated according to the time and concentration of each type of treatment. After treatment, the cells were harvested by trypsin and resuspended with fresh medium. Later, the cells were transferred into Eppendorf tube and spun down at 2000 rpm for 5 minutes then the supernatant was decanted, and the pellets were resuspended with cold PBS to wash the cells. 100 µl of cold 70% ethanol were then added to the pellets and gently resuspended. The samples with 70% ethanol were incubated for 30 minutes at 4 °C. Before analysis by flow cytometry, the ethanol-suspended cells were centrifuged for 5 minutes at 2000 rpm, and then the ethanol was decanted thoroughly. The pellets were washed with cold PBS and then resuspended with 500 µl of propidium iodide (PI)/RNase staining solution. Each sample was analysed using 488 nm, 532 nm or similar excitation and the emission was collected using a long-pass filter blue 660/20 or equivalent. The population of cells was gated in forward scatter (FSC) and side scatter (SSC) to select a single cell

and avoid any cellular debris. The gates were then used to create histograms. These represent the number of single cells and DNA contents. The flow cytometry experiments were carried out at the Medical school, University of Sheffield. Special thanks go to Mrs Susan Clark for providing training sessions on LSRII flow cytometry machine to perform the current experiments.

2.2.4 Real-time quantitative PCR assay

2.2.4.1 RNA extraction

RNA was extracted according to the instructions specified with PureLink RNA Mini kit (ambion by life technologies). After harvesting the cells, the culture medium was removed and the cells were washed with ice-cold PBS and spun down at 3500 rpm. The supernatant was removed and 0.3-0.6 ml of lysis buffer was added. The lysate was then passed through a disposable syringe with a needle gauge 18-21, 10 times. Following which, a similar volume of 70% ethanol was added to the sample and vortexed. The lysate was then transferred to a spin cartridge and centrifuged at 13400 rpm for 15 seconds. The supernatant was discarded and 350µl of the wash buffer 1 was added to the spin cartridge and then spun down again at 13400 rpm for 15 seconds. The spin cartridge was washed by adding 80 µl of DNase solution (PureLink DNase, Invitrogen) and then centrifuged for 15 seconds at 13400 rpm. 350µl of the wash buffer 1 was then added to the spin cartridge and centrifuged for 15 seconds. This step was followed by washing the spin cartridge using 500 µl of the wash buffer 2, twice, and then spun down for 1-2 minutes to dry the spin cartridge. The flow-through was discarded and the spin cartridge was transferred into a new collection tube. This was followed by adding 30-100 µl of RNase-free water to the spin cartridge and incubated for 1 minute at room temperature to elute the RNA. The eluate (RNA) was collected by centrifugation for 2 minutes at 13400 rpm. This was stored at -80C°.

2.2.4.2 Synthesis of cDNA

Complimentary of DNA (cDNA) was synthesized by using reverse transcriptase according to the instruction specified in AMV First Strand cDNA Synthesis Kit (BioLab). Briefly, 1-6 µl of total RNA (200-400 ng/ µl) was added to oligo primer d(T)₂₃ and an appropriate amount of nuclease-free water to give a final volume 8 µl. The mixture was mixed thoroughly and incubated for 5 minutes at 70 °C. This step was followed by the addition of 10 µl and 2 µl of AMV Reaction Mix and AMV Enzyme Mix to each sample, respectively. 2 µl of nuclease-free water was added to the negative control tube instead of AMV Enzyme Mix. The samples, including the negative control tube, were then incubated for 1 hour at 42 °C. The samples were then incubated for 5 minutes at 80 °C. The product was diluted with nuclease-free water to 50 µl. Finally, the samples were labelled correctly and stored at -20 °C.

2.2.4.3 Primer design and real-time quantitative PCR

PowerUp™ SYBR Green Master Mix system (Applied Biosystem) was applied to express the PRNP gene. The primers of PRNP and a housekeeping gene GAPDH were designed and tested using NCBI program to target the specific gene of interest. The sequences of primers are listed in the [table \(2-4\)](#) below. All primers were purchased from Sigma-Aldrich and were dissolved in nuclease-free water as a stock of 100 µM. The stock was kept at -20 °C, and the concentration of each primer used in qPCR was 500 nM.

Table (2-4): The sequences of primers

Primers	Sequence
PRNP Forward	5'-GGTGGTGTCTCACTCTTTCTTC-3'
PRNP Reverse	5'-CCAGCATCTCAGGTCTACTCTA-3'
GAPDH Forward	5'-CCCTTCATTGACCTCAACTACA-3'
GAPDH Reverse	5'-ATGACAAGCTTCCCGTTCTC-3'

The mixture of qPCR materials was made using 10 μ l of SYBR GREEN Mix (2X), 1 μ l each of template DNA, forward primer and reverse primer, and 7 μ l of nuclease-free water to give a total volume of 20 μ l in each well. Experiment was performed in triplicates, using 3 different samples. The amplification was performed under thermal cycling conditions i.e. 1 cycle of 50 °C for 2 minutes, 1 cycle 95 °C for 2 minutes, 50 cycles of 95 °C for 15 seconds and 58 °C for 1 minutes. This was applied using Agilant MX3005 qPCR machine, in a 96-well PCR-plate. The change of gene expression was calculated using $\Delta\Delta C_t$ method as detailed using the following equations:

$$\Delta C_t (\text{Control}) = C_t (\text{Target gene}) - C_t (\text{Reference gene})$$

$$\Delta C_t (\text{Treated sample}) = C_t (\text{Target gene}) - C_t (\text{Reference gene})$$

$$\Delta\Delta C_t = \Delta C_t (\text{Treated sample}) - \Delta C_t (\text{Control})$$

$$\text{Fold Change} = 2^{-\Delta\Delta C_t}$$

Where C_t : Threshold cycle

2.2.5 Quantification of protein expression by Western blotting

2.2.5.1 Protein quantification

After lysing the cells, protein concentration was calculated using the bicinchoninic acid (BCA) method. The protein level in the lysate was measured to determine the exact concentration of the sample that will be loaded in SDS-gel. The working reagent of BCA was prepared by mixing 50 parts of BCA Reagent A with 1 part of BCA Reagent B. Serial dilutions of BSA were made (0.0, 0.1, 0.2, 0.4, 0.6, 0.8, 1.0 mg/ml). 10 μ l from either the lysate or BSA sample was added to each well. 200 μ l of BCA working reagent was then added to each well and then the 96-well plate was left for 30 minutes in the incubator at 37 °C before the absorbance at 570 nm was read. The calibration curve was made from BSA samples to quantify the concentration of protein in the late using the formula (Figure 2-1).

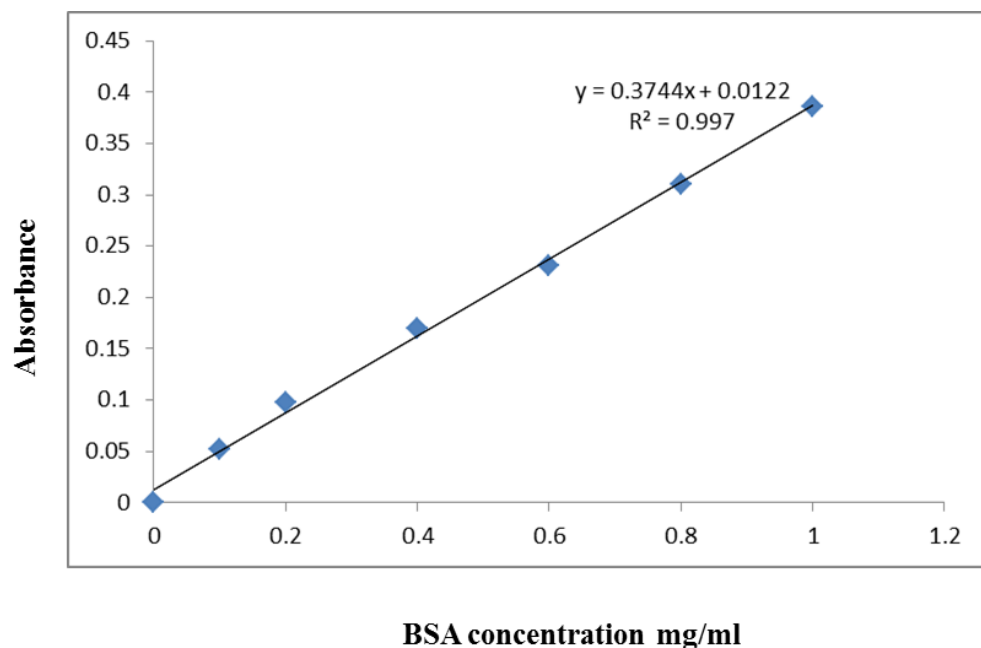


Figure (2-1): The standard curve for serial dilutions of BSA in RIPA buffer

2.2.5.2 Western blot assay

U87 cells were seeded in 6-well plates at a density which was selected according to the duration of treatments (mentioned in each chapter of results). After the treatment period, cells were harvested by trypsin-EDTA. This step was followed by adding fresh medium, and the cells were resuspended and spun down at 1500 rpm for 5 minutes. Cells were then washed twice with cold PBS and centrifuged at 1500 rpm for 5 minutes. RIPA buffer with protease inhibitor was used to lyse the pellet in ice for 25-30 minutes. The sample was spun down at 13400 rpm for 10 minutes. The lysate was collected and protein concentration was quantified by BCA method (section 2.2.5.1). The sample was then diluted with RIPA buffer to obtain 40 µg as a total concentration. 40 µl of the sample was added to 10 µl of 5x loading buffer. The sample was then denatured at 95 °C for 5 minutes.

After denaturation, 40 µl of the sample was loaded onto the precast gel. Initially, the samples were subjected to electrophoresis for 5 minutes at 300 V using 1x TGS buffer and the gel was run for further 30 minutes at 180 V. The ladder was also loaded to the gel. During this time the PVDF membrane was activated in 100 ml of methanol, and then a 100 ml of 10x TGM buffer and 800 ml double-distilled water were added to the 100 ml of methanol to create 1x TGM buffer. The gel was transferred to a suitable container. The membrane, gel, filter paper and fibre pad were stacked in the order specified in **Figure 2-2**.

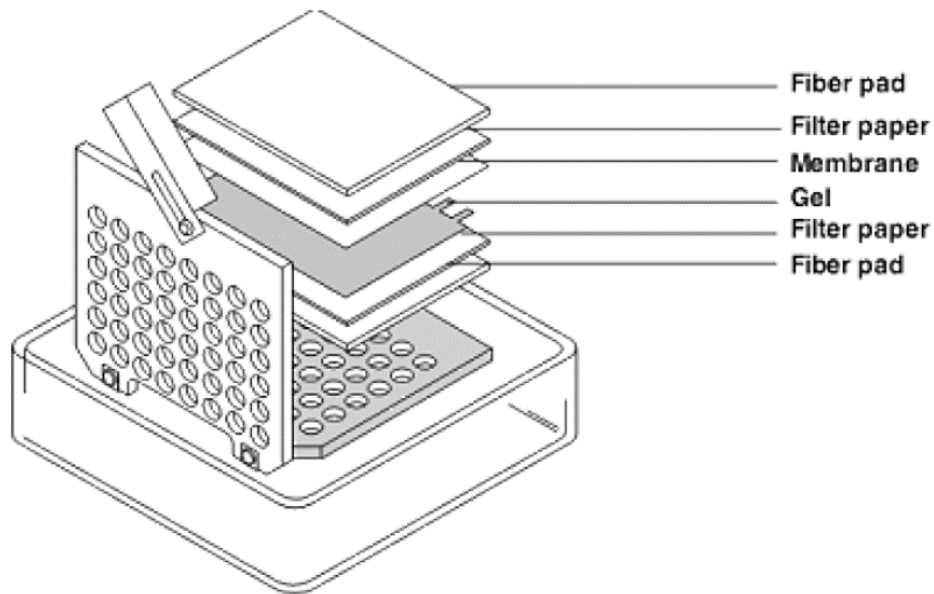


Figure (2-2): The cassette of western blotting shows the order of the membrane, gel, filter paper and fibre pad according to black and white sides²¹⁴.

The cassette was transferred into the tank, and the sample was run for 30 minutes at 400 mA. An ice pack was added to avoid overheating during the transfer process. After that, the membrane was exposed to a series of washes. First, the membrane was washed for 15 minutes with TBS-T (Tris buffer saline, 0.1% Tween 20) and this was followed by blocking for 1 hour with 20 ml of 5% of non-fat milk in TBS-T. The membrane was then exposed to primary antibody depending on the type of protein at specific dilutions mentioned in the results chapter that was diluted with 5% non-fat milk in TBS-T overnight at 4°C.

After overnight incubation, the membrane was washed three times for 5 minutes each with TBS-T to remove the remains of the primary antibody. The horseradish peroxidase-linked secondary antibody was then diluted by 1:4000 or 1:2000 in 1x TBS-T and incubated with the membrane for 1 hour at room temperature. The membrane was then washed once with TBS-T for 15 minutes and twice with TBS for

5 minutes, each. Finally, the membrane was exposed 3 minutes to ECL (Enhanced chemiluminescence) solution to allow imaging using Bio-Rad ChemiDoc system.

2.2.6 Flow cytometry analysis: protein expression

Protein expressing analysis was carried out according to the indirect flow cytometry protocol provided by Abcam. Briefly, cells were detached using the non-enzymatic dissociation solution. The cells then resuspended with fresh medium and transferred into Eppendorf tube ($1-1.5 \times 10^6$ cells) and spun down at 1500 rpm for 5 minutes. The medium was aspirated, and the cells washed by ice-cold PBS twice and then spun down again at 1500 rpm for 5 minutes. Cell viability was checked under a light microscope using trypan blue dye. Cells used in this assay were approximately 95% viable. The next steps depended upon the target (i.e. cell surface or cytosolic protein).

2.2.6.1 Live cells (surface protein) flow cytometry

Cells were resuspended with FACS buffer (PBS, 10% FBS, 1% sodium azide) and all samples were kept on ice. The pellets were washed with ice-cold PBS and centrifuged at 1500 rpm for 5 minutes. The primary antibody and/or isotype was diluted with 3% BSA. A 100 μ l of primary or isotype antibody was added to each sample (with a population of 1×10^6 cells) and then incubated in ice for 1h. Cells were then washed twice using ice-cold PBS and spun down at 1500 rpm for 5 minutes. Cells were then incubated with the secondary antibody for 45 mins on ice. Cells were then washed twice to remove any unbound secondary antibody. The samples were then resuspended in 300 μ l ice-cold PBS and transferred into the flow cytometry tube. The samples were analysed at 488 nm, and the emission was collected using a long-pass filter blue 530/30.

2.2.6.2 Fixing and permeabilising cells (cytosolic protein)

Cells were fixed using 4% paraformaldehyde for 10 minutes. The pellets were washed with ice cold PBS and centrifuged at 1500 rpm for 5 minutes. Cells were then permeabilised using 0.2% Triton 100x for 5 minutes and then spun down at 1500 rpm for 5 minutes. Following which triton was removed and blocked using 3% BSA (in PBS) for 30 minutes. The blocking reagent was then removed by centrifugation for 5 minutes at 1500 rpm.

The primary antibody and/or isotype were diluted with 3% BSA. 100 µl of primary or isotype antibody was added to each sample (containing $\sim 1 \times 10^6$ cells) and then incubated on ice for 1 hr. This was followed by incubation of secondary antibody for another hour and the finally, cells were washed two times using ice-cold PBS and then spun down at 1500 rpm for 5 minutes. Cells were washed twice to remove any remaining unbound antibodies. The samples then resuspended with 300 µl ice-cold PBS and transferred into a flow cytometry tube. The samples were analysed at a wavelength of 488nm, and the emission was collected using a long-pass filter blue 530/30.

2.2.7 ICC by Confocal Microscopy

The coverslips were rinsed in 10 M nitric acid for 1h, then washed with distilled water three times and allowed to air dry. Coverslips were autoclaved and stored in an incubator overnight to dry completely. The sterile coverslips were transferred into 24-well plate and 500 µL poly-ornithin hydrobromide was added to each well for 40 minutes at room temperature. They were washed three times using PBS.

Cells were then seeded in a certain density according to the experiment in each chapter. Allowing time for attachment, cells were then treated with a specific

treatment depending on the type of the experiments. When the time of incubation was completed, the medium was removed, and cells were washed with PBS. Cells were then fixed with 4% paraformaldehyde for 10 minutes at room temperature. The fixative reagent was removed and cells were then washed two times to remove any remaining paraformaldehyde. PBS was then removed and cells were incubated for 1h with 500 μ L blocking solution (1% BSA in PBS-T) at room temperature. Following which, the blocking solution was aspirated, and the cells were incubated with primary antibody overnight, the antibody was made up using 1% BSA with PBS-T. Next day, the primary antibody was removed and the cells washed three times with PBS-T, 5 minutes each at room temperature. The secondary antibody was added to each well and then incubated for 1h at room temperature. After aspiration of the secondary antibody, the cells were washed twice with PBS-T and one time with PBS. Cells were then incubated with DAPI for 5 minutes and washed 3 times with PBS. The coverslips were mounted with propyl galate onto a glass slide. The coverslips were sealed using transparent nail polish. The samples were imaged using a LEICA SP5 microscope and using a 40x or 63x objective. The imaging was performed in Sheffield Institute for Translational Neuroscience (SITraN), Sheffield University. I would like to express my special thanks to Dr. Cleide Souza for helping me to use the confocal microscopy.

2.2.8 ICC screening assay

Cells were seeded in 96-well plates from Greiner Bio-One Ltd, which had been treated with 100 μ g/mL poly-ornithin hydrobromide. The seeding density depended on the period of the experiment. Next day, cells were treated with the FA pathway inhibitors (FAPi) compounds at a concentration described in the methods; chapter 6. When the incubation time with the compounds finished, the medium was

aspirated and the wells were washed with PBS. Cells were then fixed by adding 50 μ l of 4% paraformaldehyde to each well for 10 minutes at room temperature. The cells then blocked with 1% BSA-T (1% BSA with 0.1% Triton 100x in PBS) for 1h at room temperature. Three times washes by TBS-T (0.1% Triton in PBS), 5 minutes each (50 μ l for each well) were followed the incubation overnight at 4 °C with primary antibody. Cells were then incubated with fluorescent secondary antibody (50 μ l for each well) for 1h at room temperature. The wells were washed three times, twice with PBS-T and once with PBS, each for 5 minutes. This was followed by 5 minutes incubation with DAPI, and washes with 50 μ l of PBS three times. Images were acquired using a Molecular Devices ImageXpress Micro microscope and at 20x objective. The figure below shows the ImageXpress Micro device. This experiment was carried out in the Department of Biomedical Science (BMS), Sheffield University. I appreciate Dr Stephen Brown's help for the training session on ImageXpress Micro imaging system.

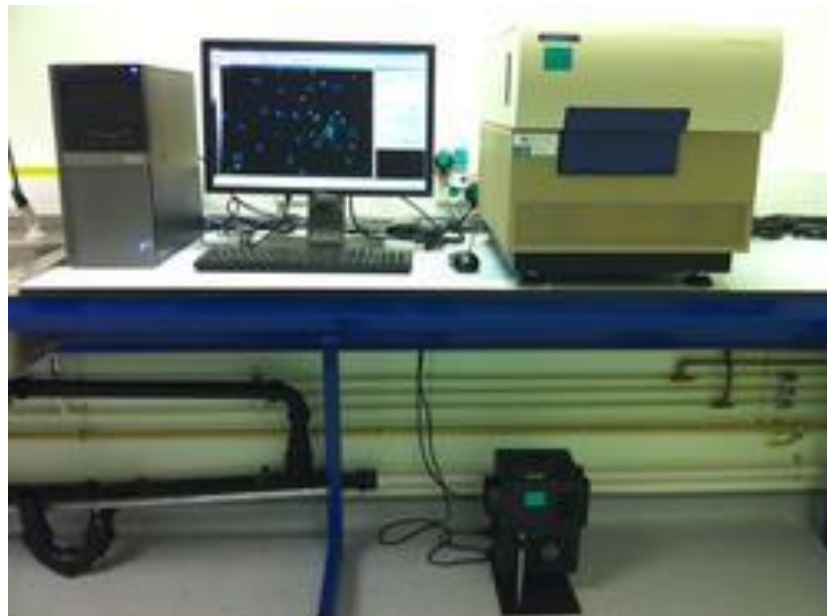


Figure (2-3): ImageXpress Micro device

2.2.9 Transfection- siRNA delivery in U87 cells

U87 cells were cultured in T25, 96-well plate, 6-well plate or 24-well plate. Next day the transfection reagent and siRNA were prepared and added. 5X siRNA buffer was diluted five times by adding RNase-free water. The target and non-target siRNA were then dissolved by adding a volume of siRNA buffer depending on the number of nanomoles of siRNA following the equation below to obtain 100 μ M as a stock solution. Later, the stock solution was diluted into 5 μ M by adding a 20x of siRNA buffer and this was aliquoted and stored at -20C°. The DharmaFECT reagent and both siRNA (PRNP and non-target) were diluted in separated tube 10 times using the optimum medium and then was left 5 minutes at RT. Later, one volume of the DharmaFECT reagent was mixed with each siRNA, and they left 20 minutes at room temperature in the fume hood. The mixture was added to 5x of the fresh antibiotic-free medium. Before treating the cells, the medium was aspirated from the attached cells, and the transfection reagent was poured onto the cells gently.

$$V = 10 \times C$$

Where V (μ l) is the volume of siRNA buffer, C is the nanomole of siRNA

To obtain the desired transfection condition, different concentrations of DarmaFECT were used to prepare the transfection medium. The optimum concentration of Darmafect was 0.08 μ l/5000cells. Besides, the optimum siRNA concentration was 50 nM. After treating cells with transfection medium, the plate or flask was placed in the incubator at 37 °C for the desired period, i.e. 24h, 48h, 3days, 4days or 5days. The table below shows examples of siRNA and DarmaFECT volume (μ l) in different cell densities and different total volumes (Table 2-5).

Table (2-5): The examples of siRNA and DarmaFECT volume (μ l) in different cell densities

Total volume (μ l)	Cell density	5 μ M siRNA (μ l)	DarmaFECT volume (μ l)
100	1000	1	0.02
100	5000	1	0.08
500	10000	5	0.16
500	20000	5	0.32
1000	25000	10	0.4
1000	50000	10	0.8
1500	25000	15	0.4
1500	50000	15	0.8
3000	100000	30	1.2
3000	400000	30	6

2.2.10 LDH assay

Lactate dehydrogenase (LDH) is a cytotoxicity assay. U87 cells were seeded in a 96-well plate at a certain density depending on the period of the experiment (see section 4.2.6). The reagents for this assay were prepared according to the manufacturer's instruction - Pierce LDH Cytotoxicity Assay Kit from Thermo Scientific. The vial of

the substrate (lyophilisate) was dissolved in 11.4 ml Mili-Q water in 15 ml centrifuge tube then mixed gently. The assay buffer vial (0.6 ml) was defrosted at room temperature then was added to the substrate to prepare the reaction mixture (RM). This mixture was aliquoted and stored at -20°C.

The medium that was used for cell culture in this assay was phenol red-free medium with 5% serum to avoid any background activity. The wells during the seeding were divided into different parts including control (part 1 and 2) and treated as triplicate for each part. After the transfection with siRNA was performed, 10 µl of 10X Lysis Buffer was added to the control (part 1) and then incubated at 37°C, 5% CO₂ for 45 minutes to obtain the Maximum LDH Activity. Next, 50 µl of medium were transferred from each well to new 96-well plate. Later, 50 µl of RM was added to all wells. The plate was incubated 30 minutes at room temperature, protected from light. This step was followed by adding 50 µl of stopping reagent. To avoid any bubbles, the plate was centrifuged for 1 minute at 4000 rpm. Finally, the absorbance was measured using the plate reader at 490 nm with background subtraction at 680 nm. The following equation was applied to determine the percentage of cytotoxicity

$$\% \text{ Cytotoxicity} = \frac{(\text{Treated LDH activity} - \text{Spontaneous LDH activity})}{(\text{Maximum LDH activity} - \text{Spontaneous LDH activity})} \times 100$$

Where Treated LDH activity is the absorbance of treated sample, Spontaneous LDH activity is the absorbance of control (part2), Maximum LDH activity is the absorbance of control (part1).

2.2.11 Alamar Blue assay

Cell proliferation for knockdown cells was analysed using Alamar blue assay. Resazurin Sodium Salt was dissolved in deionised water at 1 mM. To prepare a

working reagent of Alamar blue, one volume was diluted in 10 volumes of fresh medium.

The cells were seeded in 24-well plate at different cell density depending on the period of incubation and then transfected with siRNA. After the incubation time, the medium was removed and 500 μ l of working Alamar blue reagent was added into each well. The plate was then left 4h in the incubator at 37 °C. This step was followed by transferring 100 μ l of working alamar blue reagent in triplicate from each well into 96-well plate as shown in the figure below (Figure 2-4). The optical density was measured using plate reader spectrometry at 570 nm. The data was then calculated as a percentage to the absorbance of the control (untreated).

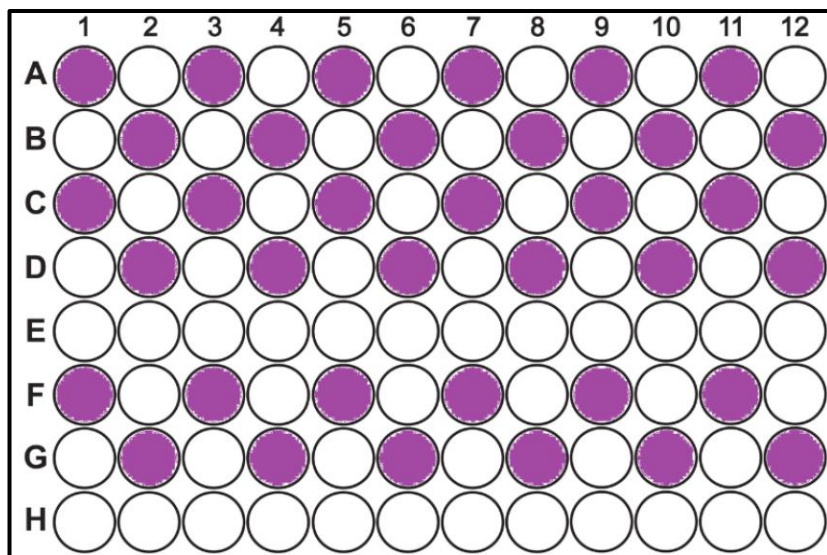


Figure (2-4): The distribution of samples in 96-well plate used to performed cell viability assay by Alamar blue assay.

2.2.12 Apoptosis assay

Apoptosis assay for U87 cells was assessed with FITC Annexin V Apoptosis Detection Kit with PI (BioLegend), according to manufacturer recommendations. The cells were seeded in a 6-well plate at a certain time point according to the experiment. Cells were harvested using a non-enzymatic dissociation solution then washed twice

with cell staining buffer which was provided by BioLegend. Cells were resuspended in Annexin V Binding Buffer, 100 µl to each 300000-500000 cells. The suspension was transferred into FACS test tube by 100 µl in each tube. Five microliters of FITC Annexin V was added to each sample and mixed gently. 10 µl of Propidium Iodide solution (PI) was then added to each tube. The tube was mixed gently and incubated for 15 minutes at room temperature. 400 µl of Annexin V binding buffer was then added to each sample. The sample was transferred to flow cytometry and analysed using 488 nm excitation. The emission was collected using a long-pass filter blue 620/20 for PI and blue 530/30 for FITC Annexin V.

2.2.13 Statistical Analyses

Data are displayed as mean \pm SD and were statistically analysed by a GraphPad Prism 7 software, using t-test (to compare each tested group with the control) and one-way ANOVA with Tukey's test (to compare between-groups and within-groups differences). The experiments were repeated at least three times and the number of replicates (n) is mentioned in the legend of figures. The results are considered statistically significant when p-value is less than 0.05.

Chapter 3: Evaluation of PrP^c and PRNP gene expression in different phases of the cell cycle and in U87 cells treated with TMZ or BCNU

3.1 Introduction

Currently, effective chemotherapies against glioblastoma are TMZ and BCNU, used alone or in combination with radiotherapy, but the chemoresistance of GBM cells remains one of the main problems. These genotoxic treatments induce DNA damage that activates DNA repair pathways and tumour suppressor p53²¹⁵. Indeed, p53 is a transcriptional factor that activates its target genes in response to cellular stresses to prevent the proliferation of damaged cells by arresting the cell cycle and triggering apoptosis,²¹⁶ a so-called DNA damage checkpoints²¹⁷. It also transactivates p21, cyclin-dependent kinase (CDK) inhibitors, which induces cell cycle arrest through suppressing CDK4 and CDK6²¹⁶. TMZ and BCNU have been shown to arrest the glioblastoma cells in G2/M, and this process delays the cells in order to allow more time to repair DNA damage induced by the alkylating agents. Thus, G2/M accumulation in these treated cells occurs due to upregulation of p53 and p21²⁰².

Several studies have reported that PrP^c is highly expressed in glioblastoma cells and that it appears to interact with many signalling pathways to protect the glioblastoma cells from the proapoptotic stimuli (reviewed in section 1.2.5.2). The behaviour of PrP^c in glioblastoma cells when they are treated with alkylating agents still needs to be elucidated, however. Indeed, to our knowledge, Zhuang *et al.* are the first researchers to have investigated the effect of TMZ on the expression of PrP^c in glioblastoma cells, which they measure by immunofluorescence and western blotting, as well as using array hybridization to assess the effect on levels of the PRNP gene. They found that PrP^c may induce the resistance to TMZ by upregulating PrP^c in the G2/M phase of the cell cycle. Similar studies have not been reported on BCNU,

however. Accordingly, in the present study, we evaluated PrP^c and its gene in U87 cells treated with either TMZ or BCNU, using western blotting and flow cytometry (for protein quantification) and qPCR (for gene quantification) at different time points and cell cycle phases. The details are described in the next section (3.2)

3.2 The aim

The work in this chapter aimed to evaluate and compare PRNP and PrP^c levels in TMZ or BCNU treated U87 cells under the assumption that they may be upregulated in response to the accumulation at G2/M resulting from these treatments. The following objectives were addressed

- The cell cycle will initially be analysed 24h after treatment with Aphidicolin and Nocodazole. These are cell-cycle modulators that are known to arrest the cell cycle at the G1 and G2/M phases, respectively. The purpose of this set of experiments is to validate the experimental design and to obtain G1 and G2/M cells. The second round of experiments was then undertaken in which U87 cells were treated with the alkylating agents, TMZ and BCNU, and then analysed using flow cytometry to determine the percentage of cells in each phase of the cell cycle at different time points (6 h, 12 h and 24 h with and without incubation for 24h and 48h).
- The regulatory cell cycle proteins p21 and p53 were then examined to confirm the arrest of the cell cycle at G2/M in response to the alkylating agents.
- The PRNP gene level of cells arrested in G1 and G2/M phases by Aphidicolin and Nocodazole were assessed and the effect of TMZ or BCNU on PRNP gene in treated U87 cells at different time points (6h+48h, 24h and 24h+48h) was also examined using qPCR

- The impact of TMZ and BCNU on the PrP^c level in treated U87 cells at 24h, 6h+24h and 24h+48h were assessed by flow cytometry and western blotting.

3.3 Methods

3.3.1 Preparation of treatments

DMSO was used as a co-solvent for all treatments and as a negative control for all experiments. MTT assay was used to determine the concentration of DMSO that could be tolerated in the cellular assay. It was observed that up to 0.5% DMSO in culture media had no effect on cell viability (see section 3.4.2.1), hence this concentration was used throughout the experiments. All compounds tested were dissolved in DMSO at 20x the working concentration. The alkylating agents, TMZ and BCNU, were prepared at 20 mM as a stock. The cell cycle synchronising agents, Aphidicolin and Nocodazole, meanwhile, were prepared at 2.96 mM and 0.2 mM, respectively. These stock solutions were divided into small aliquots and stored at -80 °C. These aliquots of stock solution were each diluted in ten times their volume of PBS to prepare a working solution. An appropriate volume of the working solution was taken and then further diluted with 20 times of fresh medium to obtain the required treatment concentration for cell culturing.

3.3.2. Cell viability assay (MTT)

3.3.2.1 Growth curve of U87 cells

MTT assay was applied to determine the doubling time of U87. The cells were seeded in four 96-well plates at 4000 cells in each well. One plate was taken to measure the viability each day, i.e. cell viability was quantified for plate 1 on day 1; this procedure was repeated to quantify the viability of cells in plate 2, plate 3 and plate 4 on days 2, 3 and 4, respectively. The absorbance of each well reflects the viability of cells.

3.3.2.2 MTT assay for treated cells

To examine the efficacy of DMSO, alkylating agents and synchronised agents, the viability of the treated cells was assessed by MTT assay. U87 cells were harvested from a T75 flask using trypsin and then counted using a haemocytometer in 10 ml resuspended medium. The volume of cell suspension containing the desired number of cells (calculated according to the incubation time of the experiment and the total number of cells required for the number of 96-well plates) was transferred into a sterile 50 ml disposable basin. A volume of fresh medium sufficient for the number of plates to be used was added, and then 100 µl was transferred into each well of the 96-well plates using a multichannel pipette. The plates were incubated overnight to allow the cells to attach.

The next day, 5 µl of treatment was added to each well using a multichannel pipette. The controls for the cell viability assay, for DMSO and the other treatments, were PBS and 0.5% DMSO, respectively. The density of cells, concentration of treatments and incubation time are shown in the [table \(3-1\)](#). For comparison purposes, the concentrations and incubation periods used for TMZ and BCNU were the same as previously reported for U87 cells in the literature^{6,202}. The concentration of Nocodazole and Aphidicolin used, and the incubation period, was also in the same range as previously reported^{218,219}.

Table (3-1): Cell density and incubation time of treated cells in MTT assay.

Treatment	Cell density	Concentration of treatment	Incubation time (h)
DMSO	10000	0.05%, 0.1%, 0.5% or 1%	24
TMZ	10000	25, 50 or 100 μ M	24
BCNU	10000	25, 50 or 100 μ M	24
Aphidicolin	10000	5, 10, or 14.8 μ M	24
Nocodazole	10000	0.125, 0.25, 0.5, 0.75 or 1 μ M	24

After incubation with these treatments for 24h, the MTT assay protocol (see section 2.2.2) was followed to quantify the cell viability.

3.3.3. Cell cycle assay by flow cytometry

The cells were seeded in a T25 flask in different densities according to the incubation time. Table (3-2) below shows the seeding density at each time point to allow for the cells' growth and to ensure 80-90% confluence was reached at the end of the incubation period. The cells were allowed to attach overnight and were then treated with 14.8 μ M Aphidicolin, 1 μ M Nocodazole, 100 μ M TMZ or 100 μ M BCNU. In the control group, the cells were treated with 0.5% DMSO in each experiment. Later, all samples were washed and the protocol for cell cycle analysis (see section 2.2.3) was followed in order to quantify the percentage of cells in each phase of the cell cycle.

Table (3-2): Seeding density of U87 cells in cell cycle experiments

Time point (h)	Seeding density
6	0.7×10^6
12	0.7×10^6
24	0.5×10^6
6+24	0.5×10^6
6+48	0.4×10^6
12+24	0.5×10^6
12+48	0.4×10^6
24+24	0.4×10^6
24+48	0.3×10^6

3.3.4. RT-qPCR

RT-qPCR was performed to assess the level of the PRNP gene in the treated cells. The cells were harvested from a T75 flask and then cultured in 6-well plates at different densities depending on the incubation time. The cell densities and the incubation times of the cells are shown in [table \(3-3\)](#).

Table (3-3): The incubation times and cell densities for RT-PCR experiment

Incubation time	Cell density	Volume of medium (ml)
24h	200000	2
6+48h	150000	2
24+48h	100000	2

Different experimental groups were designed to quantify the effect of the treatments on the PRNP gene in the U87 cells, as follows:

Experiment 1: This experiment included two parts.

- The cells were treated with TMZ or BCNU for 6h and then left for 48h in fresh medium without treatment.
- The cells were treated with Aphidicolin and Nocodazole for 24h.

Experiment 2: The cells were incubated with TMZ or BCNU treatments for 24h.

Experiment 3: The cells were treated 24h with TMZ or BCNU and incubated 48h in fresh medium.

The diagram below shows the design of these experiments (Figure 3-1).

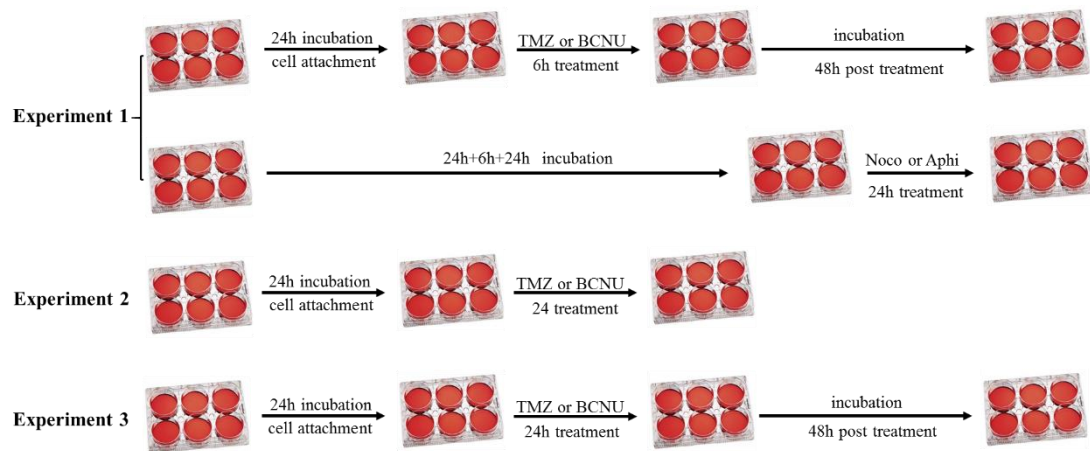


Figure (3-1): A summary of the experimental designs showing the different time points and treatments.

In each experiment, the cells were treated with TMZ, BCNU, Aphidicolin or Nocodazole by adding 100 μ l of the working solution of these treatments in each well. The control was treated with 0.5% DMSO. After incubation with the treatment, the total RNA was extracted using a PureLink RNA Mini kit (Ambion by Life Technologies) (see section 2.2.4.1). RNA extractions were normalised using RNase

free water and then 1-6 µl of RNA extraction was used to synthesise cDNA according to the protocol described in [section \(2.2.4.2\)](#). PRNP gene expression was quantified using the PowerUp™ SYBR Green Master Mix system (Applied Biosystem) and the primers that were listed in [section \(2.2.4.3\)](#).

3.3.5. Protein expression analysis by western blotting

Western blot assay was carried out to investigate the levels of p21, p53 and PrP^c in the treated cells. For p21 and p53, the cells were seeded in a 6-well plate and then, after 24h for attachment, were treated with 100 µM TMZ or BCNU for a further 24h. The medium was then replaced with fresh medium (i.e. without treatment) and the plates were left to incubate for 48h. The cells were then washed and harvested to obtain cell lysate. The procedure for western blotting was carried out according to the procedure described in [section \(2.2.5\)](#). The dilution factor for primary antibodies of p21 and p53 was 1:500 in blocking solution (5% milk in TBS-T), as recommended by the Santa Cruz Biotechnology protocol, whereas the secondary antibody (Goat anti-mouse IgG antibody) was diluted 1:4000 in TBS-T.

For PrP^c assessment, the cells were seeded and treated in the same way as described in [section \(3.3.4\)](#). When the incubation time was completed, the procedure for western blotting described in [section \(2.2.5\)](#) was performed to quantify the level of PrP^c.

3.3.6. PrP^c expression by flow cytometry

To validate the results of the western blot analysis, the PrP^c expression in the treated cells was assessed by flow cytometry. The cells were cultured and treated after 6h+48h, 24h and 24h+48h ([as described in section 3.3.4](#)). After the desired incubation time, all the samples were washed in PBS and then the protocol for flow cytometry was applied ([see Section 2.2.6](#)) to evaluate PrP^c level. The mean of the fluorescence

intensity (MFI) of each sample obtained by flow cytometry was normalised to the MFI of its isotype.

3.4 Results

3.4.1 U87 growth curve

A growth curve was plotted to ensure that the cells used in the experiments were in the growth phase. This could also be used to estimate the number of cells in each experiment. The cells were cultured in the same density, and their viability was then measured on days 1, 2, 3 and 4 by MTT assay. According to the resulting cellular growth curve, the population doubled after approximately 30 hours. The population on days 3 and 4 then increased to be about twice that of days 2 and 3, respectively.

(Figure 3-2)

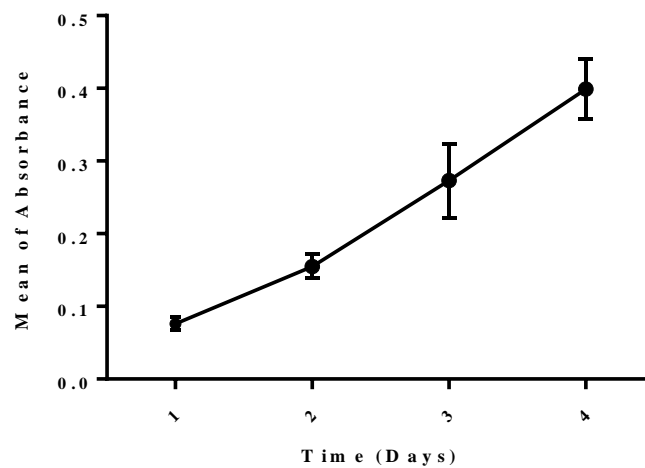


Figure (3-2): Growth curve for U87 cells over four days. The results represent mean \pm SD for the octuplicate of three independent experiments, n=24.

3.4.2 Cell viability of U87 cells

The viability of the treated cells was assessed using the MTT assay. All displayed data were calculated as a percentage in respect to the untreated sample (control).

3.4.2.1 Cell viability of U87 in DMSO

This experiment was performed to determine the concentration of DMSO that had no effect on the viability of U87 cells since DMSO was used as a co-solvent for the other treatments. The results of cell viability for various concentrations of DMSO (0.05%, 0.1%, 0.5% and 1%) after 24h are shown in **Figure (3-3)**. There was no great effect for DMSO concentrations of 0.05%, 0.1% and 0.5%, but a concentration of 1% DMSO resulted viability decreasing to $80.3\% \pm 4.2$. It was therefore decided to dissolve all the treatment compounds in 0.5% DMSO for all subsequent experiments.

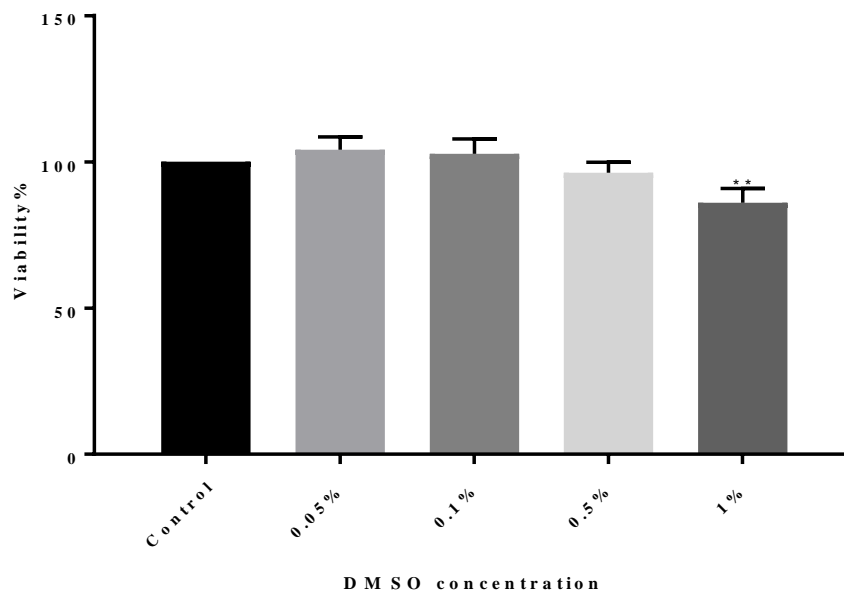


Figure (3-3): Cell viability of U87 cells in different concentrations of DMSO. The bar chart represents the percentage of viable cells in comparison to control. All the data were performed in triplicate for four different experiments and the statistical analysis was by one-way ANOVA with Tukey's test ($n=12$, $**=p<0.01$).

3.4.2.2 Viability of U87 cells treated with TMZ and BCNU

TMZ and BCNU were selected to treat U87 glioblastoma cells in this study in order to evaluate the PrP^c level. It was therefore important to evaluate the viability of U87 cells when subjected to these treatments in order to determine the concentrations of the compounds that do not affect U87 cells. Accordingly, the cells were treated with

varying concentrations of TMZ or BCNU (25 μ M, 50 μ M, 100 μ M) for 24h. The viability of the cells was calculated and normalised as a percentage in respect to the untreated control cells. **Figure (3-4)** shows that there were no significant variations in cell viability associated with any of the concentrations used. 100 μ M was therefore used for the following experiments.

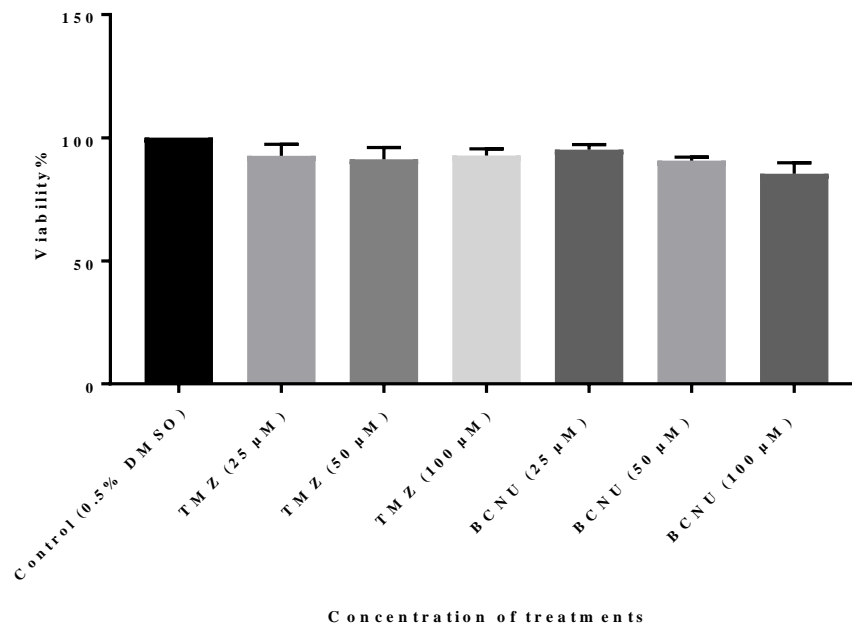


Figure (3-4): The viability of U87 cells treated with a series of concentrations of TMZ and BCNU. The chart signifies the ratio of viable cells in comparison to the control. The data represent mean \pm SD for the triplicate of three different experiments (n=9). The results were analysed using one-way ANOVA with Tukey's test.

3.4.2.3 Viability of U87 cells treated with Nocodazole and Aphidicolin

Nocodazole and Aphidicolin were used to arrest U87 cells in the G2/M and G1 phases, respectively. The MTT assay was used to determine the appropriate concentrations of these agents. The cells were therefore treated with Nocodazole and Aphidicolin at different concentrations for 24h. It was found that 1 μ M of Nocodazole significantly reduced cell viability to approximately 75% of that of the control group, while the cells with 14.8 μ M (5 μ g/ml) Aphidicolin displayed no significant change in the viable cells. (**Figure 3-5**). Despite this result, 1 μ M of Nocodazole was still used in the

subsequent experiments since it was found that lower concentrations were unable to arrest the cell cycle after 24h (data not shown). Regarding Aphidicolin, 14.8 μM was used in the subsequent experiments.

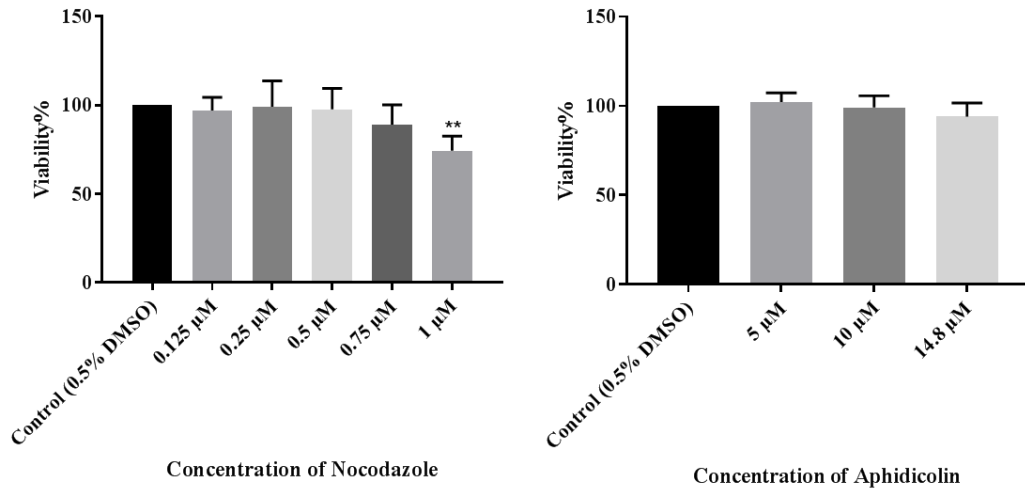


Figure (3-5): Cell viability for U87 cells in synchronised agents. The bar charts represent mean \pm SD of cell viability in respect to a series of concentrations of Nocodazole (A) and Aphidicolin (B). These experiments were repeated three times, and each conducted eight times ($n=24$). The data were analysed by one-way ANOVA with Tukey's test (**= $p<0.01$).

3.4.3 Cell cycle arrest

3.4.3.1 Cell cycle arrest by Aphidicolin and Nocodazole

To establish and optimise the assay, U87 cells were treated for 24h with the known cell cycle agents, Aphidicolin and Nocodazole to arrest the cells in the G1 and G2/M phases, respectively. The cell cycle synchronisation was performed using flow cytometry. The distribution of phases in the cell cycle changed after treatments with these compounds in comparison with untreated cells, as shown in Figure (3-6). It was found that around 83% of U87 cells were blocked in G1 when exposed to Aphidicolin (Figure 3-6, B). This result may be attributed to the blocking of DNA replication resulting from the inhibition of DNA polymerase by Aphidicolin²²⁰. Nocodazole, meanwhile, caused approximately 80% of the population of these cells to accumulate

in G2/M (Figure 3-6, C). This observation confirms that Nocodazole, a microtubule inhibitor widely used to synchronise the cycles of cell division, arrests cells in G2/M, as previously reported²¹⁸.

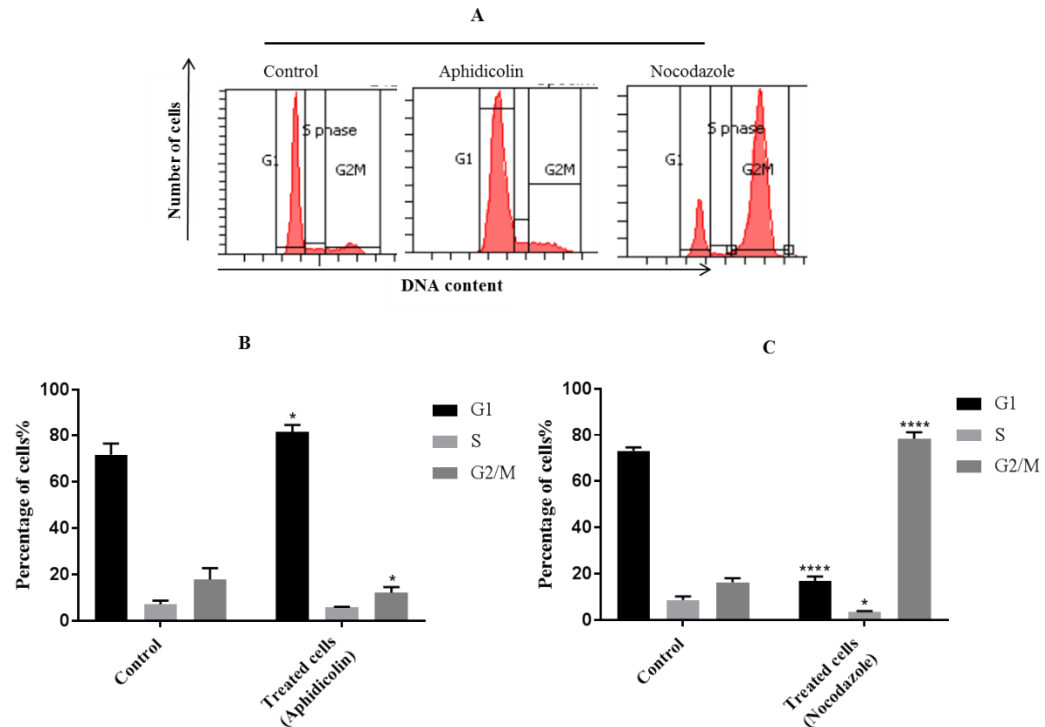


Figure (3-6): Cell cycle synchronisation of U87 cells by Nocodazole and Aphidicolin. The histograms show the cells which were synchronised by these treatments for 24h compared to the control (A). The bar charts illustrate the percentage of synchronised cells in each cell cycle phase with Aphidicolin (B) and Nocodazole (C). The results represent the mean \pm SD for three independent experiments each in duplicate and all the data were analysed using t-test ($n=6$, $*=p<0.05$, $****= p<0.0001$)

3.4.3.2 Cell cycle analysis following treatment with TMZ and BCNU

To assess the effect of alkylating agents on the cell cycle, U87 cells were treated with TMZ or BCNU at multiple time points (6h, 12h and 24h) with and without incubation for 24h and 48h. As can be seen from the histograms (Figure 3-7 A, C) and the bar charts (Figure 3-8 A), the cells that were exposed to TMZ displayed a gradual increase in G2/M arrest in a time-dependent manner compared to the control, recording the highest level (~83%) at 24h+48h. With BCNU, meanwhile, the G2/M

cells increased dramatically when the period of treatment was extended from 12h to 24h and then, on incubation, fluctuated to reach the highest level (~83%) at 24h+48h (Figure 3-7 B, D and Figure 3-8 B). Indeed, cells with BCNU showed a similar cell cycle distribution as TMZ, except that at 12h, 24h, and likewise after incubation at 6h+24h and 12h+24h, BCNU appeared more potent than TMZ in terms of arresting the cells in G2/M (Figure 3-8 C). These findings confirmed the results obtained by other studies, albeit with some variations. The distribution of the cell cycle for U87 cells was previously shown to alter in response to TMZ or BCNU but to start to lose 2N (DNA content) content after 12h exposure followed by 24h post-treatment, and this continued until 120h post-treatments²⁰². Furthermore, another study showed that TMZ began accumulating cells in G2/M from 1 day to 10 days, after just 3h of treatment²²¹. Generally, the arrest of cells by TMZ or BCNU can be ascribed to the induction of DNA damage, which serves to activate and accumulate p53 and p21²⁰². Based on these results, three time points were selected to evaluate the level of PRNP and PrP^c: 24h, 6h+48h and 24h+48h.

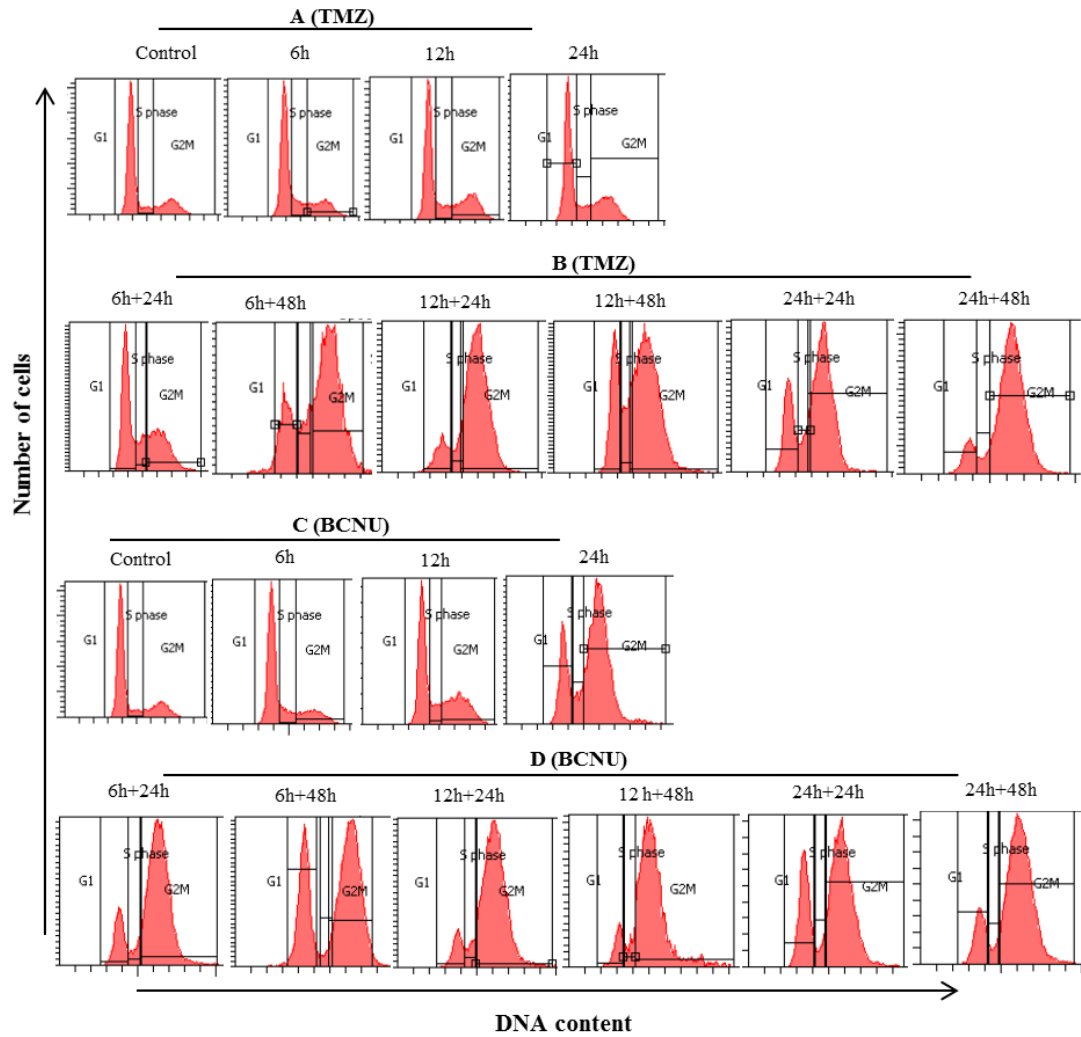


Figure (3-7): TMZ and BCNU induced cell synchronisation in the G2/M phase. Histograms shows that U87 cells were growth arrested following treatment with 100 μ M of either TMZ or BCNU. **A** and **C**, U87 cells treated for 6, 12 and 24h with TMZ or BCNU, respectively. **B** and **D**, most of cells were arrested in G2/M when the cells were subsequently incubated without treatment for 24 and 48h.

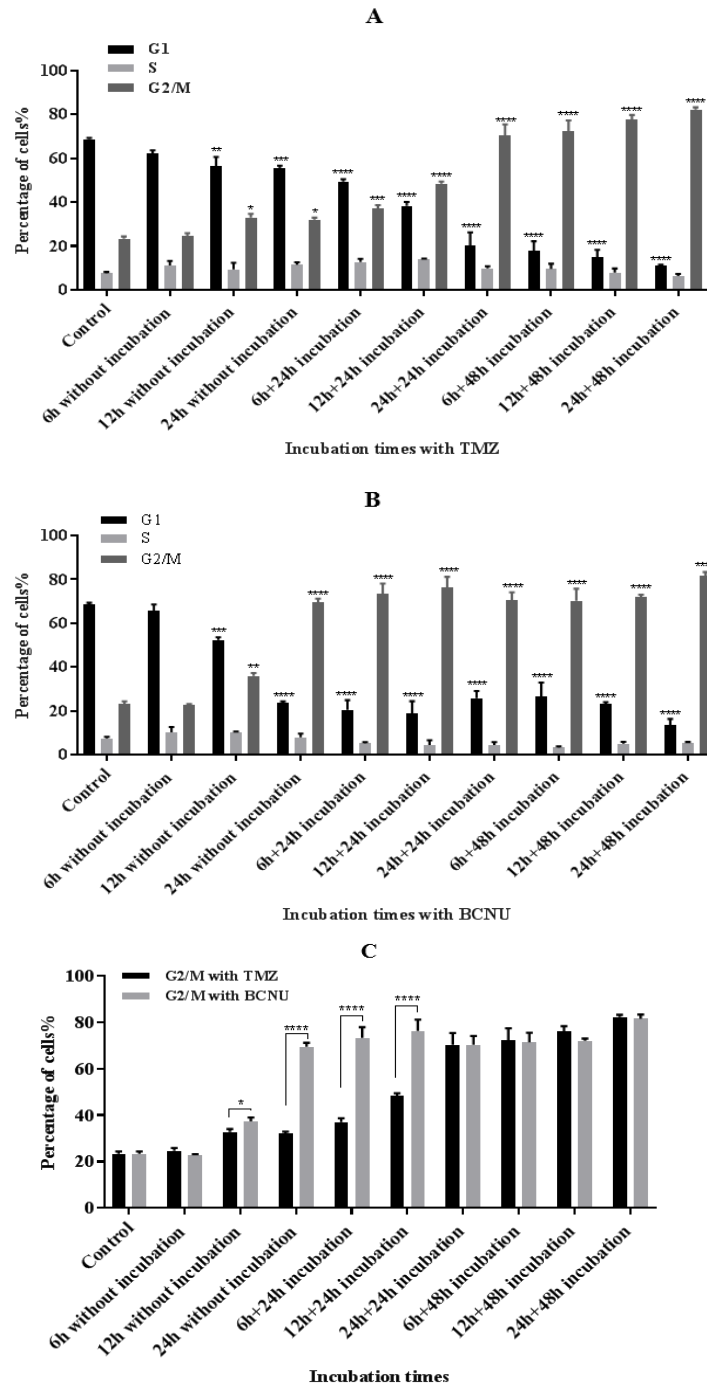


Figure (3-8): The effect of alkylating agents on the U87 cell cycle. TMZ (A) and BCNU (B) increased cells in the G2/M phase according to the period of treatment and the incubation subsequent to treatment. (C) represents the comparisons of G2/M cells among the cells treated with TMZ or BCNU at different time points. These experiments were performed in duplicate and repeated three times (n=6). The data were statistically analysed as the mean \pm SD; in this case using the t-test since we were comparing each phase of the cell cycle with its counterpart in the control (A and B) as well as between TMZ and BCNU (C) (n=6, *=p<0.05, **= p< 0.01, ***=p<0.001 ****= p<0.0001).

3.4.4 p21 and p53 expression increased in U87 cells treated by TMZ and BCNU

As shown in the previous section (3.4.3.2), TMZ and BCNU arrest U87 cells in the G2/M phase; an effect attributed to the accumulation of p21 and p53 proteins that regulate the cell cycle. To confirm this, the expression of these proteins was evaluated for treated cells at 24h+48h. Our results show that p21 levels were significantly higher in the treated cells compared to the control group (about three times higher in respect to TMZ, and four times higher in respect to BCNU). (Figure 3-9, A). p53 also increased significantly in the treated cells, relative to untreated cells, as shown in (Figure 3-9, B) – about 2 to 1.5 folds in TMZ and BCNU respectively.

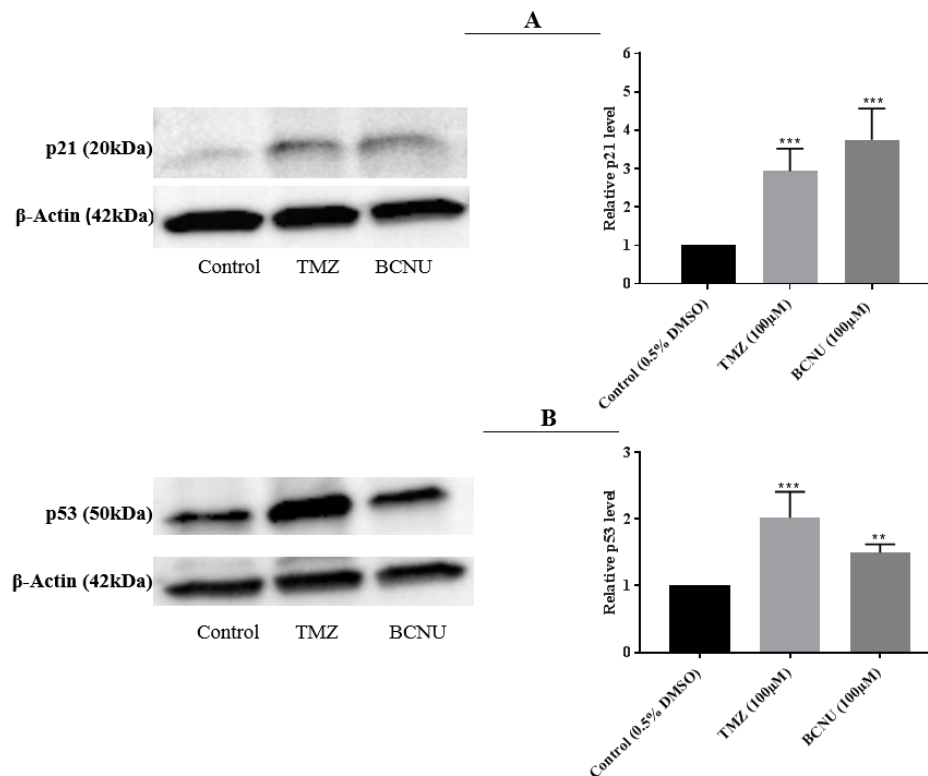


Figure (3-9): p21 and p53 expression levels in TMZ or BCNU treated cells by western blot. Expressions of p21(A) and p53 (B) in U87 cells indicated that the expressions of both proteins were markedly increased in U87 treated with TMZ or BCNU for 24h+48h. The data were analysed as the mean \pm SD using one-way ANOVA with Tukey's test, for at least three independent experiments ($n=3$, **= $p<0.01$, ***= $p<0.001$).

3.4.5 PRNP expression by qRT-PCR

To determine whether U87 cell cultures exposed to 100 μ M of TMZ or BCNU would change PRNP gene expression levels, the following experiments were designed, as mentioned in section (3.3.4):

Experiment 1: The cells were treated with TMZ or BCNU for 6h and then left for 48h without treatment. Another group of cells were treated with Aphidicolin or Nocodazole for 24h.

Experiment 2: The cells were incubated with treatments (TMZ or BCNU) for 24h.

Experiment 3: The cells were treated 24h with TMZ or BCNU and incubated 48h in fresh medium.

The purpose of experiment 1 was to assess the effect of TMZ and BCNU on the gene expression. Furthermore, the correlation of the PRNP level in the G1 and G2/M phases was also investigated. The cells were treated for 24h with the synchronising agents Aphidicolin and Nocodazole in order to evaluate the expression of the PRNP gene in cells that arrested in G1 and G2/M, respectively. **Figure (3-10 A)** shows the influence of the above treatments on the mRNA expression level of PrP^c. The PRNP gene expression was slightly increased when the cells were treated with TMZ or Nocodazole. This result revealed that the mRNA expression in the G2/M-arrested cells by TMZ or Nocodazole was increased when compared to the control. On the other hand, even though BCNU arrested the cells in the G2/M phase, the PRNP gene expression level was not affected. Furthermore, there was no significant variation in gene expression in the case of cells arrested at G1 using Aphidicolin.

In experiment 2, there was no significant variation in PRNP expression in the TMZ or BCNU when assessed after 24h of treatment alone, without resting (Figure 3-10 B).

According to Experiment 3, the expression of PRNP in the cells was significantly increased when compared with untreated cells. It is clear that a longer treatment and incubation period promotes the expression of PRNP gene in the cells arrested at G2/M by TMZ and BCNU. The significance value was higher with TMZ than with BCNU, however (Figure 3-10 C).

In general, these results confirmed that the PRNP gene in U87 cells increased in G2/M cells, resulting from G2/M-induced treatments, Nocodazole, TMZ and BCNU, with some variations depending on the duration of the treatment and the rest after the treatment. The gene profile of G2/M U87 cells resulting from TMZ treatment in the previous study showed that 83 genes were changed relative to the G1/S cells and the PRNP gene was the most significantly altered gene among these genes⁶. In our results, TMZ increased levels of the PRNP gene in U87 cells more than BCNU. In the previous section (3.4.4), the induction of p53 in TMZ treated cells was also higher than with BCNU. p53 is induced in response to DNA damage resulting from various stimuli, including chemotherapies⁶². It has been reported that PrP^c may protect the tumour cells from pro apoptotic stimuli such as chemotherapy and DNA damage¹⁸⁴. Thus, increasing the PRNP gene, as a cytoprotective factor, in cells treated with TMZ more than cells treated with BCNU may rescue the cells from the effects of anticancer treatments.

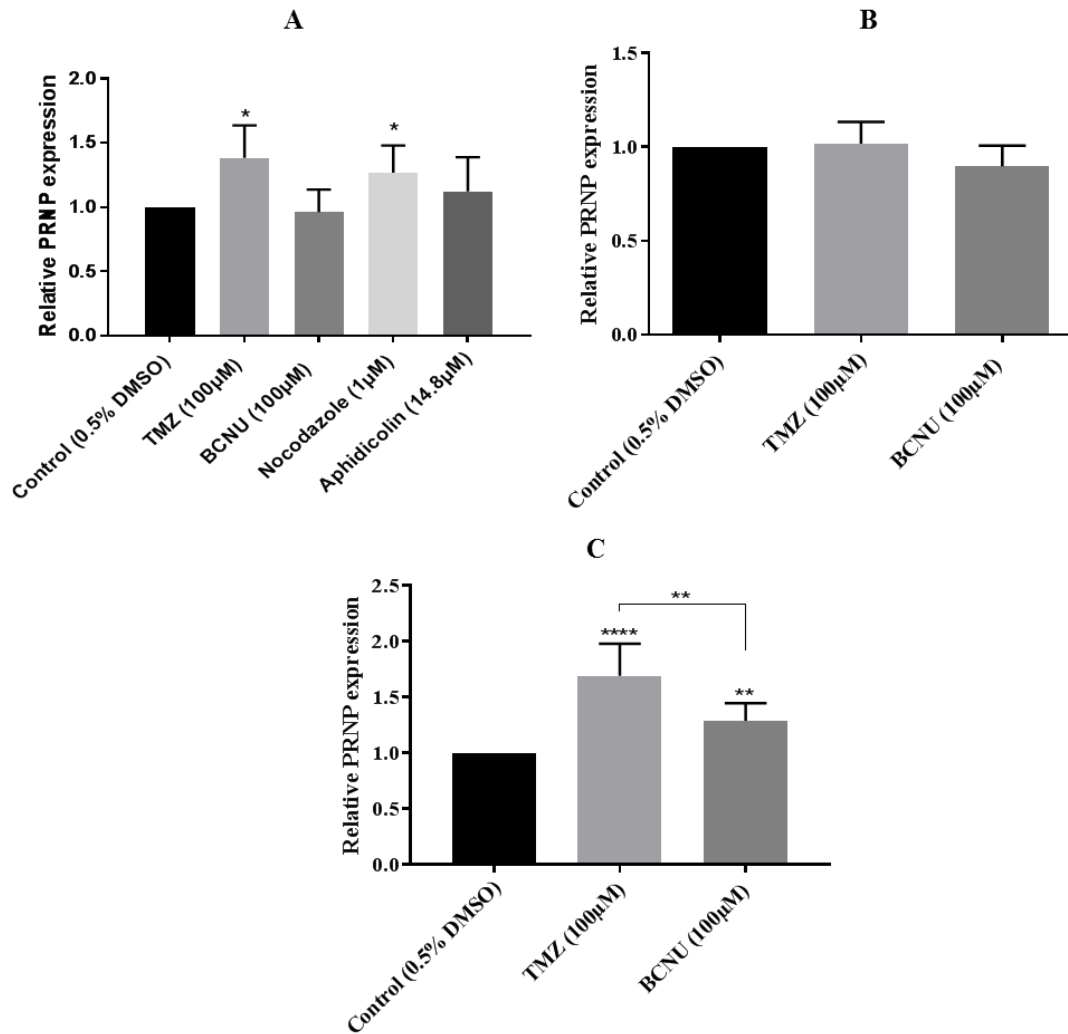


Figure (3-10): PRNP expression in treated U87 cells. mRNA expression of PRNP in cells were treated with synchronising agents and alkylating agents (Experiment 1) (A). mRNA expression of PRNP in cells were cultured with TMZ or BCNU, Experiment 2 (B) and Experiment 3 (C). The expression was measured in comparison to untreated cells as a control using the $2^{-\Delta\Delta C_t}$ method and normalised to the human housekeeping gene GAPDH. The results were performed in triplicate for three independent experiments. The data represents mean \pm SD and were analysed using one-way ANOVA, and Tukey's test ($n=9$, $*=p<0.05$, $**=p<0.01$, $****=p<0.0001$).

3.4.6 PrP^c expression level by Western blotting (Experiment 1, 2 and 3)

Western blot assay was performed to evaluate the PrP^c level in treated cells and to find out the correlation between the gene and protein level in all the experiments mentioned above (section 3.3.5). PrP^c expression was quantified in the U87 cells treated with synchronising agents (Aphidicolin and Nocodazole) or alkylating agents

(TMZ and BCNU) compared to the protein level in untreated cells. A band of ~42 kDa (β -actin) as a loading control was produced by all the treated cells and the control. A clear band of ~35 kDa represents the PrP^c level in treated and untreated cells.

Experiment 1: The band for PrP^c (~35 kDa) in cells treated with alkylating or synchronised agents had the same intensity as with the untreated cells. Thus, there was no significant change in the PrP^c level observed in any of the treated cells (Figure 3-11). The protein expression results in cells treated with TMZ or Nocodazole were therefore inconsistent with the gene expression results for cells treated with these compounds, as indicated in section (3.4.5 Experiment 1). In the case of the gene expression, there was a small bit statistically significant increase in the level of the PRNP gene, but it may be that this was not enough to produce a noticeable change in the protein level.

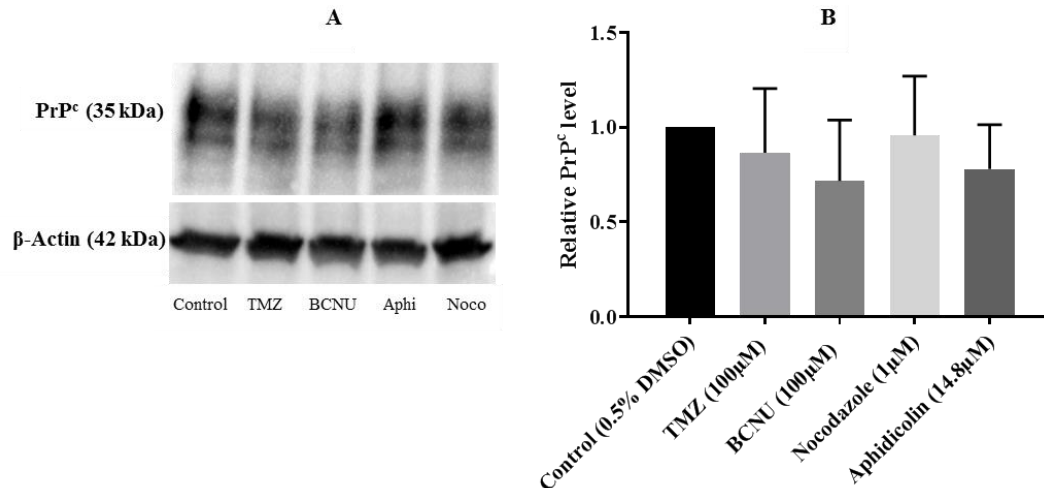


Figure (3-11): Western blotting for PrP^c in U87 cells (**Experiment 1**). Image of the membrane that was exposed to anti-prion antibody 3F4 and reprobred with β -actin as a loading control (**A**). The bar chart represents the mean \pm SD of the control and treated groups (**B**). The data were normalised to the intensity of β -actin and the control group. The results were analysed using one-way ANOVA with Tukey's test for at least three separated experiments (n=3).

In addition, the cells were treated for 24h with TMZ or BCNU (**Experiment 2**) to evaluate the expression of protein. Figure (3-12) shows that the expression of PrP^c

was not affected in the cells treated with TMZ or BCNU. These results were consistent with those for the gene expression.

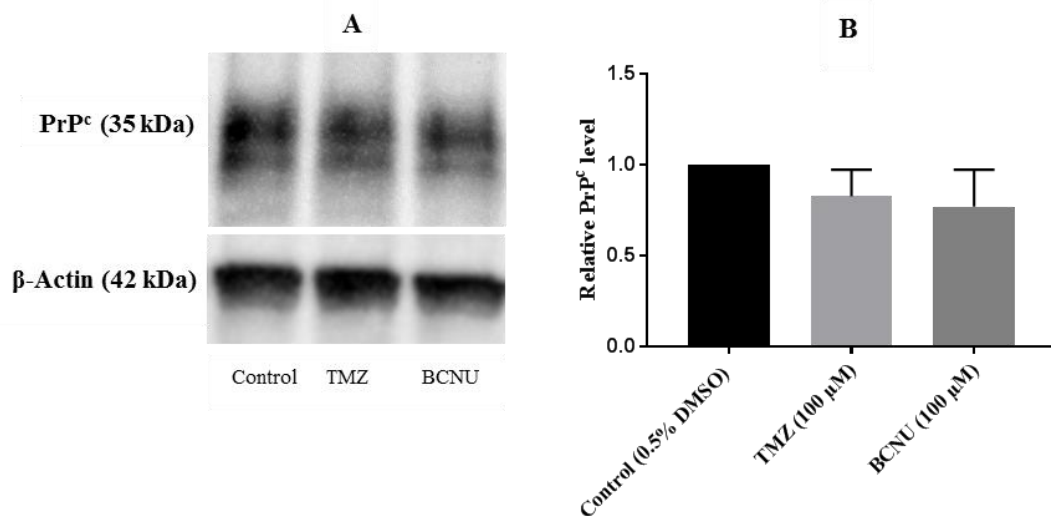


Figure (3-12): Western blotting analysis of PrP^c in U87 cells (**Experiment 2**). The cells were exposed to alkylating agents for 24h. The membrane was probed with 3F4 (PrP) antibody and β-actin as a positive control (**A**). The chart shows the analysis of the protein level in the treated cells (**B**). The data was normalised to the intensity of β-actin and control group and represents mean ± SD. The results were performed in at least three independent experiments and analysed using one-way ANOVA, with Tukey's test (n=3).

The PrP^c level in cells treated with TMZ or BCNU for 24h followed by 48h of incubation post treatment (**Experiment 3**) was also evaluated to determine the effect of a longer dosing period and longer incubation after treatment. The results in [Figure \(3-13\)](#) revealed a significant decrease in the PrP^c level in treated cells compared to the control group. These results were in contrast with the results of the PRNP gene level mentioned above ([Section 3.4.5 Experiment 3](#)), which showed a significant increase in PRNP level. One explanation could be that the transcription of the PRNP gene may be affected due to the G2/M accumulation of U87 cells for a long period. Another possible reason could be that the high expression of PRNP accelerated the degradation of PrP^c.

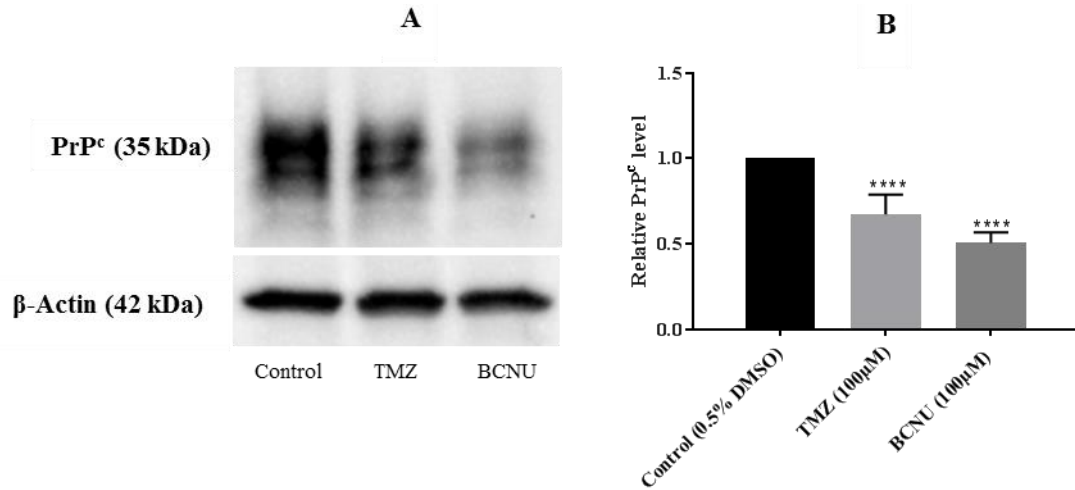


Figure (3-13): Western blotting analysis for PrP^c in U87 cells treated 24+48h with TMZ and BCNU (**Experiment 3**). The PVDF membrane was exposed to 3F4 antibody and reprobred with β-actin as a positive control (**A**). The bar chart shows the comparisons among all tested groups (**B**). The data were normalised to intensity of β-actin and control group. The results represent mean ± SD for at least three independent experiments (n=3). The statistical analysis was carried out using one-way ANOVA with Tukey's test (****=p<0.0001).

3.4.7 Characterisation of PrP^c expression by flow cytometry

Evaluation of PrP^c by flow cytometry was carried out to assess the total PrP^c (cell surface and intracellular) by fixed and permeabilised U87 cells, and cell surface PrP^c, using the live cells in each experiment. This experiment was also carried out to confirm the results of the western blotting.

3.3.7.1. PrP^c expression in treated cells (Experiment 1)

In flow cytometry, the cells were gated as a forward scatter (FSC) and side scatter (SSC) to exclude clumped cells and any cellular debris. In other words, the gates were used to select single cells. The histograms were made from the population of single cells in these gates. The histograms represent the account of single cells/events to standard filter (blue 530-30) i.e. florescent intensity (**Figure 3-14, A and B**). Our results showed that there was no significant effect on PrP^c in treated cells (fixed and

live) relative to the control group (Figure 3-14, C and D). These findings were in agreement with the western blot results.

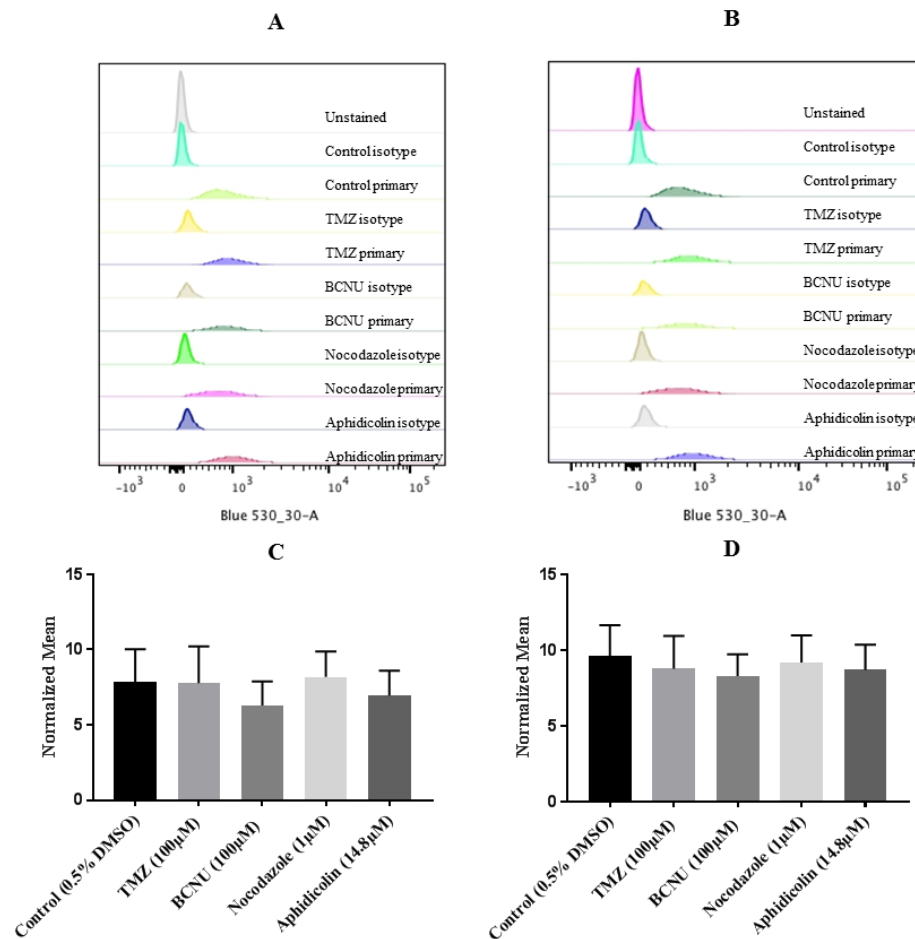


Figure (3-14): The expression of PrP^c in treated U87 cells by flow cytometry (**Experiment 1**). **A** and **B**, PrP^c expression in the gated population is demonstrated in the histograms (live cells and fixed respectively). **C** and **D** represent mean \pm SD for the expression of PrP^c for all samples (live cells and fixed respectively) that were performed in duplicate for at least three experiments and normalised to isotype (n=6). The results were analysed by one-way ANOVA, with Tukey's test.

3.4.7.2 PrP^c level in U87 cells treated with TMZ and BCNU (**Experiment 2**)

To investigate the level of PrP^c in U87 cells treated with alkylating agents over 24h, the cells were treated with 100 μ M of TMZ or BCNU and a flow cytometry assay was carried out. **Figure (3-15, A and B)** revealed the histograms of fluorescent intensity for single cells at a standard filter (blue 530-30). As can be seen, the level of PrP^c in TMZ

or BCNU treated cells was not affected relative to the control group in either experiment for either live or fixed cells (Figure 3-15, C and D respectively). These results were again consistent with the western blotting.

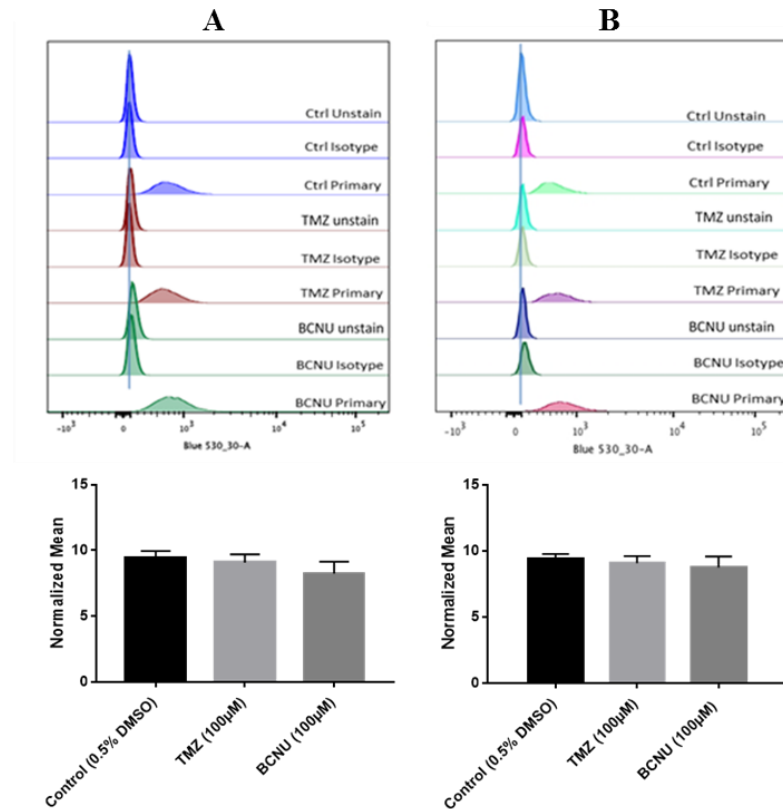


Figure (3-15): PrP^c expression in treated U87 cells by flow cytometry (**Experiment 2**). PrP^c expression in the gated population is represented in the histograms (A and B). The C and D represent mean \pm SD of the normalised expression of PrP^c in all groups (live cells and fixed respectively). These experiments were performed three times, each in duplicate (n=6). The results were analysed by one-way ANOVA, with Tukey's test. The data showed no significant change in protein level.

3.4.7.3 PrP^c level in treated cells with alkylating agents (**Experiment 3**)

To assess the level of PrP^c, the cells were treated with TMZ or BCNU for 24 h and then left to rest for 48h in fresh medium (**Experiment 3**). PrP^c level was determined using flow cytometry in live and fixed cells (Figure 3-16, A and B, respectively). This figure showed the histograms of all groups according to the value of fluorescent intensity. The results of live cells matched those in fixed cells. It is obvious that there

was a significant reduction in PrP^c level in the cells treated with TMZ or BCNU compared to the control group (Figure 3-16, C and D). These observations completely supported the results of the western blot analysis.

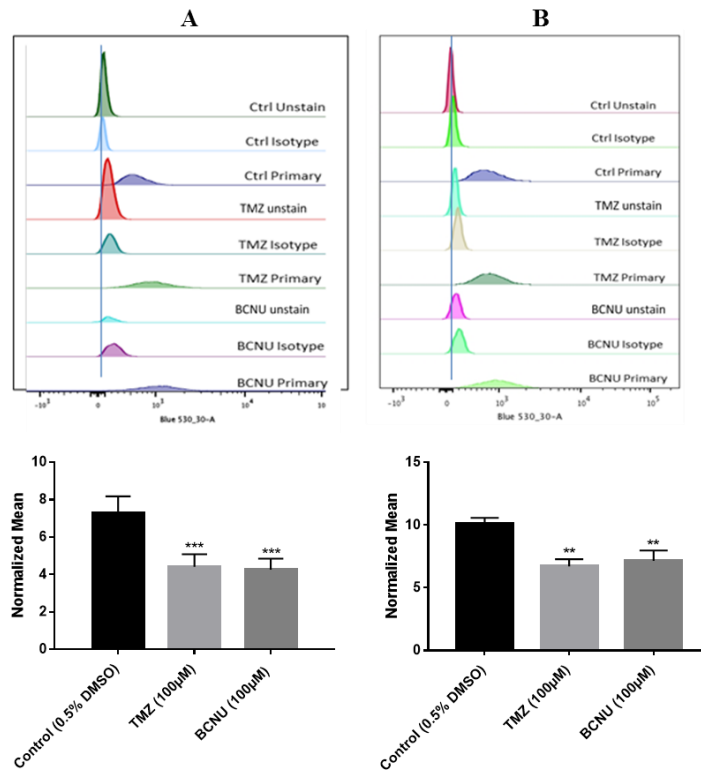


Figure (3-16): PrP^c expression in treated U87 cells by flow cytometry ((**Experiment 2**)). **A** and **B**, PrP^c expression in the gated population is represented in the histograms (live and fixed cells respectively). **C** and **D** represent the expression of PrP^c in treated cells (live and fixed cells respectively). The results reveal mean \pm SD of three independent experiment, each performed in duplicate (n=6). All data were statistically analysed by one-way ANOVA, Tukey's test (**=p<0.01, ***=p<0.001). The results showed significant decreases in protein level in both TMZ and BCNU treated cells.

3.5 Summary of key experimental results

- Aphidicolin and Nocodazole served to accumulate the U87 cells in G1 and G2/M phases, respectively. TMZ and BCNU both arrested the U87 cells in G2/M, but BCNU was more potent in the accumulation of these cells. Resting subsequent to the treatment with TMZ and BCNU increased the number of G2/M cells.
- TMZ and BCNU increased the level of regulatory cell cycle proteins p21 and p53.
- TMZ and Nocodazole arrested the cells in the G2/M phase and increased PRNP gene expression in U87 cells in **Experiment 1** (6h+48h) whereas Aphidicolin (G1 arrest) did not induce PRNP gene expression in these cells.
- In **Experiment 3** (24h+48h) TMZ and BCNU increased the level of the PRNP gene and the downregulated PrP^c level.
- Overall, both alkylating agents (TMZ and BCNU) arrested the U87 cells in G2/M and altered the level of PRNP and PrP^c, while TMZ upregulated the PRNP gene to a higher level than BCNU.

3.6 Discussion

The aim in this chapter was to assess and compare the effect of the common glioblastoma treatments, TMZ and BCNU, on the level of PrP^c using U87 cells as a model for human glioblastoma under the assumption that PrP^c may be upregulated in response to the accumulation at G2/M resulting from these treatments. To achieve this goal, various experiments were carried out, including cell cycle analysis by flow cytometry, the expression of genes by qPCR and protein expression by Western blot and flow cytometry.

The growth profile of U87 glioblastoma cells was investigated to determine the population of cells over time. The doubling time of these cells was approximately 30h, which is close to ATCC protocol reported value (34h). This growth curve also showed that the U87 cells used in this study were in the growth phase, and the data was used to estimate the seeding density in subsequent experiments (Figure 3-2). The cell viability assay was performed to determine the proportion of viable cells upon exposure to different agents or treatments. For all treatments used, MTT assay data showed that all the reagents or treatments did not reduce the cell viability at tested concentrations, except for Nocodazole at a higher concentration of 1 μ M (Figures 3-3, 3-4 and 3-5). Most concentrations of treatments (Aphidicolin, Nocodazole²¹⁸, TMZ^{6,202} and BCNU²⁰²) chosen in this study were guided by previous studies.

To develop the assay, optimise experimental conditions and make data comparable with known cell cycle arresting agents, the cells were treated with Aphidicolin or Nocodazole. The reason for synchronising cells using Aphidicolin and Nocodazole was to validate the data that resulted from TMZ and BCNU by flow cytometry measurement and to produce a model of the G1 and G2/M cells which was then used

to compare the expression of PrP^c in those cells and the TMZ- or BCNU-arrested cells. Several studies have revealed that Aphidicolin arrests mammalian cells in the G1 phase²²² and it is known that it can inhibit B-family DNA polymerases and then suppress DNA replication in eukaryotic cells²²⁰. The current study showed that 14.8 μ M of Aphidicolin over 24h can arrest U87 cells in G1 by approximately 84% (Figure 3-6 B). Nocodazole, as an antineoplastic agent, also has an effective role in cell cycle synchronisation. It can arrest most cells in G2/M by binding to tubulins and microtubules. Nocodazole disrupts the formation of the microtubule in the cell, thereby suppressing cell cycle progression²²³. Our work revealed that 1 μ M of Nocodazole arrested 80% of U87 cells in G2/M after 24h (Figure 3-6 C).

In untreated U87 cells, the population of cells distributed in G1, S and G2/M was 69%, 8%, and 22% respectively. This distribution was changed when the cells were treated with TMZ or BCNU. Our results showed that TMZ and BCNU arrested the cells in G2/M in a time-dependent manner. U87 cells were starting to lose 2N content (G1 cells) after 12h treatment with TMZ or BCNU (Figures 3-8, A and B). Indeed, the cell cycle population was slightly affected in cells that were exposed to TMZ for 12h and 24h, and gradually increased in a similar trend over the same treatment regime as BCNU in comparison to untreated cells. In addition, BCNU had more profound effects in arresting cells in G2/M than TMZ at 12h, 24h, 6h+24h and 12h+24h (Figure 3-8, C).

These results regarding TMZ are in agreement with what Hirose *et al.* reported when they found that TMZ arrested U87 cells in G2/M. They treated these cells for 3h and then left them in fresh media without treatment for 1 to 10 days, and found that the cells began to accumulate in G2/M after day 1²²⁴.

The BCNU treated cells in our study started to lose some 2N contents (G1 phase) when treated for 12h. The G2/M population was significantly increased in a time-dependent manner, particularly after the incubation of BCNU treated cells with fresh medium for 24h and 48h. Wei Xu *et al.* stated that U87 cells started to accumulate in S and G2/M after treating for 12h and rest 24h but the accumulation in G2/M was increased after 48h as a result of the upregulating of p53 and p21 proteins²⁰². Our results showed that the cells arrested in G2/M recorded a greater increase when treated for 6h, 12h and 24h with 24h and 48h incubation without TMZ or BCNU. This could be attributed to the accumulation of p53 and p21, which regulate the cell cycle, resulting from DNA damage by TMZ or BCNU. Our western blot results showed that the level of p53 and p21 was significantly increased in cells treated with TMZ or BCNU (24h+48h, **Experiment 3**). TMZ also upregulated the p21 level approximately three-fold, whereas BCNU increased the level of p21 approximately four-fold. Regarding p53, TMZ and BCNU induced the level of this protein by around 2 and 1.5 folds respectively (**Figure 3-9**). In respect to p21 and p53 in BCNU treated U87 cells, our results are in agreement with previous findings, albeit with some variations. Xu *et al.* found that BCNU at 12h+48h increased the level of p21 and p53 about ten and five-fold respectively²⁰². On the other hand, p21 and p53 in TMZ-treated cells increased about 3.6- and 2-fold at 3h+48h,²²⁴ and these results generally agreed with our results, with some variations. These variations could be ascribed to the differences in the period of treatments or to experimental techniques.

Since PrP^c has been shown to be involved in many apoptotic pathways due to its interaction with some proapoptotic molecules¹⁸⁴, it has generally been found that PRNP levels increase in different types of glioblastoma cell lines⁵. Resistance to anti-cancer therapy arises for various reasons²²⁵ but the arrest of glioblastoma cells in

G2/M by TMZ has been shown to be involved in the resistance to the treatments. We aimed to determine whether PRNP or PrP^c expressions were affected by TMZ or BCNU as common treatments for glioblastoma, examining this across different time points and cell cycle phases. In this work, PRNP expression was evaluated in U87 cells treated with synchronising agents (Aphidicolin or Nocodazole) and alkylating agents (TMZ or BCNU). The results showed that the mRNA expression of PrP^c was not affected in **Experiment 1 and 2**, except that it significantly increased following treatment with TMZ, and likewise with Nocodazole (**Experiment 1**). Cells synchronised in the G1 phase by Aphidicolin revealed no significant changes in gene expression compared to the control group, however (**Experiment 1**). Furthermore, the PRNP gene was significantly upregulated in **Experiment 3** (24h+48h) compared to the control group. TMZ was found to increase PRNP expression more than BCNU. This could be related to the high impact of TMZ on p53 induction, possibly as a result of TMZ-induced DNA damage, as shown in section (3.4.4). PrP^c may protect the tumour cells from pro-apoptotic stimuli such as chemotherapy and DNA damage¹⁸⁴. It is possible, therefore, that high induction of PRNP in TMZ treated cells may be stimulated to protect the cells from the damage caused by these treatments. In general, the sharp increase of PRNP in TMZ or BCNU treated cells may be attributed to the arrest of the cells in the G2/M phase. Zhuang *et al.* found via array hybridisation assay that alterations in the distribution of the cell population from G1/S to G2/M changed the expression of many genes and PRNP most of all. In addition, they also demonstrated that PRNP was downregulated in the arrested cells in the G1 phase,⁶ a finding that was in contrast with our result concerning Aphidicolin treated cells (G1 cells). There are no previous studies that have used qPCR to document PRNP expression in cells treated with alkylating and synchronising agents, however.

Unexpectedly, our results showed that the PrP^c expression level was incompatible with the PRNP gene level in the treated U87 cells. In both western blot and flow cytometry assay results TMZ and BCNU significantly downregulated PrP^c expression; the opposite to their effect on the PRNP level. Few studies have investigated the level of PrP^c and its gene in alkylating agents, however. According to Zhuang *et al.*, PrP^c was highly expressed in U87 cell lines which were arrested in the G2/M phase by TMZ or Nocodazole. They evaluated this protein-based upon Nocodazole (as a synchronising agent in the G2/M phase), Aphidicolin (arresting cells in the G1/S phase) and TMZ (alkylating agent 6h and 48h post-treatment). They suggested that PrP^c is upregulated when the cells accumulate in G2/M, particularly with TMZ (6h and 48h post-treatment), whereas PrP^c is downregulated in U87 cells synchronised at G1 phase⁶. Under the same conditions, however, our results showed a different trend. Regarding alkylating agents (TMZ and BCNU) (6h+48h) and synchronising agents 24h (**Experiment 1**), the western blot and FACS assay revealed that the protein level remained unchanged. In addition, the results for PrP^c level with TMZ and Nocodazole (**Experiment 1**) were inconsistent with the results for PRNP gene expression in TMZ or Nocodazole treated cells, as seen in [Section \(3.4.5 Experiment 1\)](#). This may be attributed to the fact that the increase in the PRNP gene level was only slight and may have been insufficient to induce any remarkable increase in the PrP^c protein level. To our knowledge, this is the first study which has evaluated the effects of BCNU and TMZ treatment on the expression of PrP^c at different time points. Furthermore, 24h with TMZ or BCNU treatment, followed by 48h resting (**Experiment 3**), resulted in one of the highest populations of cells accumulated in the G2/M phase. The level of PrP^c at this time point, however, was less than with the untreated control group, according to the western blot and FACS

results. This was despite the fact that qPCR showed an increase in PRNP gene levels compared to the control group. There may be several reasons for the observed result, none of which are obvious or strongly supported by the literature. One possible explanation could be that the lengthy treatment accumulation of the U87 cells at the G2/M phase may have affected the transcription of the PRNP gene. Another potential explanation could be that the high expression of PRNP may have accelerated degradation of PrP^c. A more farfetched explanation could be that treatment led to increased levels of other genes which were competing with the PRNP gene in translation.

To conclude, TMZ and BCNU accumulate the U87 cells in G2/M, particularly after incubation in fresh medium subsequent to the treatment. BCNU was more potent in the accumulation of U87 cells at G2/M. The accumulation of cells in G2/M by TMZ or BCNU led to an increase in the level of p53 and p21. The PRNP gene level was upregulated in TMZ and Nocodazole treated cells (6h+24h and 24h respectively) whereas Aphidicolin, which arrests the cells in G1, did not affect this gene. The PRNP gene level was also upregulated in TMZ and BCNU treated cells (24h+48h), but the induction of the PRNP gene in TMZ treated cells was higher than with BCNU treated cells. This may be due to the cytoprotective effect of PrP^c, suggested by previous studies. Interestingly, the protein level at this time point was downregulated. It would be interesting, therefore, to address the effect of alkylating agents TMZ and BCNU on the cellular behaviour of U87 cells, and their response by knocking down PRNP gene expression.

Chapter 4: Silencing of PRNP inhibits the proliferation of U87 cells

4.1 Introduction

Although several lines of research have demonstrated that PrP^c is involved in many cellular processes such as apoptosis and cell proliferation, its exact physiological function remains unclear³, and even in respect to proliferation and apoptosis, the exact function of PrP^c in the cell is controversial and appears to depend on the cell type. For example, overexpression of PrP^c has been shown to enhance the proliferation of mouse neuroblastoma cells¹³⁴, colon adenocarcinoma²²⁶ and stem cells of glioblastoma¹⁴⁰ whilst knockout of PrP^c induced the growth of oligodendrocyte¹⁴¹ and embryonic hippocampus cells¹⁴². Furthermore, the silencing of PrP^c in gastric carcinoma cells (AGS) reduced cell proliferation and induced apoptosis through induction of Bax and p53²²⁷, whereas cell growth and apoptosis mediated by Bax and p53 were not observed in PRNP knockdown cells, HT29 colorectal cancer cells²²⁸. p53 as tumour suppressor protein contributes to DNA repair or induces apoptosis by its downstream effect on Bax^{37,229}.

The impact on treated and untreated glioblastoma cells of knocking down PrP^c is still unclear. In untreated cells, silencing of PrP^c by PRNP antisense in T98G glioblastoma cells has been shown to have a remarkable effect on apoptosis by increasing the apoptotic factors such as caspase3/7 and p53¹⁸⁵. It was also found that silencing PrP^c reduced the growth of glioblastoma tumours in mice¹⁸⁴. In a separate study, knocking down PRNP in J889 human glioblastoma cells reduced cell proliferation and induced apoptosis via induction of caspase 3 activity¹⁸⁵. Various other studies have shown that silencing of PrP^c reduces the resistance to chemotherapy in gastric, colon and breast cancer cells^{168,228,153}. To the best of our knowledge, the effect of knockdown PrP^c on cell proliferation, apoptosis and cell resistance to TMZ and BCNU chemotherapies in

glioblastoma cells has not yet been studied. We hypothesise that the silencing of PrP^c may inhibit the proliferation of U87 cells and reduce their resistance to alkylating agents. The effect of PRNP knockdown on proliferation, apoptosis and the cell cycle will therefore be evaluated in this chapter in respect to both treated and untreated U87 cells.

4.1 The aim

This chapter aims to study the effect of PRNP knockdown on the proliferation and apoptosis of U87 cells treated with alkylating agents, based on the assumption that it might inhibit cell resistance to these treatments. To achieve this aim, the following objectives will be carried out.

- Knockdown of the PRNP gene in U87 cells using PRNP siRNA which has been produced by DharmaFect. RT-qPCR (gene level), FACS, western blot and immunocytochemistry (protein level) techniques will be used to confirm the knockdown in these cells.
- Evaluation of cell proliferation of the PrP^c silenced U87 cells using MTT and Alamar blue assay, and proliferation marker ki67 using immunocytochemistry (ICC).
- Investigation of the effect of PRNP knockdown on cell apoptosis using Annexin V with PI assay.
- Assessing the response of knockdown cells to TMZ and BCNU using MTT assay.
- Evaluation of the cell cycle for treated knockdown U87 cells with and without alkylating agents.

- Quantification of cell cycle regulatory proteins p53 and p21 in knockdown cells treated with TMZ or BCNU, as well as in untreated cells.

4.2. Methods

4.2.1. Cell proliferation and viability MTT assay

To determine cell proliferation and/or viability, U87 cells were cultured in 96-well plates. The plates were left overnight in the incubator to allow the cells to attach. The next day, transfection reagents, which were prepared as described in chapter 2 (section 2.2.9), were added to each well. The actual transfection reagents used (DharmaFect and siRNA) were different depending on the incubation time and cell density according to the manufacturer's instructions, as shown in the table below (Table 4-1).

At the end of the incubation time, the MTT assay protocol (section 2.2.2) was followed to quantify the viability of cells.

Table (4-1): Cell density and the volume of transfection reagents in the proliferation and viability assay

Incubation time	Cell density	DharmaFect (μl)	5μM PRNP siRNA (μl)	5μM (μl) Scramble siRNA (μl)
24 h	5000	0.08	1	
24 h	5000	0.08		1
48 h	4000	0.064	1	
48 h	4000	0.064		1
3 days	3000	0.048	1	
3 days	3000	0.048		1
4 days	2000	0.032	1	
4 days	2000	0.032		1
5 days	1000	0.016	1	
5 days	1000	0.016		1

4.2.2. RT-qPCR

In order to quantify the expression of the PRNP gene in transfected U87 cells, the cells were cultured in 6-well plates overnight and then the medium was removed. Transfection reagents were prepared following the instructions in [section \(2.2.9\)](#) and these were added as described below ([Table 4-2](#)). Fresh medium was added to obtain a total volume of 1500 μ l.

Table (4-2): Cell density and the volume of transfection reagents used at each time point to determine the PRNP level.

Incubation time	Cell density	DharmaFect (μ l)	5 μ M PRNP siRNA (μ l)	5 μ M Scramble siRNA (μ l)
24 h	200000	3.2	40	
24 h	200000	3.2		40
48 h	100000	1.6	40	
48 h	100000	1.6		40

After 24 h or 48 h of incubation with transfection reagents, the total RNA was extracted from the cells using the PureLink RNA Mini kit (Ambion Life Technologies) ([section 2.2.4.1](#)). RNA extractions were normalised using RNase-free water, and then 1-6 μ l of RNA extract was used to synthesise cDNA according to the protocol described in [section \(2.2.4.2\)](#). PRNP gene expression was quantified using the PowerUpTM SYBRTM Green Master Mix system (Applied Biosystem) and the primers that were described in [section \(2.2.4.3\)](#).

4.2.3. PrP^c expression by flow cytometry

PrP^c expression in knockdown cells was determined using flow cytometry after 48 h and five days as recommended by DharmaFECTTM Transfection Reagents-siRNA transfection protocol. The cells were cultured in a T25 flask at a cell density of 5×10^5

and 1×10^5 for 48 h and five days respectively. The next day, the medium was aspirated, and the transfection reagents were prepared following the instructions in [section \(2.2.9\)](#) where three millilitres of the total volume of PRNP and scrambled siRNA were prepared and added to their corresponding flasks. Fresh medium was added to another flask as a control. After the desired incubation time, all flasks (control, PRNP siRNA and scrambled siRNA) were washed with PBS, and then the flow cytometry protocol was followed ([see section 2.2.6](#)) to assess the level of PrP^c.

4.2.4. PrP^c, p53 and p21 expressions by western blot

Western blotting assay was used to evaluate the PrP^c expression level in transfected U87 cells and to confirm the results of flow cytometry. The cells were seeded in a T25 flask at a cell density of 5×10^5 , 2×10^5 and 1×10^5 for 48h, three days and five days respectively. This step was followed by treating the cells with transfection reagents as described in [section \(2.2.9\)](#) where the volume of scrambled and PRNP siRNA reagents were added, and a total volume of 3 ml was obtained. At the end of the incubation period, the western blotting procedure in [section \(2.2.5\)](#) was performed to quantify the level of PrP^c.

Western blotting assay was also used to evaluate the level of p53 and p21 in transfected cells. The cells were first treated for three days with transfection reagents and then treated for 48 h with 100 μ M of TMZ or BCNU. The control group was treated with 0.5% of DMSO alone for five days (three days + 48 h). The western blotting assay, as described in [section \(2.2.5\)](#) was carried out to quantify the level of p53 and p21. The dilution factor for primary antibodies of p53 and p21 was 1:500 in blocking solution (5% milk in TBS-T), as recommended in the protocol published by Santa Cruz Biotechnology. The horseradish antibody (secondary antibody) was probed at 1:4000 in TBS-T.

4.2.5. Proliferation assay using Alamar Blue

Alamar blue assay was used to quantify the proliferation of transfected cells at different time points (between one and five days) in order to validate the results of the MTT assay. The cells were cultured in a 24-well plate as shown in [figure \(4-1\)](#). In the figure, the columns 1, 2, 3 and 4 represent the blank (without cells), control (untransfected cells), scrambled and PRNP siRNA, respectively. One 24-well plate was used for each time point. The table below [\(4-3\)](#) shows the cell densities and transfection reagents used for all time points. After 24 h, the transfection reagents were prepared in 500 μ l medium as described in [section \(2.2.9\)](#) and then added to the cells. The blank and control wells were left without treatment, and 500 μ l of fresh medium was added to each well. Alamar blue protocol in [section \(2.2.11\)](#) was followed to quantify cell viability after the desired incubation time.

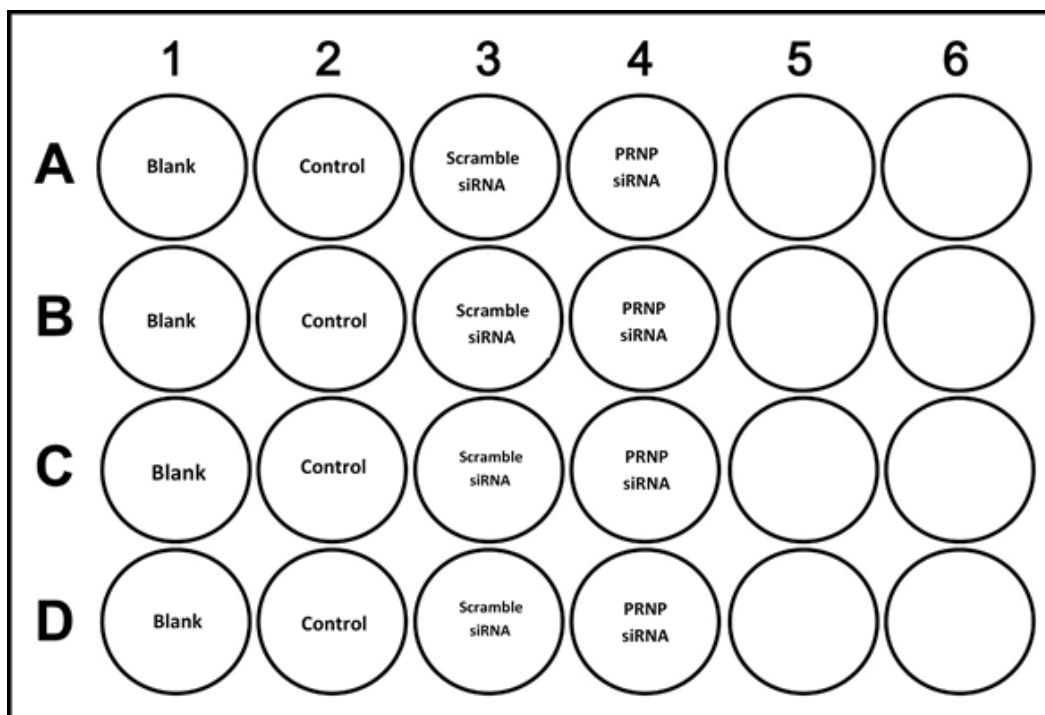


Figure (4-1): The design of Alamar blue experiment.

Table (4-3): A summary of the cell densities and transfection reagents for all incubation periods in the Alamar blue assay

Plate Number	Incubation time	Cell density in each well	DharmaFect (μ l)	5 μ M Scramble or PRNP siRNA (μ l)
1	24 h	30000	0.48	5
2	48 h	20000	0.32	5
3	3 days	10000	0.16	5
4	4 days	7500	0.12	5
5	5 days	5000	0.08	5

4.2.6. Cytotoxicity LDH assay

LDH assay was performed to evaluate the toxicity of transfection reagents on U87 cells over the course of five days. This experiment was conducted to ensure that any reduction in proliferation did in fact result from the knockdown of the PRNP gene and not from toxicity due to the transfection reagents. The cells were cultured in five 96-well plates at 1500 cells per well. The figure below (Figure 4-2) shows the design of this experiment. The transfection reagents were prepared according to the protocol mentioned in section (2.2.9). The LDH assay protocol was applied (see section 2.2.10) to collect the data each day.

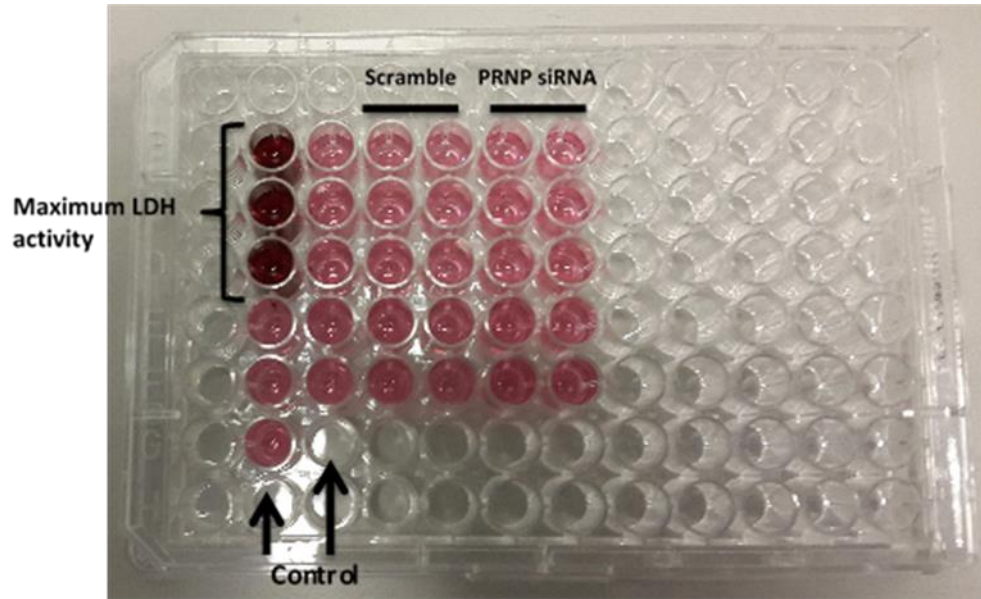


Figure (4-2): The experimental design for LDH assay. The cultured cells were divided into four groups Maximum LDH activity, Control, Scramble and PRNP siRNA.

4.2.7. Immunocytochemistry (ICC) by confocal microscopy

ICC assay was used to investigate the PrP^c and ki67 proteins in transfected U87 cells. The cells were cultured onto sterile coverslips which were previously mounted in a 24-well plate as mentioned in [section \(2.2.7\)](#). ICC for PrP^c expression in transfected cells was evaluated here to validate the results of FACS and western blotting. The cells were seeded and transfected as in [table \(4-3\)](#) above for two days (48 h) and five days, respectively. Ki67 was assessed in knockdown cells, both treated and untreated with TMZ, in order to investigate the proliferation of these cells. To evaluate if the cells were positive for ki67, the cells treated with transfection reagent for five days as described in [table \(4-3\)](#) above. During the incubation, 100 μ M of TMZ (25 μ l of 20 mM stock solution to each well) were added at day 3, and the plate was then left for 48 h. Later, the protocol for ICC using confocal microscopy was followed to image the coverslips, as described in [section \(2.2.7\)](#).

4.2.8. Apoptosis assay by Annexin V with PI

The apoptosis assay was carried out in order to evaluate the apoptotic cells in the transfection reagents. The cells were seeded in a 6-well plate at a seeding density of 25×10^3 cells per well. The next day, the cells were treated with transfection reagents as described in [section \(2.2.9\)](#) and incubated for five days. The Annexin V protocol ([see section 2.2.3](#)) was applied in order to quantify the rate of apoptosis.

4.2.9. Cell cycle assay by flow cytometry

The population of TMZ treated and untreated knockdown cells in each cell cycle phase was assessed by flow cytometry. The cells were cultured in a 6-well plate at a seeding density of 25×10^3 cells per well. The following day, the cells were treated with transfection reagents as described in [section \(2.2.9\)](#) and then incubated for five days. In this experiment, the samples were grouped as a control, PRNP siRNA, scrambled siRNA, control/TMZ, PRNP siRNA/TMZ and scrambled/TMZ. The control/TMZ, PRNP siRNA/TMZ and scrambled/TMZ samples were treated with 100 μ M of TMZ (25 μ l of 20 mM stock solution to each well) on day 3, then left for 48 h. Later, all samples were washed, and the protocol for cell cycle analysis ([see section 2.2.3](#)) was followed in order to assess the cell cycle in each phase.

4.3 Results

4.3.1 Assessment of U87 cell viability in PRNP siRNA and Dharmafect reagents

According to the recommendations in the DharmaFect protocol, at least 80% of the cells in the transfection reagents should be viable if transfection is to be successful. To validate the effect of siRNA and DharmaFect reagents on U87 cells, the cells were treated with the recommended concentrations: 0.1 μ l/5000 cells of DharmaFect reagent and 25 nM siRNA **Figure (4-3 A)**. The results showed that 0.1 μ l of the DharmaFect reagent with 25 nM siRNA reduced cell viability to around 62% after 48 h. It was therefore necessary to optimise the viability of the U87 cells by testing different concentrations of DharmaFect reagent and siRNA over a period of 48 h so as to obtain the best concentration of these reagents. **Figure (4-3 B)** revealed that 0.05, 0.06 or 0.08 μ l with 25 or 50 nM siRNA recorded cell viability of more than 80%. There was also no significant change in cell viability (around 80%) between 50 nM scrambled siRNA (NON-TARGET) and 50 nM PRNP siRNA (ON-TARGET) over the 48 hours **(Figure 4-3 C)**. To achieve the maximum knockdown effect, 0.08 μ l DharmaFect reagent with 50 nM siRNA was used to transfect U87 cells.

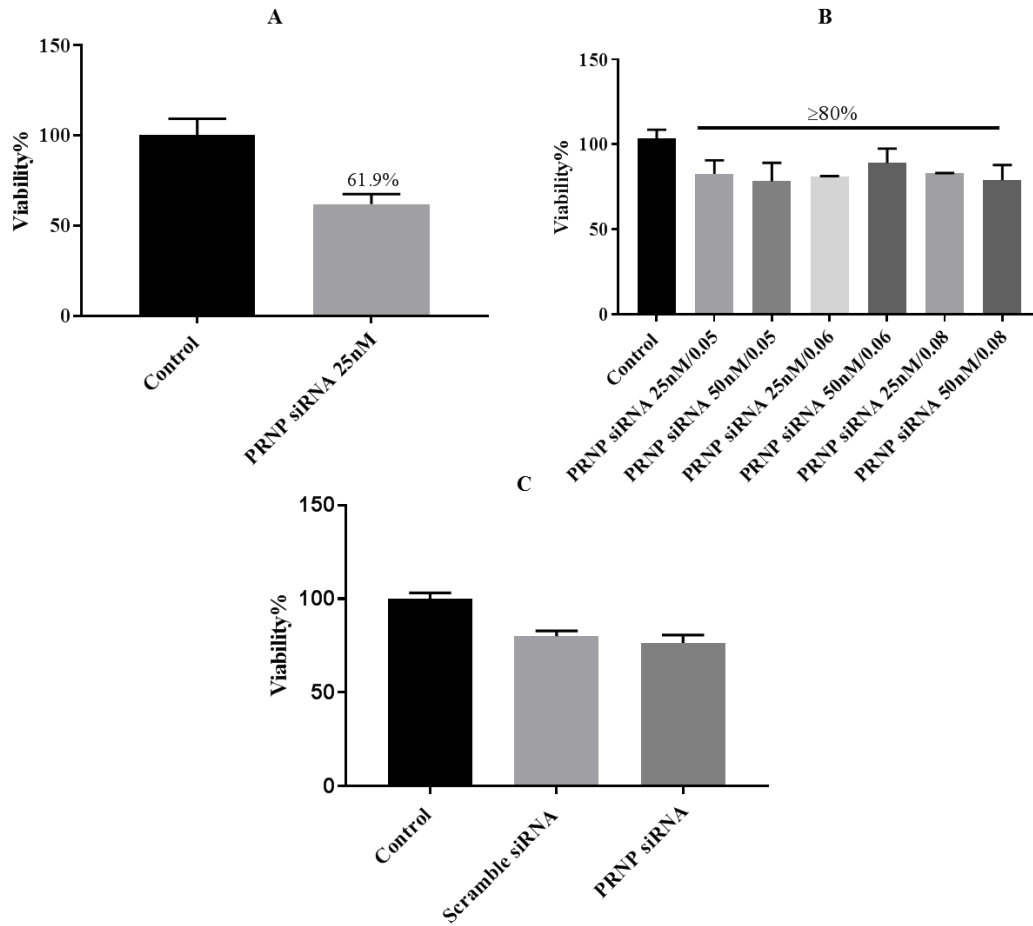


Figure (4-3): Quantification of cell viability in transfected U87 cells using MTT assay. **A**, the bar chart shows the viability in transfected cells with 25 nM siRNA and 0.1 μ l/5000 cells DarmaFect reagent for 48 h. **B**, the chart reveals the viability of cells in the serial concentrations of siRNA/DarmaFect (25 nM/0.05, 50 nM/0.05, 25 nM/0.06, 50 nM/0.06, 25 nM/0.08 and 25 nM/0.08). **C**, the chart shows that 50 nM scrambled and PRNP siRNA with 0.08 μ l/5000 cells DarmaFect exhibits cell viability around 80%. These data represent mean \pm SD of three independent experiments and each experiment was performed in six wells (n=18).

4.3.2 The effectiveness of PRNP gene knockdown in transfected cells

To assess the efficiency of PRNP gene knockdown in transfected U87 cells, the cells were treated with the transfection reagent for 24 h and 48 h, as recommended by the DarmaFect protocol, followed by qPCR analysis. The bar charts below (Figure 4-4) illustrate the level of the PRNP gene in the transfected and control groups. Gene expression decreased by approximately 90% and 86% in knockdown cells compared to the control group at 24 h and 48 h, respectively (Figure 4-4).

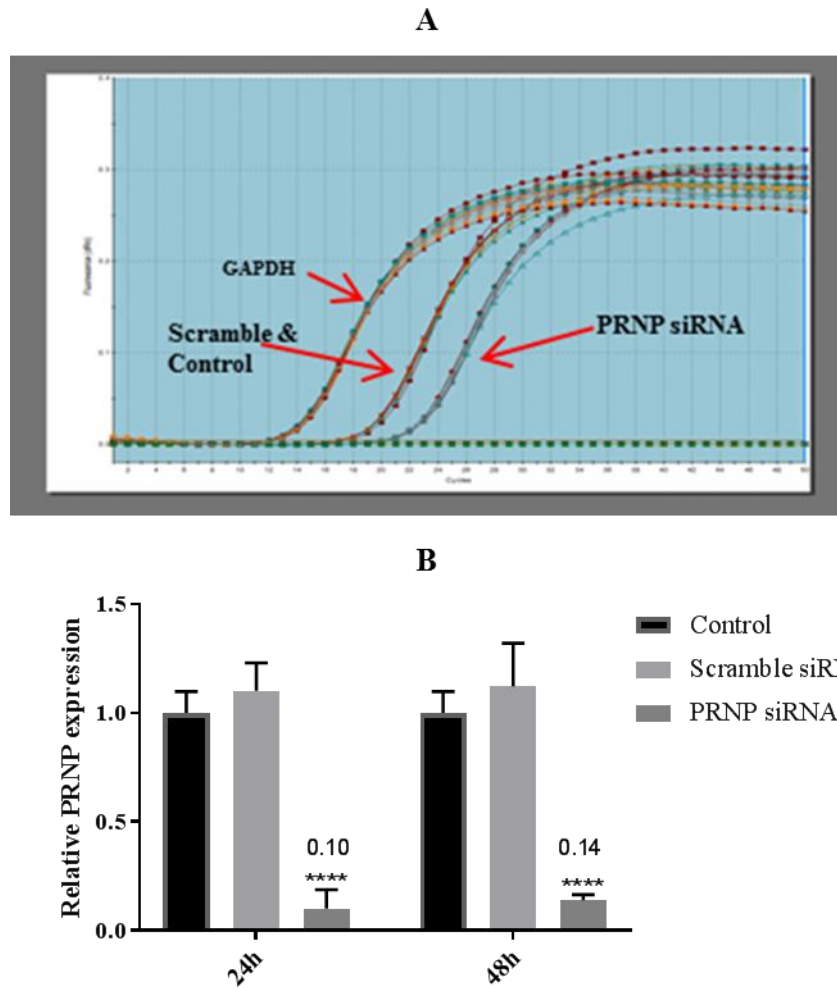


Figure (4-4): Relative PRNP gene expression in transfected and non-transfected U87 cells. Amplification plot for the cDNA of three samples was quantified using qPCR (**A**). Expression of the PRNP gene in transfected cells with siRNA reagents for 24 h and 48 h (**B**). The expression was measured in comparison to the control group using the $2^{-\Delta\Delta C_t}$ method and normalised to human housekeeping gene GAPDH. The results represent mean \pm SD of three separate experiments, each performed in triplicate (n=9) (****=p<0.001).

4.3.3 PrP^c expression in knockdown cells

To ensure that subsequent experiments obtained the largest reduction of PrP^c protein expression in the transfected cells, the level of PrP^c in knockdown cells was examined at different time points (two, three and five days) by flow cytometry, western blot and ICC by confocal microscopy.

4.3.3.1 PrP^c expression in transfected cells by Flow cytometry

To quantify the level of PrP^c in the knockdown U87 cells, the cells were transfected for two and five days and then flow cytometry assay was performed. The level of the protein was found to have declined by around 80% in cells treated with PRNP siRNA in comparison with scrambled and untreated cells, while the percentage of positive cells in PRNP siRNA (i.e. cells with PrP^c expression) decreased to 23% after 48 h (Figure 4-5 Day 2). In addition, the protein level was assessed after five days using flow cytometry. The protein level of each sample was normalised to the comparable isotype and the percentage of positive cells in each sample was calculated as a percentage to the control. Figure (4-5 Day 5) illustrates that the protein level remaining decrease by about 83% and the positive cells were around 20% compared to control, the level of protein in scramble cells was decreased in day 5 when compared with the control group.

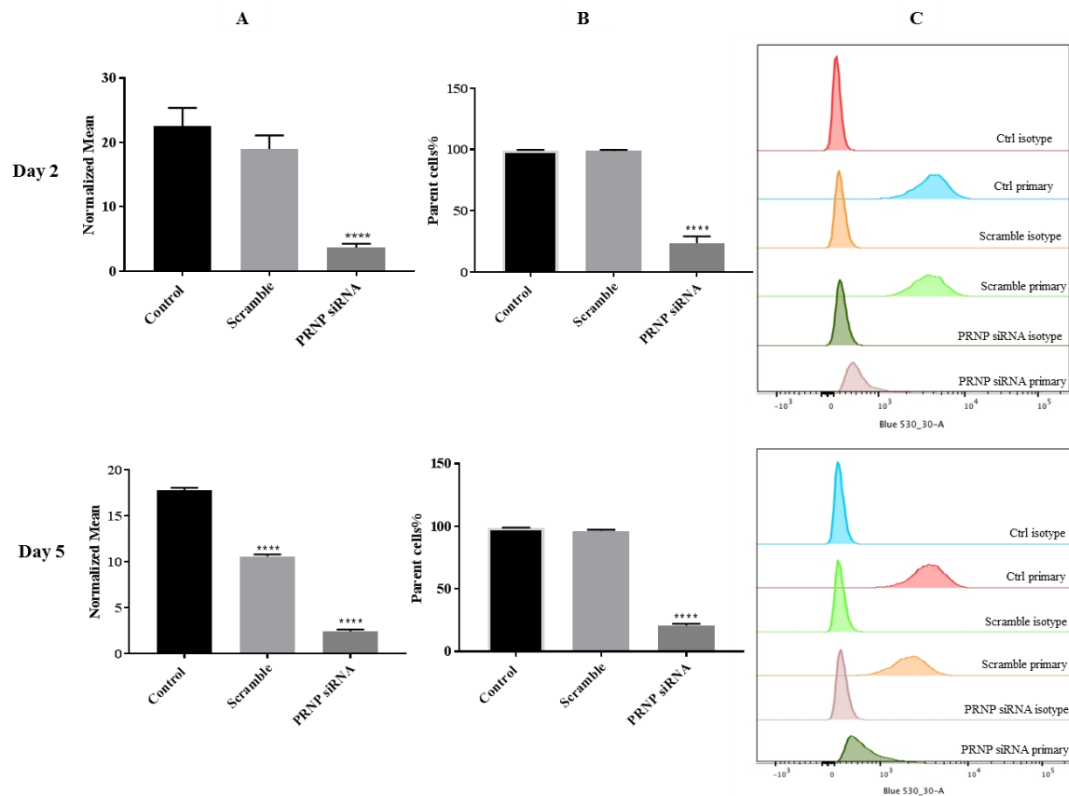


Figure (4-5) Expressions of PrP^c in transfected U87 cell according to flow cytometry. The level of PrP^c and percentage of positive parent cells both decreased in PRNP siRNA cells (after two and five days) (A) and (B) respectively. The histograms showed the cell number and fluorescent intensity of all samples (C). The data represents mean \pm SD of three different experiments, each performed in duplicate (n=6). The data was statistically analysed using t-test (****=p<0.001).

4.3.3.2 PrP^c expression in transfected cells by Western blot and ICC

To further confirm the results of PrP^c expression in knockdown cells, western blot and confocal microscopy were carried out for untreated, scrambled and PRNP siRNA cells. As can be seen in [Figure \(4-6 A\)](#), the PrP^c level was significantly decreased in PRNP siRNA cells compared to the control and scrambled cells on days 2, 3 and 5. The PrP^c level in knockdown cells was significantly decreased on days 2 and 3 relatives to the scrambled and untreated cells, by $79\% \pm 7\%$ and $81\% \pm 3\%$, respectively. On day 5, the protein level was also significantly reduced relative to untreated cells, while the protein level in the scrambled cells was slightly decreased compared to the control (untreated cells). In addition, ICC images showed that the

PrP^c level in PRNP siRNA cells declined on days 2 and 5 in comparison to the control and scrambled cells. It can be seen that the intensity of PrP^c (green colour) was reduced in knockdown cells relative to the scrambled and control groups (Figure 4-6, B and C).

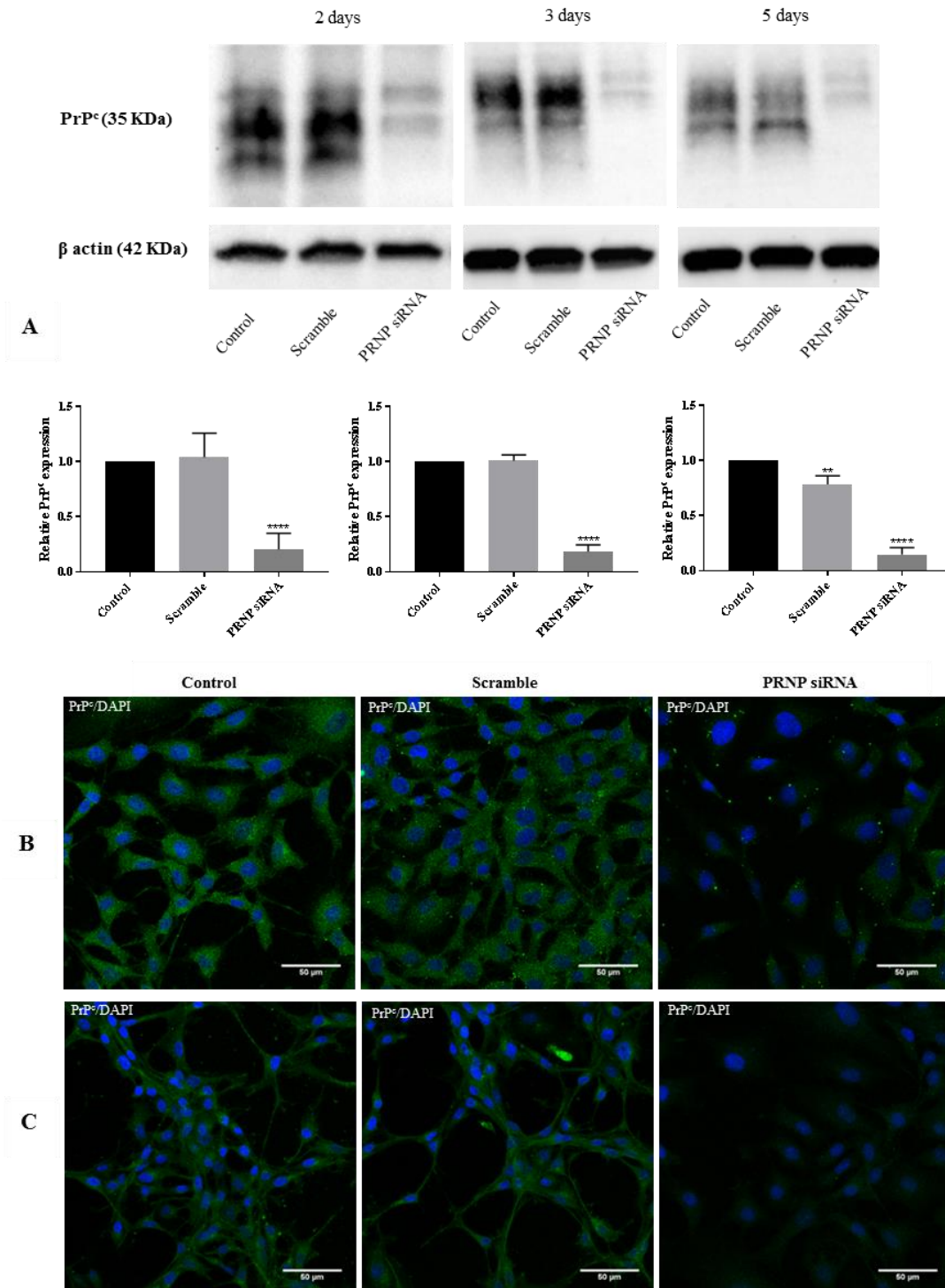


Figure: (4-6) Expressions of PrP^c in transfected U87 cells. According to western blot analysis, the level of PrP^c decreased in PRNP siRNA cells (2, 3 and 5 days), the data were normalised to the intensity of β -actin and the control group (A). Confocal microscopy images show the expression of PrP^c in control, scrambled and PRNP siRNA cells after two days (B) and five days (C). The western blot results represent mean \pm SD of three independent experiments (n=3) (**=p<0.01, ****=p<0.0001).

4.3.4 PRNP knockdown reduces the proliferation of U87 cells

The MTT cell proliferation assay was carried out to study the effect of PrP^c silencing on the proliferation of U87 cells. The proliferation rate of PRNP knockdown cells was decreased in comparison with the scrambled cells in a time dependent manner (Figure 4-7 A and B). The line graph (Figure 4-7, A) shows that the proliferation of PRNP siRNA cells decreased dramatically over five days, with the lowest value of approximately 45% recorded on the fifth day. This graph represents five experiments (i.e. each experiment represents a single time point) using different cell seeding densities and incubation times (1 to 5 day/s). In these experiments, the cell density on days 1, 2, 3, 4 and 5 was 5000, 4000, 3000, 2000 and 1000 cells, respectively, in order to avoid the over confluence of cell culture in the well plate at the end of the experiment. The quantity of transfection reagent (DharmaFect) was added in proportion to the cell seeding density, as described in section (2.2.9). The trends in Figure (4-7, A) were confirmed using the same cell density (1000 cells) and quantity of DharmaFect over 5 days to avoid potential cytotoxicity resulting from variability in DharmaFect concentrations (Figure 4-7, B). These results were also confirmed using Alamar blue assay as shown in Figure (4-7, C). These observations indicate that silencing of PrP^c reduces the proliferation of U87 cells. A possible explanation for the downregulation of PrP^c is that the proliferation of cancer cells is indirectly inhibited due to downregulation of PI3K/Akt pathway and Cyclin D1, both of which are activated and regulated by PrP^c¹⁶⁹.

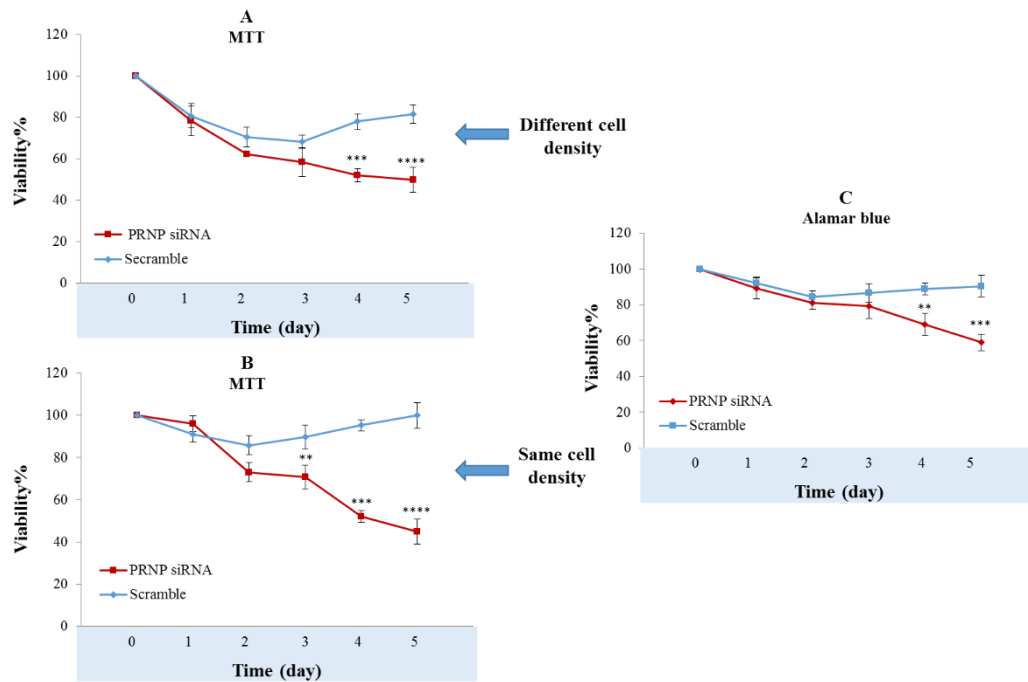


Figure (4-7): Cell proliferation of transfected U87 cells. Knockdown of PRNP gene in U87 cells reduces cell viability using the proliferation assays MTT (**A and B**) and Alamar blue (**C**). All data were calculated as a percentage to the control group. These results represent mean \pm SD for three different experiments, each performed six times (n=18). The results were statistically analysed using t-test (**= $p < 0.01$, ***= $p < 0.001$ ****= $p < 0.0001$).

4.3.5 Knockdown of PrP^c in U87 cells does not induce cytotoxicity according to

LDH assay

According to MTT and Alamar blue assays, the number of cells was reduced due to the knockdown of the PRNP gene. Both of these techniques depend on the metabolic activity of viable cells²³⁰. LDH assay, on the other hand, measures the activity of lactate dehydrogenase (LDH) as a result of damaged cells²³¹. The LDH assay was performed in order to prove that the reduction of cells did not result from the toxicity of the transfection reagent. The line graph in **Figure (4-8)** shows that there was no significant change in cytotoxicity between PRNP siRNA and scrambled lines. The toxicity was approximately 20% or less at all time points, which is acceptable

according to the DarmaFect protocol. These results indicated that the transfection reagents were not significantly cytotoxic during the incubation periods.

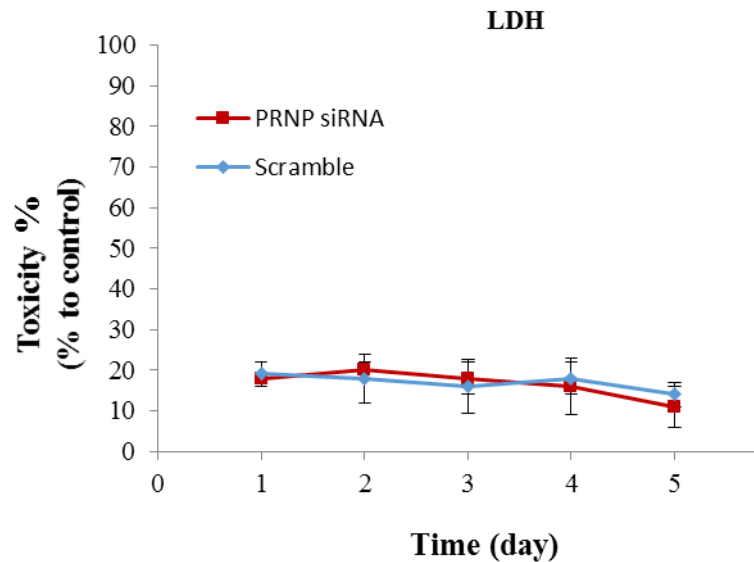


Figure (4-8): Cytotoxicity of transfection reagents in U87 cells by LDH assay. The line graph shows no significant change across all time points. The results were calculated as a percentage of the control. The data represent mean \pm SD of three separate experiments, each performed at least five times (n=15). These data were analysed using one-way ANOVA with Tukey's test.

4.3.6 PrP^c knockdown inhibits proliferating marker ki67

Proliferation marker ki67 was evaluated to confirm the reduction of cell proliferation in PRNP knockdown cells. Many studies have used ki67 as an independent index for predicting cancer progression²³². ICC by confocal microscopy was used to estimate the number of ki67 positive cells. The images in **Figure (4-9, A)** show the total positive cells in the scrambled and PRNP siRNA samples after five days. The bar chart below (**Figure 4-9, B**) shows that the percentage of ki67 positive cells among the knockdown cells decreased significantly after five days to about 55% of the total, compared to scrambled cells where approximately 70% of the total number of cells were positive for ki67. Thus, knockdown of PRNP reduced the proliferation rate of U87 cells.

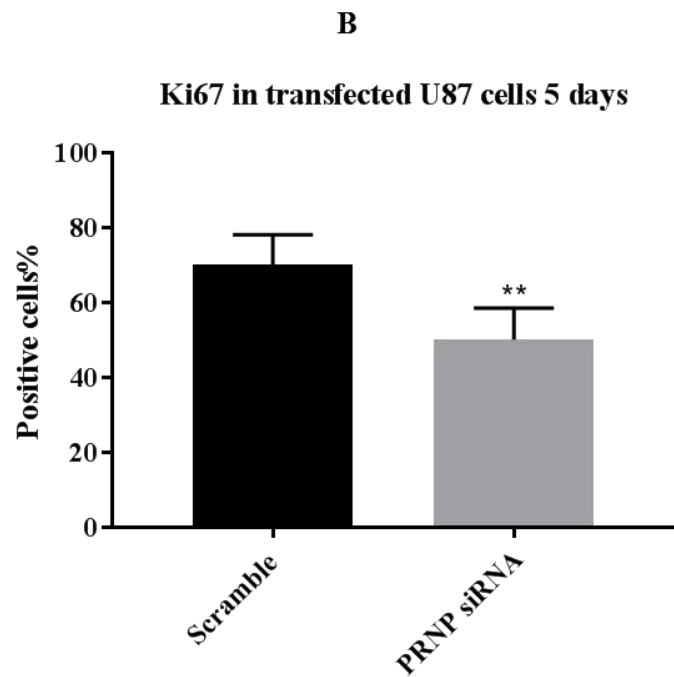
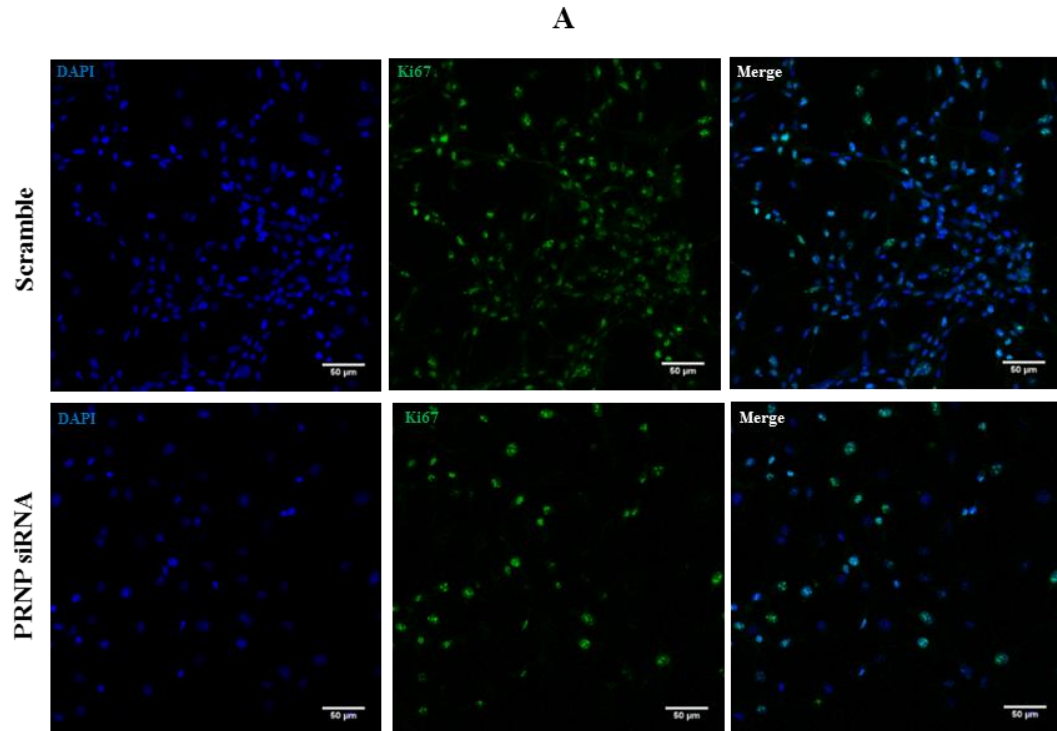


Figure (4-9): ICC for ki67 in PRNP knockdown cells. **(A)** In the ICC images, cell nuclei were stained with DAPI (blue) and ki67 was stained with anti ki67 antibody (green), the analysis of these images was performed using Image J. **(B)** The bar chart reveals the percentage of cells to the total number of cells in each sample as mean \pm SD of three experiments, each performed in duplicate, and the data were calculated for 30 images for each sample (10 images per experiment) $n=6$. These data were statistically analysed by t-test (**= $p<0.01$).

4.3.7 Knockdown of PRNP gene does not induce apoptosis in U87 cells either when treated with TMZ or untreated

To find out whether knockdown of PrP^C in U87 cells induced or inhibited the apoptosis, Annexin V assay with PI staining was carried out with and without TMZ. The flow cytometry blots (Figure 4-10) show the population of apoptotic, live and dead cells. As reviewed in sections 1.7.2.3, PrP^C may improve the viability of cancer cells by inhibiting pro-apoptotic stimuli. We, therefore, expected that the knockdown of PrP^C would induce the apoptosis of U87 cells. Unexpectedly, however, statistical analysis of the current results indicated that the apoptosis in both untreated and treated knockdown cells was not significantly different to that of the scrambled cells (Figure 4-10, A and B).

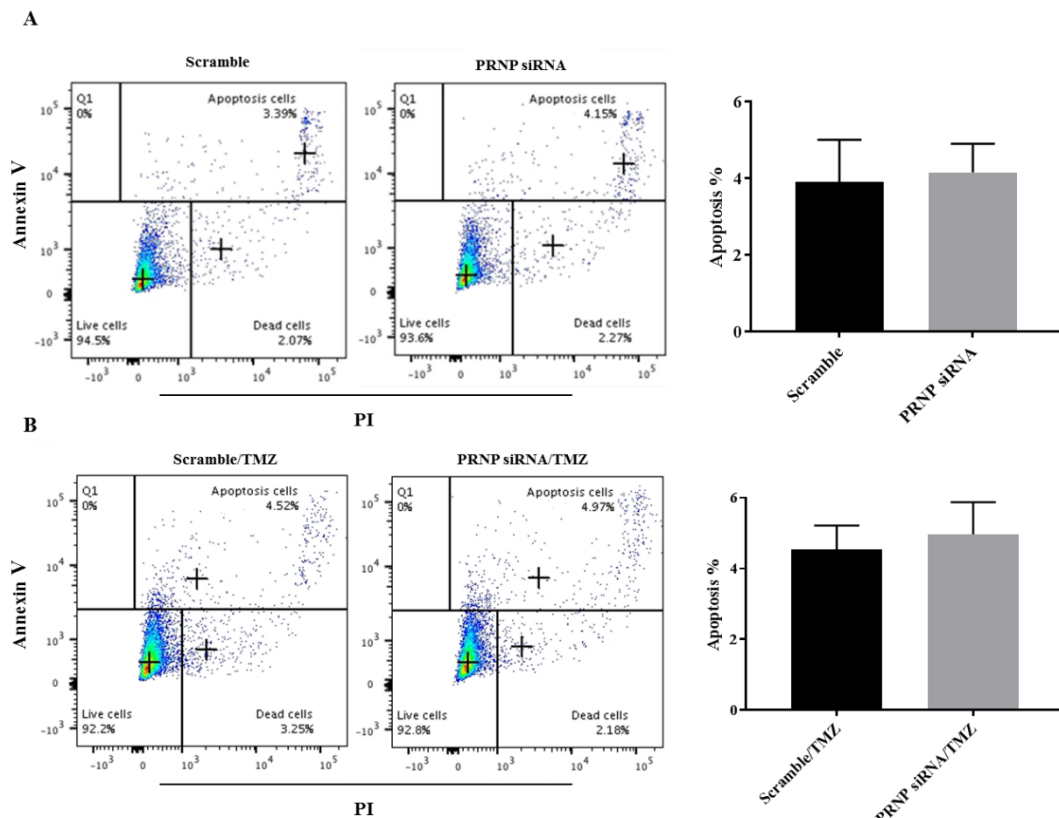


Figure (4-10): The apoptosis of PrP^C knockdown cells using Annexin V with PI. The dot blots and bar chart reveal the apoptosis ratio of scrambled and PRNP siRNA cells, **A** (untreated) and **B** (treated with TMZ). The results represent mean \pm SD of three different experiments and each experiment was performed in duplicate (n=6). The data were statistically analysed by t-test.

4.3.8 PrP^c silencing does not influence chemotherapeutic resistance in U87 cells by MTT assay

To examine whether the PRNP knockdown affects the response of U87 cells towards alkylating agents TMZ and BCNU, MTT assay was carried out using a range of TMZ and BCNU treatment doses which have previously shown dose-dependent effects on U87 cells. The scrambled and PRNP siRNA cells were treated for 48 h with TMZ and BCNU at low (20-100 μ M) and high doses (100-300 μ M and 50-200 μ M, respectively). The line graphs reveal that there were no significant differences in the cell viability of treated PRNP siRNA cells compared to treated scrambled cells over 48 h (Figure 4-11). Thus, the knockdown of PrP^c in U87 cells did not increase or decrease the response to these treatments according to MTT assay. To our knowledge, this is the first study to have evaluated the effect of TMZ and BCNU on PRNP knockdown U87 cells. One other study, however, has explored the knockdown of PrP^c in the breast cancer cell line, MDA-MB-435, showing that this knockdown induced resistance to doxorubicin but was not affected by other treatments (paclitaxel and staurosporine) after 48 h⁸.

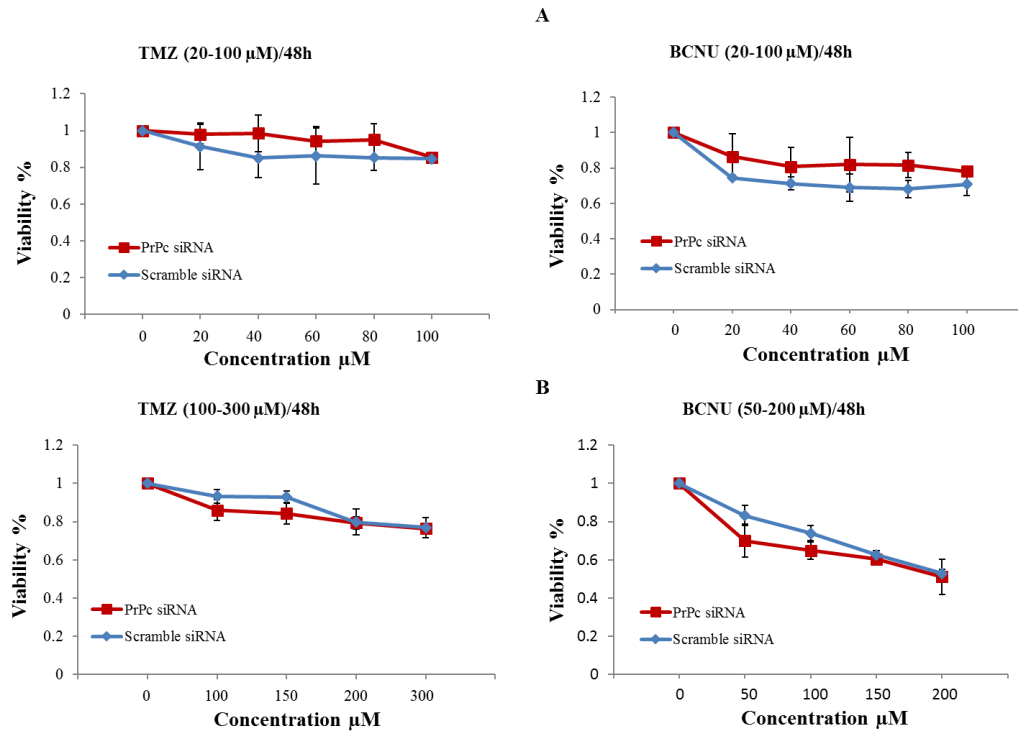


Figure (4-11): Knockdown of PrP^c in U87 cells does not affect the response to TMZ or BCNU. **A**, the line graphs show the cell viability in low dose treatments for 48 h. **B**, the line graphs revealed the viability of cells treated with a high dose of TMZ and BCNU for 48 h. The data represent mean \pm SD of three independent experiments, each performed in six wells for (n=18). These results were analysed by t-test.

4.3.9 PRNP knockdown cells affect the cell cycle of TMZ treated U87 cells

Cell cycle analysis was performed in order to assess the population of transfected U87 cells in each phase with and without TMZ treatment. Our previous results in [section 3.3.3.2](#) showed that TMZ arrested U87 cells at different time points. Transfected cells were therefore treated with TMZ for 48 h. The histograms show the percentage of cells in each phase, and the bar chart reveals the analysis of this experiment ([Figure 4-12, A and B](#)). The cell cycle phases in untreated PRNP siRNA and scrambled cells were identical to those in the control group, whereas the G1 and G2/M populations were significantly changed in treated PRNP siRNA cells in comparison with treated control and scrambled cells [Figure \(4-12\)](#). The mechanism of how the knockdown of PrP^c alters the population of cell cycle phases in glioblastoma cells treated with

alkylating agents has not as yet been described in the literature, however. Our results, though, suggest that the decrease in treated knockdown cells at G2/M may be ascribed to the alteration of the regulatory cell cycle proteins p53 and p21. This based on the evidence that the accumulation of TMZ-treated U87 cells in G2/M required both p53 and p21²³³. The levels of these proteins will be assessed in the next section (4.3.10).

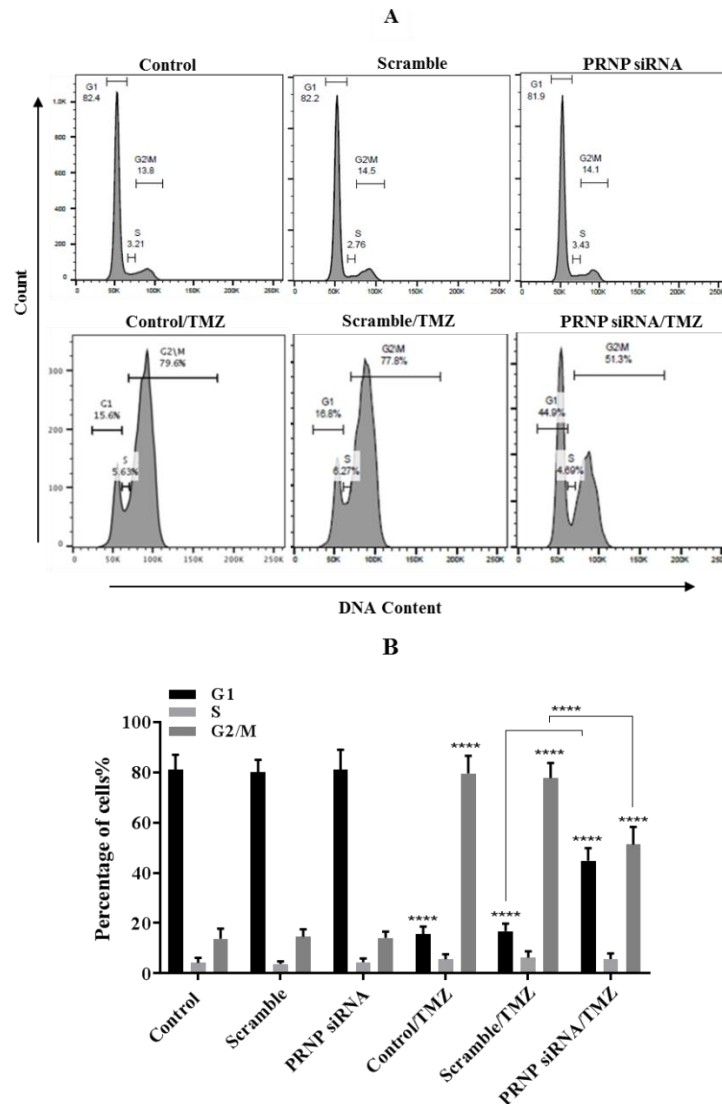


Figure (4-12): Determination of cell cycle phases in knockdown cells using PI. **A**, the histograms show the population of cell cycle phases in the control, scrambled and PRNP siRNA cells with and without TMZ. **B**, the bar chart shows that there is no change among the groups without TMZ but that the cells were accumulated in G2/M in groups treated with TMZ. The treated PRNP siRNA cells showed less accumulation in G2/M compared to treated control and scramble cells. The bars represent mean \pm SD of three separate experiments, and each experiment was performed in duplicate (n=6). The data were analysed using one-way ANOVA, Tukey's test (****= p<0.0001).

4.3.10 p53 and p21 in PRNP knockdown cells treated with TMZ and BCNU

As shown in the previous section (4.3.9), knockdown of the PRNP gene in U87 cells altered the population of cell cycle phases when the cells were treated with TMZ. This led us to investigate the effect of TMZ and BCNU on p53 and p21, as regulators of the cell cycle, in knockdown cells. In each case, U87 cells were treated with transfection reagents for three days to obtain PRNP or scrambled knockdown lines. The transfection reagents were then withdrawn, and the cells were immediately treated with either TMZ or BCNU for 48 h before the analysis was carried out by western blot assay. Our results showed that the p53 level increased in both treated scrambled and PRNP siRNA cells compared to the control (cell treated with 0.5% DMSO). In addition, there was no significant change in the p53 level between treated PRNP siRNA and scrambled cells (Figure 4-13, A). The western blot assay showed that the level of p21 increased significantly in PRNP siRNA cells treated with TMZ or BCNU when compared with comparable treated scrambled cells (Figure 4-13, B), however. It appears, therefore, that, regardless of the type of alkylating agent, p21 significantly increased in treated knockdown cells, and a higher value of p53 level was recorded in these cells, but without significant differences between PRNP siRNA and scrambled cells when treated with either TMZ or BCNU. In general, p53 is upregulated in response to the DNA damage induced by alkylating agents and p21, as a p53 transcription target, also induced in response to these agents²⁰². Although the effect of knockdown of PrP^c on TMZ or BCNU treated glioblastoma cells has not been studied yet, we may speculate that the consequent upregulation of p21 may serve to rescue the PRNP knockdown cells from the cytotoxic effects of alkylating agents in that it acts like a tumour suppressor protein. In addition, upregulation of p21 has been previously shown to induce resistance of glioblastoma cells to BCNU and cisplatin²³⁴.

Although previously, the accumulation of treated U87 cells with alkylating agents in G2/M was thought to require both p53 and p21²³³, in our results it seems that the upregulation just of p21 in treated knockdown cells may induced G1 arrest, perhaps due to its effect on cyclin dependant kinases (CDKs)²³⁵.

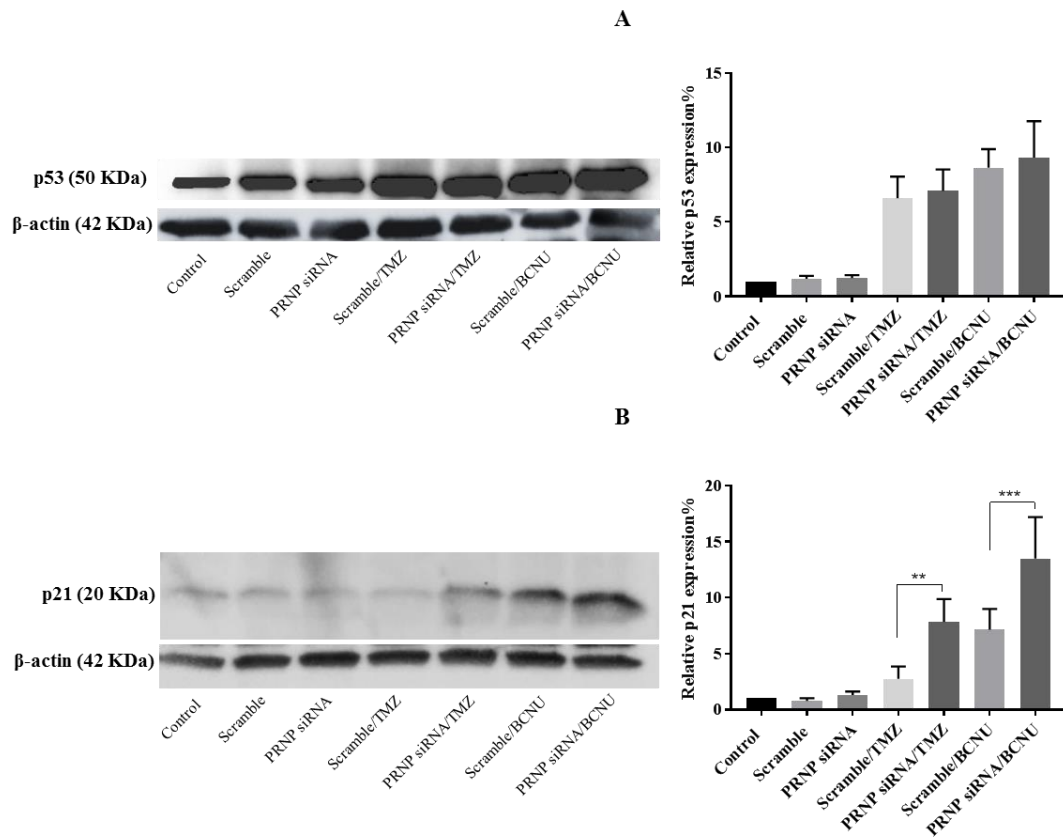


Figure (4-13): Western blot for p53 and p21 in treated and untreated transfected U87 cells. **(A)** p53 increased in treated transfected cells with TMZ or BCNU and there is no significant changes in p53 level between treated scrambled and PRNP siRNA cells in both treatments. **(B)** TMZ and BCNU upregulated p21 in treated knockdown and scrambled cells and the level of p21 significantly increased in treated PRNP siRNA cells in comparison with treated scrambled cells. The data was normalised to β -actin and calculated as a percentage of the control group. These results represent mean \pm SD of three experiments (n=3). The data were analysed using one-way ANOVA, Tukey's test (**= $p < 0.01$, ***= $p < 0.001$).

4.4. Summary of key experimental results

- PRNP gene expression was reduced in knockdown cells in comparison to scrambled and untreated cells to approximately 10% and 14% of the control values after 24 h and 48 h treatment with transfection reagents, respectively.
- The level of PrP^c protein was decreased in knockdown cells approximately by 80% after 2, 3 and 5 days compared to the scrambled and control groups according to flow cytometry, western blot and confocal microscopy assays.
- Knockdown of the PRNP gene inhibited the proliferation of U87 cells according to MTT and Alamar blue assays and reduced the proliferation marker ki67 in knockdown cells compared to scrambled cells after five days.
- PRNP knockdown did not induce the apoptosis of U87 cells according to Annexin V with PI assay.
- There was no significant change in cell viability between TMZ or BCNU treated knockdown cells and scrambled cells.
- The proportion of cells in the G1 and G2/M cell cycle phases changed in TMZ treated knockdown cells in comparison with treated scrambled and control cells.
- The level of p21 increased in TMZ or BCNU treated knockdown cells compared to the treated scrambled cells, whilst p53 was not significantly affected.

4.5. Discussion

The expression of PrP^c may rescue different type of cells, such as neurons, from the environmental and internal stress¹⁸⁴. In addition, however, the overexpression of PrP^c may protect tumour cells from the pro-apoptotic initiators such as DNA damage and chemotherapy²³⁶. The level of PrP^c expression in U87 cells treated with TMZ and BCNU has not yet been examined in depth, however. Our speculation was that knockdown of PrP^c in U87 glioblastoma cells may affect cellular behaviour and sensitivity to alkylating agents. This chapter aimed to address this speculation by knocking down PRNP gene in U87 cells using PRNP siRNA and investigating the impact of this on cell proliferation and apoptosis when those cells were treated with TMZ and BCNU alkylating agents.

In this work, the optimum condition for knocking down PrP^c in U87 cells was identified initially using PRNP siRNA. We found that PRNP siRNA suppressed PrP^c expression in U87 cells by approximately 80% after 48 h, as quantified by qPCR, western blot, flow cytometry, and confocal microscopy (Figures 4-4, 4-5 and 4-6). Although a higher level of protein reduction was not obtained, 80% reduction in protein level is a good measure for the effectiveness of knockdown in cell lines as recommended by the DharmaFect protocol. The knockdown of PrP^c continued until day 5 day, but thereafter the level of PrP^c in scrambled cells decreased by around 20-30% compared to the control group. In respect of positive cells (PrP⁺ cells), there was no significant change in scrambled cells at day 5 relative to the control. This change may be attributed to the long period of exposure to the transfection reagent. It is difficult to explain why the protein level decreased in scrambled cells because the sequence of the non-target siRNA was not provided in the manufacturer's instruction. One possible explanation, however, is that the decrease in protein level could be

subjected to two different pathways including deficiency in protein synthesis or inducing protein degradation. Our result regarding the knockdown of PrP^c level in U87 cells is an agreement with that of Silber *et al.* who reported that PRNP siRNA inhibited the level of PrP^c in T98G glioma cells after two days by approximately 80%¹⁸.

To determine whether the knockdown of PrP^c induces or reduces the proliferation of U87 cells, the cells were transfected for different durations from day 1 to day 5. A reduction in the number of cells was observed after day 2 in a time-dependent manner according to MTT and Alamar blue assays (Figure 4-7). In addition, to exclude the effect of the potential toxicity of DharmaFect (the transfection reagent) on U87 cells over this period, LDH assay was performed with the results showing that the toxicity was not significant over the transfection periods (1-5 days) (Figure 4-8). These findings indicate that knockdown of PrP^c in U87 inhibits the proliferation. This may be ascribed to the PI3K/Akt pathway and Cyclin D1 protein which are probably regulated and activated by PrP^c¹⁶⁹. Our results are in agreement with those of Li *et al.*, who found a reduction in the proliferation of J889 glioblastoma cells in response to PRNP siRNA¹⁸⁵. In addition, inhibition of PrP^c in many glioblastoma cells using DNA-antisense oligonucleotide decreased the viability of these cells¹⁸⁴. Indeed, the role of PrP^c in the proliferation may depend on the type of cells as reviewed in section (1.2.5.2.5). For example, suppression of PRNP in gastric cancer cells SW620 and HT29 and breast cancer cells MDA-MB-435 did not reduce the proliferation of cells^{228,8}. Furthermore, we also quantified the proliferation marker ki67 in knockdown and scrambled cells using confocal microscopy to confirm the reduction in proliferation. Although the function of ki67 is still unclear, it is a commonly accepted marker for assessing cell proliferation. It is observed in all cell cycle phases apart

from the G₀ and G₁ phases at which point it is undergoing proteasome-mediated degradation²³⁷. In our results, the positive ki67 cells in PRNP knockdown cells were significantly less than in scrambled cells by around 55% and 70% of total cells respectively after five days incubation with the transfection reagent (Figure 4-9). This may be related to the decrease in the proliferation of knockdown cells. Regarding the proliferation marker ki67 there is no literature to support this result. Nonetheless, we suggest that the reduction of ki67 positive cells is a marker for the reduction of proliferation in U87 knockdown cells.

Furthermore, in our results, the knockdown of PrP^c in U87 cells did not lead to more extensive apoptosis in TMZ or BCNU treated and untreated knockdown cells, according to Annexin V assay with PI staining (Figure 4-10). On the one hand, we expected that knockdown of PrP^c in untreated cells would induce apoptosis due to PrP^c's known anti-apoptotic effect in many types of cells (reviewed in 1.2.5.2.3). Our result is in line with previous findings that have shown that the knockdown of PrP^c using DNA-antisense oligonucleotides did not induce the apoptosis of cells from another glioblastoma cell line (T98G)¹⁸⁴. In contrast, Li *et al.* found that knockdown of PrP^c in untreated J889 glioblastoma cells using PRNP siRNA induced the apoptosis of these cells by upregulating caspase 3¹⁸⁵. Another study showed that knockdown of PrP^c in AGS gastric carcinoma cells promoted cell apoptosis through activation of Bax and p53²²⁷. On the other hand, the effect of PrP^c knockdown in glioblastoma cells treated with alkylating agents has not been studied in detail. Our result contradicts Zhuang *et al.*'s finding that knockdown of PrP^c in U87 cells induced apoptosis when treated with TMZ by activation caspase 3⁶. Other results showed that knockdown PrP^c in breast cancer cells MDA-MB-435 reduced the apoptosis mediated by doxorubicin

and chemotherapy-induced cytotoxicity, by increasing some of Bcl-2 family proteins such as Bcl-xL and Bcl-2⁸.

Resistance to chemotherapy has been considered a big issue in cancer treatment. The overexpression of PrP^c may be implicated in the sensitivity of many kinds of cancer cells to the chemotherapy and indeed knockdown of PrP^c has been shown to improve the sensitivity of several cancer cells to chemotherapy^{168,152}. The work concerning PrP^c in glioblastoma cells treated with TMZ and BCNU is very limited, however. We speculated that knockdown of PrP^c in U87 cells may decrease cell viability when treated with TMZ or BCNU. Unexpectedly, our work demonstrated that the knockdown of PrP^c in U87 cells did not affect cell viability in treated cells with TMZ or BCNU compared to treated scrambled cells, even with high doses (Figure 4-11). This indicated that knockdown of PrP^c by PRNP siRNA in U87 cells does not improve the sensitivity of these cells to chemotherapeutic agents TMZ or BCNU. Our result is in agreement with Yu *et al.* who found that knockdown of PrP^c in breast cancer cells MDA-MB-435 did not induce resistance to other chemotherapies, paclitaxel and staurosporine (treatments that induce apoptosis)⁸. In contrast, the overexpression of PrP^c in gastric cancer cells has been shown to induce resistance to Adriamycin whereas the silencing of this protein promotes sensitivity towards Adriamycin¹⁶⁸. Meslin and co-workers also found that the depletion of PrP^c promotes the sensitivity of breast cancer cells to Adriamycin through TRAIL-mediated apoptosis and upregulation of pro-apoptotic protein Bax¹⁵². In addition, it has been reported that the overexpression of PrP^c protected the astrocytes from staurosporine-induced apoptosis by activation of caspase 3²³⁸, whereas the knockdown of PRNP in astrocyte cells promoted sensitivity towards staurosporine²³⁹.

As mentioned in chapter three, TMZ treated U87 cells accumulated in the G2/M phase after 24 h. To investigate the effect of PrP^c knockdown on the cell cycle, therefore, the cells were exposed to TMZ for 48 h. Our results indicated that the population of treated knockdown cells was less arrested in G2/M compared to treated control or scrambled cells (Figure 4-12). We speculated that this change may be attributed to the variation of the regulated cell cycle proteins p53 and p21. p53 has been shown to be upregulated in response to the DNA damage mediated by alkylating agents, while p21, the transcriptional target of p53, is also induced in response to these treatments²⁰². The influence of knockdown PrP^c on TMZ or BCNU treated glioblastoma cells has not been reported yet. To validate our speculation, the level of these proteins was evaluated using western blot analysis. We found that the level of p53 in knockdown cells treated with TMZ or BCNU increased when compared with the control (untreated cells) but there was no significant variation between PRNP knockdown and scrambled cells treated with either TMZ or BCNU. Surprisingly, p21 significantly increased in knockdown cells treated with TMZ or BCNU in comparison with treated scramble cells (Figure 4-13). To our knowledge, this observation has not been reported by other researchers. We found that the increase of p21 induces the treated knockdown cells to accumulate in G1 rather than G2/M. A possible explanation is that the upregulation of p21 may be promoted in response to TMZ or BCNU and this induction may protect the knockdown cells from the cytotoxicity of these treatments. Many studies have indeed shown that p21 protects various types of cells from apoptosis and that the silencing of this protein induces tumourigenesis²³⁵. Furthermore, the high level of p21 may induce G1 arrest due to its effect on cyclin-dependent kinases (CDKs). Also, the accumulation of cells in G2/M after the DNA damage by TMZ or BCNU requires both p53 and p21 in U87 cells²³³.

It has also been reported that p53 might contribute to sensitising tumour cells to chemotherapy²⁴⁰ or inducing the resistance due to its function in DNA repair²²⁹. Kay *et al.*, for example, reported that p53 has an active role in the induction of p21 during DNA damage in response to intrinsic or extrinsic stimuli. Furthermore, p21 can be induced independently to p53 in many conditions such as the development of normal tissue, wild type p53 cells, mutant p53 cells and through cell differentiation²⁴¹. Other studies have reported that upregulation of p21 in glioblastoma cells induces resistance to cisplatin and BCNU²³⁴. p21 is upregulated in a downstream effect of p53 and is a key for regulating the cell cycle arrest in response to DNA damage. In addition, p21 may also have an oncogenetic function due to its roles as a pro-cancer and antiapoptosis^{242,235}. Accordingly, the knockdown of PrP^c in U87 cells increased the level of p21 in response to DNA damage-mediated by TMZ or BCNU. The resistance of knockdown cells to alkylating agents might not be detectable by MTT assay, where there was no significant change in treated knockdown cells compared to treated scramble cells.

To summarise, this is the first study to have evaluated the effect of knockdown of PRNP gene on U87 cells treated with alkylating agents. A high level of PRNP knockdown was obtained using PRNP siRNA. Knockdown of PrP^c significantly reduced the proliferation of U87. Furthermore, the knockdown of PrP^c did not induce apoptosis in U87 cells regardless of whether or not they were treated with TMZ. It was also seen that cell cycle populations in TMZ treated knockdown cells changed in comparison to treated scrambled and control cells. The knockdown of the PRNP gene may induce the resistance to alkylating agents TMZ and BCNU. This may be attributed to increasing the level of p21 in TMZ or BCNU treated knockdown cells.

Chapter 5: Evaluation of the effect of proteasomal inhibitor, MG132, on PrP^c in U87 cells and on the apoptosis when combined with TMZ

5.1 Introduction

In eukaryotes, proteasomes are located in the nucleus and the cytoplasm. Abnormal, misfolded or damaged proteins are degraded by the the proteasome. These proteins are usually tagged by ubiquitin (a protein consisting of 76 amino acids)²⁴³. Cancer cells produce a large amount of damaged proteins when compared to normal cells, and this can overwhelm and deactivate proteasome²⁴⁴. The term of proteasome refers to 26S (S means Svedberg, which is the unit for sedimentation coefficient) proteasome, a large multi-catalytic ATP-dependent protease complex, containing 20S protein and 19S regulatory subunits. At least four ubiquitins are linked and guide the unneeded protein to the 19S subunits and 20S core to produce 3-22 amino acid peptides (peptide fragments) (Figure 5-1)²⁴⁵.

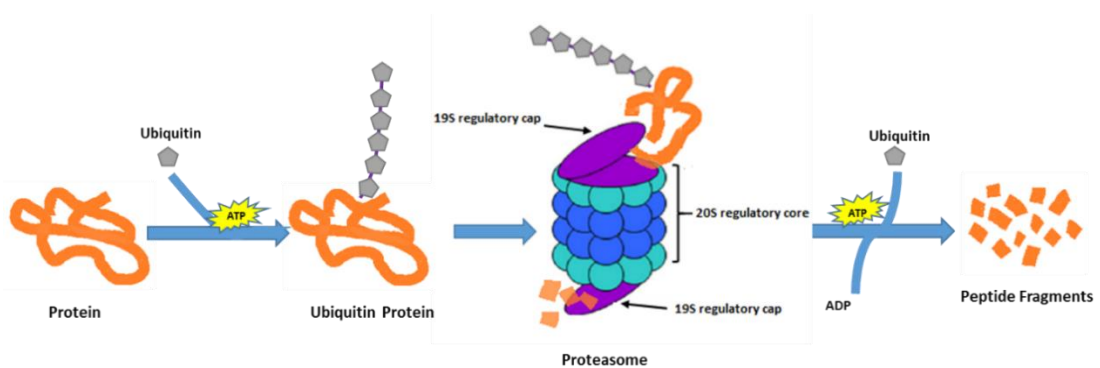


Figure (5-1): The proteasome structure and its function. Protein is conjugated with ubiquitins then served into the proteasome. The protein is degraded to a peptide which fragments the protease in the core particle. Adapted from Teicher, B. A. and Tomaszewski, J. E. under the Creative Commons Attributed Licence²⁴⁵.

Proteasome inhibitors have in general been used to investigate the function of the proteasome in malignant cells²⁴⁴. It has been reported that proteasome inhibitors induce apoptosis *in vitro* for many types of cancer such as breast cancer²⁴⁶, multiple

myeloma²⁴⁷, melanoma²⁴⁸ and glioblastoma¹³. There are different classes of proteasome inhibitors such as peptide aldehydes, streptomyces metabolite, dipeptidyl boronic acids, vinyl sulfone tripeptides and natural products which can inhibit the degradation of protein by various mechanisms²⁴⁴. MG132 or (carbobenzoxy-L-leucyl-L-leucyl-L-leucinal) is a peptide (Figure 5-2) which suppresses the proteasome by inhibiting serine protease²⁴⁵. It precisely inhibits the activity of the 20S subunit by binding with the beta subunit and then blocking the action of the 26S proteasome¹⁰.

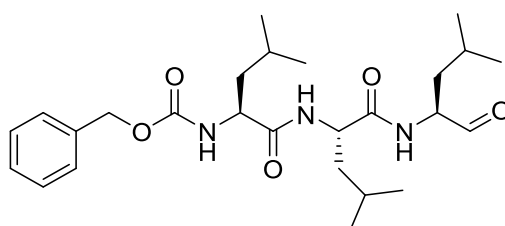


Figure (5-2): The structure of MG132

It has been reported that MG132 induces apoptosis through different pathways. One such pathway is the formation of reactive oxygen species (ROS) and loss of glutathione production. This process may affect the function of mitochondria and cause the release of cytochrome c, which inhibits cell viability (Figure 5-3 A)¹¹. The coordination of MG132 with TRAIL upregulates the death receptor 5 in cancer cells and this combination induces the intrinsic apoptosis by activation of caspases 3 and 8 (Figure 5-3 B)²⁴⁹. Another process for MG132-mediated apoptosis is the inhibition of the transcriptional regulator protein NF- κ B, which can promote the survival of tumour cells¹⁰. Various factors such as TNF, IL-1, IL-6, viruses and bacteria can activate the I κ B kinase enzyme complex, which is upstream of NF- κ B²⁵⁰. MG132, meanwhile, can suppress the degradation of I κ B kinase complex²⁵¹. As a consequence, downregulated NF- κ B inhibits the anti-apoptotic protein Bcl-2, and this then induces cell death (Figure 5-3 C)²⁵². In addition, MG132 can induce p53-independent apoptosis in cancer cells¹⁰ since p53 is mutated in most cancer cells²⁵³. Noxa is one of

the pro-apoptotic proteins that are activated in response to proteasome inhibitor MG132. The anti-apoptotic proteins in the Bcl-2 family interact with Noxa and then release cytochrome c, which activates caspase-induced apoptosis (Figure 5-3 D)²⁵⁴.

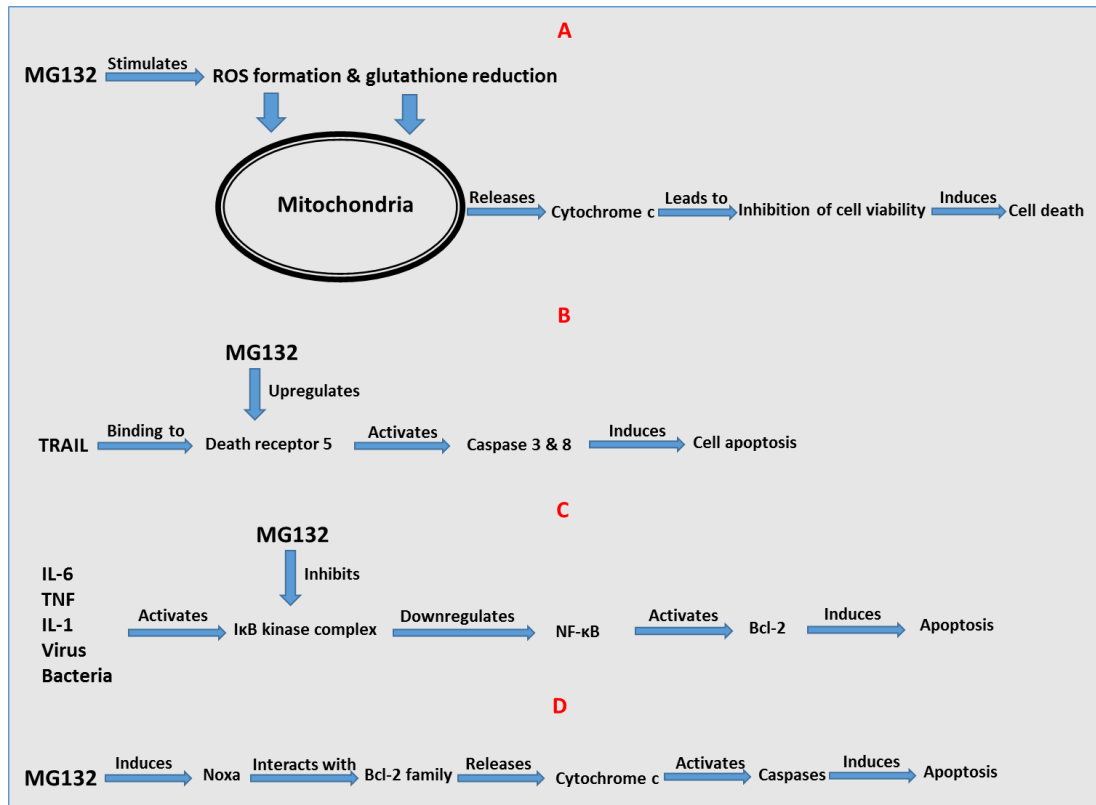


Figure (5-3): Diagram showing MG132-induced apoptosis. **A.** MG132 mediated apoptosis by ROS formation and glutathione reduction. **B.** MG132-induce cell death through upregulating TRAIL-death receptor 5. **C.** MG132-induced cell apoptosis by inhibition of NF-κB. **D.** p53-independent apoptosis by MG132. Adapted from Guo, N. and Peng, Z. under the Creative Commons Attributed Licence¹⁰

Bettina *et al.* showed that p53 was increased in glioblastoma cells treated with MG132, and apoptosis was induced in a p53-dependant manner. In wild type p53 glioblastoma cells LN-229, MG132 mediated p53-dependant apoptosis, whilst in mutant p53 cells LN-18, the apoptosis was in a p53-independent. In both cell types, p21 was accumulated due to the toxic effect and inhibition of protein degradation resulting from MG132²⁵⁵. Another study confirmed these results using other types of glioblastoma cells. Generally, MG132 induced G2/M arrest in both types of

glioblastoma cells (wild type and mutant p53 cells)²⁵⁶. In MG132 treated glioblastoma cells, the G2/M arrest in wild type p53 cells is associated with the induction of p53 as a regulator of the cell cycle^{255,256}. In contrast, Xue-Feng *et al.* found that MG132 arrested glioblastoma cells U87 and U251 in G2/M due to the increase in p53 and decrease in the p21 level¹³. MG132 in combination with chemotherapy was shown to increase the apoptosis of cancer cells in few studies. For example, the combination of MG132 with cisplatin was found to induce apoptosis in human oesophageal squamous cell carcinoma cells²⁵⁷. The combination of MG132 with TMZ has not been tested before, however, and needs to be elucidated.

Since the ubiquitin/proteasome system is a part of the endoplasmic reticulum (ER)-associated machinery for protein degradation (ERAD), proteasome inhibitors may accumulate some unfolded and misfolded proteins in the cytoplasm that subjected to retrograde transport from the ER²⁵⁸. This accumulation may then cause ER stress. The ER stress resulting from proteasome inhibitors may reduce the translocation of PrP and accumulate the cytosolic PrP²⁵⁹. It has been found that the accumulation of PrP by proteasome inhibitor MG132 may occur as a result of two different cellular processes: ERAD which contributes to about 10% of nascent PrP and the post-Golgi turnover of PrP (33-35 kDa species) which is interfered by MG132¹⁴.

In light of this, we hypothesised that U87 cells treated with MG132 may increase the level of PrP^c expression due to the induction of ER stress and inhibition of proteasome function. Furthermore, the apoptotic effect of MG132 may promote the death of U87 cells when combined with TMZ. These actions will be addressed in this chapter.

5.2 The aim

In this chapter, we aimed to evaluate the effect of MG132 upon the level of PrP^c and GBM treatment, TMZ.

To achieve this aim, the following objectives will be addressed:

- Evaluate cell viability in U87 cells treated with MG132 and calculate the IC₅₀ using MTT assay.
- Quantify the level of PrP^c in MG132 treated cells using western blot, flow cytometry and ICC assays.
- Assess the apoptosis rate of U87 cells treated with MG132 and/or TMZ by annexin V with PI staining.
- Evaluate the proliferation of U87 cells treated with MG132 or MG132/TMZ by MTT assay
- Quantify the effect of MG132 or MG132/TMZ combination on the cell cycle using flow cytometry assay.
- Estimate the level of p53 and p21 in cells treated with MG132 or MG132/TMZ.

5.3 Methods

5.3.1 Preparation of treatments

MG132 and TMZ were dissolved in DMSO at 1 mM and 5 mM respectively as stock solution. The stock solution was aliquoted and kept at -80 °C. The desired concentration was prepared by diluting the stock solution in DMSO depending on the final concentration and then diluting ten times using PBS.

5.3.2 Cell viability assay

MTT assay was used to determine the viability of U87 cells treated with the proteasome inhibitor MG132. The cells were seeded in a 96-well plate at 10000 cells in each well. The plate was incubated overnight and then treated with MG132 at different concentrations (1, 2, 3, 4 and 5 μ M) for 12 h. The purpose of this experiment was to check the efficacy of MG132 on U87 cell viability during this period, which will be used to assess the level of PrP^c in treated cells, as previously reported with neuron cells¹⁴. The second 96-well plate with the same cell seeding density was treated with different concentrations of MG132 (0.1, 0.5, 1, 2, 3, 4, and 5 μ M) for 24 h in order to determine the IC₅₀ of MG132, and these concentrations were within the same range as previously reported²⁵⁶. The third 96-well plate was seeded with 5000 cells to evaluate the proliferation of U87 cells treated with 25 μ M TMZ and/or MG132 (0.1, 0.5, 1, 2) for 48 h. The concentrations for MG132 over 48 h were within the range of concentrations previously reported²⁵⁶, whereas the combination with TMZ has not been reported yet. After the cells had been incubated with the treatments for the desired time, the MTT assay protocol (see section 2.2.2) was followed to evaluate the viability of the U87 cells in all 96-well plates.

5.3.3 Western blot assay

PrP^c, p21 and p53 levels in cells treated with MG132 were evaluated using western blot. Regarding PrP^c level, the cells were seeded in a 6-well plate at 200000 cells in each well. On the next day, they were treated with 2 and 4 μ M of MG132 for 12 h or 0.5 and 1 μ M of MG132 for 24 h. To evaluate p21 and p53, another 6-well plate was seeded at 80000 cells and treated with MG132 (0.1, 0.5 and 1 μ M) or a combination with 25 μ M TMZ for 48 h. In all experiments, the control group was treated with 0.5% DMSO for the same time incubation. After the desired incubation time, cell lysate

was prepared, and the protein levels were assessed using the western blot method described in [section \(2.2.5\)](#).

5.3.4 Flow cytometry assay for protein level

To validate the results of the PrP^c level in MG132 treated cells obtained by western blot, flow cytometry assay was carried out. The cells were seeded and treated in a 6-well plate as described in the western blot method above ([section 5.2.3](#)). The cells were then harvested and the protocols for live and fixed cells ([see section 2.2.6](#)) were performed in order to assess the level of PrP^c in treated cells.

5.3.5 Microscopical assay

ICC by confocal microscopy was used to confirm the PrP^c level in MG132 treated U87 cells that had been obtained from western blot and flow cytometry. The cells were seeded onto sterile coverslips which were mounted in a 24-well plate, as shown in the figure below ([Figure 5-4](#)). Next, 30000 cells were seeded in each well, and then next day treated with 2 μ M or 4 μ M of MG132 for 12 h. The control group was treated with 0.5% DMSO for the same incubation time. Later, the confocal microscopic images were obtained as described in [section \(2.2.7\)](#).

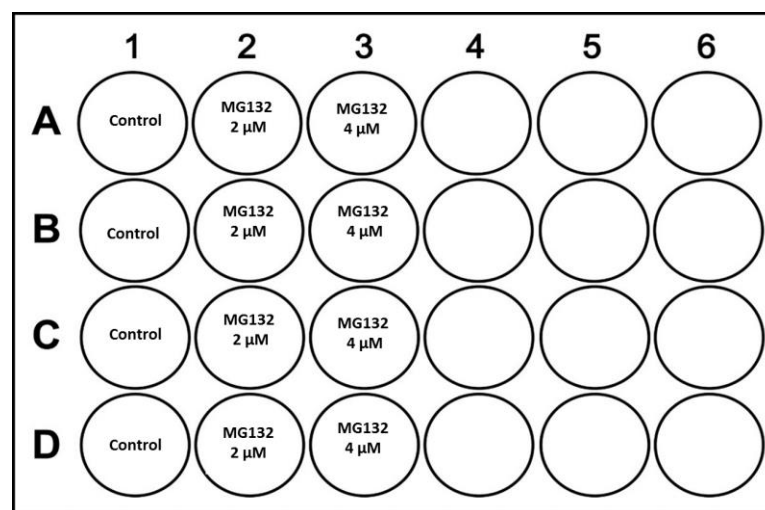


Figure (5-4): The experimental design for using confocal microscopy to evaluate PrP^c in treated cells with MG132.

5.3.6 Annexin V with PI assay

Annexin V with PI assay was used to determine the apoptosis rate in MG132 and/or TMZ treated U87 cells. The cells were cultured in 6-well plates at a density of 80000 cells per well and then, the following day, the cells were treated with MG132 and/or TMZ, as shown in [figure 5-5](#) below. The plates were incubated for 48 h, and then the protocol of Annexin V with PI assay ([see section 2.2.13](#)) was applied to quantify the number of apoptotic cells.

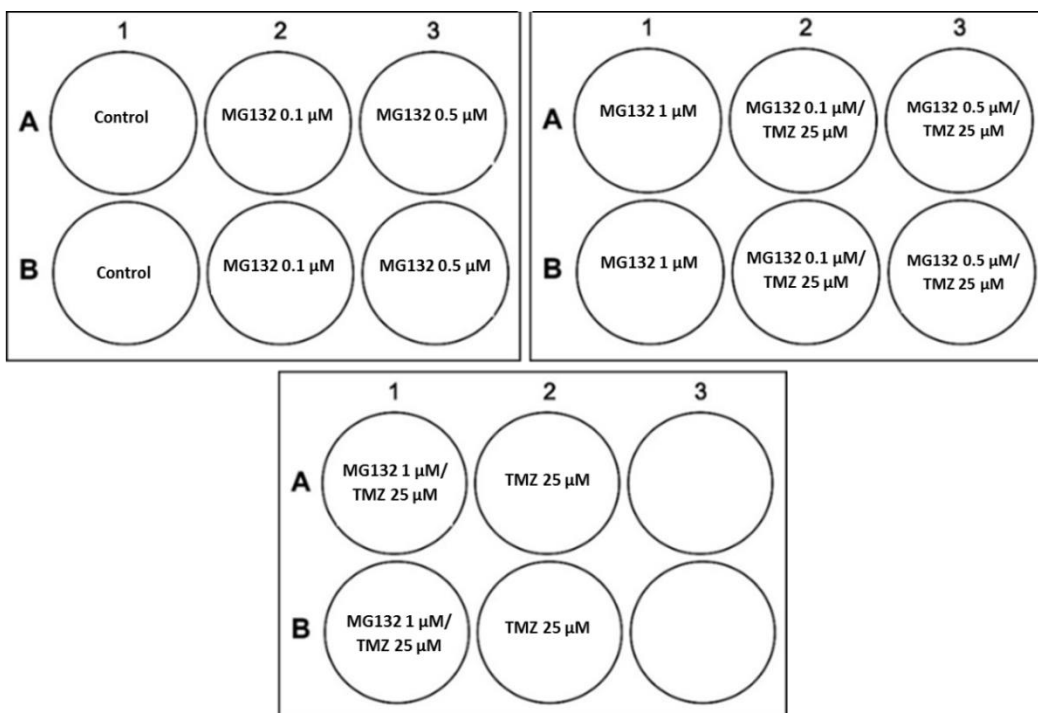


Figure (5-5): The experimental design for U87 cells treated with MG132 and/or TMZ for apoptosis assay.

5.3.7 Cell cycle assay by flow cytometry

Cell cycle assay using flow cytometry was carried out to quantify the number of cells treated with MG132 and/or TMZ in each phase of the cell cycle. The cells were seeded and treated in 6-well plates as described for the apoptosis assay above ([section 5.3.7](#)). After 48 h of incubation with the treatments, the cells were washed and

detached. The cell cycle protocol was then applied (see section 2.2.3) to quantify the population of cells in each phase.

5.4 Results

5.4.1 Cell viability for U87 treated with MG132

Since different concentrations of MG132 were to be tested in this work it was important to check the viability of cells treated with different concentrations of this treatment. MTT assay was therefore carried out to assess the viability of U87 cells treated with MG132. The bar chart below (Figure 5-6, A) revealed the viability of U87 cells in serial concentrations of MG132 (1, 2, 3, 4 and 5 μM) for 12 h. The concentrations 3, 4 and 5 μM of MG132 led to a significant decrease in the viability of cells after 12 h. The lowest value of cell viability was $57\% \pm 5.8$ at 5 μM (Figure 5-6, A). In the next experiment, we therefore decided to use 2 or 4 μM to determine the level of PrP^c after 12 h (section 5.3.2).

A cell viability assay was carried out after 24 h to estimate the IC_{50} for MG132. The line graph shows the viability of U87 cells using different concentrations of MG132 (0.1, 0.5, 1, 2, 3, 4 and 5 μM). Our results indicate that there was a dramatic decrease in the cell viability of U87 cells treated with MG132 in a dose-dependent manner with $\text{IC}_{50} = 2.26 \mu\text{M}$ (Figure 5-6, B). This could be related to the apoptotic effect of MG132 cells²⁵⁵ as will be described in section (5.4.6). In a previous study, it was demonstrated that MG132 decreased the viability of many glioblastoma and this reduction resulted from the alteration of many survival pathways such as the antiapoptotic pathway²⁵⁶.

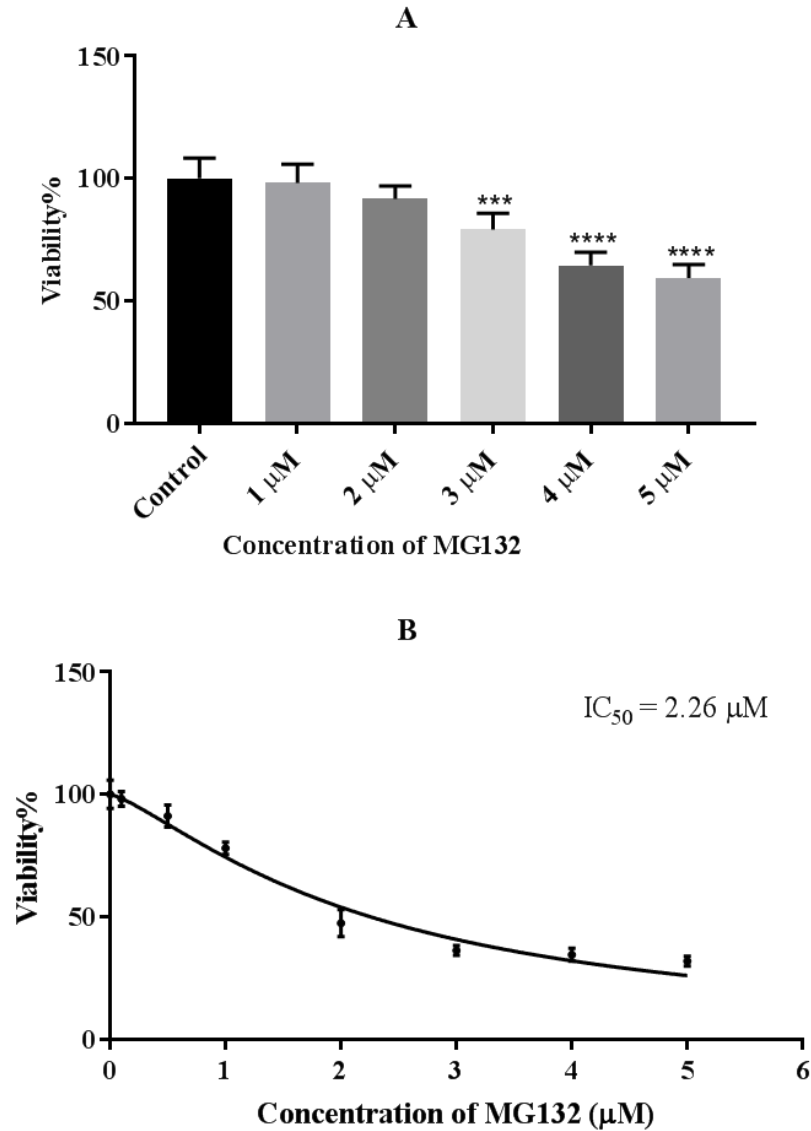


Figure (5-6): Viability of U87 cells in different concentrations of MG132. (A) The bar chart represents the percentage of viable cells relative to the control after 12 h. (B) The line graph shows the IC₅₀ of MG132 in treated cells after 24 h. Quantification of mean \pm SD of three repeats, each performed in octuplicates (n=24). The data were analysed using one-way ANOVA with Tukey's test (***=p<0.001, ****=p<0.0001).

5.4.2. MG132 increases the PrP^c level according to the western blot assay

Western blot assay using PrP(3F4) was carried out to determine the level of PrP^c in MG132 treated U87 cells. The result of this experiment showed that the PrP^c level increased after 12 h treatment with 2 and 4 μM of MG132. The protein level was not affected when the cells were treated for 24 h at 0.5 and 1 μM (Figure 5-7 A). According to this experiment, the level was increased by about 1.5- to 1-fold in cells

treated with 2 and 4 μM for 12 h respectively (Figure 5-7 B). The induction of PrP^c could be attributed to the ER stress resulting from MG132 and/or to the inhibition of the ERAD-proteasome degradation pathway, which may inhibit the degradation of nascent PrP^c or the post-Golgi species of PrP^{c14}.

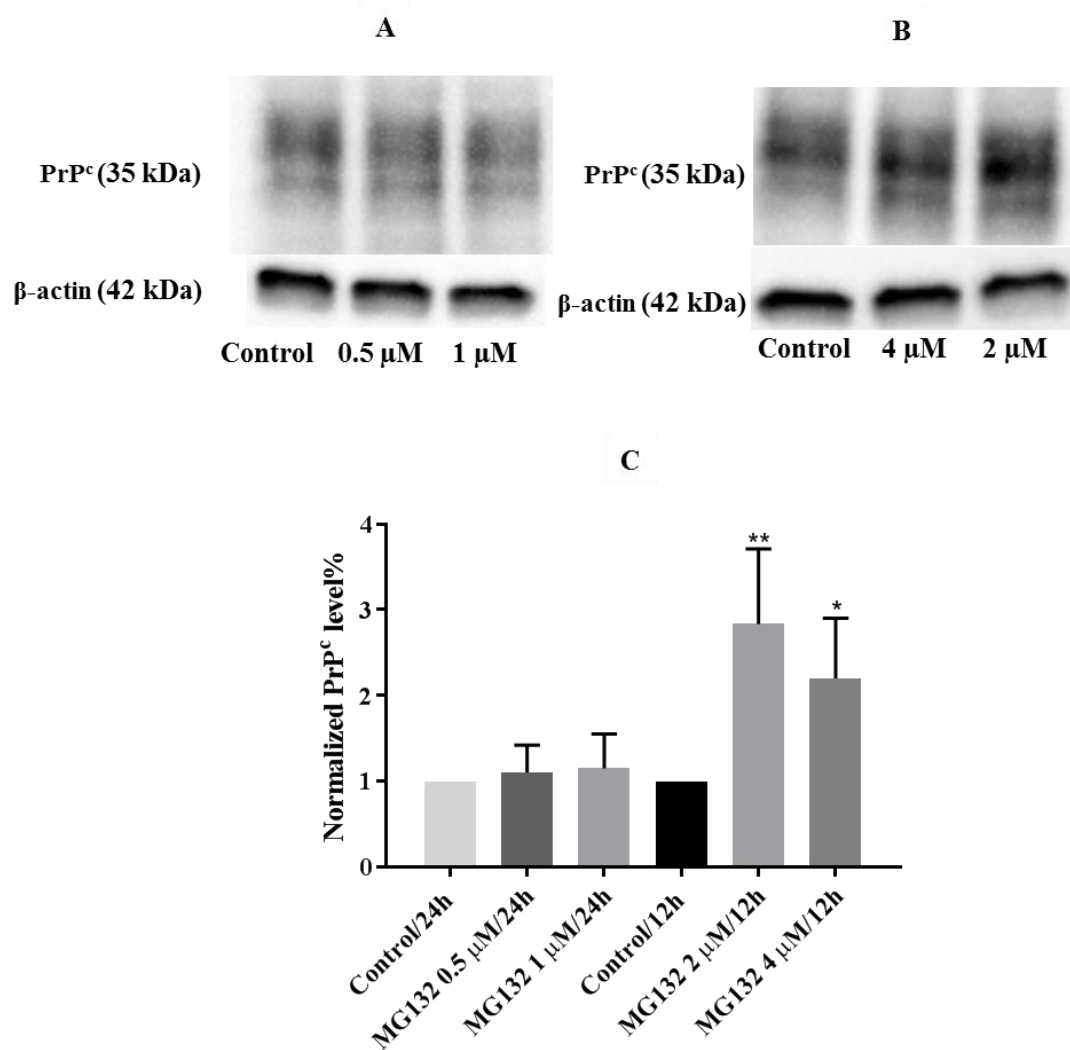


Figure (5-7): PrP^c level in U87 treated with MG132 by western blotting. The western blot image of PrP^c and β -actin in the control and treated groups for 24 h with 0.5 and 1 μM of MG132 (A) and for 12 h with 2 and 4 μM of MG132 (B). The bar chart shows the analysis of images (C). The data were normalised to the control and represents mean \pm SD for at least three independent experiments (n=3). The results were analysed using t-test (*= $p < 0.05$, **= $p < 0.01$).

5.4.3 Assess PrP^c level in treated cells with MG132 by flow cytometry

A flow cytometry assay was carried out to confirm the results of the western blotting. This experiment was applied on live cells to evaluate the protein level on the cell surface, as well as to fixed and permeabilised cells to assess the total protein level. The figure below reveals that the protein level increases significantly in live and fixed cells that had been treated by MG132 for 12 h in comparison to the control group. There was no significant change in protein levels between cells treated with 2 and 4 μ M. The protein level increased about 1.4-fold in treated cells compared to untreated cells (Figure 5-8) confirming the results by western blot section (5.4.2).

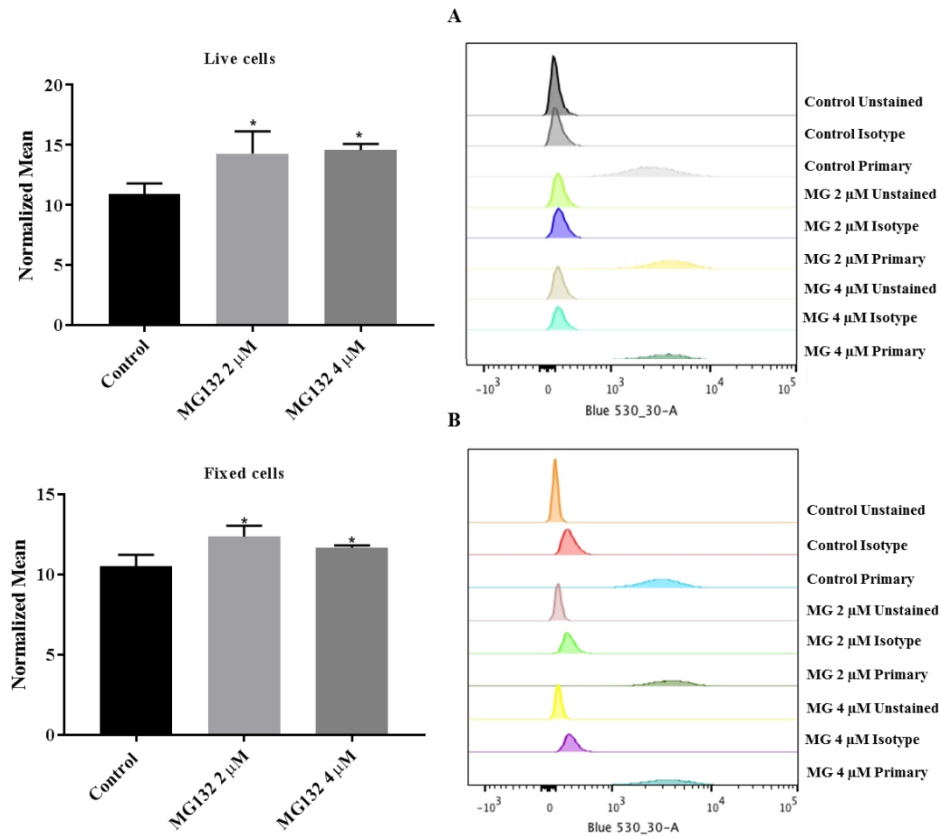


Figure (5-8): The expression of PrP^c in MG132 treated U87 cells after 12 h according to flow cytometry assay. PrP^c expression in the live cells (A) and fixed cells (B). The bar charts in A and B show that protein level increases in treated cells with 2 and 4 μ M MG132 compared to control group. The results were normalised to isotype and represent mean \pm SD of three different experiments, each performed in duplicate (n=6). All data were statistically analysed using t-test (*=p<0.05).

5.4.4 PrP^c level in MG132 treated U87 cells using confocal microscopy

To confirm the results of western blot and flow cytometry, the cells were treated with MG132 at 2 and 4 μ M, and then the PrP^c level was assessed using ICC confocal microscopy to show the expression of PrP^c in treated and untreated cells (Figure 5-9 A). The fluorescent intensity of PrP^c in treated cells (2 and 4 μ M) was higher than that in the control group (Figure 5-9 B). This reflects the increase of PrP^c level in U87 cells treated with MG132. These results are consistent with the findings of western blot and flow cytometry assays (section 5.4.2 and 5.4.3).

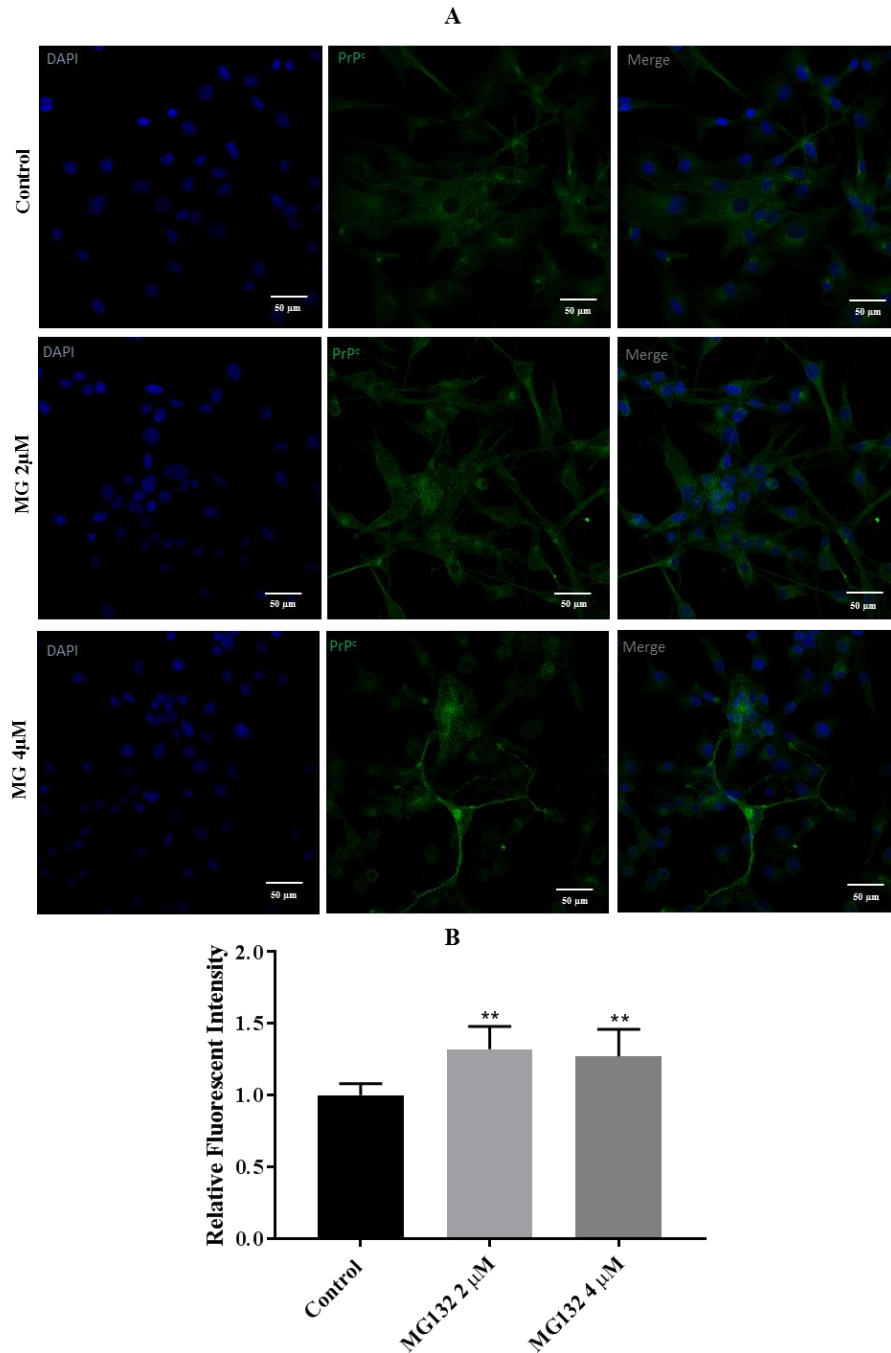


Figure (5-9): PrP^c expression in MG132 treated and untreated cells by confocal microscopy. **(A)** The cells were exposed to anti-prion protein antibody 8H4 and then labelled with Alexa Fluor 488 (green). The nuclei were labelled with DAPI (blue). **(B)**. The fluorescent intensity was calculated using Image J. The fluorescent intensity was normalised to the control and the bars represent mean ± SD of three repeats, each performed in duplicate and three images were taken for each sample (n=18). Statistical analysis was carried out using t-test (**=p<0.01).

5.4.5 MG132/TMZ combination does not promote the apoptosis of U87 according to Annexin V with PI staining assay

Annexin V assay with PI staining was carried out to determine the effect of MG132 alone and in combination with TMZ on the apoptosis of U87 cells. The cells were treated with MG132 (0.1, 0.5 and 1 μ M) and/or 25 μ M TMZ. The apoptosis rate increases in cells treated with MG132 in a dose-dependent manner for 48 h (Figure 5-10). MG132 induced the apoptosis due to its effect on many signalling survival pathways, as reviewed in section (5.1). To date, however, there has been no published experimental work on the MG132/TMZ combination. We expected that the combination of MG132 with TMZ may sensitise U87 cells to TMZ. In our results, however, the combination of MG132 with TMZ did not promote any significant change in the apoptosis rate compared to single treatment (MG132 alone) (Figure 5-10).

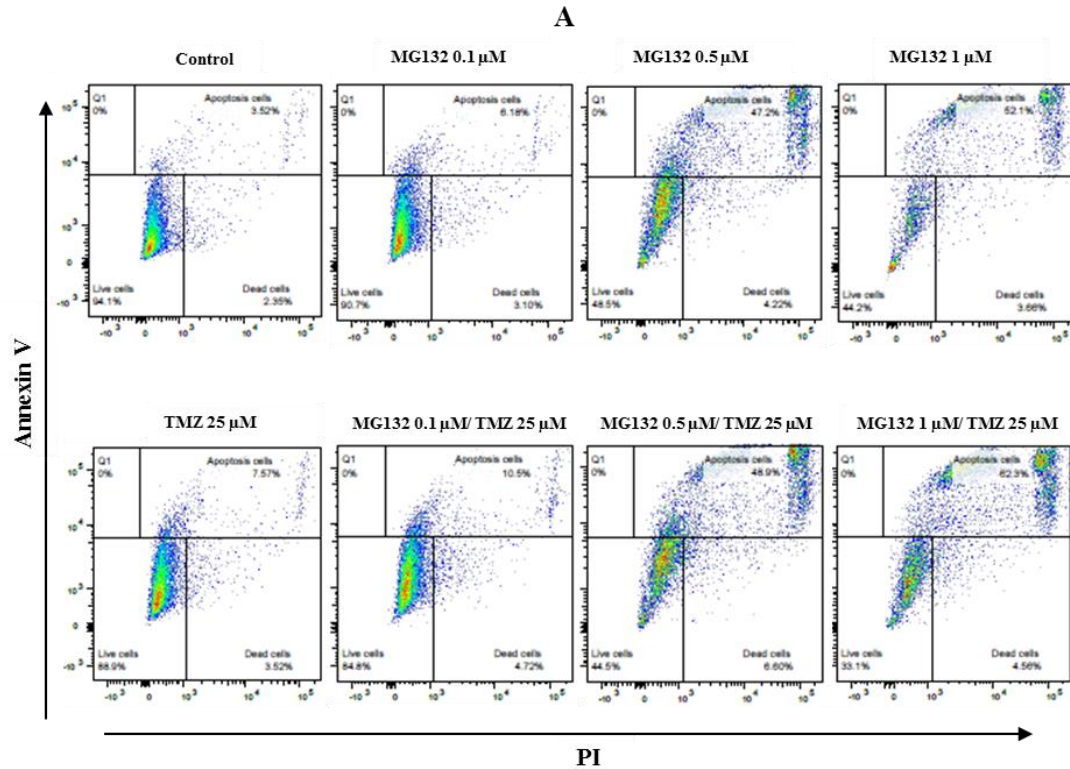


Figure (5-10): Apoptosis assay by flow cytometry for MG132 treated cells. U87 cell lines treated with TMZ, MG132 and MG132/TMZ for 48 h. The right-hand quadrante in the dot plot represents the apoptosis cells that were exposed to the treatments (A). The bar chart shows that the apoptosis increases in MG132-treated cells in a dose-dependent manner (B). These bars represent mean \pm SD of three different experiments, and each experiment was performed in duplicate (n=6). The data were analysed using one-way ANOVA, Tukey's test (*= $p < 0.05$, **= $p < 0.01$, ****= $p < 0.0001$).

5.4.6 The effect of MG132/TMZ combination upon the proliferation of U87 cells

An MTT proliferation assay was carried out to evaluate the effect of MG132 on cell viability when combined with TMZ. The cells were treated with MG132 (0.1, 0.5, 1, and 2 μM) alone and in combination with 25 μM TMZ for 48 h. The viability of the cells decreased dramatically with or without TMZ combination and there were no significant changes in cell viability in cells treated with MG132/TMZ in combination compared to MG132 alone (Figure 5-11). The results of MG132 alone (black line in Figure 5-11) over 48 h confirmed the results in section (5.3.1), namely a decrease in MG132 treated cells in a dose dependent manner. This reduction of cell proliferation could be attributed to the effect of MG132 on the PI3/Akt pathway which correlated with cell proliferation²⁵⁶. In addition, the high impact of MG132 on cell viability can be ascribed to the apoptotic effect of this treatment, as shown in section (5.4.5). It has been reported that MG132 reduces the viability of different types of cells due to its effect on many survival pathways (see section 5.1). For example, Alfeu *et al.* found that MG132 decreased the proliferation of glioblastoma cell through inhibition of the PI3/Akt pathway which is upregulated in glioblastoma cells²⁵⁶.

Concerning the effect of the MG132/TMZ combination on U87 cell proliferation, we expected that this combination may enhance the efficacy of TMZ on U87 cells. Our results, however, showed that the combination of MG132 with TMZ did not reduce the proliferation of U87 cells after 48 h compared to MG132 alone (Figure 5-11). This finding supported the results in respect to apoptosis in section (5.4.5). Further investigations will be performed in the next sections to elaborate the effect of the MG132/TMZ combination on the proliferation and apoptosis of U87 cells by evaluating the cell cycle and p53/p21, respectively.

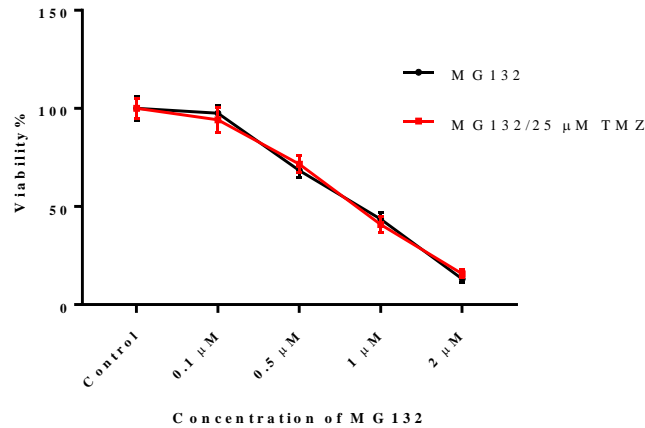


Figure (5-11): Cell viability for U87 cells treated with MG132 and/or TMZ over 48 h by MTT assay. The line graph shows the viability of treated cells with the different concentrations of MG132 in (0.1, 0.5, 1 and 2 μM) with and without combination with TMZ. There was no significant change in cell viability of the MG132/TMZ combination compared to cells treated with MG132 alone. The values represent mean \pm SD of three separated experiments, each performed eight times ($n=24$) and analysed using t-test.

5.4.7 MG132 induces cell cycle arrest

A flow cytometry assay was now carried out to evaluate the effect of MG132 and/or TMZ on the cell cycle of U87 cells. A low 0.1 μM concentration of MG132 did not affect the cell cycle, but 0.5 and 1 μM did induce cell cycle arrest in G2/M after 48 h by around 32% and 29%, respectively (Figure 5-12). The accumulation of MG132 treated cells in G2/M may be attributed to the induction of p53 and p21, which serve to regulate the cell cycle, as shown in the next section (5.4.8). Additionally, the G2/M arrest by MG132 supported the results of section (5.4.6) concerning the decrease of the cell proliferation with MG132 alone.

It is obvious that TMZ arrests the cells in G2/M after 48 h by approximately 72%. The combination of 0.1 μM MG132 and 25 μM TMZ reduced G2/M cells to about 68%, but this was non-significant relative to TMZ alone. Interestingly, the combination of TMZ with 0.5 or 1 μM MG132 reduces the number of G2/M cells

approximately from 72% to 32% and 25% respectively (Figure 5-12). Furthermore, the population of the cell cycle in cells treated with 0.5 and 1 μ M MG132 alone was insignificant compared to the comparable combination groups (0.5 and 1 μ M MG132/TMZ). These results indicated that the combination did not affect the cell proliferation when compared with MG132 and this supported the results of section 5.4.6 concerning the combination effect. Since it seems as if the target of both treatments is different, MG132 may deactivate or counteract the action of TMZ.

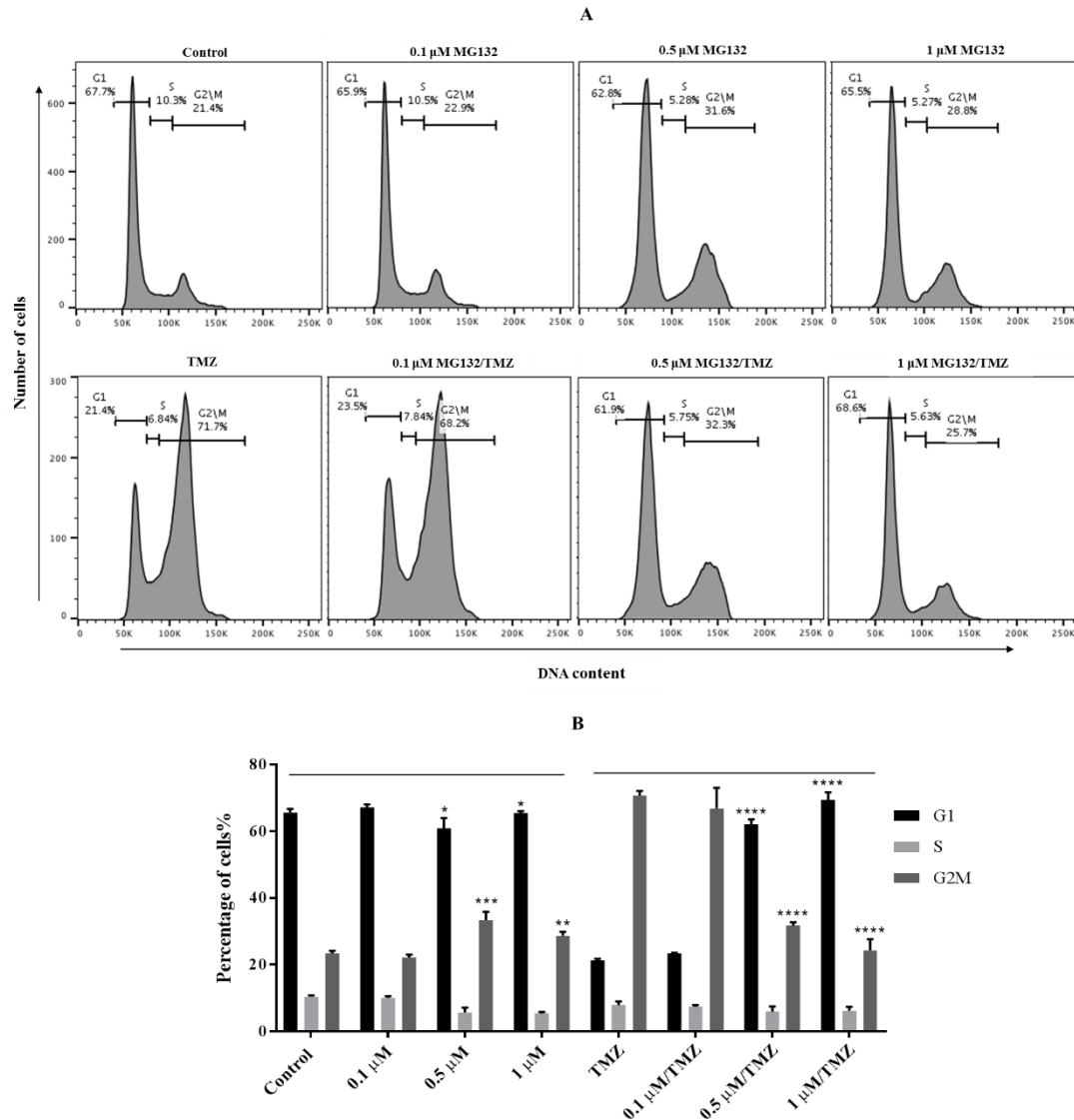


Figure (5-12): Cell cycle analysis for MG132 treated U87 cells. **A**, the histograms reveal the cells in the population of each phase after treatment with MG132 and/or TMZ. **B**, the bar chart illustrates the percentage of cells in each cell cycle phase. Quantification of mean \pm SD for three repeats, each carried out in duplicate ($n=6$). The data were statistically analysed using one-way ANOVA, Tukey's test ($*=p<0.05$, $**=p<0.01$, $***=p<0.001$, $****=p<0.0001$).

5.4.8 MG132 increases the level of p53 and p21

MG132 altered the population of cell cycle phases and induced apoptosis in U87 cells as shown in previous sections. p53 and p21 are regulators of the cell cycle and may play a role in the apoptosis of MG132 treated cells. Western blot analysis was therefore carried out to estimate the effect of MG132 and/or TMZ on p53 and p21 in

the U87 cell line. It has been mentioned in chapter 3 that TMZ accumulated the cells in the G2/M phase due to the increase of regulatory cell cycle proteins, p21 and p53. **Figure (5-13)** shows that the level of these proteins increases significantly in cells with 0.5 and 1 μM MG132 for 48 h, by approximately 3-folds for p21 and 1.5-fold for p53. The induction of p53 and p21 may be attributed to the genotoxic stress of MG132. p53, as a tumour suppressor protein, plays an important role in the regulation of the cell cycle, in apoptosis and chemoresistance²⁵⁶. In our results, the accumulation of p53 in treated cells may induce p53-dependent apoptosis.

The combination of 25 μM TMZ with 0.1 μM of MG132 for 48 h did not affect these proteins compared with TMZ-treated cells. The combination of 0.5 or 1 μM MG132 with 25 μM TMZ increased p21 and p53 levels by around 2.5-3.5 and 1.8-1.5 fold respectively. Furthermore, the level of these proteins in 0.5 and 1 μM MG132/TMZ treated cells was insignificant compared to MG132 treated cells (single treatment). These results therefore showed that the combination did not affect p53 and p21 and this confirmed the results of cell cycle **section (5.4.7)** and proliferation **section (5.4.6)**.

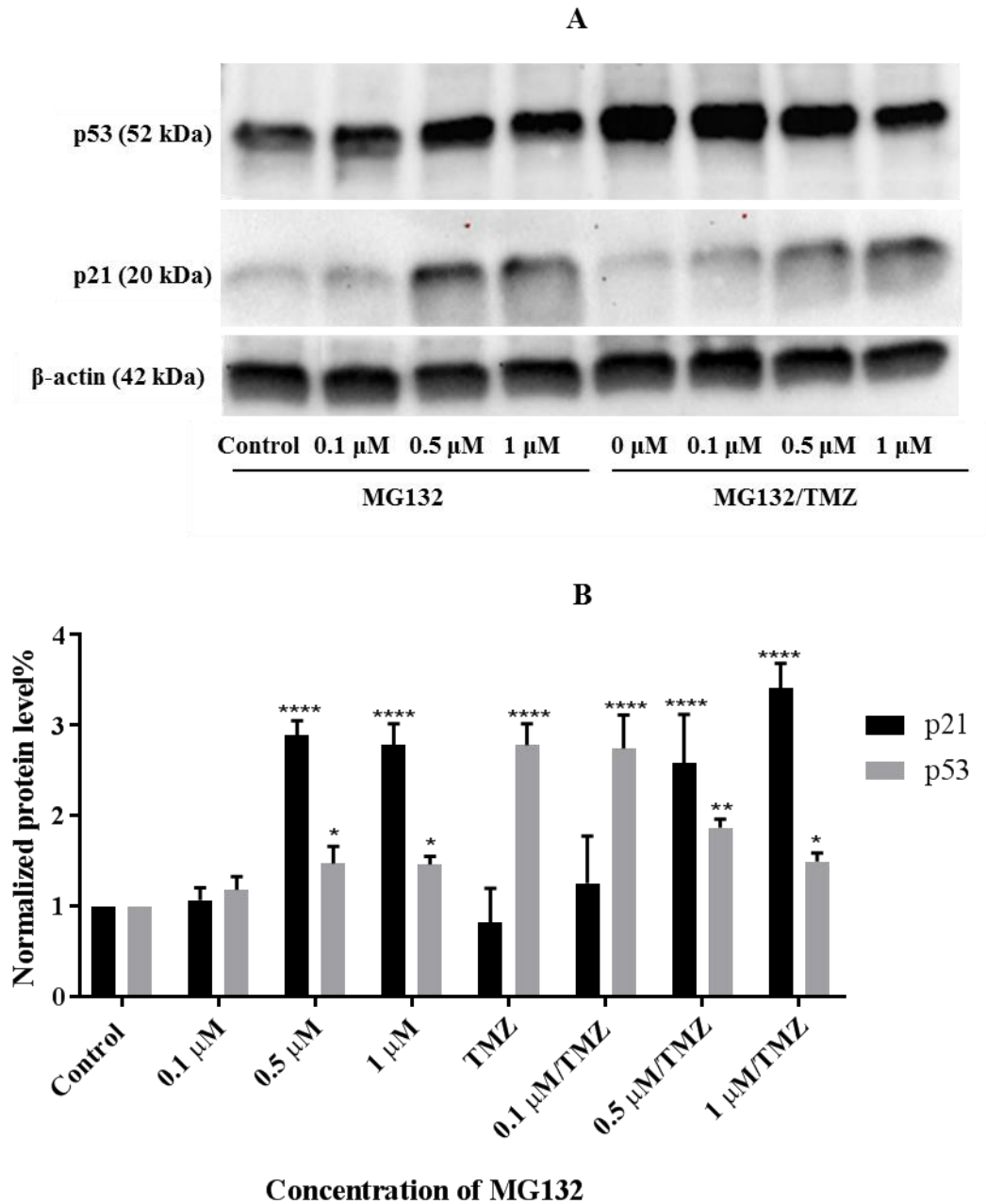


Figure (5-13): The expression of p53 and p21 and in MG132 treated U87 cells with and without TMZ. **A**, shows the western blot images for p53 and p21 in treated cells with MG132 and/or TMZ. **B**, reveals the analysis of data. Both of these proteins are upregulated in treated cells with 0.5 and 1 μM MG132 and/or TMZ. The results represent mean \pm SD of three independent experiments (n=3) and statistically analysed using one-way ANOVA, Tukey's test (*=p<0.05, **=p<0.01, ****=p<0.0001).

5.5 Summary of key experimental results

- The viability of U87 cells decreased in MG132 treated cells in a dose-dependent manner by $IC_{50} = 2.26 \mu\text{M}$
- MG132 upregulates the level of PrP^c in U87 cells after a short incubation time at high concentrations of 2 and 4 μM .
- The morphology of U87 cells was changed when treated with MG132.
- The apoptosis rate of U87 cells increased when treated with MG132, whereas there was no significant change in apoptosis between MG132 and MG132/TMZ treated cells.
- MG132 arrested the cells in the G2/M phase of the cell cycle and induced p21 and p53 levels in a dose-dependent manner, but there was no significant change in the G2/M population when comparing MG132, and MG132/TMZ treated cells.

5.6 Discussion

The ubiquitin proteasomal pathway has been shown to play a vital role in the proteolysis of most intracellular proteins and regulates many cellular processes such as differentiation, apoptosis and cell cycle. The proteasome, therefore, is considered an effective target for cancer treatment¹⁰. Proteasome inhibitors such as MG132, lactacystin and bortezomib (PS341) have been introduced in the literature and have been found to inhibit cell proliferation and induce apoptosis through different survival pathways²⁶⁰. MG132, as a proteasome inhibitor, has been specifically shown to reduce cell viability and promote the apoptosis of different glioma cells^{255,256}. The combination of MG132 with cisplatin has also been shown to enhance the apoptosis of various cancer cells such as human oesophageal cancer cells²⁵⁷. The combination of MG132 with TMZ has not been investigated yet, however. Although the targets of

MG132 and TMZ are different, we speculated that the combination of these molecules may sensitise U87 cells to TMZ.

In our work, we found that MG132 can remarkably reduce the growth of U87 cells in a dose-dependent manner, with an $IC_{50} = 2.26 \mu\text{M}$ over a 24 h treatment period (Figure 5-6). This may be attributed to the apoptotic and cytotoxic effect of MG132. Generally, this finding is in agreement with another study by Alfeu *et al.*; they found that MG132 reduced cell viability of different glioma cells such as C6, U138 MG, U87 and U373 in a dose-dependent manner with $IC_{50} = 2.8, 2.5, 5.1$ and $2.6 \mu\text{M}$ respectively after 48 h, but did not affect astrocytes²⁵⁶. Xue-Feng *et al.* stated that MG132 suppressed the proliferation of U87 and U251 glioma cells in both a time- and dose-dependent manner according to MTT assay¹³.

The proliferation of U87 cells was also decreased when treated with MG132 for 48 h both in combination with TMZ and without combination. These results therefore indicate that the combination of MG132 with TMZ does not affect the proliferation of U87 relative to treatment with MG132 alone (Figure 5-13). The reduction in the proliferation of cells when they are treated with MG132 may be related to the effect of this treatment on many survival pathways. For instance, MG132 decreased the proliferation of glioblastoma cells by inhibition of the PI3/Akt pathway, which is upregulated in glioblastoma cells²⁵⁶. Furthermore, in our results, the apoptosis of U87 cells was increased in cells treated with MG132, and this could be attributed to the accumulation of p53 and p21. p53 plays an important role in cell cycle regulation, apoptosis and chemoresistance²⁵⁶. Other studies have found that MG132 can promote the activation of caspase 3 and the release of cytochrome c in glioblastoma cell lines, LN-308 and LN-18. These studies showed that apoptosis is p53/p21 dependent due to the increase of p53 and p21 in wild type p53 cells treated with any apoptotic stimuli

such as MG132. In addition, MG132 induced the apoptosis in U87 cells through upregulation of p53 and p21. In contrast, apoptosis in glioma cells with the p53 mutation undergo a p53 independent mechanism^{261,12,256}. Furthermore, MG132 promotes the apoptosis of U87 by increasing p53 and downregulating p21¹³.

In our results, MG132 accumulated the cells in G2/M by increasing the level of p53 and p21 since these regulate the cell cycle. The induction of G2/M arrest could also elucidate a decrease in the proliferation of MG132 treated cells. These results are in agreement with the previous results that showed that MG132 induces G2/M arrest in glioblastoma cells which results from the increase of p53 and p21^{255,256}. Furthermore, proteasome inhibitors can reduce p21 and p27 degradation thus initiating growth arrest and apoptosis^{262,256}. In contrast, our results partially disagree with Xue-Feng *et al.* who ascribed the accumulation of cells in G2/M to the increase in the level p53 level and a decrease in p21 expression in U87 cells treated with MG132¹³.

Similar observations concerning proliferation, apoptosis and cell cycle arrest were found in this work when combined MG132 with TMZ. It has been reported that TMZ accumulates glioma cells in G2/M²²⁴. TMZ arrests U87 cells in G2/M by 71% of total cells after 48 h whereas the combination with MG132 reduces the G2/M to around 31% which is the same percentage of G2/M cells in U87 cells treated with MG132 alone (Figure 5-11). Furthermore, the apoptosis rate and the level of p21 and p53 in MG132/TMZ-treated cells were consistent with those in cells treated with MG132 alone. This is a somewhat unexpected result. To our knowledge, the effect of the combination of TMZ and MG132 on U87 cells have not been studied prior to this work but our results show that there is no cumulative effect when TMZ is combined with MG123. It is unclear as to why this is, but a potential explanation could be that MG132 competes with or counteracts TMZ.

Regarding the effect of MG132 on PrP^c, in our results, high concentrations of MG132 (2 and 4 μ M for 12 h) increased the level of PrP^c in U87 cells whereas 0.5 and 1 μ M for 24 h did not affect the PrP^c level in these cells. The upregulation of this protein was about 1.5-2-fold possibly due to MG132's ability to reduce the protein degradation resulting from the function of the ERAD proteasome pathway (Figure 5-7, 5-8, 5-9). Yifat *et al.* showed that MG132 increases the level of PrP^c in CHO-MHM2 and N2a cells due to resistance of PrP^c to proteolysis by endoplasmic-reticulum-associated protein degradation (ERAD) in the metabolism of PrP^c¹⁴. Other studies reported that MG132 upregulates the cytosolic 27-34 kDa of PrP^c in Hela-PrP, N2a-PrP and N2a cell lines. This has been linked to the blockage of the proteasome which results in the unfolded protein response (UPR) as a consequence of endoplasmic reticulum stress²⁵⁹. Furthermore, Jiyan Ma *et al.*¹²² suggested that the metabolism of PrP^c was partially regulated by the ERAD-proteasome degradation pathway when the proteasome was inhibited, suggesting that a similar pathway may regulate cytosolic PrP^c and potentially membrane PrP^c levels in U87 cells. There is no literature to our knowledge to support the contention that inhibition of the ERAD-proteasome degradation pathway increases membrane associated PrP^c levels, and thus further analysis is needed.

Furthermore, the toxicity of high doses of MG132 (2 and 4 μ M) changes the morphology and promotes the detachment of U87 cell as is clearly seen in the actin filaments staining (phalloidin 488) reported in this chapter. Alfeu *et al.* mentioned that in the case of U138MG cells more than 1 μ M of MG132 causes the cell membrane to lose its integrity, weakens the attachment of cells and changes the cell morphology²⁵⁶.

To conclude, MG132 induces the apoptosis of U87 cells in a p53-dependent manner. Unexpectedly, however, the combination of MG132 with TMZ does not improve the

apoptosis rate compared to cells treated with MG132 alone. The efficacy of TMZ on U87 was null when combined with MG132. Our results have also showed for the first time that a short period of treatment of U87 cells with high concentration of MG132 reduces the degradation of PrP^c and, therefore, increase its level.

Chapter 6: Investigation of the effect of small molecules (Fanconi anaemia pathway inhibitors, FAPi) on the level of PrP^c in U87 cells

6.1 Introduction

The Fanconi Anaemia (FA) pathway is operated by a network of proteins responsible for DNA repair, with 22 genes/proteins so far discovered in this family.²⁶³ Any defect in these genes will result in a disease called Fanconi Anaemia which is a recessive genetic disorder (Table 6-1)²⁶⁴. In addition to its connection with FA disease, however, FA pathway plays an important role in DNA repair in mammalian cells. It was revealed that 12 of these proteins is a minimum requirement in the normal function of the FA pathway (Figure 6-1)¹⁶. The 22 proteins in FA pathway can be divided into three groups according to their role in the complex:

- 1- Upstream proteins or FA core complex involve 10 proteins, FANCA, FANCB, FANCC, FANCE, FANCF, FANCG, FANCL (E3 ligase), FANCM²⁶³, FANCT²⁶⁵ and FANCW²⁶⁴.
- 2- Nexus ID2 complex includes FANCI and FANCD2 which are substrates for E3 ubiquitin ligase and constitutes monoubiquitin (Ub) that follows DNA damage²⁶³.
- 3- Downstream of FANCD2/FANCI complex consists of FANCD1, FANCI, FANCN, FANCO, FANCP, FANCQ²⁶³, FANCR, FANCS²⁶⁵, FANCU and FANCV²⁶⁴ which play effective roles in DNA repair.

Table (6-1): The FA genes and their function.

Protein's group	Gene's name	Function
A	FANCA	FA core complex member
B	FANCB	FA core complex member
C	FANCC	FA core complex member
D1	FANCD1/BRCA2	Downstream of FANCD/FANCI complex
D2	FANCD2	Formation FANCD/FANCI complex
E	FANCE	FA core complex member
F	FANCF	FA core complex member
G	FANCG/XRCC9	FA core complex member
I	FANCI/KIAA1794	Monoubiquitinated. Forms heterodimer with FANCD2
J	FANCI/BRIP1/BACH1	Downstream of FANCD/FANCI complex
L	FANCL/PHF9	FA core complex member
M	FANCM	FA core complex member
N	FANCN/PALB2	Downstream of FANCD/FANCI complex
O	FANCO/RAD51C	Downstream of FANCD/FANCI complex
P	FANCP/SLX4	Downstream of FANCD/FANCI complex
Q	FANQ/ERCC4/XPF	Downstream of FANCD/FANCI complex
R	FANCR	Downstream of FANCD/FANCI complex
S	FANCS	Downstream of FANCD/FANCI complex
T	FANCT	FA core complex member
U	FANCU	Downstream of FANCD/FANCI complex
V	FANCV	Downstream of FANCD/FANCI complex
W	FANCW	FA core complex member

FANCD2 monoubiquitination occurs after DNA damage, with a complex of upstream proteins being required to activate this process. Monoubiquitination is directed to nuclear foci, and this interaction repairs the DNA damage²⁶⁶. Specifically, the interaction of FANCD2 protein with BRCA1 and BRCA2 proteins promotes the

repair of DNA lesions. Furthermore, FANCD2 monoubiquitination and the formation of nuclear foci occur in the S phase of the cell cycle¹⁶.

Sims *et al.* stated that FANCI has the second most important role in the FA pathway after FANCD2. They confirmed this role by determination of FANCI monoubiquitination in cell lines in which the core complex protein was knocked down. Inhibition of FANCA and FANCG entirely rescinded the ubiquitination of FANCI in these cells. Thus, the ubiquitin ligase stimulates FANCI during the DNA damage process²⁶⁷.

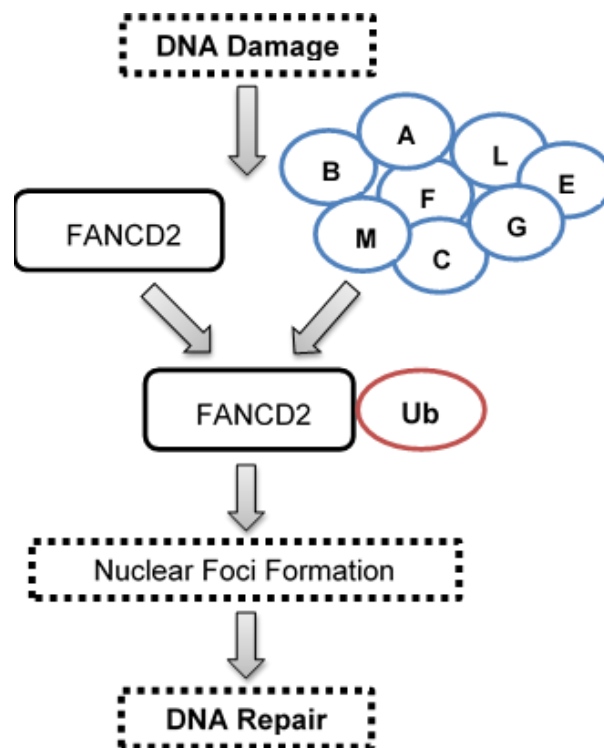


Figure (6-1): The mechanism of DNA repair via the FA pathway. Adapted from Chen *et al.* with kind permission of Springer Nature Group¹⁶.

Chemotherapeutic agents such as cisplatin, TMZ and BCNU kill cancer cells by producing DNA interstrand crosslink (ICL) which prevents DNA disentangling and blocks its replication and transcription. Eukaryotic cells, however, use the FA

pathway to repair such damage rendering anti-cancer drug inactive and causing resistance. The FA pathway also has an important role in assisting other types of DNA repair processes such as nucleotide excision repair, translesion synthesis, homologous recombination²⁶⁸.

According to previous studies, resistance to chemotherapies arises from the complex pathways which are associated with many processes of DNA repair. TMZ and BCNU increase monoubiquitinated FANCD2 and nuclear foci formation in glioblastoma cells that have proficient FA pathway and the sensitivity to these treatments was increased in deficient FA pathway's cells¹⁶. Patil and co-workers confirmed these findings when they found that FANCD2 has a significant level of expression in high-grade gliomas when compared with lower grades in GBM tissue samples. They also reported that silencing of the FA pathway or inhibiting of FANCD2 improved the efficacy of TMZ and BCNU¹⁷. In addition, Nimustine (ACNU) and TMZ were used *in vitro* to evaluate the FA pathway, which causes DNA damage as a result of these treatments. FANCD1 and FANCG particularly contribute to DNA repair after the damage by ACNU or TMZ. Silencing of FANCD1 improved the efficacy of these agents in A172 glioblastoma cells²⁶⁹. These results attracted the researcher to develop novel molecules that may inhibit the FA pathway and thence increase the sensitivity of glioblastoma cells to chemotherapy.

In previous work within our group by Drs. Matthew Sellwood and Peng Hua it was demonstrated that novel small molecules FA pathway inhibitors (FAPi compounds) could downregulate FANCD2, which is activated in response to TMZ or BCNU treatment and this action may improve the effectiveness of these alkylating agents on U87 cells (unpublished results). In addition to the effect of FAPi compounds on the

level of FANCD2, some of these molecules may also suppress the level of PrP^c in glioblastoma cells. Although there is no specific structure of compounds targeting PrP^c, many different scaffolds may have a potential active hit to PrP^c¹⁸. It has been found that different analogues of amide compounds and other scaffolds have a possible potential effect to suppress the level of PrP^c in glioblastoma cells T98G according to SPC (single point confirmation) and ELISA. It is not known why some compounds selectively reduced PrP^c levels in glioblastoma cells, T98G¹⁸. We hypothesise that these compounds may have a dual function by inhibiting the FA pathway and reducing the level of PrP^c in U87 cells. In this chapter, ICC by ImageXpress Micro imaging system as a high throughput screening system (HTS) will be used for the first time to evaluate the PrP^c expression level in treated U87 cells with the combination of TMZ or BCNU with FAPi compounds or with FAPi compounds alone.

6.2 The aim

The aim of this chapter is to assess the level of PrP^c in U87 cells when treated with small molecules (benzimidazole amide derivatives, [Figure 6-2](#)) and possible effects upon treatment by TMZ and BCNU. The aim of this work will be addressed via following objectives:

- Investigate the effect of these molecules on cell viability in treated cells with FAPi compounds in combination with TMZ or BCNU.
- Evaluation of FANCD2 level in cells treated cells with TMZ or BCNU using western blotting.
- The ICC method using the ImageXpress Micro as a high-throughput or high content screening assay (HTS), will be employed to evaluate the level of PrP^c in treated cells with FAPi compounds in combination with TMZ or BCNU.

Prior to this, since this method was not used in the context of PrP^c level in U87 cells, the optimization and validation of this method will be performed using the following experiment.

- Optimising the concentration of anti-prion antibodies (3F4 and 8H4)
- Evaluation of PrP^c expression level in transfected cells with PRNP siRNA and compare that with previous results in chapter 4.

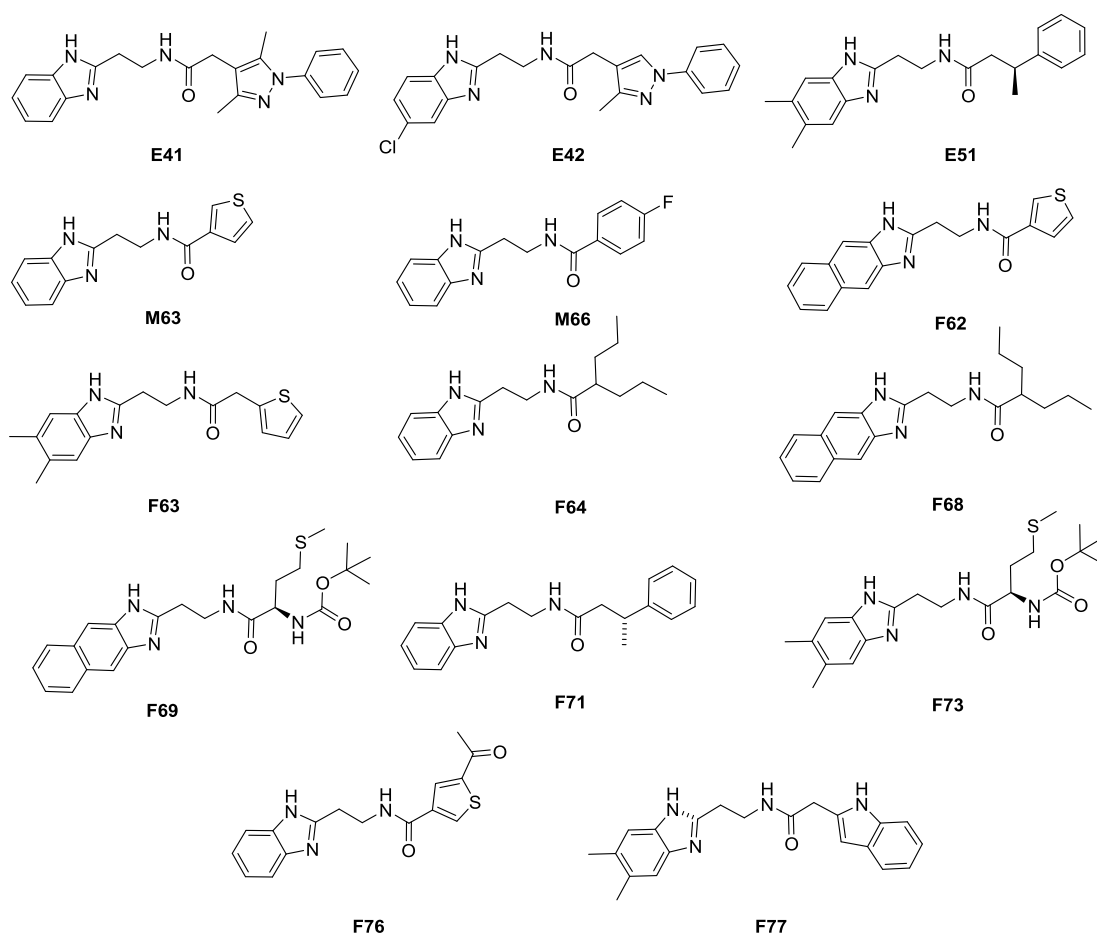


Figure (6-2): The structures of FAPi compounds.

6.3 Methods

In this chapter the incubation times and the concentrations of FAPi compounds and alkylating agents were used according to the previous work by Drs. Matthew Sellwood and Peng Hua.

6.3.1 Preparation of treatments

The small molecules and alkylating agents (TMZ and BCNU) were dissolved in DMSO at 10 mM and 20 mM respectively as a stock solution. The stock solutions were then aliquoted into smaller portions in small vials and kept at -80 °C. The working solution was prepared by diluting the stock solution with DMSO (1:5) and then with PBS (1:20). The final concentration of small molecules (FAPi compounds) and alkylating agents was 5 µM and 50 µM, respectively; as used in previous work by Drs. Matthew Sellwood and Peng Hua (unpublished data).

6.3.2. Cell viability assay

MTT assay was carried out to evaluate the cell viability of U87 treated with the small molecules in combination with TMZ or BCNU. The cells were cultured in 96-well plate at 5000 cells in each well and left overnight for attachments. The cells were treated with small molecules by adding 2.5 µl of working solution (i.e 5 µM final concentration) using a multichannel pipette. The control group was treated with 2.5 µl of 10% DMSO. The plate was then incubated for 8 h in the incubator at 37 °C. This step was followed by adding 2.5 µl of working solution of TMZ or BCNU (i.e 50 µM final concentration) to each well of the treated groups and 2.5 µl of 10% DMSO to each well of the control group. The plate was then left for 40 h under standard incubation conditions before the MTT protocol (section 2.2.2) was performed to evaluate the viability of the treated U87 cells. The Figure (6-3) below shows the design of this experiment.

	1	2	3	4	5	6	7	8	9	10	11	12
A												
B		E41/TMZ or BCNU			F63/TMZ or BCNU			F76/TMZ or BCNU				
C		E42/TMZ or BCNU			F64/TMZ or BCNU			F77/TMZ or BCNU				
D		E51/TMZ or BCNU			F68/TMZ or BCNU			Contrl/TMZ or BCNU				
D		M63/TMZ or BCNU			F69/TMZ or BCNU			Contrl				
F		M66/TMZ or BCNU			F71/TMZ or BCNU							
G		F62/TMZ or BCNU			F73/TMZ or BCNU							
H												

Figure (6-3): The experimental design of MTT assay used to evaluate cell viability of U87 cells treated with FAPi compounds/TMZ or BCNU.

6.3.3 Western blot assay

To assess the level of FANCD2 in treated U87, the cells were cultured in a 6-well plate at 200000 cells and allowed to attach overnight, the cells were then treated with 50 μ M TMZ or BCNU. The plate was then incubated for 24 h and the protocol for western blotting was applied (section 2.2.5) to quantify the FANCD2 level. In this experiment, the PVDF membrane was exposed to anti FANCD2 antibody and secondary antibody (goat anti-mouse IgG) at 1:500 and 1:4000, respectively, as described in the manufacturer's instructions for these antibodies. The membrane was re-probed with β -actin as a loading control.

6.3.3 High throughput and high content small molecule screening method

High-throughput screening (HTS) technology is an automated microscope-based assay which provides information on individual and multiple cells using several fluorescent stains to evaluate accurately many targets that are triggered by drugs and small molecules²⁷⁰. The large number of cell images is rapidly quantified by image analysis using specific algorithms to provide initial evidence of the predictive validity for the cytotoxicity and efficacy of drug candidates²⁷¹. This technique has therefore become an effective tool in drug discovery and in the pharmaceutical industry and has also attracted the interest of cell researchers²⁷². To date, however, this method has not been

used to quantify the binding of PrP^c to anti-prion antibodies hence the following experiments will elucidate this binding further.

6.3.3.1 Optimisation of ImageXpress Micro as a high content screening assay

This method was used to evaluate the level of PrP^c in cells treated with FAPI compounds in combination with TMZ or BCNU. Prior to this experiment, the concentration of anti-prion antibodies (3F4 and 8H4) had to be optimised. These anti-prion antibodies were selected because they are commonly used for immunostaining in various studies^{273,184}. The 3F4 antibody binds strongly to PrP human and hamster with a specific requirement of two Met residues at positions 109 and 112 of the human PrP²⁷⁴, while the 8H4 antibody reacts with PrP monkey, bovine, rat, human, sheep and mouse, and its epitope residues found in amino acids 145-180 of the human prion protein²⁷⁵. The 96-well plate (Greiner Bio-One Ltd, cat no. 655098) was treated with polyornithine bromide, as described in [section \(2.2.8\)](#) and the cells were then cultured with 10000 cells in each well. Next day, the cells were fixed and the ICC protocol was followed ([see section 2.2.8](#)) to evaluate the fluorescent intensity of the PrP^c level. In this protocol, the cells were exposed to different concentrations of primary and secondary antibodies. Two kinds of anti-prion antibodies (3F4 and 8H4) in serial dilution and two dilution factors for secondary antibody (Donkey anti-mouse Alexa flour 488) were used to evaluate PrP^c expression level ([Figure 6-4](#)).

	1	2	3	4	5	6	7	8	9	10	11	12
A	1:100/3F4	1:100/3F4	1:100/3F4	1:100/8H4	1:100/8H4	1:100/8H4	1:100/3F4	1:100/3F4	1:100/3F4	1:100/8H4	1:100/8H4	1:100/8H4
B	1:250/3F4	1:250/3F4	1:250/3F4	1:250/8H4	1:250/8H4	1:250/8H4	1:250/3F4	1:250/3F4	1:250/3F4	1:250/8H4	1:250/8H4	1:250/8H4
C	1:500/3F4	1:500/3F4	1:500/3F4	1:500/8H4	1:500/8H4	1:500/8H4	1:500/3F4	1:500/3F4	1:500/3F4	1:500/8H4	1:500/8H4	1:500/8H4
D	1:750/3F4	1:750/3F4	1:750/3F4	Sec 1:1000	Sec 1:1000	Sec 1:1000	1:750/3F4	1:750/3F4	1:750/3F4	Sec 1:500	Sec 1:500	Sec 1:500
E	1:1000/3F4	1:1000/3F4	1:1000/3F4	Sec 1:1000	Sec 1:1000	Sec 1:1000	1:1000/3F4	1:1000/3F4	1:1000/3F4	Sec 1:500	Sec 1:500	Sec 1:500

Figure (6-4): The experimental design to optimise the PrP^c antibodies.

6.2.3.2 Validating the screening method

Since the ICC method using ImageXpress Micro have not been used to evaluate the PrP^c level. The cells were seeded in a 96-well plate (Greiner Bio-One Ltd, cat no. 655098) at a density of 5000 cells per well. After overnight attachment, the cells were transfected with scrambled and PRNP siRNA for 48 h as described in [section \(2.2.9\)](#). The ICC protocol ([section 2.2.8](#)) was followed to assess the level of PrP^c in the transfected U87 cells.

6.3.3.3 The screening of FAPi compounds to evaluate PrP^c level

The Greiner 96-well plate was prepared and coated with polyornithine bromide as described in [section \(2.2.8\)](#). The cells were seeded with 5000 cells in each well and then next day treated with FAPi compounds and alkylating agents TMZ or BCNU as described in [section \(6.3.2\)](#). After the incubation hours, the protocol for ICC was followed ([section 2.2.8](#)) to quantify the PrP^c level. In this experiment, the wells were exposed to primary antibody 8H4 at 1:250 and secondary antibody (Donkey anti-mouse Alexa flour 488) as shown in the [Figure \(6-5\)](#) below.

	1	2	3	4	5	6	7	8	9	10	11	12
A												
B		E41/TMZ or BCNU-Primary			F63/TMZ or BCNU-Primary			F76/TMZ or BCNU-Primary				
C		E42/TMZ or BCNU-Primary			F64/TMZ or BCNU-Primary			F77/TMZ or BCNU-Primary				
D		E51/TMZ or BCNU-Primary			F68/TMZ or BCNU-Primary			Contrl/TMZ or BCNU-Primary				
D		M63/TMZ or BCNU-Primary			F69/TMZ or BCNU-Primary			Contrl-Primary				
F		M66/TMZ or BCNU-Primary			F71/TMZ or BCNU-Primary			Contrl-Secondary				
G		F62/TMZ or BCNU-Primary			F73/TMZ or BCNU-Primary							
H												

Figure (6-5): The design of screening compounds by ImageXpress Micro. All wells were exposed to primary and secondary antibody except six wells (Control-primary, Control-Secondary), which were exposed to primary or secondary antibody only to determine the non-specific binding.

6.3.4 The analysis of the images

The procedure of the imaging was followed from the main menu of the MetaXpress software. A 20x objective was used to image all the selected wells. The acquired images were then analysed by designing a protocol using MetaXpress software

version 6.1. Briefly, the nuclear area was identified by DAPI staining (Blue channel, excitation 374/50, emission 447/60), then the PrP^c signal (Green channel, excitation 438/24, emission 483/32) was localised by aligning the cell shape on the segment of DAPI staining. Using a special algorithm, the total number of cells was calculated based on the fluorescent intensity of the blue channel. The intensity of the green areas represents PrP^c level in each cell. The total intensity of all cells was then calculated and then divided by the total number of cells to obtain the mean of individual intensity.

The collected data were normalised as a percentage to the control group. The results were statistically analysed using student's t-test as mean \pm SD.

6.4 Results

6.4.1 Cell viability for U87 cells treated with FAPi compounds in combination with TMZ or BCNU

To investigate whether FAPi compounds induce toxicity to U87 cells in combination with TMZ or BCNU, an MTT assay was carried out. The cells were treated for 8 h with 5 μ M FAPi compounds and then treated with TMZ or BCNU for 40 h. **Figure (6-6)** reveals that none of these compounds affects the viability of U87 cells. The cell viability was between 84% \pm 11 to 103% \pm 12 and between 88% \pm 11 to 110% \pm 7 for treated cells with FAPi compounds in combination with TMZ or BCNU respectively in comparison with the control group. Due to the non-toxic effect of these compounds when combined with TMZ or BCNU, they were used in the ImageXpress Micro screening method (**section 6.4.4**). Our findings confirm the results of previous work by Drs. Matthew Sellwood and Peng Hua using the same combinations (unpublished data).

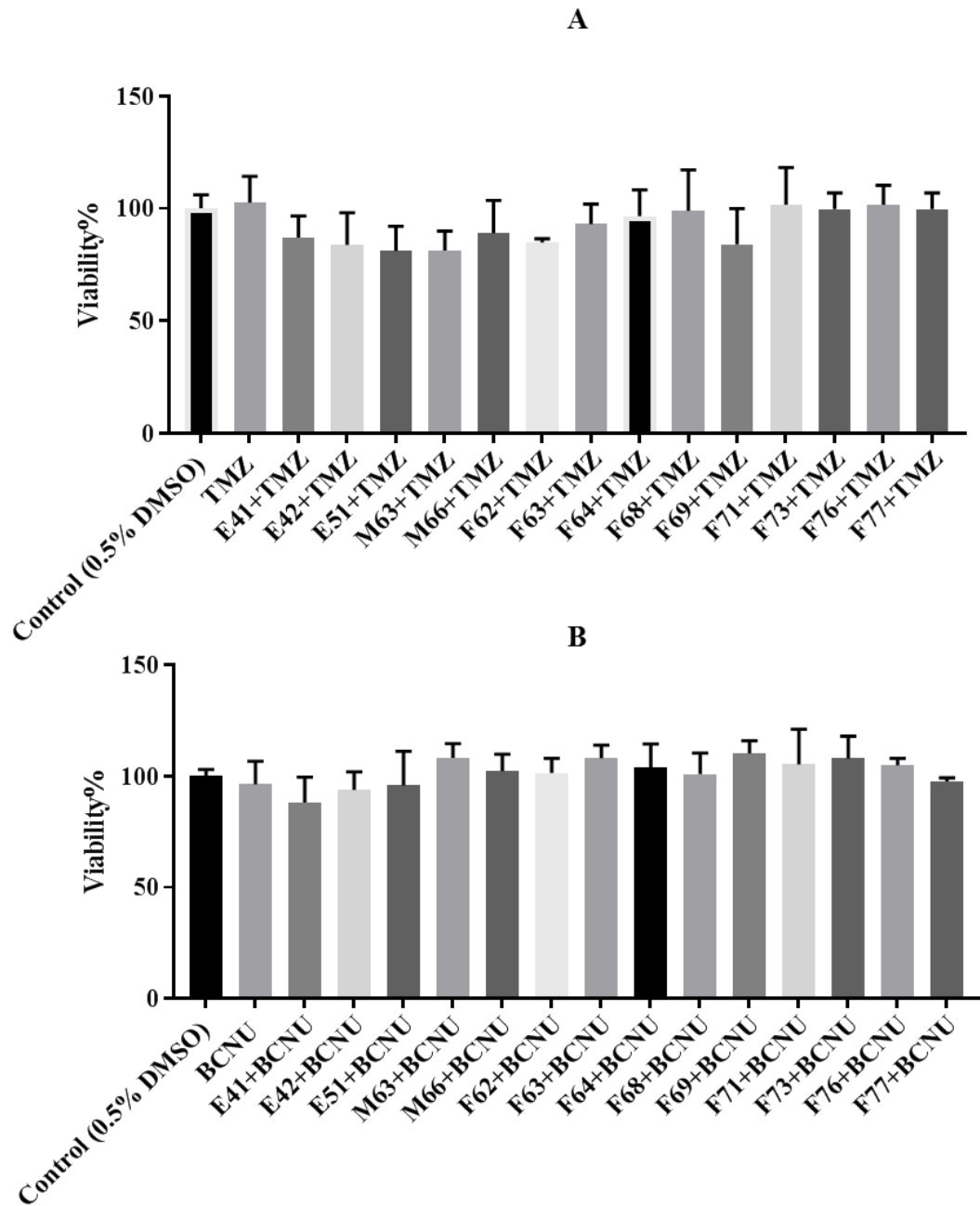


Figure (6-6): Cell viability assay for U87 cells treated with FAPi compounds in combination with TMZ or BCNU. The **A** and **B** bar charts reveal cell viability of U87 cells treated with FAPi compounds in combination with TMZ or BCNU respectively. The cell viability was normalised to the control group. The bars represent mean \pm SD of three independent experiments, each performed in triplicate (n=9). The data were statistically analysed using one-way ANOVA, Tukey's test (each compound was compared to the control and TMZ or BCNU treated cells).

6.4.2 FANCD2 expression in treated U87 cells with TMZ or BCNU

To find out whether TMZ or BCNU induced the FA pathway in U87 cells through upregulation of the FANCD2 level, the cells were treated with these agents for 24 h and western blot assay was then used to evaluate FANCD2 expression. **Figure (6-7)** shows that the level of FANCD2 was significantly increased in treated cells compared to the control group. This induction was in response to the DNA damage caused by alkylating agents which activated many pathways such as the FA pathway to repair this damage. This pathway is required to protect the cells from the DNA interstrand cross-links resulting from alkylating agents²⁷⁶.

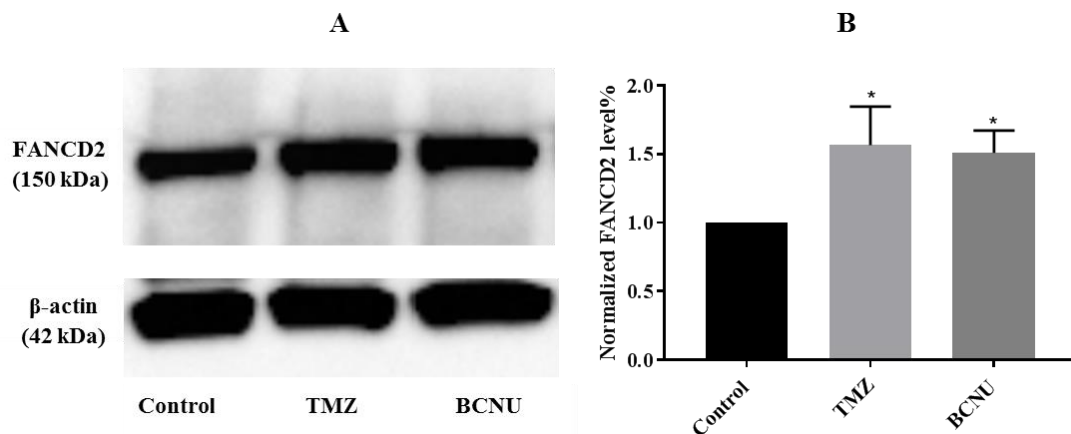


Figure (6-7): Western blot for FANCD2 in U87 cells treated with TMZ and BCNU for 24h. **(A)**, represents the image of western blot. **(B)**, the bar chart represent mean \pm SD and shows the significant increase of FANCD2 in treated cells in comparison to the control group. This experiment was repeated three times and normalised to the control group (n=3). The results were analysed using t-test (*= $p < 0.05$).

6.4.3 FAPi compounds suppress FA pathway

In previous work by this research group, ICC and western blot assays were used to investigate the level of FANCD2 in U87 cells treated with FAPi/TMZ or FAPi/BCNU combinations. Seven compounds were chosen to present in this chapter.

These small-molecule compounds have reliable inhibition against FA re-activated by chemotherapeutic agents, TMZ and BCNU (Figure 6-8 A and B). In western blot assay, although there was no significant difference between the TMZ or BCNU band on the one hand and the compounds' pre-dosing bands on the other when using 1 μ M (data not shown). When the pre-dosing concentration was increased to 5 μ M, the band of FANCD2 FAPi conditions was observed to be significantly fainter than those TMZ or BCNU, even reaching the DMSO control level (Figure 6-8 B and C). Altogether, therefore, this family of small-molecules has great potential to be developed for specifically inhibiting FA pathway in U87 cells.

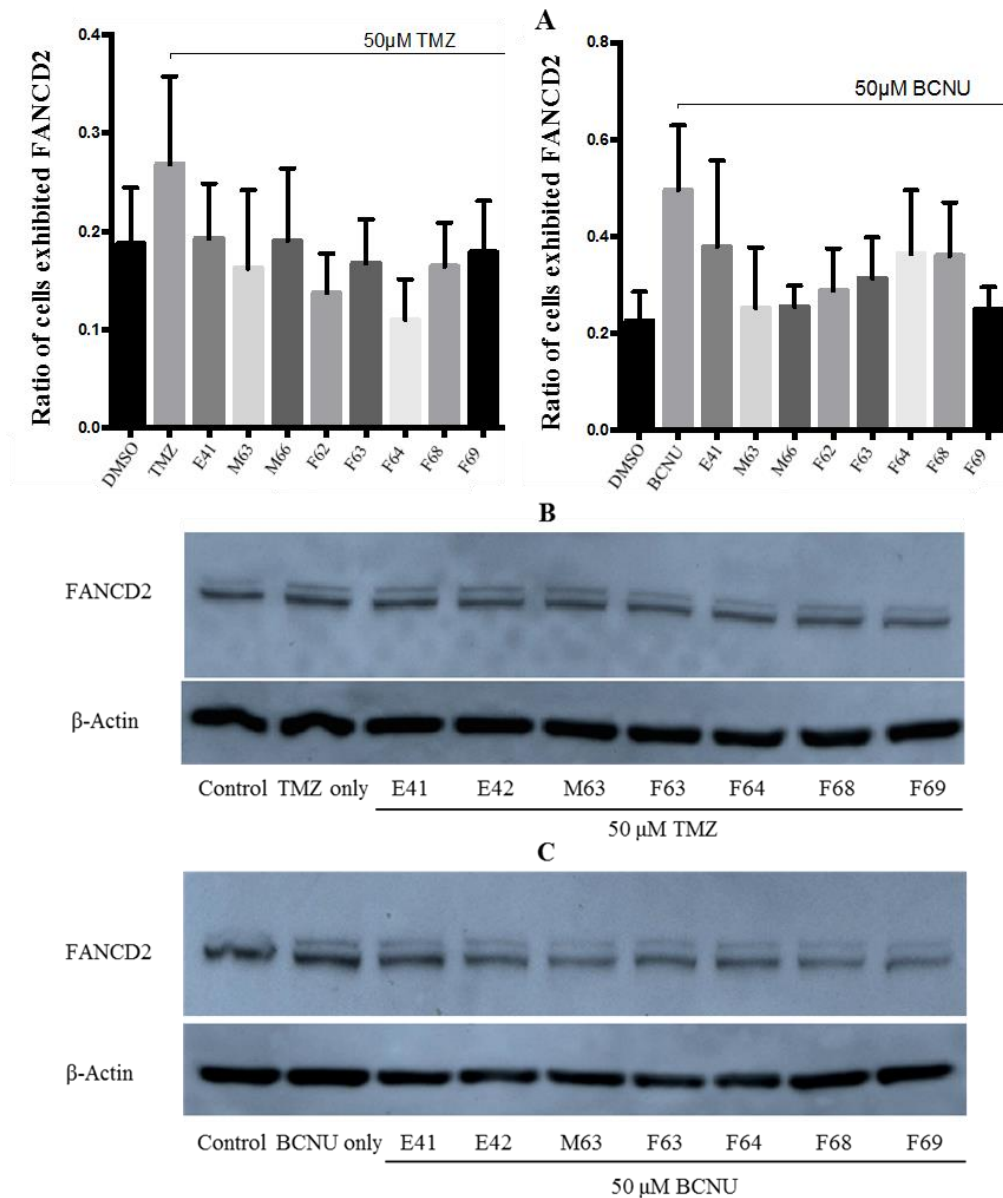


Figure (6-8): The level of FANCD2 in FAPi treated U87 cells. **A**, Immunofluorescence detection and quantification of U87 cells exhibiting nuclear FANCD2 foci (a marker of an active FA pathway). The cells were treated with 5 μ M compounds prior to 50 μ M TMZ or BCNU for 40 h. Images were captured and analysed using Volocity software. Error bars represent the standard deviation of the means. All duplicated data suggest that these compounds offer a reliable inhibition of FANCD2 signalling. **B** and **C**, Representative western blots showing FANCD2 and actin (loading control) expression in U87 cells treated with TMZ or BCNU activate the FA pathway. Pre-treatment with FAPi and then the combination with TMZ or BCNU inhibit FA pathway activation as evidenced by significantly reduced FANCD2 after TMZ or BCNU treatment. These experiments were performed by Drs. Matthew Sellwood and Peng Hua.

6.4.4 Development of high throughput and high content small molecule screening method

High-content imaging by ImageXpress Micro has numerous applications in the drug discovery field including target identification and screening of chemical compounds. Since, so far, this method has not been used to assess the binding of the anti-PrP^c antibodies to PrP^c, the next set of experiments were aimed to evaluate whether ICC by ImageXpress Micro is suitable to evaluate PrP^c level in U87 cells or not.

6.4.4.1 Optimisation and validation of ImageXpress Micro as a high throughput and high content screening assay

To optimise this method and to obtain an accurate indication of the binding of PrP^c with the anti-prion antibody, ICC was carried out using different concentrations of 3F4 and 8H4 anti-prion antibodies. **Figure (6-9, A)** reveals the profile of the 96-well plate which was exposed to the serial dilution of both primary antibodies and two dilutions of secondary Alexa Fluor 488 (1:1000 and 1:500). The profile image of the 96-well plate shows a gradient of brightness indicating the binding of both antibodies to the fluorescent secondary antibody. The fluorescent intensities of both primary antibodies decreased gradually with 1:1000 of the secondary antibody, whereas with 1:500 of secondary antibody the fluorescent intensities fluctuated (**Figure 6-9, B**). These results would suggest that both 3F4 and 8H4 are suitable for use in this experiment since they displayed proper binding with PrP^c when these antibodies were exposed to 1:1000 of the secondary antibody. The two yellow squares in the image A (**Figure 6-9, A**) show that no obvious background was seen when the cells were exposed to only secondary Alexa Fluor 488, leading to a low level of non-specific binding as shown in the value of fluorescence compared to the primary antibody in

both dilutions of secondary antibody, 1:1000 and 1:500 (Figure 6-9, B). It was therefore decided to use 1:250 of 8H4 with 1:1000 of secondary antibody in the ICC experiment in this chapter. To our knowledge, this method concerning PrP^c has not been reported previously.

To validate the ICC technique using ImageXpress Micro, the cells were transfected with PRNP siRNA for 48h and the level of PrP^c was evaluated in both the transfected and untreated cells. Nine images were taken for each well and all images were analysed using MetaXpress Software. Figure 6-9, B shows that the transfected cells displayed a decreasing fluorescent intensity for PrP^c in knockdown cells. The level of PrP^c decreased relative to scrambled and untreated cells (control) to around 30% (Figure 6-9, C). These results confirmed our western blot and flow cytometry assay findings in the previous chapter of this thesis where we found that the level of PrP^c in knockdown cells decreased to approximately 23% and 21%, respectively compared to scrambles and control groups after 48 h incubation with transfection reagents (see chapter 4, section 4.3.3.1 and 4.3.3.2). The slight variation in the values of PrP^c level therefore, could be related to the experimental or system variations.

As shown in these experiments, this method might be appropriate to screen the effect of small molecules on PrP^c level in U87 glioblastoma cells.

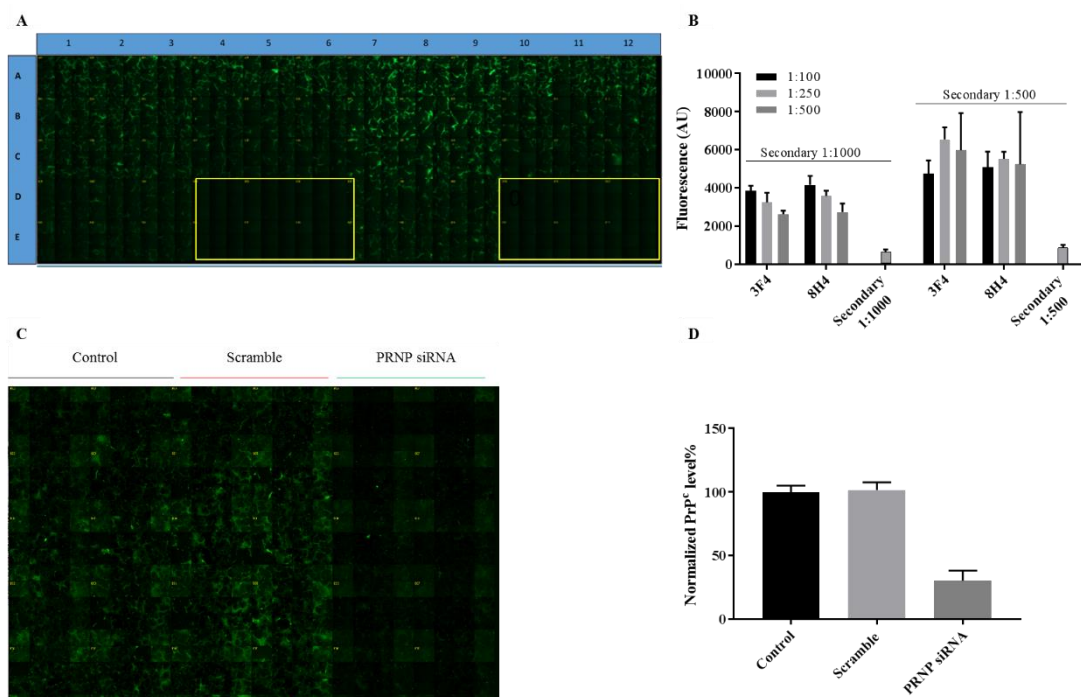


Figure (6-9): The level of PrP^c by ICC using ImageXpress Micro. **A**, shows the profile of a 96-well plate for determining PrP^c level in U87 cells exposed to 3F4 and 8H4 antibodies. **B**, the bar chart reveals the fluorescent intensity of PrP^c in U87 as mean \pm SD using 3F4 and 8H4 antibodies. The experiment was repeated three times, each performed in triplicate (n=9). **C**, the image represents the profile of 96-well plate which reflects the fluorescent of PrP^c in transfected cells for 48h. **D**, the chart shows mean \pm SD of three different experiments and each experiment was performed in six wells (n=18). The data were normalised to the control group.

6.4.4.2. PrP^c expression in treated U87 cells with FAPi compounds/TMZ or BCNU combination using ImageXpress Micro

ICC using ImageXpress Micro imaging was applied to assess PrP^c expression level in cells treated with FAPi compounds/TMZ or BCNU combination as described in [section 6.3.4](#). In previous studies by Drs. Matthew Sellwood and Peng Hua, FAPi compounds were found to suppress the activity of that FA pathway which is otherwise activated in response to alkylating agents. In brief, the combination of these compounds with TMZ or BCNU inhibited the FA pathway when compared with treated cells with TMZ or BCNU alone ([section 6.4.3](#)). We speculated that these

compounds might also reduce the level of PrP^c in glioblastoma cells. Figure (6-10) shows that the combination of FAPi compounds with TMZ or BCNU did not exhibit any remarkable change in PrP^c protein level compared to the control group after 48 h (8 h with FAPi compounds+40 h in combination with TMZ or BCNU). The structure of these compounds has an amide group. Michael *et al.* showed that some of amide analogues and other molecules may be hit PrP^c in T98 glioblastoma cells and then decrease its level¹⁸. This combination may distract or disturb the hit. The next experiment was therefore performed to evaluate the PrP^c level in cells treated with FAPi compounds alone.

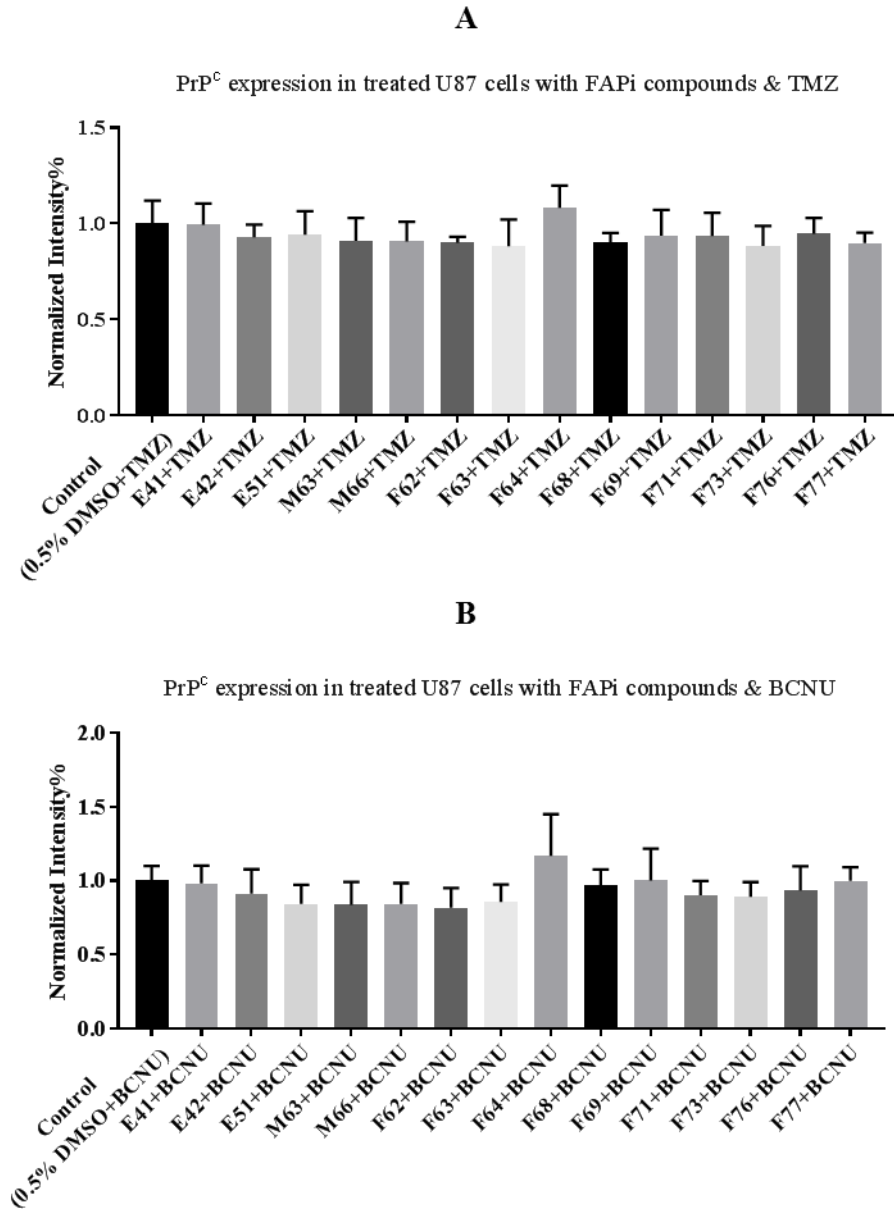


Figure (6-10): FAPi compounds do not affect PrP^c expression in combination with TMZ or BCNU. The **A** and **B** bar charts show the expression of PrP^c in treated cells. The data were normalised to the control as a percentage and represents mean \pm SD of four independent experiments, each performed in triplicate (n=12). The data were statistically analysed using t-test (each compound compared to the control group).

6.4.4.3 The expression of PrP^c in treated U87 cells with FAPi compounds

To evaluate the effect of FAPi compounds on the PrP^c level in U87 cells, the cells were treated with FAPi compounds for 48 h at 5 μ M and ICC using ImageXpress Micro. We expected that the single treatment with FAPi compounds may affect PrP^c

level in U87 cells. **Figure (6-11, A)** shows the profile image for the 96-well plate which was treated with FAPi compounds. The bar chart reveals that FAPi compounds did not affect PrP^c expression in U87 cells compared to the control group after 48 h (**Figure 6-11, B**).

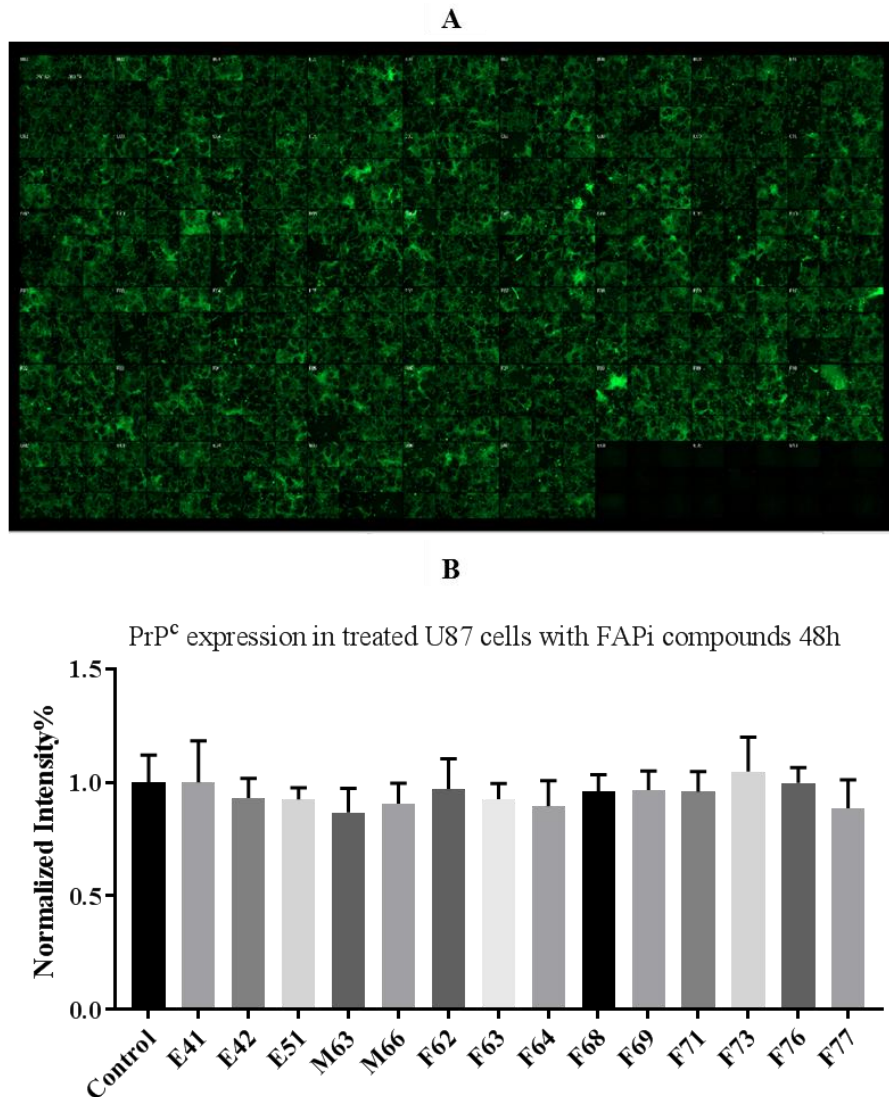


Figure (6-11): FAPi compounds do not affect PrP^c level in U87 cells after 48 h of treatment with 5 μ M FAPi compounds. **A**, represents the profile of the 96-well plate of treated cells. **B**, reveals no significant effect on PrP^c level compared to the control group. The results were normalised to the control group and represent mean \pm SD of three different experiments, each performed in triplicate (n=9). The data were statistically analysed using t-test (each compound compared to the control group).

6.5 Summary of key experimental results

- The FAPi compounds did not induce cytotoxicity to U87 cells in combination with TMZ or BCNU at 5 μ M.
- FANCD2 was upregulated in TMZ or BCNU treated cells after 24 h
- FAPi compounds inhibited the FA pathway, which was activated by TMZ or BCNU through suppressing FANCD2.
- ICC using ImageXpress Micro as a high content screening assay provided suitable results in the optimisation and validation of this method using; different concentration of primary antibodies and in the evaluation of PrP^c in knockdown cells.
- The expression of PrP^c in FAPi compounds in U87 cells treated in combination or without combination with TMZ or BCNU did not affect using ImageXpress Micro imaging assay.

6.6 Discussion

The FA pathway is considered to be one of the main DNA repair pathways in mammalian cells. It has been found to be induced in glioblastoma cells treated with alkylating agents such as TMZ and BCNU by the formation of monoubiquitinated FANCD2, the key part of the FA pathway¹⁶. This pathway is very sensitive to a variety of DNA damage or crosslinking stimuli, thus, many attempts have been carried out to identify novel small molecules as inhibitors to this pathway²⁷⁷. In our western blot assay results, TMZ and BCNU increase the level of FANCD2 when U87 cells were treated for 24 h (Figure 6-7). This result is in line with previous work reporting that TMZ or BCNU induced the level of FANCD2 in U87 cells^{16,17}. It has been demonstrated that glioma cells with an inhibited FA pathway are more sensitive to alkylating agents when pre-dosed with FA inhibitors such as Curcumin¹⁷. FAPi

compounds were synthesised and used in previous work by our group (Drs. Matthew Sellwood and Peng Hua) revealing that these compounds have a reliable inhibitory effect on the highly-stimulated FA pathway induced by chemotherapeutic drugs, by significantly reducing the level of FANCD2 (Figure 6-8). The exact mechanism of these molecules has not been elucidated yet, even for the commercially available FA pathway inhibitors such as curcumin^{278,277}.

Since these novel compounds inhibit the FA pathway, we speculated that they may also have a possible potential to hit PrP^c level in glioblastoma cells and inhibit the expression level of this protein. This possibility could be related to the structure of these compounds, which have an amide group with different substitution groups. In another study, the amide analogues (have an amide with different substitutions) may have an active hit on PrP^c in glioblastoma cells¹⁸.

The ICC method using ImageXpress Micro was employed to evaluate the level of PrP^c in U87 cells treated with FAPi compounds with or without TMZ or BCNU. Prior to the screening of FAPi compounds in the ImageXpress Micro imaging assay we had to evaluate the viability of U87 cells in the combination of these compounds with TMZ or BCNU and validate this imaging method. The results of the MTT assay showed that the combination of these compounds with TMZ or BCNU did not induce any obvious cell death at the intended dose (Figure 6-6).

To our knowledge, this is the first time that ICC by ImageXpress Micro has been used to evaluate the PrP^c level in glioblastoma cells. Thus, it is necessary to validate this method for PrP^c evaluation. Different concentrations of two types PrP^c primary antibodies (3F4 and 8H4) which are commonly used in immunofluorescent staining^{273,184} showed graduated brightness in the images and gave a linear

proportional fluorescent intensity with the increase of the antibodies' concentrations (1:100, 1:250 and 1:500 of primary antibodies with 1:1000 of fluorescent secondary antibody) (Figure 6-9 A and B). Both of these antibodies were suitable to be used in this experiment, however, 8H4 was used in the next experiments at 1:250 with 1:1000 of Alexa flour secondary antibody. Furthermore, to confirm the validity of this method, the cells were transfected with PRNP siRNA in order to suppress the level of PrP^c in these cells. As has been mentioned in chapter 5, the transfection of U87 cells by PRNP siRNA silenced about 78% of PrP^c after 48h. The result of PrP^c knockdown using ImageXpress Micro shows that the level of PrP^c in PRNP siRNA cells decreased by approximately 70% relative to scramble and untreated cells (Figure 6-9, B and C) and this result coincides with the previous result in chapter 5. Therefore, ICC using ImageXpress Micro could be an appropriate method to screen many compounds.

Consequently, in this chapter, we investigated whether or not FAPi compounds inhibit the level of PrP^c in U87 using ImageXpress Micro. These compounds may have a potential to suppress the level of PrP^c due to the amide group in their structure. For this reason, we speculated that FAPi compounds might have a dual function inhibition of the FA pathway and reduce the level of PrP^c. The combination of these compounds with TMZ or BCNU, however, did not cause any reduction in the PrP^c level in treated U87 cells after 48 h (8 h with FAPi and 40 h in combination with TMZ or BCNU (Figure 6-10). We expected that the combination of FAPi compounds with TMZ or BCNU might disrupt the ability of these compounds to decrease PrP^c protein in U87 cells. The ICC experiment was therefore carried out for treated cells with FAPi compounds alone. The results revealed that there is no significant change in the level of PrP^c in relative to the control group (Figure 6-11). Our results did not agree with

the findings of Michael *et al.* who found that many scaffolds such as the amide analogues reduced the level of PrP^c in T98G glioblastoma cells. Using ELISA assay they identified and confirmed that these compounds have a potential effect to hit the PrP^c in T98G cells¹⁸. Further investigations could be carried out to determine the effect of FAPi compounds on PrP^c level in glioblastoma cells. For example, increasing the incubation time with FAPi compounds may exhibit a remarkable decrease in the level of PrP^c in these cells. In addition, other measurements may confirm our results such as flow cytometry, western blot and ICC by confocal microscopy which may be more accurate than ICC by ImageXpress Micro.

To conclude, these preliminary results demonstrated that the FAPi compounds examined are FA pathway-specific compounds, and do not have much effect on the PrP pathway, especially on PrP^c expression itself. This is the first time ICC has been used alongside by ImageXpress Micro for high content image for screening several compounds to evaluate the effect of these compounds on PrP^c level in glioblastoma cells U87. Further investigation could be carried out, such as increasing the duration of treatment or using other quantification methods to confirm and validate the effect of these molecules on PrP^c levels.

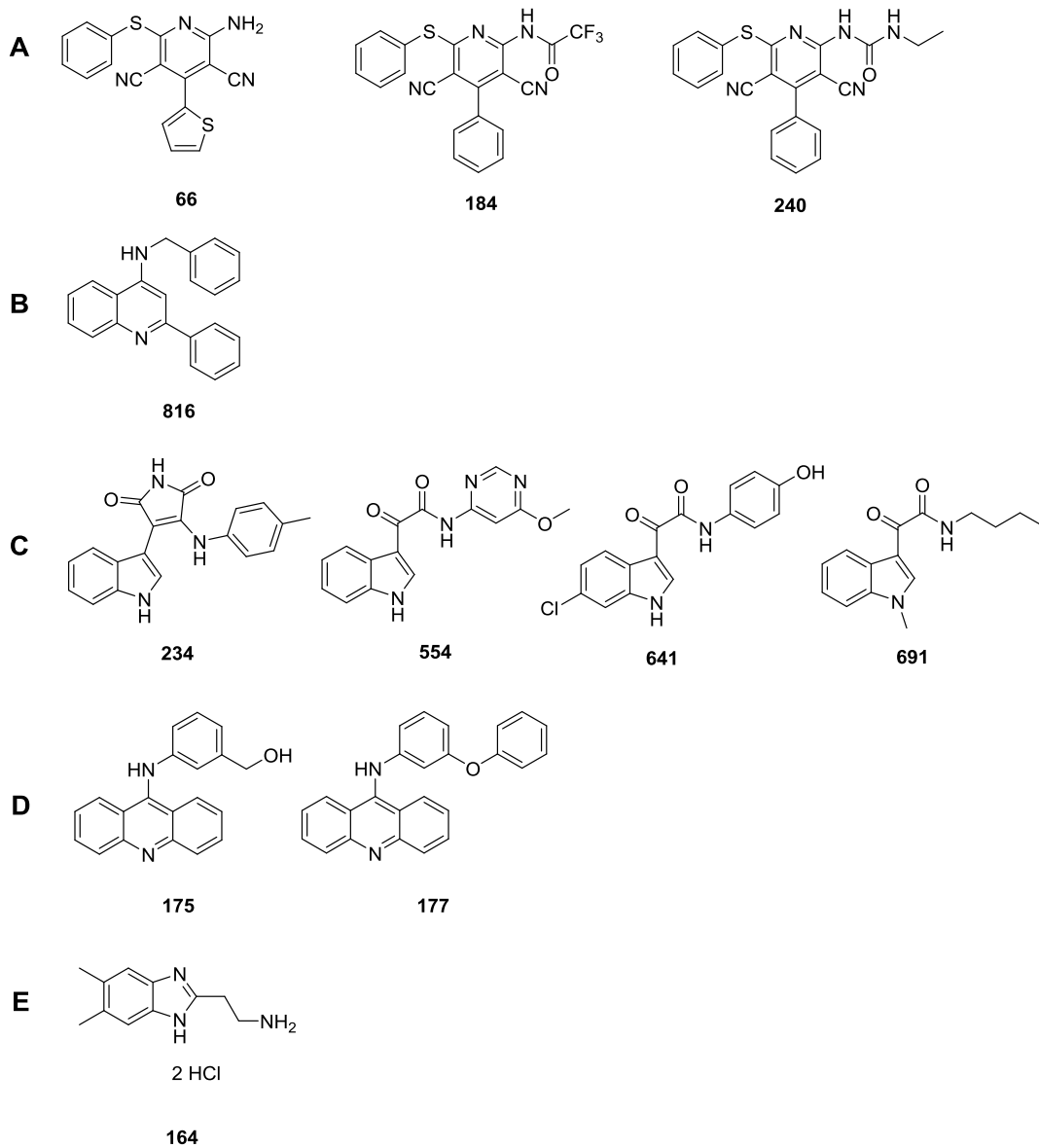
Chapter 7: Screening of small molecule chemical libraries as anticancer agents

using U87 glioblastoma cells.

7.1 Introduction

Substituted heteroaromatic compounds have been known to have a wide range of biological activity including anti-cancer activities²⁷⁹. Most anti-cancer therapies act via promoting programmed cell death, such as apoptosis²⁸⁰. A previous member of the Chen group (Dr Peng Hua) has tested a library of heteroaromatic compounds from which dicynopyridine (A), pyridine (B), indole (C), acridine (D), benzimidazole (E), thiazol (F) and oxazole (G) (Figure 7-1) displayed obvious cytotoxicities to teratocarcinoma stem cell line Ntera2 (NT2) while he was searching for compounds that enhance the proliferation of NT2 cells. The potential applications of these compounds as anticancer drugs have not yet explored. In addition, some of these compounds may have an activity to lower PrP^c level. For example, the previous work for the group found that some analogues of 9-aminoacridines may bind PrP^c according to surface plasmon resonance (SPR) binding assay²⁸¹. These compounds have been also tested previously by a member of group (Dr Jennifer Louth) on SMB cells (prion-infected brain cell of mouse²⁸²) and zebrafish, where it was found that these molecules did not induce cytotoxicity with $IC_{50} \leq 20 \mu\text{M}$ (unpublished data)

These novel small molecules were synthesised previously by the members of group (Tummalu Reddy, Paul Taylor, Steven Farrara, Vinciane Borsenberger, Aziz Mekhalfia, Claire Pascoe, Hannah Hope, Mark Thompson and Katie Judd). Their anticancer activities in NT2 cells inspired us to hypothesis that these molecules might also inhibit the growth of U87 cells and act via PrP^c route.



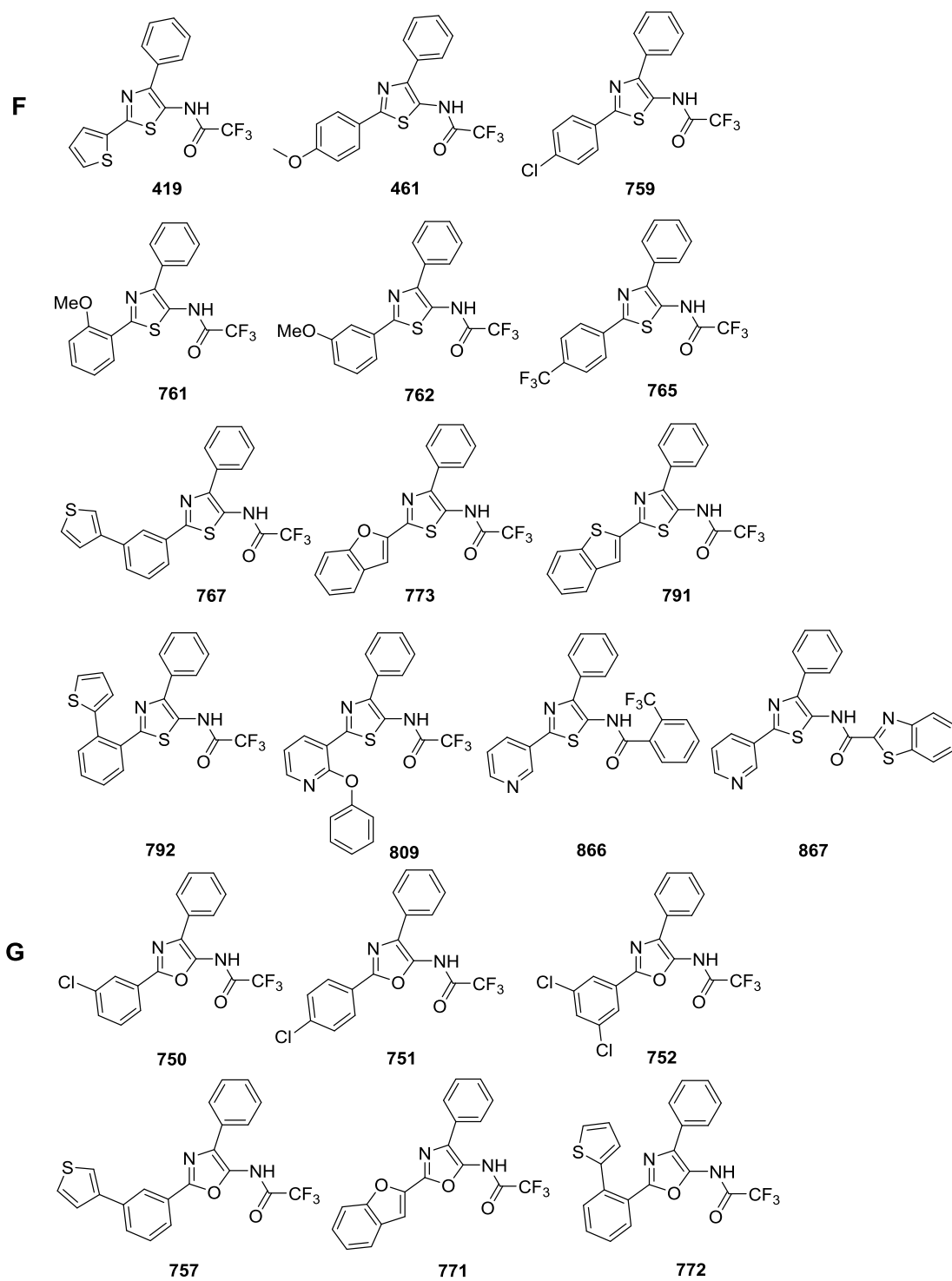


Figure (7-1): List of the small molecules subdivided into seven families.

7.2 The aim

This chapter aims to evaluate the effect of small molecule chemical libraries, that previously displayed anticancer activities on NT2 cells, on U87 glioblastoma cells. The influence of the effective small molecules on PrPc expression and other biomarkers will also be evaluated. To achieve this aim, the following objectives will be carried out:

- Evaluate the cell viability for U87 cells treated with these small molecules using MTT assay.
- Assess the apoptotic effect of small molecules on U87 cells using Annexin V with PI.
- Evaluate the population of treated cells in each cell cycle phase using flow cytometry.
- Assess the level of p53 and p21 in treated cells.
- Evaluate the effect of the compound that induced apoptosis on the level of PrP^c to determine whether it induces or reduces the level of this protein.

7.3 Methods

7.3.1 Compounds preparation

The novel small molecules were synthesised and purified using HPLC by the previous members in the group, as listed in [section 7.1](#). These compounds were dissolved in DMSO at 10 mM and then aliquoted into small portion and placed in small vials, which were kept at -20 °C before use. The desired working concentration was prepared by diluting the stock solution with an appropriate volume of DMSO and PBS prior to each experiment.

7.3.2 Cell viability by MTT assay

MTT assay was used to determine the viability of U87 cells treated with the small molecules. The cells were seeded in 96-well plates at a density of 10000 cells in each well, and the following day were treated with the compounds as illustrated in [Figure \(7-2\)](#). The cells were incubated at 37 °C for 24 h. The protocol for MTT assay ([section 2.2.2](#)) was applied in order to determine the viability of cells in these compounds. The data were analysed as a percentage to the untreated cells (control group).

Furthermore, MTT assay was used to calculate the IC₅₀ for compound **175**. The cells were seeded in 96-well plate at 1000 cells and then treated with serial concentrations (1, 2.5, 5, 10, 20 µM) of this compound for five days.

	1	2	3	4	5	6	7	8	9	10	11	12
A	Control	1 µm	5 µm	10 µm	20 µm	Control	1 µm	5 µm	10 µm	20 µm		
B	Compound 1					Compound 3						
C												
D												
D	Compound 2					Compound 4						
F												
G												
H												

Figure (7-2): The experimental design of MTT assay for the small molecules.

7.3.3 Apoptosis assay

Annexin V with PI staining was carried out as described in [section 2.2.13](#) to evaluate the apoptotic effect of small molecules on U87 cells. The cells were seeded in a 6-well plate at 50000 cells in each well and then treated with 5 µM of the small molecules for 48 h, as reported by other groups using glioblastoma cells for anticancer drug screening^{262,13}. The apoptosis for all samples was quantified using flow cytometry. The apoptotic cells were calculated as a percentage of total cells.

7.3.4 Cell cycle assay

To quantify the population of cells in each cell cycle phase, the cells were cultured in 6-well plates, and then left overnight for attachments. This step was followed by treating the cells with compound **175** at 1, 2.5 and 5 μM . After five days, the cells were washed and harvested using non-enzymatic dissociation solution. The protocol for cell cycle using PI with RNase (section 2.2.3) was followed to assess the number of cells in each cell cycle phase. In this chapter, we focused on compound **175** due to its significant apoptotic impact on U87 cells (section 7.4.2). Although 48 h incubation with the treatment led to only a slight change in cell cycle over the used concentrations (data not shown), the incubation time was extended to five days to ensure the effectiveness of this compound on cell cycle phases clearly seen.

7.3.5 Western blot assay

PrP^c, p21 and p53 levels in treated cells with compound **175** were evaluated using western blot. To evaluate these proteins, the 6-well plate was seeded at 25000 cells and then the on the following day the cells treated with compound **175** (1, 2.5 and 5 μM) for five days. The control group was treated with 0.5% DMSO. This step was followed by the preparation of cell lysate, and the protein levels were then assessed using the western blot method described in section (2.2.5).

7.4 Results

7.4.1 Cell viability of U87 treated with the small molecules

To determine the effect of 30 compounds on the viability of U87 glioblastoma cells, MTT assay was carried out for all these compounds after 24 h treatment with different concentration of these compounds (1, 5, 10 and 20 μM). Most of these compounds did not induce any reduction in cell number of the cultured cells (data not shown) except for eight compounds. For these eight, MTT assay exhibited different responses. The

bar chart below shows the viability of U87 cells in treated cells compared to the control group (Figure 7-3). Our results indicate that these compounds are generally non-toxic for U87 cells at 5 μM except compound **765**. As can be seen, that compound **752** in group G and **759**, **762**, **765** and **866** in F group reduce the viability of U87 cells at a high concentration of 20 μM to just 25%-45% compared to the control group. Compound **816** and **175** slightly decrease the cell viability to approximately 72% and 83% at 20 μM respectively. It was therefore decided to use 5 μM as single treatment concentration in the subsequent experiments.

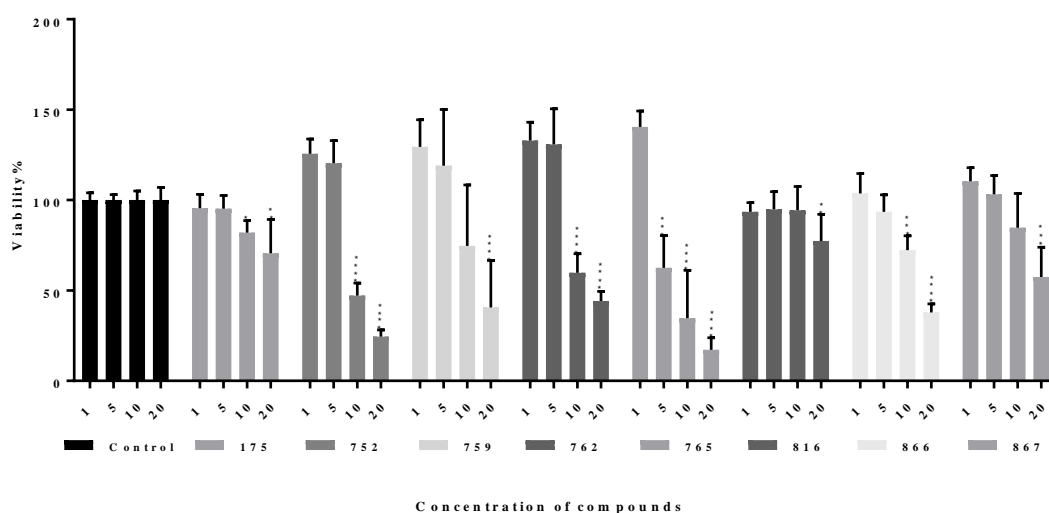


Figure (7-3): Cell viability of U87 cells treated with eight compounds. The viability was calculated as a percentage to the control group. The bars represent mean \pm SD of three different experiments and each experiment was performed in triplicate (n=9) and analysed using t-test (each concentration of compound compared to the control group), *= $p < 0.05$, **= $p < 0.01$, ***= $p < 0.001$, ****= $p < 0.0001$.

7.4.2 Apoptosis assay for the treated U87 cells with small molecules

Eight of the small molecules displayed a reduction in cell viability at variable concentration due to the cytotoxic effect of these molecules, as shown in the previous experiment (section 7.4.1). To quantify this effect, an apoptosis assay was performed in U87 cells treated with these compounds for 48 h at 5 μM for each compound. The scatter charts show the population of live, dead and apoptotic cells in flow cytometry

analysis. The upper right square in each scatter chart (Figure 7-4, A) reveals the total apoptotic cells in each sample. It can be seen that compound **175** increased the apoptosis rate in U87 cells, whereas other compounds did not induce any apoptotic effect (Figure 7-4, A). The bar chart shows the statistical analysis for this experiment (Figure 7-4, B). These results indicate that compound **175** can increase the apoptosis rate by about 12% after 48 h (Figure 7-4, B). This could be attributed to the general cytotoxic effect of this compound, which is one of the 9-aminoacridine family. Some of the acridine compounds bind to the DNA and then induce cytotoxicity^{283,284}.

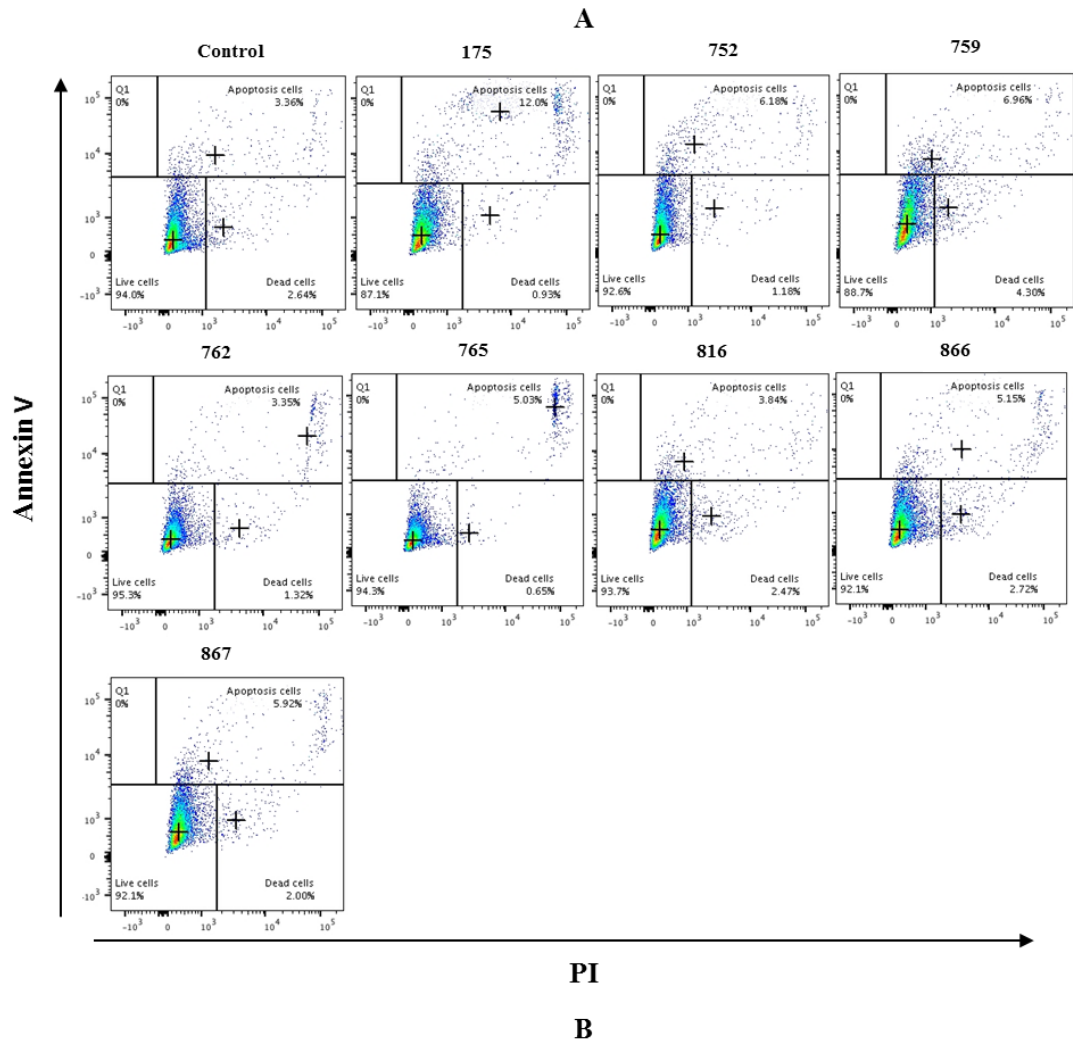


Figure (7-4): The effect of eight small molecules on the apoptosis of U87 cells using Annexin V with PI. **A**, represents scatter charts of U87 cells treated for 48 h. **B**, the bars show mean \pm SD of three different experiments, each performed in duplicate ($n=6$). The data were analysed using t-test (each compound was compared to the control) (**= $p<0.01$).

7.4.3 Dose-dependent studies of U87 cells treated with compound 175 over 5 days

According to apoptosis assay, compound **175** induces the most apoptosis of U87 cells after 48 h. A cell viability assay was therefore carried out as described in [section 7.3.2](#) to calculate IC_{50} for this compound over five days treatment period. The time was extended to five days because 24 h and 48 h did not show any remarkable decrease in cell viability. In addition, this compound did not dissolve properly when its concentration increased where we observed that this compound aggregated at 40 and 50 μ M. The line graph shows that the viability of U87 cells was decreased dramatically in a dose-dependent manner with $IC_{50}=10.9 \mu$ M ([Figure 7-5](#)).

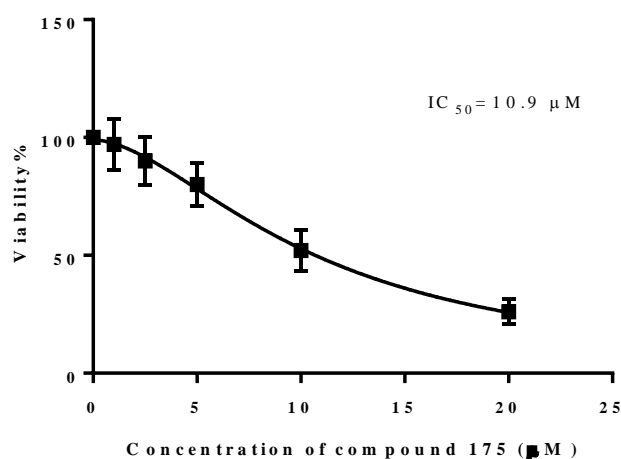


Figure (7-5): Viability of U87 cells in the different concentrations of compound **175**. The line graph represents mean \pm SD of the percentage of viable cells compared to the control. Cell viability was calculated in treated cells after five days to evaluate the IC_{50} of compound **175**. This experiment was performed in triplicate and repeated three times (n=9).

7.4.4 Cell cycle studies by compound 175

To evaluate the effect of compound **175** on the cell cycle of U87 cells, a flow cytometry assay for cell cycle was carried out after five days as described in [section 7.3.4](#). [Figure \(7-6, A\)](#) shows the histograms which represent the population of cells in each phase of the cell cycle. These results reveal that compound **175** arrested the cells

in G2/M in a dose-dependent manner (1, 2.5 and 5 μ M) after 5 days by around 18%, 27% and 46%, respectively whereas the G1 cells were dramatically decreased depending on the concentration of compound **175** (Figure 7-6, B). These results support the cell viability result with the decrease in cell proliferation possibly attributable to the arrest of cells in G2/M. Furthermore, the G2/M arrest may result from the DNA damage induced by this compound, or possibly from p53 induction resulting from the effect of acridine compound (see section 7.4.5). The induction of p53 as a tumour suppressor protein in response to DNA damage induces the cell cycle arrest or apoptosis²⁸⁵. p53 and p21 as regulators for cell cycle will therefore be evaluated in the next section (7.4.5).

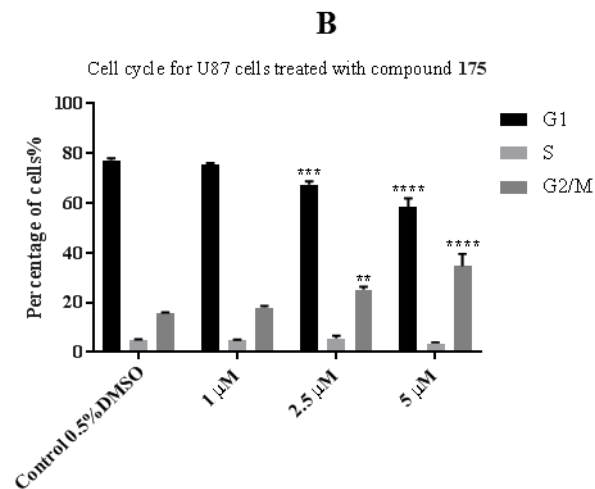
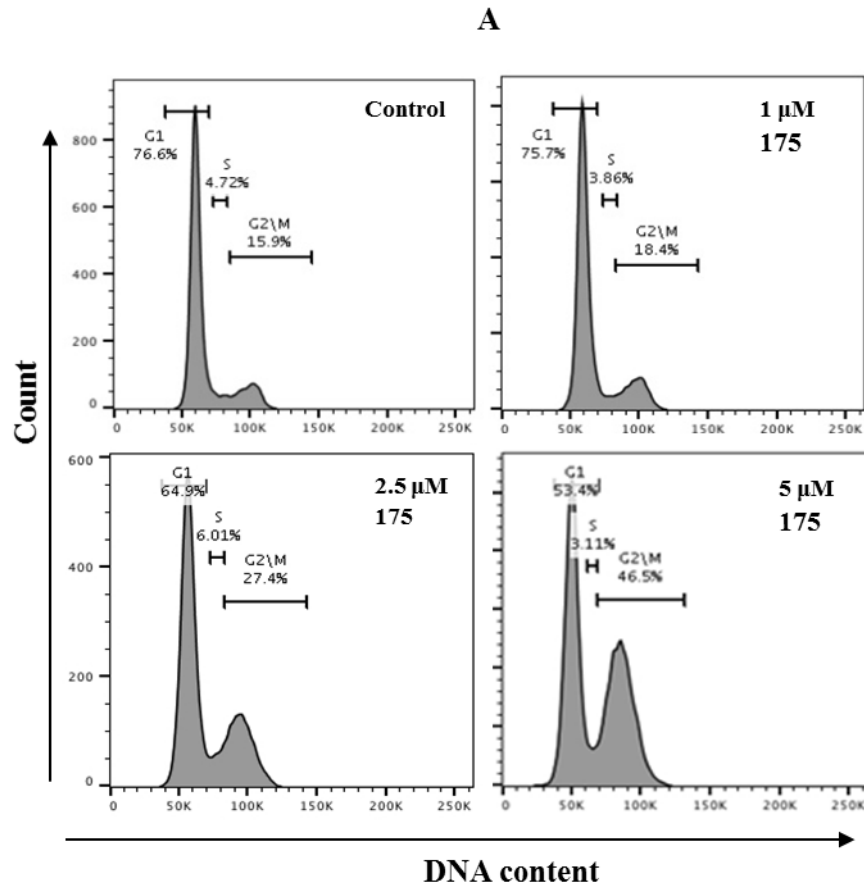


Figure (7-6): The cell cycle analysis of U87 cells treated with compound **175**. **A**, the histograms reveal the population of treated cells with compound **175** in each cell cycle phase. **B**, the bar chart represents mean \pm SD and shows the percentage of cells in each cell cycle phase. The treated cells were accumulated in G2/M in a dose-dependent manner. The experiment was performed in triplicate and repeated three times (n=6). All data were analysed using one-way ANOVA, Tukey's test (**= $p < 0.01$, ***= $p < 0.001$, ****= $p < 0.0001$).

7.4.5 The level of p21 and p53 by compound 175

Since compound **175** accumulates U87 cells in the G2/M phase, as shown in section (7.4.4), western blot analysis was carried out in U87 cells to estimate the effect of this compound on the regulators of the cell cycle p53 and p21 as described in section 7.3.5. Figure (7-7) shows that these proteins dramatically increased when treated with 1, 2.5 and 5 μ M of compound **175** for five days. p53 and p21 were significantly increased in treated U87 cells with compound **175** in a dose-dependent manner. This induction may be ascribed to the arrest of U87 cells in G2/M (section 7.4.4) allowing repair of the DNA damage caused by compound **175**. The G2/M accumulation required both p53 and p21 in glioblastoma cells. As a further explanation, the p53 may be increased as a result of the apoptotic effect of compound **175**, as shown in section (7.4.2) where p53 was induced in response to DNA damage or apoptotic stimuli²⁸⁵. Another study has revealed that acridine derivatives promoted the apoptosis of tumour cells by induction of p53 and Bax²⁸⁶.

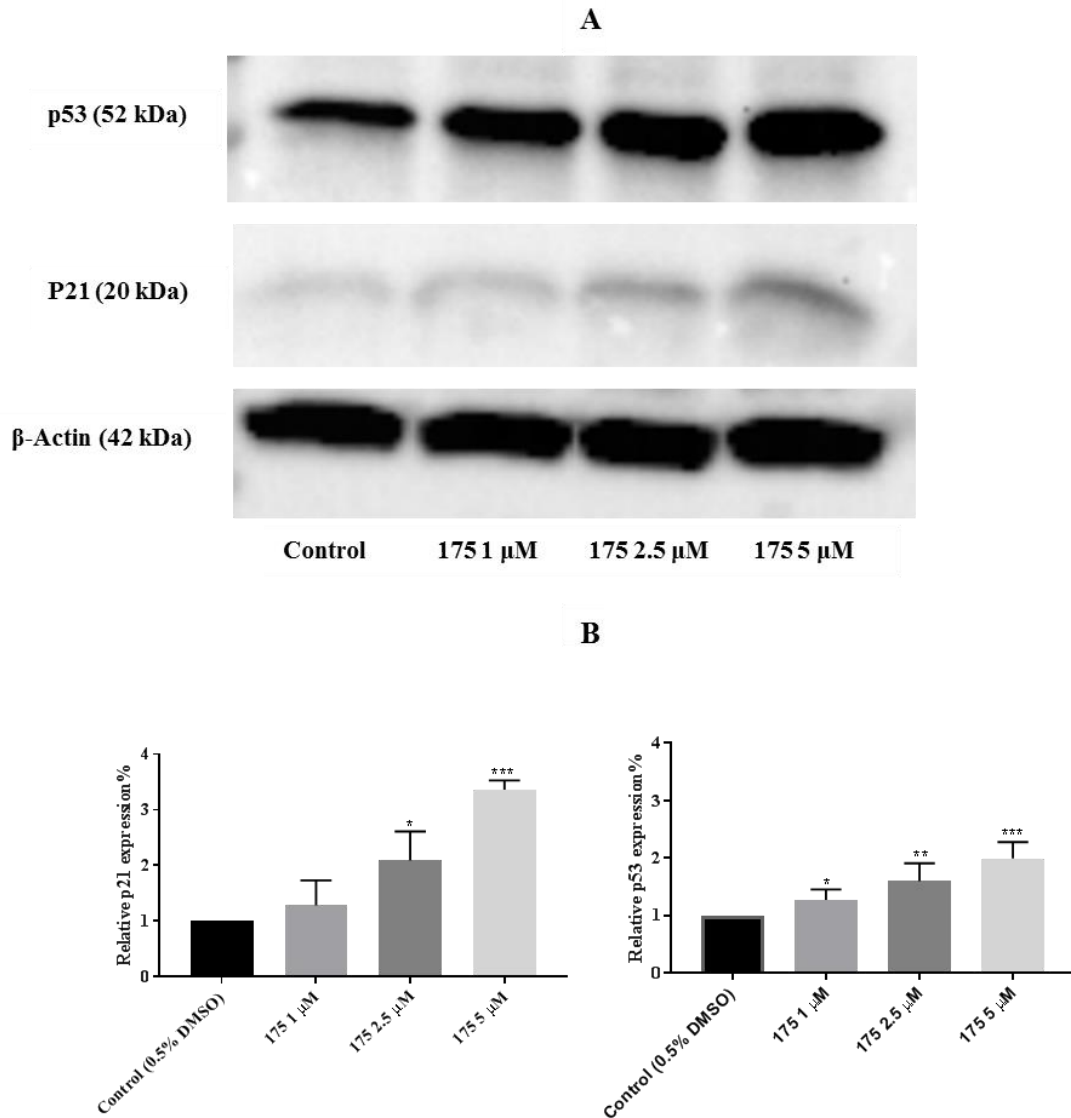


Figure (7-7): Compound **175** upregulates p21 and p53 in U737 cells. **A**, shows the western blot images for p53 and p21 in treated cells with compound **175**. **B**, the bar charts reveal the analysis of data as mean \pm SD of three independent experiments ($n=3$). The data were normalised to the control group. Both of these proteins are upregulated in treated cells with 1, 2.5 and 5 μM of compound **175**. The results were statistically analysed using one-way ANOVA, Tukey's test (*= $p<0.05$, **= $p<0.01$, ***= $p<0.001$).

7.4.6 The effect of compound **175** on PrP^c level in U737 cells

Besides the apoptotic impact of compound **175** on U737 cells, we expected that the compound may change the level of PrP^c in U737 cells on the basis that previous work for the group found that some analogues of 9-aminoacridines may bind PrP^{c281}. The level of PrP^c in U737 cells treated with compound **175** was evaluated using western

blot assay as described in section 7.3.5. Figure (7-8) below indicates that there was no significant change in the level of PrP^c in cells treated with compounds **175** over five days at tested concentrations of 1, 2.5 and 5 μM when compared to the control. The level of PrP^c was normalised to the loading control (β -actin) for each sample and then calculated as a percentage to the control group.

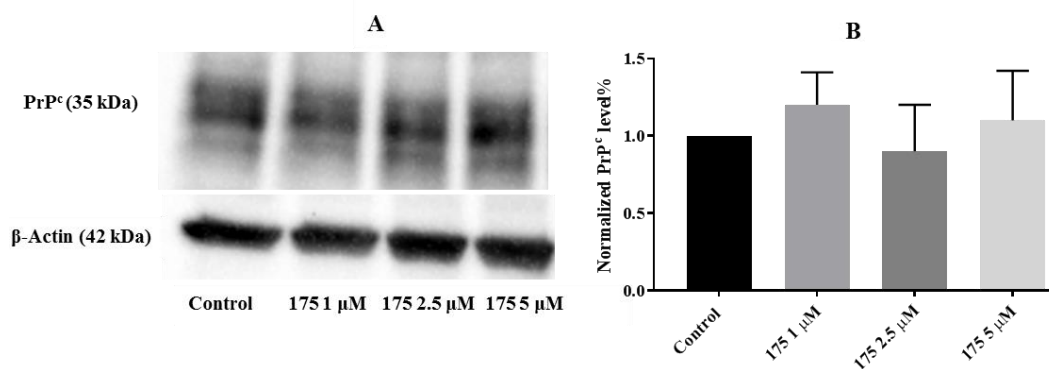


Figure (7-8): PrP^c level in treated U87 cells with compound **175**. **A**, the western blot image shows the expression of PrP^c in **175**-treated cells. **B**, the bars represent mean \pm SD of PrP^c level in treated cells in relative to the control. There was no significant change in proteins level in **175**-treated cells compared to the control. This experiment was repeated for at least three times ($n=3$) and the data were analysed using one-way ANOVA, Tukey's test.

7.5 Summary of key experimental results

- Thirty compounds were tested as an anti-cancer treatment on glioblastoma cells U87 cells, with just eight compounds reducing the viability of U87 cells.
- One of the eight compounds, compound **175**, increased the apoptosis rate of U87 cells after 48 h.
- Compound **175** decreased the viability of U87 cells in a dose-dependent manner and the IC₅₀ was 10.9 μM.
- Compound **175** arrested the cells in G2/M phase after five days in a dose-dependent manner.
- p21 and p53 levels increased in a dose-dependent manner in compound **175** treated cells as a result to G2/M arrest.
- Compound **175** did not induce the level of PrP^c in U87 cells.

7.6 Discussion

Many of heteroaromatic compounds have promising bioactivities against cancers as well as other physiochemical properties²⁷⁹. In this work, 30 novel compounds were tested on U87 cells. these compounds were selected based on these compounds have been tested previously by a member of group (Dr Jennifer Louth) on SMB cells (Scrapie mouse brain cells infected with Chandler scrapie strain²⁸²) and zebrafish, where it was found that these molecules did not induce cytotoxicity with IC₅₀ ≤ 20 μM (unpublished data); further cytotoxicity work has also been carried out by the group (Dr Peng Hus) on the teratocarcinoma stem cell line Ntera2 (NT2), and they found that these compounds displayed cytotoxicity on this cell (unpublished data). We therefore speculated that these compounds may have a potent toxic effect on U87 cells.

Our results showed that most of these compounds did not induce any cytotoxicity, even at high concentrations (20 μM). Eight of these compounds reduced the viability of U87 cells, and this reduction was fluctuated from compound to another compound but 5 μM did not induce any cytotoxic effect on U87 cells, except for compound **765** (Figure 7-3). The results of the apoptosis assay by Annexine V with PI staining for the eight compounds showed that only compound **175** promoted apoptosis for U87 cells after 48 h compared to the control group (Figure 7-4), possibly related to the cytotoxic effect of this compound. Furthermore, compound **175** inhibited the growth of U87 cells after five days with an IC_{50} of 10.9 μM according to MTT assay (Figure 7-5). To our knowledge, this is the first time that compound **175** has been shown to be active against glioblastoma cells, we, therefore, focused on this compound as a treatment for glioblastoma cancer. This compound belongs to the 9-aminoacridine family which has previously been reported as inducing cytotoxicity for some cancer cells. Com and co-workers synthesised various 9-aminoacridine derivatives and they tested them on leukaemia L1210 cells. They stated that some of these compounds suppressed the growth of these cells, although the IC_{50} results varied depending on the variation of the structure of these compounds²⁸³. Also, another study revealed that 9-phenoxyacridines and 9-(phenylthio) acridines have moderate toxicity to mouse and human leukaemia cell lines L1210 and HL60, respectively²⁸⁴. Furthermore, Christopher *et al.* stated that di and tri substituted 9-aminoacridine reduced the viability of human ovarian carcinoma A2780²⁸⁷. Goodell *et al.* stated that the growth of pancreas cancer cells BxPC-3, MIA PaCa-2 and SU.86.86 was inhibited when treated with some 9-aminoacridine derivatives^{288,289}.

To investigate the effect of compound **175** on U87 cells, a cell cycle assay was carried out. The results of this test showed that compound **175** has a crucial impact on the cell

cycle phases of U87 cells. This compound accumulates the cells in the G2/M phase in a dose-dependent manner. It arrests the cells in G2/M by around 48% when the cells were treated for five days at 5 μ M (Figure 7-6). These results may support the results regarding cell viability in that the accumulation of cells in G2/M would have reduced the proliferation of cells. The G2/M arrest may be attributed to the effect of this compound on DNA through intercalating. It has been reported that some acridine compounds intercalate to DNA due to its planar structure and then bind covalently via the amine group to DNA. This binding thereby may also exert cytotoxicity^{283,284}. In addition, other studies have shown that some of the 9-aminoacridine derivatives compounds inhibit topoisomerase II (topo II) which regulates the over-winding or under-winding of DNA^{283,290,291}. The disruption of Topo II by some of 9-aminoacridine derivatives compounds leads to a change in cell cycle phases and accumulates the cells in the G2 phase^{292,293}.

Furthermore, the induction of G2/M arrest in cells treated with compound **175** may increase the level of p53 and p21 which arises in response to DNA damage (Figure 7-7). These results are in agreement with previous findings which have illustrated that p53 induced G2 arrest in response to the inhibitors of topo II²⁹³. On the other hand, as we mentioned before, according to Annexine V assay, compound **175** increased the apoptosis in U87 cells (Figure 7-4) and this induction may be as a result of increasing the level of p53 since this induces apoptosis in some cancer cells through the p53-dependent apoptotic pathway, particularly in wild-type p53 cells. Wenge *et al.* found that 9-aminoacridine derivatives promoted the apoptosis in various cancer cells through upregulating p53 and Bax²⁸⁶. The increase in the level of p53 in response to DNA damage stimuli may induce cell cycle arrest or apoptosis transiently or permanently²⁸⁵.

Beside the cytotoxic effect of compound **175** and the consequent increase in apoptosis, which may correlate with the induction of p53, we expected that the level of PrP^c in U87 treated with compound **175** would also change due to the potential binding of this compound to PrP^c. The expectation was that compound **175** may target PrP^c then subsequently reduce the level of this protein in U87 cells. In this work, however, we found that the level of PrP^c was not affected in treated cells (Figure 7-8). It has been reported that 9-aminoacridine, phenothiazine and other tricyclic derivatives exhibited an excellent binding to PrP^c through specific amino acid residues^{294,281}. Furthermore, the previous work for the group revealed that some analogues of 9-aminoacridines could bind PrP^c according to surface plasmon resonance (SPR) binding assay²⁸¹.

To our knowledge, this is the first study concerning the effect of the acridine compound on glioblastoma cells. Due to the effect of compound **175** on U87 cells, however, further investigation should be carried out to investigate the impact of 9-aminoacridine derivatives on glioblastoma cells. Furthermore, the other eight compounds which induced cytotoxicity to U87 cells need further study to determine the cause of their cytotoxic effect.

To conclude, 30 compounds were tested as anti-glioblastoma. Eight of these compounds reduced the viability of U87 cells. Compound **175** decreased the proliferation of cells by IC₅₀ = 10.9 μM after five days. It also increased the apoptosis rate of U87 after 48 h. In addition, compound **175** arrested the cells in G2/M and accumulated p53 and p21 in a dose-dependent manner. This compound belongs to the acridine derivatives, and this work is the first to examine an acridine compound in the context of glioblastoma cells. More in-depth work is needed, however, to investigate the effect of acridine compounds as anti-glioblastoma treatment.

Chapter 8: General discussion, Conclusions and Future perspectives

Glioblastoma is an aggressive and fatal disease that affects brain cells. It is more resistant to chemotherapy than other astrocytomas. Currently, TMZ and BCNU with radiotherapy are the standard treatments for GBM patients following surgery². PrP^c has been reported to be implicated in GBM and PRNP gene is highly expressed in GBM than other brain cancers⁵. Despite this, the precise physiological role of PrP^c is still unclear. It is involved in many cellular functions such as apoptosis and proliferation. PrP^c is linked to resistance towards treatments for many cancers cells³ and notably, it has been implicated in causing resistance to TMZ in glioblastoma cells⁶. However, an in-depth investigation of PrP^c and its gene expressions affected by GBM treatments; TMZ and BCNU, were yet under covered. In this thesis, experiments were carefully designed to evaluate the level of PrP^c in glioblastoma cell line U87 treated with alkylating agents, TMZ and BCNU. The effects of alkylating agents on cells with PrP^c knockdown were also investigated. The impact of proteasome inhibitor MG132 on PrP^c apoptosis, proliferation and sensitisation in U87 cells treated with TMZ were also evaluated. Further investigations were carried out to evaluate the polypharmacological effects of combinations of TMZ or BCNU with novel small molecules that suppress the FA pathway on PrP^c level. Cytotoxic studies of novel small molecules (30 compounds) that are active against embryonic carcinoma (EC) cells Ntera 2 and U87 cells were also performed to evaluate their potentials as anti-GBM agents and their effects on PrP^c. In the following sections, the main findings of this thesis are discussed.

8.1 The level of PrP^c, its gene expressions and cell cycle phases change in U87 cells treated with TMZ or BCNU

The effects of alkylating agents TMZ and BCNU on the level of PrP^c in U87 cells were evaluated based on our hypothesis that PrP^c level may be increased during G2/M phase induced by the alkylating agents.

Our results confirmed that Aphidicolin and Nocodazole arrest U87 cells in G1 and G2/M respectively. These treatments are commonly used to synchronise the eukaryotic cells in G1 (Aphidicolin)²²² and G2/M (Nocodazole)²²³ phases. These experiments were performed to produce a model of G1 and G2/M cells which were used to evaluate the PrP^c level in these cells and to validate the data resulting from the treatment of the cells with TMZ and BCNU. Our results revealed that TMZ and BCNU arrested U87 cells in G2/M in a time-dependent manner. The accumulation of cells in G2/M phase increased when treated cells were incubated without the treatment. BCNU has more potency to arrest the cells in G2/M at 12h, 24h, 6h+24h and 12h+24h and the trend was similar for TMZ in the rest time points. Generally, it has been found that TMZ and BCNU arrested U87 cells in G2/M^{224,202}. The G2/M arrest of U87 could be ascribed to the upregulation of p53 and p21, regulators of the cell cycle, resulting from DNA damage by TMZ or BCNU. We found that p53 and p21 levels were significantly upregulated in treated cells with TMZ or BCNU. It was also found that p53 and p21 were accumulated in U87 cells in response to TMZ and BCNU^{224,202}. Our results are in agreement with those reported.

The levels of PRNP and PrP^c were evaluated in U87 cells synchronized at G1 and G2/M by Aphidicolin and Nocodazole respectively, as well as in U87 cells treated by TMZ or BCNU at different time points (6h+24h, 24h, and 24h+48h). Our results

showed that PRNP gene expression was significantly increased in synchronized cells by Nocodazole (i.e. G2/M cells) and in treating cells with TMZ (6h+48h), while the protein level was not affected. Furthermore, cells treated with TMZ and BCNU (24h+48h) were significantly upregulated, whereas the protein levels were significantly downregulated. PrP^c may protect the cells from pro-apoptotic or DNA damage stimuli such as chemotherapy¹⁸⁴.

Overall, TMZ and BCNU arrested the U87 cells in G2/M and altered the level of PRNP and PrP^c but TMZ upregulated the PRNP gene to a higher level than BCNU. The induction of the PRNP gene in treated cells may be ascribed to G2/M accumulation induced by TMZ or BCNU. It has been found that PrP^c and its gene were upregulated in G2/M cells mediated by TMZ. According to array hybridization assay, PRNP was one of the group of genes that were upregulated in G2/M synchronized cells⁶. However, these findings were inconsistent with our results in respect to the protein level. The study of PrP^c in glioblastoma cells treated with both TMZ and BCNU treatments has not been previously reported. Thus, the downregulation of PrP^c in treated cells could be attributed to different reasons. A possible reason may be that the protein could be degraded due to the higher expression of the PRNP gene. In addition, cells remaining for a long period at G2/M phase may affect the translation of this gene.

We concluded that BCNU is more potent in accumulating U87 cells in G2/M than TMZ. The accumulation of cells in G2/M phase may be attributed to the increase of the level of p21 and p53 which are regulators of the cell cycle. PRNP gene was elevated in treating cells with Nocodazole, which synchronizes cells in G2/M phase, whereas there is no significant change in the gene level in treated cells with Aphidicolin that arrested the cells in G1 phase. In addition, PRNP gene expression

was upregulated in treating cells with alkylating agents, 24h and 48h post-treatment. This may be an indication of may perhaps be due to the cytoprotective function of PrP^c, suggested by other previous studies. PrP^c expression under this condition was downregulated and these results were not in agreement with the gene expression results. This reduction of PrP^c may be attributed to the degradation of this protein or the competition of other genes in translation.

Further studies could be carried out to evaluate PRNP, and PrP^c using different types of glioblastoma cells such as U251 and T98G treated with TMZ or BCNU in a dose and time-dependent manner, with and without post-treatment. The accumulation of cells in G2/M phase may induce the resistance to chemotherapy, and the level of PRNP may increase in this cell phase. Therefore, apoptosis and proliferation assays may help to investigate whether upregulation of PrP^c promotes or inhibits the apoptosis rate. It is also possible that the combination of TMZ or BCNU with Aphidicolin may decrease the level of G2/M cells, which may improve the sensitivity of cells toward these treatments. Furthermore, more investigation is needed to detect PrP^c after prolonged cell arrest at G2/M by these treatments.

8.2 Knockdown of PRNP inhibits the proliferation of U87 cells

As mentioned in the previous [section \(8.1\)](#) the levels of PrP^c and its gene were altered in response to alkylating agents. The effect of PrP^c levels in treated glioblastoma cells with these agents has not been studied yet. We speculated that knockdown of PrP^c may reduce cell proliferation and induce apoptosis rate in untreated and treated cells with alkylating agents due to its anti-apoptotic effect in many cell types. Hence, knockdown experiments were performed in U87 cells to investigate the effect of this gene in untreated and treated cells with alkylating agents. These experiments showed

80% knocking down after 48h using siRNA, and the silencing continued after 5 days. It has been found that PRNP siRNA reduced the level of PrP^c in T98G glioma cells after 48h by approximately 80%¹⁸. Silencing of the PRNP gene in U87 cells inhibited the proliferation of untreated cells and did not improve the proliferation in treated cells. In addition, our results also showed that knockdown of PrP^c in U87 did not affect apoptosis in both untreated and treated cells. The effect of PrP^c knockdown on the proliferation of untreated U87 cells may be attributed to the PI3K/Akt pathway and Cyclin D1 protein which may be regulated and activated by PrP^c¹⁶⁹. Li *et al.* found that silencing of PrP^c in J889 glioblastoma cells reduced the proliferation and induced the apoptosis of these cells¹⁸⁵. Another study showed that suppressing PrP^c in many glioblastoma cells using DNA-antisense oligonucleotide decreased cell proliferation¹⁸⁴. The effect of PrP^c on cell proliferation depends on the cell type as reviewed in [section \(1.7.2.5\)](#). For instance, silencing of PRNP in gastric cancer cells SW620 and HT29 and breast cancer cells MDA-MB-435 did not affect the proliferation of cells^{228,8}. Silencing of PrP^c in gastric carcinoma cells AGS induced apoptosis by activation Bax and p53²²⁷. Zhuang *et al.* revealed that knockdown of PrP^c in U87 cells increase the apoptosis rate when treated with TMZ through activation of caspase 3⁶. The knockdown of PrP^c in breast cancer cells MDA-MB-435 did not induce resistance to chemotherapies (paclitaxel and staurosporine) that induced apoptosis⁸. Silencing of prion protein promoted sensitivity toward Adriamycin in gastric¹⁶⁸ and breast¹⁵² cancer cells. In addition, the knockdown of PRNP in astrocyte cells promoted sensitivity to staurosporine²³⁹.

Further investigations were performed to elucidate the effect of PRNP knockdown on U87 cells. The knockdown cells were treated with TMZ for 48h to evaluate the cell cycle phases and the level of p53 and p21, the regulators of the cell cycle. Results

here showed that the population of treated knockdown cells was less arrested in G2/M than treated control or scramble cells. This may be ascribed to the level of p53 and p21 where the G2/M arrest in glioblastoma cells required both of these proteins²³³. The results showed that these proteins were upregulated, but it is interesting to note that p21 was more upregulated in treated knockdown cells than cells treated with the scrambled control. These findings have not been reported in the literature before. The high level of p21 may induce G1 arrest due to its effect on cyclin-dependent kinases (CDKs). It has been reported that p21 may protect many types of cells from apoptosis²³⁵. Other studies reported that the induction of p21 in glioblastoma cells induces resistance to cisplatin and BCNU²³⁴. In addition, p21 may be considered as an oncogene due to its effect as a pro-cancer and antiapoptosis^{242,235}. Therefore, it is possible that p21 induces the resistance to alkylating agents and this resistance may be undetectable by MTT assay.

In conclusion, this is the first study to evaluate the effect of PRNP knockdown on U87 cells treated with TMZ or BCNU. The level of knockdown was approximately 80% after 48h. Knockdown of PrP^c significantly reduced the proliferation of U87 but did not induce cell proliferation in treated cells with TMZ or BCNU. Furthermore, the knockdown of PrP^c did not induce apoptosis in untreated and treated U87 cells with TMZ. In TMZ treated knockdown cells, the distribution of cell populations in cell cycle phases was changed in relative to treated scramble and control cells. Surprisingly, the expression of p21 was significantly upregulated in the treated silencing cells with alkylating agents and this upregulation may induce the resistance to TMZ and BCNU.

For future perspective, the effect of PrP^c knockdown on the resistance to alkylating agents needs further study. PrP^c in two types of glioblastoma cells (one of which has a wild type p53, and the other group has a mutant p53) can be silenced and then treated with TMZ or BCNU at different time points. Cell cycle assay can be used to quantify the cells in each phase. The results of cell cycle assay correlate with the level of p21 and p53 which regulate the cell cycle and have an active role in the apoptosis. Furthermore, apoptosis markers such as Bax and caspase 3 could be evaluated to explain whether the knockdown of the PRNP gene induces resistance or promotes sensitivity of cells toward alkylating agents.

8.3 Proteasomal inhibitor, MG132, does not improve the apoptosis when combined with TMZ but it affects PrP^c level in U87 cells

Several proteasome inhibitors such as MG132, lactacystin and bortezomib (PS341) have been reported to decrease cell proliferation and induce apoptosis through their effects on many survival pathways²⁶⁰. MG132 reduced cell proliferation and promoted the apoptosis of many glioblastoma cell lines^{255,256}. The combination of MG132 with cisplatin improved apoptosis in several cancer cells such as human oesophageal cancer cells²⁵⁷. The combination of MG132 with TMZ has not been investigated yet. It was hypothesised that this combination may sensitise U87 cells to TMZ. Furthermore, ERAD is a ubiquitin/proteasome system that blocks unfolded and misfolded proteins in the ER. MG132 may induce ER stress, reducing the translocation of PrP^c and causing an accumulation of nascent PrP¹⁴ or cytosolic PrP^c²⁵⁹. We also speculated that MG132 may upregulate PrP^c in U87 cells.

Our results showed that MG132 significantly decreases the growth of U87 cells with IC₅₀ values of 2.26 µM after 48h. The combination of MG132 with TMZ did not

reduce the proliferation of cells compared to MG132 alone. The reduction of cell growth could be related to the apoptotic effect of MG132. It has been found that MG132 reduces the viability of many glioblastoma cells with a different IC_{50} depending on cell type through differing survival pathways, but did not affect astrocytes^{256,13}. The results for the combination with TMZ have not been previously reported.

Further investigations have been performed to evaluate the effect of MG132 on U87 cells. MG132 induced apoptosis in U87 cells whereas there is no significant change in the apoptosis rate when compared with the combination of MG132 with TMZ. MG132 arrested the cells in the G2/M phase and induced the level of p53 and p21. The combination treatment did not exhibit any significant change in cell cycle or the level of these proteins compared to single treatment with MG132. The accumulation of p53 and p21 could be explained by the apoptotic effect of MG132 where these proteins are upregulated in response to cytotoxic stimuli and may promote the apoptosis. p53 plays an important role in cell cycle regulation and apoptosis. It has been shown that MG132 induced p53-dependent apoptosis in glioblastoma cells and upregulated caspase 3, particularly in p53 wild type cells^{261,12,256}. The effects of the combination of TMZ and MG132 on U87 cells have not been previously studied. Although the targets for MG132 and TMZ are different, the mechanisms of the actions could possibly be that MG132 competes or counteracts TMZ. It has been found that the combination of cisplatin with MG132 sensitised different cancer cells such as human oesophageal cancer cells to cisplatin and enhanced the apoptosis in these cells²⁵⁷.

Further studies were carried out to study the effect of MG132 on PrP^c in U87 cells. MG132 increases the level of PrP^c in U87 cells, and this action may be attributed to

the ability of this treatment to reduce protein degradation resultant from the pathway of ERAD. Yifat *et al* stated that MG132 upregulated the level of PrP^c in CHO-MHM2 and N2a cells due to resistance of PrP^c to proteolysis by ERAD¹⁴. Other studies found that MG132 increased cytosolic 27-34 kDa of PrP^c in HeLa-PrP, N2a-PrP and N2a cell lines. This has been associated with disruption of the proteasome function that results in the unfolded protein response (UPR) in a sequence to ER stress²⁵⁹.

To summarise, despite the effect of MG132 on cell proliferation and apoptosis, its combination with TMZ showed that there is no accumulative effect on U87 cells. Therefore, it implies that the combination treatment of MG132 and TMZ may counteract the effect of TMZ. Furthermore, MG132 affected the metabolism of PrP^c and then increased its level.

Further investigations could be carried out to elucidate the exact effect on PrP in U87 cells (cell surface and intracellular). For example, immunostaining using MG132 and other types of proteasome inhibitors could be used. In addition, pre-treatment with MG132 followed by treatment with different concentrations at various time points could be performed to sensitise U87 cells to TMZ treatment.

8.4 Novel FAPi (FA pathway inhibitors) small molecules do not affect the level of PrP^c in U87 cells

FA pathway is one of the DNA repair pathways that is activated through DNA replication or in response to DNA lesion²⁹⁵. This pathway is induced in glioblastoma cells treated with TMZ and BCNU by upregulating FANCD2, the key part of this pathway¹⁶. Previous work from our group (Drs. Matthew Sellwood and Peng HUA) showed that FAPi compounds inhibit the FA pathway in U87 cells (induced by TMZ or BCNU) by reducing the expression of FANCD2 (unpublished data). These

compounds, which have an amide group with different substitution groups, may have an ability to hit PrP^c in glioblastoma cells¹⁸. Therefore, we speculated that these compounds may disrupt PrP^c pathway.

In this work, we used ICC by ImageXpress Micro as high content small molecule screening method to evaluate PrP^c in treated cells. To our knowledge, this is the first time that this method was performed to evaluate the PrP^c level in glioblastoma cells. Therefore, it was validated using different concentrations of two types of prion protein antibodies (3F4 and 8H4) which are commonly used in immunofluorescent staining^{273,184}. Our results showed that both of these antibodies are suitable for screening.

The screening of FAPi compounds in combination with or without TMZ or BCNU did not show any reduction of PrP^c level in treated U87 cells after 48h (8h with FAPi compounds and 40h in combination with TMZ or BCNU). Michael *et al.* found that a group of some amide analogs and other molecules decreased the level of PrP^c in glioblastoma cells T98G and the hits that lower PrP^c level on cell surface were confirmed using ELISA¹⁸. Despite the negative results, ICC by ImageXpress Micro screening assay is a useful technique to examine many compounds that have a possible potential to lower the expression of PrP.

To conclude, many compounds of benzimidazole derivatives (FAPi compounds) were synthesised and purified by previous members of the group. In a separate study, it was found by the other member of the group (Drs. Matthew Sellwood and Peng HUA) that these small molecules inhibited the FA pathway by downregulation of FANCD2 protein in treated U87 cells with TMZ or BCNU. In our work, PrP^c level was assessed in U87 cells treated with FAPi compounds, and in combination with TMZ or BCNU

using ICC by ImageXpress Micro. These compounds however did not show any significant changes.

Further experiments could be performed to assess the effect of FAPi compounds on PrP^c level in glioblastoma cells. For instance, the duration of treatment could be extended. Other biochemical assays such as flow cytometry, western blot and ICC by confocal microscopy may be carried out to confirm the findings of this study.

8.5 Novel small molecules are cytotoxic to U87 cells

Heteroaromatic molecules are an important class of heterocyclic compounds, which have a wide range of biological activities such as anticancer²⁷⁹. The anticancer activity of several compounds is associated with their ability to activate some signalling pathways that promote cell death²⁸⁰. In this work, we examined groups of small molecules of heteroaromatic compounds (30 compounds) on U87 cells. According to previous work of the group, these molecules exhibit a cytotoxic effect on teratocarcinoma stem cells NT2. Therefore, we hypothesized that these compounds may have efficacy to induce cell death in U87 cells.

Our results showed that 8 of these compounds exhibited a cytotoxic effect on U87 cells. To further investigate the mechanism of toxicity, apoptosis assay using Annexin V and PI was employed. Only one compound (**175**) induced apoptosis of U87 cells. Besides, compound **175** inhibits the viability of U87 cells with an IC₅₀ value of 10.9 μM, according to MTT assay. This compound belongs to acridine 9-aminoacridine derivatives that were previously reported to induce cytotoxicity in different types of cancer cells including^{283,284} ovarian²⁸⁷ and pancreatic cancer^{288,289}. To our knowledge, these derivatives have not been tested against glioblastoma cells.

The effect of compound **175** on U87 cells was further studied. Cell cycle assay showed that this compound arrests the cells in G2/M, which supports the cell viability findings where the G2/M arrest decreases cell proliferation. The G2/M arrest may be ascribed to the interaction of compound **175** with DNA through intercalation. Several studies have previously shown that some acridine compounds intercalate with DNA by the amine group and this action may cause cytotoxicity^{283,284}. Furthermore, several 9-aminoacridine derivatives compounds were found to inhibit topoisomerase II (topo II) that participates in the over-winding or under-winding of DNA^{283,290,291}. The disruption of this enzyme may affect cell cycle phases and induce G2 phase accumulation^{292,293}.

Due to G2/M accumulation resulting from compound **175**; p53 and p21 were evaluated in treated cells. Both of these proteins were upregulated, and this upregulation may be resultant of the toxicity to compound **175**, where p53 and p21 were induced in response to DNA damage. It has been found that p53 induced G2 arrest in response to the inhibition of topo II²⁹³. Additionally, the induction of p53 in treated cells with compound **175** may induce apoptosis of U87 cells, and this effect was supported by the results from the Annexin V assay. Wang *et al.* found that 9-aminoacridine derivatives increased the apoptosis rate in several cancer cells via upregulating p53 and Bax²⁸⁶. p53, as a tumour suppressor protein, is accumulated in response to DNA damage and induces cell cycle arrest or apoptosis transiently or permanently²⁸⁵.

On the other hand, it was expected that this compound may reduce PrP^c level due to its binding to prion protein as previously observed. Surprisingly, compound **175** did not change the expression of PrP^c in U87 cells. Other studies showed that 9-aminoacridine derivatives bind to PrP^c through specific amino acid residues (Tyrosine

225, Tyrosine 226, and Glutamine 227)^{294,281}. In addition, according to SPR assay, the previous work of our group found that some of 9-aminoacridine derivatives can bind PrP^c²⁸¹.

To summarise, several novel heteroaromatic compounds from the libraries (30 compounds) synthesised by the previous members in the group, were tested as new anti-glioblastoma agents. These compounds previously exhibited cytotoxicity effects on NT2 cells. In our work, 8 of these molecules induced toxicity in U87 cells. Compound **175** (acridine derivative) has the efficacy to reduce cell viability with an IC₅₀ value of 10.9 µM and increased the apoptosis rate of U87 cells. It also arrested the cells in G2/M and upregulated p53 and p21 levels.

To our knowledge, this is the first study concerning the effect of the acridine compounds on glioblastoma cells. Therefore, further studies are required to investigate other acridine derivatives as potential anti-glioblastoma agents. Many biological tests may be applied to investigate the apoptotic pathway of these compounds. For example, caspase 3 is a useful biomarker to determine the apoptosis of treated cells. Pro-apoptotic factors such as Bax, Bak and Bcl-X or anti-apoptotic factors such as Bcl-2 and Bcl-XL can also be estimated using western blot.

References

1. Bastien, J. I. L., McNeill, K. a. & Fine, H. a. Molecular characterizations of glioblastoma, targeted therapy, and clinical results to date. *Cancer* **121**, 502–516 (2015).
2. Ramirez, Y. P., Weatherbee, J. L., Wheelhouse, R. T. & Ross, A. H. Glioblastoma multiforme therapy and mechanisms of resistance. *Pharmaceuticals* **6**, 1475–1506 (2013).
3. Yang, X. *et al.* Prion protein and cancers. *Acta Biochim. Biophys. Sin. (Shanghai)*. **46**, 431–440 (2014).
4. Lopes, M. H. *et al.* Disruption of prion protein–HOP engagement impairs glioblastoma growth and cognitive decline and improves overall survival. *Oncogene* **34**, 3305–3314 (2015).
5. Comincini, S. & Facoetti, A. Differential expression of the prion-like protein doppel gene (PRND) in astrocytomas: a new molecular marker potentially involved in tumor progression. *Anticancer Res.* **1518**, 1507–1517 (2004).
6. Zhuang, D. *et al.* TMZ-induced PrPc/par-4 interaction promotes the survival of human glioma cells. *Int. J. Cancer* **130**, 309–318 (2012).
7. Song, X. *et al.* Temozolomide – perillyl alcohol conjugate downregulates O⁶-methylguanine DNA methyltransferase via inducing ubiquitination-dependent proteolysis in non-small cell lung cancer. *Cell Death Dis.* (2018). doi:10.1038/s41419-017-0193-2
8. Yu, G. *et al.* Silencing prion protein in MDA-MB-435 breast cancer cells leads to pleiotropic cellular responses to cytotoxic stimuli. *PLoS One* **7**, e48146–e48146 (2012).
9. Park, J. E., Miller, Z., Jun, Y., Lee, W. & Kim, K. B. Next-generation proteasome inhibitors for cancer therapy. *Transl. Res.* **198**, 1–16 (2018).
10. Guo, N. & Peng, Z. MG132, a proteasome inhibitor, induces apoptosis in tumor cells. *Asia. Pac. J. Clin. Oncol.* **9**, 6–11 (2013).

11. Han, Y. H. & Park, W. H. MG132, a proteasome inhibitor decreased the growth of Calu-6 lung cancer cells via apoptosis and GSH depletion. *Toxicol. Vitro.* **24**, 1237–1242 (2010).
12. Wagenknecht, B. *et al.* Proteasome inhibitor-induced apoptosis of glioma cells involves the processing of multiple caspases and cytochrome c release. *J. Neurochem.* **75**, 2288–2297 (2000).
13. Yang, X. *et al.* SAHA and / or MG132 reverse the aggressive phenotypes of glioma cells : An in vitro and vivo study. *Oncotarget* **8**, 3156–3169 (2017).
14. Yedidia, Y., Horonchik, L., Tzaban, S., Yanai, A. & Taraboulos, A. Proteasomes and ubiquitin are involved in the turnover of the wild-type prion protein. *EMBO J.* **20**, 5383–5391 (2001).
15. Collins, N. & Kupfer, G. M. Molecular pathogenesis of Fanconi anemia. *Int. J. Hematol.* **82**, 176–183 (2005).
16. Chen, C. C., Taniguchi, T. & D'Andrea, A. The Fanconi anemia (FA) pathway confers glioma resistance to DNA alkylating agents. *J. Mol. Med.* **85**, 497–509 (2007).
17. Patil, A. a *et al.* FANCD2 re-expression is associated with glioma grade and chemical inhibition of the Fanconi Anaemia pathway sensitises gliomas to chemotherapeutic agents. *Oncotarget* **5**, 1–11 (2014).
18. Silber, B. M. *et al.* Novel compounds lowering the cellular isoform of the human prion protein in cultured human cells. *Bioorganic Med. Chem.* **22**, 1960–1972 (2014).
19. Ouyang, L. *et al.* Programmed cell death pathways in cancer: A review of apoptosis, autophagy and programmed necrosis. *Cell Prolif.* **45**, 487–498 (2012).
20. He, C. & Klionsky, D. J. Regulation Mechanisms and Signalling Pathways of Autophagy. *Annu. Rev. Genet.* **43**, 67 (2009).
21. Liu, B., Cheng, Y., Liu, Q., Bao, J. K. & Yang, J.-M. M. Autophagic pathways as new targets for cancer drug development. *Acta Pharmacol. Sin.*

- 31**, 1154–1164 (2010).
22. Feoktistova, M. & Leverkus, M. Programmed necrosis and necroptosis signalling. *FEBS J.* **282**, 19–31 (2015).
 23. Amelio, I., Melino, G. & Knight, R. a. Cell death pathology: Cross-talk with autophagy and its clinical implications. *Biochem. Biophys. Res. Commun.* **414**, 277–281 (2011).
 24. Eum, K. H. & Lee, M. Crosstalk between autophagy and apoptosis in the regulation of paclitaxel-induced cell death in v-Ha-ras-transformed fibroblasts. *Mol. Cell. Biochem.* **348**, 61–68 (2011).
 25. Sayers, T. J. Targeting the extrinsic apoptosis signaling pathway for cancer therapy. *Cancer Immunol. Immunother.* **60**, 1173–1180 (2011).
 26. Baig, S. *et al.* Potential of apoptotic pathway-targeted cancer therapeutic research: Where do we stand? *Cell Death Dis.* **7**, e2058 (2016).
 27. Shen, Y. & White, E. in *Encyclopedia of Cancer* 55–84 (Springer Berlin Heidelberg, 2001). doi:10.1016/S0065-230X(01)82002-9
 28. Green, D. R. & Llambi, F. Cell Death Signaling. *Cold Spring Harb. Perspect. Biol.* **7**, a006080 (2015).
 29. Xu, W. *et al.* Bax-PGAM5L-Drp1 complex is required for intrinsic apoptosis execution. *Oncotarget* **6**, 30017–34 (2015).
 30. Bai, L. & Wang, S. Targeting apoptosis pathways for new cancer therapeutics. *Annu Rev Med* **65**, 139–155 (2014).
 31. Engel, T. & Henshall, D. C. Apoptosis, Bcl-2 family proteins and caspases: The ABCs of seizure-damage and epileptogenesis? *Int. J. Physiol. Pathophysiol. Pharmacol.* **1**, 97–115 (2009).
 32. Llambi, F. & Green, D. R. Apoptosis and oncogenesis: Give and take in the BCL-2 family. *Curr. Opin. Genet. Dev.* **21**, 12–20 (2011).
 33. Wen, X., Lin, Z. Q., Liu, B. & Wei, Y. Q. Caspase-mediated programmed cell death pathways as potential therapeutic targets in cancer. *Cell Prolif.* **45**, 217–

- 224 (2012).
34. Irene M. Ghobrial MD; Alex A. Adjei, M. T. E. W. Targeting apoptosis pathways in cancer. *CA Cancer J Clin* **55**, 178–194 (2005).
 35. Li, P. *et al.* Cytochrome c and dATP-dependent formation of Apaf-1/caspase-9 complex initiates an apoptotic protease cascade. *Cell* **91**, 479–489 (1997).
 36. Kelly, P. N. & Strasser, a. The role of Bcl-2 and its pro-survival relatives in tumourigenesis and cancer therapy. *Cell Death Differ.* **18**, 1414–1424 (2011).
 37. Yu, J., Wang, Z., Kinzler, K. W., Vogelstein, B. & Zhang, L. PUMA mediates the apoptotic response to p53 in colorectal cancer cells. *PNAS* **100**, 1931–1936 (2003).
 38. Leva, G. Di, Garofalo, M. & Croce, C. M. PM09CH13-Croce MicroRNAs in Cancer. *Annu. Rev. Pathol. Mech. Dis* **9**, 287–314 (2014).
 39. Wang, S. Y., Yu, Q. J., Zhang, R. D. & Liu, B. Core signaling pathways of survival/death in autophagy-related cancer networks. *Int. J. Biochem. Cell Biol.* **43**, 1263–1266 (2011).
 40. Yun, C., Lee, S., Yun, C. W. & Lee, S. H. The Roles of Autophagy in Cancer. *Int. J. Mol. Sci.* **19**, 3466 (2018).
 41. Agostinis, P., Buytaert, E., Breysens, H. & Hendrickx, N. Regulatory pathways in photodynamic therapy induced apoptosis. *Photochem. Photobiol. Sci.* **3**, 721–729 (2004).
 42. Diaz-Moralli, S., Tarrado-Castellarnau, M., Miranda, A. & Cascante, M. Targeting cell cycle regulation in cancer therapy. *Pharmacol. Ther.* **138**, 255–271 (2013).
 43. Sancar, A. *et al.* Molecular mechanisms of mammalian DNA repair and the DNA damage checkpoints. *Annu. Rev. Biochem.* **73**, 39–85 (2004).
 44. Cuddihy, A. R. & O’Connell, M. J. in *Review Literature And Arts Of The Americas* **222**, 99–140 (2003).
 45. Lara-Gonzalez, P., Westhorpe, F. G. & Taylor, S. S. The Spindle Assembly

- Checkpoint. *Curr. Biol.* **22**, R966–R980 (2012).
46. Vermeulen, K., Van Bockstaele, D. R. & Berneman, Z. N. The cell cycle: A review of regulation, deregulation and therapeutic targets in cancer. *Cell Prolif.* **36**, 131–149 (2003).
 47. Dash, B. C. & El-Deiry, W. S. in *Checkpoint Controls and Cancer* **280**, 099–162 (Humana Press, 2004).
 48. Dickson, M. a. & Schwartz, G. K. Development of cell-cycle inhibitors for cancer therapy. *Curr. Oncol.* **16**, 36–43 (2009).
 49. Adamsen, B. L., Kravik, K. L. & De Angelis, P. M. DNA damage signaling in response to 5-fluorouracil in three colorectal cancer cell lines with different mismatch repair and TP53 status. *Int. J. Oncol.* **39**, 673–682 (2011).
 50. Peltier, S., Oger, J. M., Lagarce, F., Couet, W. & Benoît, J. P. Enhanced oral paclitaxel bioavailability after administration of paclitaxel-loaded lipid nanocapsules. *Pharm. Res.* **23**, 1243–1250 (2006).
 51. Stupp, R., Brada, M., van den Bent, M. J., Tonn, J.-C. & Pentheroudakis, G. High-grade glioma: ESMO Clinical Practice Guidelines for diagnosis, treatment and follow-up. *Ann. Oncol.* **25**, 93–101 (2014).
 52. Szopa, W., Burley, T. A., Kramer-Marek, G. & Kaspera, W. Diagnostic and Therapeutic Biomarkers in Glioblastoma: Current Status and Future Perspectives. *Biomed Res. Int.* **2017**, 1–13 (2017).
 53. Adamson, C. *et al.* Glioblastoma multiforme: a review of where we have been and where we are going. *Expert Opin.* **18**, 1061–1084 (2009).
 54. Furnari, F. B. *et al.* Malignant astrocytic glioma: genetics, biology, and paths to treatment. *Genes Dev.* **21**, 2683–2710 (2007).
 55. Eisele, G. & Weller, M. Targeting apoptosis pathways in glioblastoma. *Cancer Lett.* **332**, 335–345 (2013).
 56. Krajewski, S. *et al.* Immunohistochemical analysis of Bcl-2, Bcl-X, Mcl-1, and Bax in tumors of central and peripheral nervous system origin. *Am. J.*

- Pathol.* **150**, 805–814 (1997).
57. McDonald, F. E. *et al.* The prognostic influence of bcl-2 in malignant glioma. *Br. J. Cancer* **86**, 1899–1904 (2002).
58. Vogler, M. *et al.* Different forms of cell death induced by putative BCL2 inhibitors. *Cell Death Differ.* **16**, 1030–1039 (2009).
59. Voss, V. *et al.* The pan-Bcl-2 inhibitor (-)-gossypol triggers autophagic cell death in malignant glioma. *Mol. Cancer Res.* **8**, 1002–1016 (2010).
60. Shi, L. *et al.* MiR-21 protected human glioblastoma U87MG cells from chemotherapeutic drug temozolomide induced apoptosis by decreasing Bax/Bcl-2 ratio and caspase-3 activity. *Brain Res.* **1352**, 255–264 (2010).
61. Chan, J. A., Krichevsky, A. M. & Kosik, K. S. MicroRNA-21 Is an Antiapoptotic Factor in Human Glioblastoma Cells. *Cancer Res.* **65**, 6029–6033 (2005).
62. Farnebo, M., Bykov, V. J. N. & Wiman, K. G. The p53 tumor suppressor: A master regulator of diverse cellular processes and therapeutic target in cancer. *Biochem. Biophys. Res. Commun.* **396**, 85–89 (2010).
63. McLendon, R. *et al.* Comprehensive genomic characterization defines human glioblastoma genes and core pathways. *Nature* **455**, 1061–1068 (2008).
64. Ohgaki, H. *et al.* Genetic Pathways to Glioblastoma : A Population-Based Study Genetic Pathways to Glioblastoma : A Population-Based Study. *Cancer Res* **64**, 6892–6899 (2004).
65. Galanis, E. *et al.* Phase II Trial of Temsirolimus (CCI-779) in Recurrent Glioblastoma Multiforme: A North Central Cancer Treatment Group Study. *J. Clin. Oncol.* **23**, 5294–5304 (2005).
66. Wang, M. Y. *et al.* Mammalian Target of Rapamycin Inhibition Promotes Response to Epidermal Growth Factor Receptor Kinase Inhibitors in PTEN-Deficient and PTEN-Intact Glioblastoma Cells. *Cancer Res.* **66**, 7864–7869 (2006).

67. Kichev, A. *et al.* Tumor necrosis factor-related apoptosis-inducing ligand (TRAIL) signaling and cell death in the immature central nervous system after hypoxia-ischemia and inflammation. *J. Biol. Chem.* **289**, 9430–9439 (2014).
68. Grund, K. *et al.* Troglitazone-mediated sensitization to TRAIL-induced apoptosis is regulated by proteasome-dependent degradation of FLIP and ERK1/2-dependent phosphorylation of BAD. *Cancer Biol. Ther.* **7**, 1982–1990 (2008).
69. Nagane, M., Shimizu, S., Mori, E., Kataoka, S. & Shiokawa, Y. Predominant antitumor effects by fully human anti-TRAIL-receptor2 (DR5) monoclonal antibodies in human glioma cells in vitro and in vivo. **12**, 687–700 (2010).
70. Rieger, J., Frank, B. & Weller, M. Cellular Physiology Biochemistry and Biochemistr y Mechanisms of Resistance of Human Glioma Cells to Apo2 Ligand / TNF-Related Apoptosis-Inducing Ligand. *Cell. Physiol. Biochem.* 23–34 (2007).
71. Calzolari, A. *et al.* Salinomycin Potentiates the Cytotoxic Effects of TRAIL on Glioblastoma Cell Lines. *PLoS One* **9**, e94438 (2014).
72. Colby, D. W. & Prusiner, S. B. Prions. *Cold Spring Harb. Lab. Press* **3**, (2011).
73. Pruisner, S. B. Novel proteinaceous infectious particles cause scrapie. *Science* (80-.). **216**, 136–44 (1982).
74. Puckett, C., Concannon, P., Casey, C. & Hood, L. Genomic structure of the human prion protein gene. *Am. J. Hum. Genet.* **49**, 320–329 (1991).
75. Acevedo-Morantes, C. & Wille, H. The Structure of Human Prions: From Biology to Structural Models — Considerations and Pitfalls. *Viruses* **6**, 3875–3892 (2014).
76. Castle, A. R. & Gill, A. C. Physiological Functions of the Cellular Prion Protein. *Front. Mol. Biosci.* **4**, 19 (2017).
77. Atkinson, C. J., Zhang, K., Munn, A. L., Wiegman, A. & Ming, Q. Prion protein scrapie and the normal cellular prion protein Prion protein scrapie and

- the normal cellular prion protein. *Prion* **10**, 63–82 (2016).
78. Lawson, V. A., Collins, S. J., Masters, C. L. & Hill, A. F. Prion protein glycosylation. *J. Neurochem.* **93**, 793–801 (2005).
79. Harris, D. A. Trafficking, turnover and membrane topology of PrP. *Br. Med. Bull.* **66**, 71–85 (2003).
80. Cancellotti, E. *et al.* Altered glycosylated PrP proteins can have different neuronal trafficking in brain but do not acquire scrapie-like properties. *J. Biol. Chem.* **280**, 42909–42918 (2005).
81. Harris, D. A. Cellular biology of prion diseases. *Clin. Microbiol. Rev.* **12**, 429–44 (1999).
82. Giachin, G., Biljan, I., Ilc, G., Plavec, J. & Legname, G. Probing early misfolding events in prion protein mutants by NMR spectroscopy. *Molecules* **18**, 9451–9476 (2013).
83. Peters, P. J. *et al.* Trafficking of prion proteins through a caveolae-mediated endosomal pathway. *J. Cell Biol.* **162**, 703–17 (2003).
84. Harris, D. A. Trafficking, turnover and membrane topology of PrP. *Br. Med. Bull.* **66**, 71–85 (2003).
85. Kim, Y., Lee, J. & Lee, C. In silico Comparative Analysis of DNA and Amino Acid Sequences for Prion Protein Gene. *Transbound. Emerg. Dis.* **55**, 105–114 (2008).
86. Schmitt-Ulms, G., Ehsani, S., Watts, J. C., Westaway, D. & Wille, H. Evolutionary descent of prion genes from the ZIP family of metal Ion transporters. *PLoS One* **4**, (2009).
87. Spevacek, A. R. *et al.* Zinc drives a tertiary fold in the prion protein with familial disease mutation sites at the interface. *Structure* **21**, 236–246 (2013).
88. Watt, N. T., Griffiths, H. H. & Hooper, N. M. Neuronal zinc regulation and the prion protein. *Prion* **7**, 203–208 (2013).
89. Aguzzi, A., Baumann, F. & Bremer, J. The Prion's Elusive Reason for Being.

- Annu. Rev. Neurosci.* **31**, 439–477 (2008).
90. Restelli, E. *et al.* The hydrophobic core region governs mutant prion protein aggregation and intracellular retention. *Biochem. J.* **430**, 477–486 (2010).
 91. Wille, H., Requena, J., Wille, H. & Requena, J. R. The Structure of PrP^{Sc} Prions. *Pathogens* **7**, 20 (2018).
 92. Linden, R. *et al.* Physiology of the prion protein. *Physiol. Rev.* **88**, 673–728 (2008).
 93. Pauly, P. C. & Harris, D. a. Copper stimulates endocytosis of the prion protein. *J. Biol. Chem.* **273**, 33107–33110 (1998).
 94. Brown, D. R. *et al.* The cellular prion protein binds copper in vivo. *Nature* **390**, 684–687 (1997).
 95. Jackson, G. S. *et al.* Location and properties of metal-binding sites on the human prion protein. *Proc. Natl. Acad. Sci.* **98**, 8531–8535 (2001).
 96. Cheng, F., Lindqvist, J., Haigh, C. L., Brown, D. R. & Mani, K. Copper-dependent co-internalization of the prion protein and glypican-1. *J. Neurochem.* **98**, 1445–1457 (2006).
 97. Marella, M., Lehmann, S., Grassi, J. & Chabry, J. Filipin Prevents Pathological Prion Protein Accumulation by Reducing Endocytosis and Inducing Cellular PrP Release. *J. Biol. Chem.* **277**, 25457–25464 (2002).
 98. Herms, J. *et al.* Evidence of presynaptic location and function of the prion protein. *J. Neurosci.* **19**, 8866–8875 (1999).
 99. Watt, N. T., Routledge, M. N., Wild, C. P. & Hooper, N. M. Cellular prion protein protects against reactive-oxygen-species-induced DNA damage. *Free Radic. Biol. Med.* **43**, 959–967 (2007).
 100. Zocche Soprana, H., Canes Souza, L., Debbas, V. & Martins Laurindo, F. R. Cellular prion protein (PrPC) and superoxide dismutase (SOD) in vascular cells under oxidative stress. *Exp. Toxicol. Pathol.* **63**, 229–236 (2011).
 101. Sakudo, A. *et al.* Impairment of superoxide dismutase activation by N-

- terminally truncated prion protein (PrP) in PrP-deficient neuronal cell line. *Biochem. Biophys. Res. Commun.* **308**, 660–667 (2003).
102. Klamt, F. *et al.* Imbalance of antioxidant defense in mice lacking cellular prion protein. *Free Radic. Biol. Med.* **30**, 1137–1144 (2001).
103. Wong, B. S. *et al.* Increased levels of oxidative stress markers detected in the brains of mice devoid of prion protein. *J. Neurochem.* **76**, 565–572 (2001).
104. Chacón, M. a, Barría, M. I., Lorca, R., Huidobro-Toro, J. P. & Inestrosa, N. C. A human prion protein peptide (PrP(59-91)) protects against copper neurotoxicity. *Mol. Psychiatry* **8**, 835,853-862 (2003).
105. Choi, C. J. *et al.* Normal cellular prion protein protects against manganese-induced oxidative stress and apoptotic cell death. *Toxicol. Sci.* **98**, 495–509 (2007).
106. Haigh, C. L., McGlade, A. R. & Collins, S. J. MEK1 transduces the prion protein N2 fragment antioxidant effects. *Cell. Mol. Life Sci.* **72**, 1613–1629 (2015).
107. Haigh, C. L., Tumpach, C., Drew, S. C. & Collins, S. J. The Prion Protein N1 and N2 Cleavage Fragments Bind to Phosphatidylserine and Phosphatidic Acid; Relevance to Stress-Protection Responses. *PLoS One* **10**, e0134680 (2015).
108. Bravard, A. *et al.* The prion protein is critical for DNA repair and cell survival after genotoxic stress. *Nucleic Acids Res.* **43**, 904–16 (2015).
109. Hutter, G., Heppner, F. L. & Aguzzi, A. No Superoxide Dismutase Activity of Cellular Prion Protein in vivo. *Biol. Chem.* **384**, 1279–85 (2003).
110. Steinacker, P. *et al.* Neuroprotective function of cellular prion protein in a mouse model of amyotrophic lateral sclerosis. *Am. J. Pathol.* **176**, 1409–20 (2010).
111. Vassallo, N. *et al.* Activation of phosphatidylinositol 3-kinase by cellular prion protein and its role in cell survival. *Biochem. Biophys. Res. Commun.* **332**, 75–82 (2005).

112. Yin, X.-M., Oltvai, Z. N. & Korsmeyer, S. J. BH1 and BH2 domains of Bcl-2 are required for inhibition of apoptosis and heterodimerization with Bax. *Nature* **369**, 321–323 (1994).
113. Bounhar, Y., Zhang, Y., Goodyer, C. G. & LeBlanc, A. Prion Protein Protects Human Neurons against Bax-mediated Apoptosis. *J. Biol. Chem.* **276**, 39145–39149 (2001).
114. Kurschner, C. & Morgan, J. I. The cellular prion protein (PrP) selectively binds to Bcl-2 in the yeast two-hybrid system. *Brain Res. Mol. Brain Res.* **30**, 165–168 (1995).
115. Chen, S., Mangé, A., Dong, L., Lehmann, S. & Schachner, M. Prion protein as trans-interacting partner for neurons is involved in neurite outgrowth and neuronal survival. *Mol. Cell. Neurosci.* **22**, 227–233 (2003).
116. Roucou, X., Guo, Q., Zhang, Y., Goodyer, C. G. & LeBlanc, A. C. Cytosolic Prion Protein Is Not Toxic and Protects against Bax-mediated Cell Death in Human Primary Neurons. *J. Biol. Chem.* **278**, 40877–40881 (2003).
117. Roucou, X. *et al.* Cellular prion protein inhibits proapoptotic Bax conformational change in human neurons and in breast carcinoma MCF-7 cells. *Cell Death Differ.* **12**, 783–795 (2005).
118. Westergard, L., Christensen, H. M. & Harris, D. a. The cellular prion protein (PrP(C)): its physiological function and role in disease. *Biochim. Biophys. Acta* **1772**, 629–644 (2007).
119. Roucou, X. & LeBlanc, A. C. Cellular prion protein neuroprotective function: Implications in prion diseases. *J. Mol. Med.* **83**, 3–11 (2005).
120. Lin, D. T. S., Jodoin, J., Baril, M., Goodyer, C. G. & LeBlanc, A. C. Cytosolic prion protein is the predominant anti-Bax prion protein form: Exclusion of transmembrane and secreted prion protein forms in the anti-Bax function. *Biochim. Biophys. Acta - Mol. Cell Res.* **1783**, 2001–2012 (2008).
121. A. Rambold D. Rapaport, T. Bartke, M. Baier, K. Winklhofer, and J. Tatzelt, M. M. Association of Bcl-2 with Misfolded Prion Protein Is Linked to the

- Toxic Potential of Cytosolic PrP. *Mol. Biol. Cell* **17**, 3356–3368 (2006).
122. Ma, J. & Lindquist, S. Wild-type PrP and a mutant associated with prion disease are subject to retrograde transport and proteasome degradation. *Proc. Natl. Acad. Sci. U. S. A.* **98**, 14955–14960 (2001).
123. Ma, J., Wollmann, R. & Lindquist, S. Neurotoxicity and neurodegeneration when PrP accumulates in the cytosol. *Science* **298**, 1781–1785 (2002).
124. Zhang, S. & Yu, D. Targeting Src family kinases in anti-cancer therapies: turning promise into triumph. *Trends Pharmacol. Sci.* **33**, 122–128 (2012).
125. Zanata, S. M. *et al.* Stress-inducible protein 1 is a cell surface ligand for cellular prion that triggers neuroprotection. *EMBO J.* **21**, 3307–3316 (2002).
126. Roffé, M. *et al.* Prion protein interaction with stress-inducible protein 1 enhances neuronal protein synthesis via mTOR. *Proc. Natl. Acad. Sci. U. S. A.* **107**, 13147–52 (2010).
127. Chiarini, L. B. *et al.* Cellular prion protein transduces neuroprotective signals. *EMBO J.* **21**, 3317–3326 (2002).
128. Martini, M., De Santis, M. C., Braccini, L., Gulluni, F. & Hirsch, E. PI3K/AKT signaling pathway and cancer: an updated review. *Ann. Med.* **46**, 372–383 (2014).
129. Bakkebo, M. K. *et al.* The Cellular Prion Protein: A Player in Immunological Quiescence. *Front. Immunol.* **6**, 450 (2015).
130. Mouillet-Richard, S. *et al.* Signal transduction through prion protein. *Science* **289**, 1925–1928 (2000).
131. Lopes, M. H. *et al.* Interaction of cellular prion and stress-inducible protein 1 promotes neuritogenesis and neuroprotection by distinct signaling pathways. *J. Neurosci.* **25**, 11330–11339 (2005).
132. Nah, J. *et al.* BECN1/Beclin 1 is recruited into lipid rafts by prion to activate autophagy in response to amyloid β 42. *Autophagy* **9**, 2009–2021 (2013).
133. Shin, H.-Y., Park, J.-H., Carp, R. I., Choi, E.-K. & Kim, Y.-S. Deficiency of

- prion protein induces impaired autophagic flux in neurons. *Front. Aging Neurosci.* **6**, 207 (2014).
134. Llorens, F. *et al.* PrP^C regulates epidermal growth factor receptor function and cell shape dynamics in Neuro2a cells. *J. Neurochem.* **127**, n/a-n/a (2013).
135. Sempou, E., Biasini, E., Pinzón-Olejua, A., Harris, D. A. & Málaga-Trillo, E. Activation of zebrafish Src family kinases by the prion protein is an amyloid- β -sensitive signal that prevents the endocytosis and degradation of E-cadherin/ β -catenin complexes in vivo. *Mol. Neurodegener.* **11**, 18 (2016).
136. Steele, A. D., Emsley, J. G., Ozdinler, P. H., Lindquist, S. & Macklis, J. D. Prion protein (PrP^c) positively regulates neural precursor proliferation during developmental and adult mammalian neurogenesis. *Proc. Natl. Acad. Sci. U. S. A.* **103**, 3416–3421 (2006).
137. Zhang, C. C., Steele, A. D., Lindquist, S. & Lodish, H. F. Prion protein is expressed on long-term repopulating hematopoietic stem cells and is important for their self-renewal. *Proc. Natl. Acad. Sci. U. S. A.* **103**, 2184–2189 (2006).
138. Haigh, C. & Collins, S. Oxidative Modulation of Neural Stem Cell Growth by Prion Protein Cleavage Fragments. *Free Radic. Biol. Med.* **76**, S24 (2014).
139. Chieng, C. K.-L. & Say, Y.-H. Cellular prion protein contributes to LS 174T colon cancer cell carcinogenesis by increasing invasiveness and resistance against doxorubicin-induced apoptosis. *Tumor Biol.* **36**, 8107–8120 (2015).
140. Corsaro, A. *et al.* Cellular prion protein controls stem cell-like properties of human glioblastoma tumor-initiating cells. *Oncotarget* **7**, 38638–38657 (2016).
141. Bribián, A. *et al.* Role of the Cellular Prion Protein in Oligodendrocyte Precursor Cell Proliferation and Differentiation in the Developing and Adult Mouse CNS. *PLoS One* **7**, e33872 (2012).
142. Kim, B.-H., Kim, J.-I., Choi, E.-K., Carp, R. I. & Kim, Y.-S. A neuronal cell line that does not express either prion or doppel proteins. *Neuroreport* **16**,

- 425–429 (2005).
143. Morel, E. *et al.* The cellular prion protein PrP(c) is involved in the proliferation of epithelial cells and in the distribution of junction-associated proteins. *PLoS One* **3**, e3000–e3000 (2008).
 144. Diarra-Mehrpour, M. *et al.* Prion protein prevents human breast carcinoma cell line from tumor necrosis factor alpha-induced cell death. *Cancer Res.* **64**, 719–727 (2004).
 145. Antonacopoulou, A. G. *et al.* Prion protein expression and the M129V polymorphism of the PRNP gene in patients with colorectal cancer. *Mol. Carcinog.* **49**, 693–699 (2010).
 146. Antony H Wei MQ, Chernoff YO, Khanna KK, and Munn AL, W. A. P. Potential roles for prions and protein-only inheritance in cancer. *Cancer Metastasis* **31**, (2013).
 147. Mehrpour, M. & Codogno, P. Prion protein: From physiology to cancer biology. *Cancer Lett.* **290**, 1–23 (2010).
 148. Sy, M.-S. *et al.* Association of prion protein expression with pancreatic adenocarcinoma survival in the SEER residual tissue repository. *Cancer Biomark.* **10**, 251–258 (2012).
 149. Sollazzo, V., Galasso, M., Volinia, S. & Carinci, F. Prion proteins (PRNP and PRND) are over-expressed in osteosarcoma. *J. Orthop. Res.* **30**, 1004–1012 (2012).
 150. Déry, M.-A. *et al.* Endoplasmic reticulum stress induces PRNP prion protein gene expression in breast cancer. *Breast Cancer Res.* **15**, R22–R22 (2013).
 151. Diarra-mehrpour, M. *et al.* Prion Protein Prevents Human Breast Carcinoma Cell Line from Tumor Necrosis Factor alfa-Induced Cell Death. 719–727 (2004).
 152. Meslin, F. *et al.* Silencing of prion protein sensitizes breast adriamycin-resistant carcinoma cells to TRAIL-mediated cell death. *Cancer Res.* **67**, 10910–10919 (2007).

153. Li, Q.-Q. *et al.* The role of P-glycoprotein/cellular prion protein interaction in multidrug-resistant breast cancer cells treated with paclitaxel. *Cell. Mol. Life Sci.* **66**, 504–515 (2009).
154. Meslin, F. *et al.* Efficacy of adjuvant chemotherapy according to Prion protein expression in patients with estrogen receptor-negative breast cancer. *Ann. Oncol.* **18**, 1793–1798 (2007).
155. Cheng, Y. *et al.* CD44/cellular prion protein interact in multidrug resistant breast cancer cells and correlate with responses to neoadjuvant chemotherapy in breast cancer patients. *Mol. Carcinog.* **53**, 686–697 (2014).
156. Li, Q.-Q. *et al.* Cellular prion protein promotes glucose uptake through the Fyn-HIF-2 α -Glut1 pathway to support colorectal cancer cell survival. *Cancer Sci.* **102**, 400–406 (2011).
157. De Wit, M. *et al.* Cell surface proteomics identifies glucose transporter type 1 and prion protein as candidate biomarkers for colorectal adenoma-to-carcinoma progression. *Gut* **61**, 855–864 (2012).
158. Antonacopoulou, A. G. *et al.* POLR2F , ATP6V0A1 and PRNP Expression in Colorectal Cancer : New Molecules with Prognostic Significance ? *Anticancer Res.* **1228**, 1221–1227 (2008).
159. Wang, Q., Qian, J., Wang, F. & Ma, Z. Cellular prion protein accelerates colorectal cancer metastasis via the Fyn-SP1-SATB1 axis. *Oncol. Rep.* **28**, 2029–2034 (2012).
160. Han, H. *et al.* Identification of Differentially Expressed Genes in Pancreatic Cancer Cells Using cDNA Microarray. *Cancer Res.* **62**, 2890–2896 (2002).
161. Li, C. *et al.* Binding of pro-prion to filamin A disrupts cytoskeleton and correlates with poor prognosis in pancreatic cancer. *J. Clin. Invest.* **119**, 2725–2736 (2009).
162. Yang, L. *et al.* Glycosylphosphatidylinositol Anchor Modification Machinery Deficiency Is Responsible for the Formation of Pro-Prion Protein (PrP) in BxPC-3 Protein and Increases Cancer Cell Motility. *J. Biol. Chem.* **291**,

- 3905–17 (2016).
163. Pammer, J., Cross, H. S., Frobert, Y., Tschachler, E. & Oberhuber, G. The pattern of prion-related protein expression in the gastrointestinal tract. *Virchows Arch.* **436**, 466–472 (2000).
 164. Konturek, P. C. *et al.* Helicobacter pylori upregulates prion protein expression in gastric mucosa: a possible link to prion disease. *World J. Gastroenterol.* **11**, 7651–7656 (2005).
 165. Amieva, M., Peek, R. M. & Jr. Pathobiology of Helicobacter pylori-Induced Gastric Cancer. *Gastroenterology* **150**, 64–78 (2016).
 166. Tang, Z. *et al.* The Role of Prion Protein Expression in Predicting Gastric Cancer Prognosis. *J. Cancer* **7**, 984–90 (2016).
 167. Zhao, Y. *et al.* Differentially expressed gene profiles between multidrug resistant gastric adenocarcinoma cells and their parental cells. *Cancer Lett.* **185**, 211–218 (2002).
 168. Du, J. *et al.* Overexpression and significance of prion protein in gastric cancer and multidrug-resistant gastric carcinoma cell line SGC7901/ADR. *Int. J. Cancer* **113**, 213–220 (2005).
 169. Liang, J. *et al.* Cellular prion protein promotes proliferation and G1/S transition of human gastric cancer cells SGC7901 and AGS. *FASEB J.* **21**, 2247–2256 (2007).
 170. Liang, J. *et al.* Inhibition of PI3K/Akt partially leads to the inhibition of PrP(C)-induced drug resistance in gastric cancer cells. *FEBS J.* **276**, 685–694 (2009).
 171. Liang, J. *et al.* Function of PrPC (1-OPRD) in biological activities of gastric cancer cell lines. *J. Cell. Mol. Med.* **13**, 4453–4464 (2009).
 172. Pan, Y. *et al.* Cellular prion protein promotes invasion and metastasis of gastric cancer. *FASEB J.* **20**, 1886–1888 (2006).
 173. Wang, J.-H. *et al.* Dynamic changes and surveillance function of prion protein

- expression in gastric cancer drug resistance. *World J. Gastroenterol.* **17**, 3986–3993 (2011).
174. Zhou, L. *et al.* Overexpression of PrPc, combined with MGr1-Ag/37LRP, is predictive of poor prognosis in gastric cancer. *Int. J. Cancer* **135**, 2329–2337 (2014).
175. Pammer, J., Weninger, W. & Tschachler, E. Human keratinocytes express cellular prion-related protein in vitro and during inflammatory skin diseases. *Am. J. Pathol.* **153**, 1353–1358 (1998).
176. Li, C. *et al.* Pro-prion binds filamin A, facilitating its interaction with integrin beta1, and contributes to melanomagenesis. *J. Biol. Chem.* **285**, 30328–30339 (2010).
177. Sauer, H., Dagdanova, A., Hescheler, J. & Maria, W. Redox-regulation of intrinsic prion expression in multicellular prostate tumor spheroids. *Free Radic. Biol. Med.* **27**, 1276–1283 (1999).
178. Conti, A. *et al.* Identification of novel candidate circulating biomarkers for malignant soft tissue sarcomas: Correlation with metastatic progression. *Proteomics* **16**, 689–697 (2016).
179. Kikuchi, Y. *et al.* G1-dependent prion protein expression in human glioblastoma cell line T98G. *Biol. Pharm. Bull.* **25**, 728–733 (2002).
180. Lopes, M. H. *et al.* Interaction of cellular prion and stress-inducible protein 1 promotes neuritogenesis and neuroprotection by distinct signaling pathways. *J. Neurosci.* **25**, 11330–11339 (2005).
181. Erlich, R. B., Kahn, S. A., Lima, F. R. S. & Muras, A. G. STI1 promotes glioma proliferation through MAPK and PI3K pathways. *Glia* **1698**, 1690–1698 (2007).
182. Iglesia, R. P. *et al.* Engagement of cellular prion protein with the co-chaperone Hsp70/90 organizing protein regulates the proliferation of glioblastoma stem-like cells. *Stem Cell Res. Ther.* **8**, 1–14 (2017).
183. Da Fonseca, a. C. C. *et al.* Microglial stress inducible protein 1 promotes

- proliferation and migration in human glioblastoma cells. *Neuroscience* **200**, 130–141 (2012).
184. Barbieri, G. *et al.* Silencing of cellular prion protein (PrPC) expression by DNA-antisense oligonucleotides induces autophagy-dependent cell death in glioma cells. *Autophagy* **7**, 840–853 (2014).
185. Li, W. *et al.* Expression of prion protein in glioblastoma and related mechanisms. *Int J Clin Exp Pathol* **9**, 10973–10980 (2016).
186. El-Guendy, N., Zhao, Y., Gurumurthy, S., Burikhanov, R. & Rangnekar, V. M. Identification of a unique core domain of par-4 sufficient for selective apoptosis induction in cancer cells. *Mol. Cell. Biol.* **23**, 5516–25 (2003).
187. Lawson, H. C. *et al.* Interstitial chemotherapy for malignant gliomas: The Johns Hopkins experience. *J. Neurooncol.* **83**, 61–70 (2007).
188. Ozdemir-Kaynak, E., Qutub, A. A. & Yesil-Celiktas, O. Advances in Glioblastoma Multiforme Treatment: New Models for Nanoparticle Therapy. *Front. Physiol.* **9**, (2018).
189. Sarkaria, J. N. *et al.* Mechanisms of chemoresistance to alkylating agents in malignant glioma. *Clin. Cancer Res.* **14**, 2900–2908 (2008).
190. Moody, C. & Wheelhouse, R. The Medicinal Chemistry of Imidazotetrazine Prodrugs. *Pharmaceuticals* **7**, 797–838 (2014).
191. Dna, C. *et al.* Identification of the Cross-Link between Human O⁶-Methylguanine-DNA Methyltransferase and Identification of the Cross-Link between Human O⁶-Methylguanine-DNA. 6052–6058 (1992).
192. Schäfer, O. D. Chemistry and Biology of DNA Repair. *Angew. Chemie Int. Ed.* **42**, 2946–2974 (2003).
193. Lee, E. Q., Nayak, L., Wen, P. Y. & Reardon, D. a. Treatment options in newly diagnosed glioblastoma. *Curr. Treat. Options Neurol.* **15**, 281–288 (2013).
194. Chen, C., Xu, T., Lu, Y., Chen, J. & Wu, S. The efficacy of temozolomide for

- recurrent glioblastoma multiforme. *Eur. J. Neurol.* **20**, 223–230 (2013).
195. Pegg, A. E. Repair of O6-alkylguanine by alkyltransferases. *Mutat. Res. - Rev. Mutat. Res.* **462**, 83–100 (2000).
196. Hegi, M. E. *et al.* *MGMT* Gene Silencing and Benefit from Temozolomide in Glioblastoma. *N. Engl. J. Med.* **352**, 997–1003 (2005).
197. Hegi, M. E. & Stupp, R. Withholding temozolomide in glioblastoma patients with unmethylated *MGMT* promoter—still a dilemma?: Table 1. *Neuro. Oncol.* **17**, 1425–1427 (2015).
198. Carlsson, S. K., Brothers, S. P. & Wahlestedt, C. Emerging treatment strategies for glioblastoma multiforme. *EMBO Mol. Med.* **6**, 1359–1370 (2014).
199. Beier, D. *et al.* Temozolomide Preferentially Depletes Cancer Stem Cells in Glioblastoma. *Cancer Res.* **68**, 5706–5715 (2008).
200. Fritzell, S. *Combined chemotherapy and immunotherapy against experimental malignant brain tumors.* (2013).
201. Liu, X. Y. *et al.* Inhibition of elongation factor-2 kinase augments the antitumor activity of temozolomide against glioma. *PLoS One* **8**, e81345–e81345 (2013).
202. Xu, G. W., Mymryk, J. S. & Cairncross, J. G. Pharmaceutical-mediated inactivation of p53 sensitizes U87MG glioma cells to BCNU and temozolomide. *Int. J. Cancer* **116**, 187–192 (2005).
203. Xu, Y., Stamenkovic, I. & Yu, Q. CD44 attenuates activation of the Hippo signaling pathway and is a prime therapeutic target for glioblastoma. *Cancer Res.* **70**, 2455–2464 (2010).
204. Gutenberg, a. *et al.* The combination of carmustine wafers and temozolomide for the treatment of malignant gliomas. A comprehensive review of the rationale and clinical experience. *J. Neurooncol.* **113**, 163–174 (2013).
205. Dörner, L., Mustafa, A., Rohr, A., Mehdorn, H. M. & Nabavi, A. Growth

- pattern of tumor recurrence following bis-chloroethylnitrosourea (BCNU) wafer implantation in malignant glioma. *J. Clin. Neurosci.* **20**, 429–434 (2013).
206. Ogawa, J., Pao, G. M., Shokhirev, M. N. & Verma, I. M. Glioblastoma Model Using Human Cerebral Organoids. *Cell Rep.* **23**, 1220–1229 (2018).
207. Heffernan, J. M. & Sirianni, R. W. Modeling Microenvironmental Regulation of Glioblastoma Stem Cells: A Biomaterials Perspective. *Front. Mater.* **5**, 7 (2018).
208. Li, D. *et al.* Cover image: Primary diagnosis of a right frontal glioblastoma following acquisition of axial slices of T1-weighted gadolinium-enhanced MRI (left) and 18F-FDG PET (right). See page 158, chapter 9 for details. **63**, (2017).
209. Clark, M. J. *et al.* U87MG decoded: the genomic sequence of a cytogenetically aberrant human cancer cell line. *PLoS Genet.* **6**, e1000832 (2010).
210. Xie, Y. *et al.* The Human Glioblastoma Cell Culture Resource: Validated Cell Models Representing All Molecular Subtypes. *EBioMedicine* **2**, 1351–1363 (2015).
211. Allen, M., Bjerke, M., Edlund, H., Nelander, S. & Westermarck, B. Origin of the U87MG glioma cell line: Good news and bad news. *Sci. Transl. Med.* **8**, (2016).
212. Chio, C. C. *et al.* Honokiol enhances temozolomide-induced apoptotic insults to malignant glioma cells via an intrinsic mitochondrion-dependent pathway. *Phytomedicine* **49**, 41–51 (2018).
213. Clark, M. J. *et al.* U87MG Decoded: The Genomic Sequence of a Cytogenetically Aberrant Human Cancer Cell Line. *PLoS Genet.* **6**, e1000832 (2010).
214. Bio-Rad. Bio-Rad. www.bio-rad.com (2018).
215. Annovazzi, L. *et al.* Chemotherapeutic Drugs: DNA Damage and Repair in

- Glioblastoma. *Cancers (Basel)*. **9**, 57 (2017).
216. Benson, E. K. *et al.* p53-dependent gene repression through p21 is mediated by recruitment of E2F4 repression complexes. *Oncogene* **33**, 3959–3969 (2014).
217. Barnum, K. J. & O’Connell, M. J. Cell cycle regulation by checkpoints. *Methods Mol. Biol.* **1170**, 29–40 (2014).
218. Panopoulos, A., Howell, M., Fotedar, R. & Margolis, R. L. Glioblastoma motility occurs in the absence of actin polymer. *Mol. Biol. Cell* **22**, 2212–20 (2011).
219. Mizenina, O. A. & Moasser, M. M. S-phase Inhibition of Cell Cycle Progression by a Novel Class of Pyridopyrimidine Tyrosine Kinase Inhibitors. *Cell Cycle* **3**, 794–801 (2004).
220. Baranovskiy, A. G. *et al.* Structural basis for inhibition of DNA replication by aphidicolin. *Nucleic Acids Res.* **42**, 14013–14021 (2014).
221. Hirose, Y., Berger, M. S., Pieper, R. O. & Cells, T. H. G. p53 Effects Both the Duration of G₂ / M Arrest and the Fate of p53 Effects Both the Duration of G₂ / M Arrest and the Fate of. *Cancer Res.* **61**, 1957–1963 (2001).
222. Hofstetrova, K. *et al.* Giardia intestinalis: Aphidicolin influence on the trophozoite cell cycle. *Exp. Parasitol.* **124**, 159–166 (2010).
223. Choi, H. J., Fukui, M. & Zhu, B. T. Role of cyclin B1/Cdc2 up-regulation in the development of mitotic prometaphase arrest in human breast cancer cells treated with nocodazole. *PLoS One* **6**, (2011).
224. Hirose, Y. *et al.* p53 Effects Both the Duration of G₂ /M Arrest and the Fate of Temozolomide-treated Human Glioblastoma Cells 1. *Cancer* 1957–1963 (2001).
225. Karbownik, M. S., Pietras, T., Szemraj, J., Kowalczyk, E. & Nowak, J. Z. The ability of hyaluronan fragments to reverse the resistance of C6 rat glioma cell line to temozolomide and carmustine. *Wspolczesna Onkol.* **18**, 323–328 (2014).

226. Chieng, C. K. L. & Say, Y. H. Cellular prion protein contributes to LS 174T colon cancer cell carcinogenesis by increasing invasiveness and resistance against doxorubicin-induced apoptosis. *Tumor Biol.* **36**, 8107–8120 (2015).
227. Liang, J. *et al.* Overexpression of PrPC and its antiapoptosis function in gastric cancer. *Tumor Biol.* **27**, 84–91 (2006).
228. Atkinson, C. The expression of the prion protein (PrP) in common cancers and its role in the metastasis of breast cancer and development of chemotherapeutic drug resistance in colon and breast cancer. (2015).
229. Fan, S. *et al.* Disruption of p53 Function Sensitizes Breast Cancer MCF-7 Cells to Cisplatin and Pentoxifylline. *Cancer Res.* **55**, 1649–1654 (1995).
230. Stockert, J. C., Horobin, R. W., Colombo, L. L. & Blázquez-Castro, A. Tetrazolium salts and formazan products in Cell Biology: Viability assessment, fluorescence imaging, and labeling perspectives. *Acta Histochem.* **120**, 159–167 (2018).
231. Kumar, P., Nagarajan, A. & Uchil, P. D. Analysis of Cell Viability by the Lactate Dehydrogenase Assay. *Cold Spring Harb. Protoc.* **2018**, pdb.prot095497 (2018).
232. Yang, C. *et al.* Ki67 targeted strategies for cancer therapy. *Clin. Transl. Oncol.* **20**, 570–575 (2018).
233. Xu, G. W. *et al.* Inactivation of p53 sensitizes U87MG glioma cells to 1,3-bis(2-chloroethyl)1-nitrosourea. *Cancer Res.* **61**, 4155–4159 (2001).
234. Gartel, A. L. & Tyner, A. L. The role of the cyclin-dependent kinase inhibitor p21 in apoptosis. *Mol Cancer Ther* **1**, 639–649 (2002).
235. Karimian, A., Ahmadi, Y. & Yousefi, B. Multiple functions of p21 in cell cycle, apoptosis and transcriptional regulation after DNA damage. *DNA Repair (Amst)*. **42**, 63–71 (2016).
236. Roucou, X. *et al.* Cellular prion protein inhibits proapoptotic Bax conformational change in human neurons and in breast carcinoma MCF-7 cells. *Cell Death Differ.* **12**, 783–795 (2005).

237. Miller, I. *et al.* Ki67 is a Graded Rather than a Binary Marker of Proliferation versus Quiescence. *Cell Rep.* **24**, 1105–1112.e5 (2018).
238. Hartmann, C. A., Martins, V. R. & Lima, F. R. S. High levels of Cellular Prion Protein improve astrocyte development. *FEBS Lett.* **587**, 238–244 (2013).
239. Arantes, C. *et al.* Prion protein and its ligand stress inducible protein 1 regulate astrocyte development. *Glia* **57**, 1439–1449 (2009).
240. Lowe, S. W., Ruley, H. E., Jacks, T. & Housman, D. E. p53-dependent apoptosis modulates the cytotoxicity of anticancer agents. *Cell* **74**, 957–67 (1993).
241. Macleod, K. F. *et al.* p53-Dependent and independent expression of p21 during cell growth, differentiation, and DNA damage. *Genes Dev.* **9**, 935–944 (1995).
242. Gartel, A. L. Is p21 an oncogene? *Mol. Cancer Ther.* **5**, 1385–1386 (2006).
243. Di Giovanni, C. *et al.* Identification of noncovalent proteasome inhibitors with high selectivity for chymotrypsin-like activity by a multistep structure-based virtual screening. *Eur. J. Med. Chem.* **121**, 578–591 (2016).
244. Almond, J. B. & Cohen, G. M. The proteasome: a novel target for cancer chemotherapy. *Leuk. Off. J. Leuk. Soc. Am. Leuk. Res. Fund, U.K* **16**, 433–443 (2002).
245. Teicher, B. A. & Tomaszewski, J. E. Proteasome inhibitors. *Biochem. Pharmacol.* **96**, 1–9 (2015).
246. Ames, E., Hallett, W. H. D. & Murphy, W. J. Sensitization of human breast cancer cells to natural killer cell-mediated cytotoxicity by proteasome inhibition. *Clin. Exp. Immunol.* **155**, 504–513 (2009).
247. Chauhan, D., Hideshima, T. & Anderson, K. C. PROTEASOME INHIBITION IN MULTIPLE MYELOMA: Therapeutic Implication. *Annu. Rev. Pharmacol. Toxicol.* **45**, 465–476 (2005).

248. Lecis, D. *et al.* Novel SMAC-mimetics synergistically stimulate melanoma cell death in combination with TRAIL and Bortezomib. *Br. J. Cancer* **102**, 1707–1716 (2010).
249. He, Q., Huang, Y. & Sheikh, M. S. Proteasome inhibitor MG132 upregulates death receptor 5 and cooperates with Apo2L/TRAIL to induce apoptosis in Bax-proficient and -deficient cells. *Oncogene* **23**, 2554–2558 (2004).
250. Nakano, H. *et al.* Reactive oxygen species mediate crosstalk between NF- κ B and JNK. *Cell Death Differ.* **13**, 730–737 (2006).
251. Furman, R. R., Asgary, Z., Mascarenhas, J. O., Liou, H.-C. & Schattner, E. J. Modulation of NF- κ B Activity and Apoptosis in Chronic Lymphocytic Leukemia B Cells. *J. Immunol.* **164**, 2200–2206 (2000).
252. Liu, S. F. NF- κ B activation as a pathological mechanism of septic shock and inflammation. *AJP Lung Cell. Mol. Physiol.* **290**, L622–L645 (2006).
253. Erdal, H. *et al.* Induction of lysosomal membrane permeabilization by compounds that activate p53-independent apoptosis. *Proc. Natl. Acad. Sci.* **102**, 192–197 (2005).
254. Pandit, B. & Gartel, A. L. Proteasome inhibitors induce p53-independent apoptosis in human cancer cells. *Am. J. Pathol.* **178**, 355–360 (2011).
255. Wagenknecht, B., Hermisson, M., Eitel, K. & Weller, M. Proteasome Inhibitors Induce p53/p21-Independent Apoptosis in Human Glioma Cells. *Cell Physiol Biochem* **9**, 117–125 (1999).
256. Zanutto-Filho, A., Braganhol, E., Oliveira Battastini, A. M. & Fonseca Moreira, J. C. Proteasome inhibitor MG132 induces selective apoptosis in glioblastoma cells through inhibition of PI3K/Akt and NF κ B pathways, mitochondrial dysfunction, and activation of p38-JNK1/2 signaling. *Invest. New Drugs* **30**, 2252–2262 (2012).
257. Dang, L. *et al.* Proteasome inhibitor MG132 inhibits the proliferation and promotes the cisplatin-induced apoptosis of human esophageal squamous cell carcinoma cells. *Int. J. Mol. Med.* **33**, 1083–8 (2014).

258. Ma, J. & Lindquist, S. Wild-type PrP and a mutant associated with prion disease are subject to retrograde transport and proteasome degradation. *Proc. Natl. Acad. Sci.* **98**, 14955–14960 (2001).
259. Orsi, A., Fioriti, L., Chiesa, R. & Sitia, R. Conditions of endoplasmic reticulum stress favor the accumulation of cytosolic prion protein. *J. Biol. Chem.* **281**, 30431–30438 (2006).
260. Wu, W. K. K. *et al.* Proteasome inhibition: A new therapeutic strategy to cancer treatment. *Cancer Lett.* **293**, 15–22 (2010).
261. Kitagawa, H. *et al.* Proteasome inhibitors induce mitochondria-independent apoptosis in human glioma cells. *FEBS Lett.* **443**, 181–186 (1999).
262. Yin, D. *et al.* Proteasome inhibitor PS-341 causes cell growth arrest and apoptosis in human glioblastoma multiforme (GBM). *Oncogene* **24**, 344–354 (2005).
263. Longerich, S., Li, J., Xiong, Y., Sung, P. & Kupfer, G. M. Stress and DNA repair biology of the Fanconi anemia pathway. *Blood* **124**, 2812–2819 (2014).
264. Niraj, J., Färkkilä, A. & D’Andrea, A. D. The Fanconi Anemia Pathway in Cancer. *Annu. Rev. Cancer Biol.* **3**, 457–478 (2019).
265. Dong, H. *et al.* Update of the human and mouse Fanconi anemia genes. *Hum. Genomics* **9**, 32 (2015).
266. Garcia-Higuera, I. *et al.* Interaction of the Fanconi anemia proteins and BRCA1 in a common pathway. *Mol. Cell* **7**, 249–262 (2001).
267. Sims, A. E. *et al.* FANCI is a second monoubiquitinated member of the Fanconi anemia pathway. *Nat. Struct. Mol. Biol.* **14**, 564–567 (2007).
268. Moldovan, G.-L. & D’Andrea, A. D. How the fanconi anemia pathway guards the genome. *Annu. Rev. Genet.* **43**, 223–249 (2009).
269. Kondo, N. *et al.* FANCD1/BRCA2 plays predominant role in the repair of dna damage induced by ACNU or TMZ. *PLoS One* **6**, 1–8 (2011).
270. Joshi, P. & Lee, M.-Y. High Content Imaging (HCI) on Miniaturized Three-

- Dimensional (3D) Cell Cultures. *Biosensors* **5**, 768–90 (2015).
271. Zanella, F., Lorens, J. B. & Link, W. High content screening: seeing is believing. *Trends Biotechnol.* **28**, 237–245 (2010).
272. van Vliet, E. *et al.* Current approaches and future role of high content imaging in safety sciences and drug discovery. *ALTEX* **31**, 479–493 (2014).
273. Gu, Y., Luo, X., Basu, S., Fujioka, H. & Singh, N. Cell-specific metabolism and pathogenesis of transmembrane prion protein. *Mol. Cell. Biol.* **26**, 2697–715 (2006).
274. Lund, C., Olsen, C. M., Tveit, H. & Tranulis, M. A. Characterization of the prion protein 3F4 epitope and its use as a molecular tag. *J. Neurosci. Methods* **165**, 183–190 (2007).
275. Zanusso, G. *et al.* Prion protein expression in different species: Analysis with a panel of new mAbs. *Proc. Natl. Acad. Sci. U. S. A.* **95**, 8812–8816 (1998).
276. Kee, Y. & D'Andrea, A. D. Expanded roles of the Fanconi anemia pathway in preserving genomic stability. *Genes Dev.* **24**, 1680–94 (2010).
277. Lanclais, I., Sobeck, A., Stone, S., LaChapelle, A. & Hoatlin, M. E. A novel cell-free screen identifies a potent inhibitor of the fanconi anemia pathway. *Int. J. Cancer* **124**, 783–792 (2009).
278. Landais, I. *et al.* Monoketone analogs of curcumin, a new class of Fanconi anemia pathway inhibitors. *Mol. Cancer* **8**, 133 (2009).
279. Martins, P. *et al.* Heterocyclic Anticancer Compounds: Recent Advances and the Paradigm Shift towards the Use of Nanomedicine's Tool Box. *Molecules* **20**, 16852–16891 (2015).
280. Malki, A. *et al.* New 3-Cyano-2-Substituted Pyridines Induce Apoptosis in MCF 7 Breast Cancer Cells. *Molecules* **21**, 230 (2016).
281. Cope, H. *et al.* Synthesis and SAR study of acridine, 2-methylquinoline and 2-phenylquinazoline analogues as anti-prion agents. *Eur. J. Med. Chem.* **41**, 1124–1143 (2006).

282. Wolf, H., Vorberg, I., Grassmann, A., Graham, J. & Hofmann, J. *Cellular Aspects of Prion Replication In Vitro. Viruses* **5**, (2013).
283. Watanabe, K. A. & Takahashi, K. PCT, US005229395A. (1993).
284. Su, T. L. *et al.* 9-Substituted Acridine Derivatives with Long Half-Life and Potent Antitumor Activity: Synthesis and Structure-Activity Relationships. *J. Med. Chem.* **38**, 3226–3235 (1995).
285. Vogelstein, B., Lane, D. & Levine, A. J. Surfing_the_p53_network. *Nature* **408**, 307–310 (2000).
286. Wang, W. *et al.* Acridine derivatives activate p53 and induce tumor cell death through bax. *Cancer Biol. Ther.* **4**, 893–898 (2005).
287. Incles, C. M., Schultes, C. M. & Neidle, S. Telomerase inhibitors in cancer therapy: current status and future directions. *Curr Opin Investig Drugs* **4**, 675–685 (2003).
288. Goodell, J. R. *et al.* Acridine-based agents with topoisomerase II activity inhibit pancreatic cancer cell proliferation and induce apoptosis. *J. Med. Chem.* **51**, 179–182 (2008).
289. Opegard, L. M. *et al.* Novel acridine-based compounds that exhibit an anti-pancreatic cancer activity are catalytic inhibitors of human topoisomerase II. *Eur J Pharmacol* **602**, 223–229 (2010).
290. Denny, W. A. & Baguley, B. C. Dual topoisomerase I/II inhibitors in cancer therapy. *Curr. Top. Med. Chem.* **3**, 339–53 (2003).
291. Nial J. Wheate, Craig R. Brodie, J. Grant Collins, Sharon Kemp & Janice R. Aldrich-Wright. DNA Intercalators in Cancer Therapy: Organic and Inorganic Drugs and Their Spectroscopic Tools of Analysis. *Mini-Reviews Med. Chem.* **7**, 627–648 (2007).
292. Kaufmann, S. H. Cell death induced by topoisomerase-targeted drugs: More questions than answers. *Biochim. Biophys. Acta - Gene Struct. Expr.* **1400**, 195–211 (1998).

293. Clifford, B., Beljin, M., Stark, G. R. & Taylor, W. R. G2 arrest in response to topoisomerase II inhibitors: The role of p53. *Cancer Res.* **63**, 4074–4081 (2003).
294. Vogtherr, M. *et al.* Antimalarial drug quinacrine binds to C-terminal helix of cellular prion protein. *J. Med. Chem.* **46**, 3563–3564 (2003).
295. Kupfer, G. M. Fanconi anemia: a signal transduction and DNA repair pathway. *Yale J. Biol. Med.* **86**, 491–497 (2013).